



**University of
Reading**

Effects of PAMAM dendrimers on model and biological membranes

By Marleen Wilde

Thesis for the degree of Doctor of Philosophy

Submitted in June 2021

SCFP – School of Pharmacy

DECLARATION OF ORIGINAL AUTHORSHIP

I confirm that this is my own work and the use of all material from other sources has been properly and fully acknowledged.

Marleen Wilde

For my family and friends who supported me during this journey –

I am nothing without you!

ACKNOWLEDGEMENT

I would like to say a heart-felt THANK YOU to everyone who was in one way, or another, involved in this long journey. I am not a fan of big words, so I will keep this brief – apologies that I don't mention every single one of you, but be assured, I am extremely grateful for you being by my side.

I am grateful to my supervisors Dr Francesca Greco and Prof Rebecca Green, and the School of Pharmacy, for providing this opportunity and enabling me to achieve this goal in parallel to my employment.

I also like to thank my teaching and PhD student colleagues for their support, advice, and encouragement throughout my time in the department. It was a pleasure to be part of the team and I enjoyed working with you.

Last but not least, a huge THANK YOU goes out to my family and my friends inside and outside University life (You know who you are!) - not only for your emotional support, but sharing my happiness in my good times and bearing my emotional rollercoaster in my bad ones. You helped me through it when I was close to give up. Now, that it's done, we are going to celebrate together!

ABSTRACT

Poly(amidoamine) (PAMAM) dendrimers are nanosized, highly defined, hyperbranched polymeric vehicles designed for targeted delivery of drugs or bioactive molecules. Whilst heavily researched, their mechanism of interaction with biological systems is barely understood.

Here, medium-generation PAMAMs (-COOH-terminus (G4.5); -NH₂-terminus (G5)) were characterized by UV-Vis and fluorescence, small-angle X-ray scattering and computational simulations. Biophysical (surface pressure measurements, neutron reflectometry) and microbiological techniques were used to assess modulating factors (i.e. solvent pH, residual methanol) of dendrimer-membrane interactions and related toxicity.

PAMAM surface groups are charged at pH 7, and in phosphate buffer solution the dendrimers assumed a compact, near-globular shape (radius \approx 2.5 – 3 nm). PAMAM G5 penetrated anionic phosphatidylglycerol (DPPG, model bacterial lipid) monolayers rapidly but showed lesser membrane-activity on supported bilayers. Electrostatic effects could be potential drivers but also hinder PAMAM G4.5 penetration into DPPG monolayers.

Across techniques, it was shown that solvent pH influenced dendrimer core (tertiary amines) and surface charge, with higher impact on structural characteristics of zwitterionic PAMAM G4.5 than of G5. At pH 4, the charge effect led to higher penetration levels into DPPG monolayers and bilayers for both dendrimers (G5 > G4.5) compared to pH 7.

Methanol as co-solvent affected PAMAM radii and spectroscopic properties across the pH range tested. Additionally, it increased DPPG monolayer penetration compared to the methanol-free buffer environment, which could be explained by both, the impact on PAMAMs and on lipid layer organization.

Anti-bacterial efficacy was studied on gram-negative and gram-positive bacteria. Amine-terminated PAMAMs led to growth-inhibition of most strains, but specifically gram-positive *Staphylococcus spp.* which are rich in anionic

membrane lipids (i.e. PG lipids). Whilst overall less inhibitory than G5, PAMAM G4.5 was bactericidal against *Staphylococcus saprophyticus*.

Taken together, our findings highlight the significance of the PAMAM characteristics and the solvent-PAMAM-lipid interplay and explain, at least partially, potential drivers of PAMAM membrane-toxicity.

DEFINITION OF CONTRIBUTOR ROLES

The CRediT – Contributor Roles Taxonomy (<https://casrai.org/credit/>) was used to attribute contributions of each author to the experimental chapters 3-6.

Conceptualization – Ideas; formulation or evolution of overarching research goals and aims.

Data curation – Management activities to annotate (produce metadata), scrub data and maintain research data (including software code, where it is necessary for interpreting the data itself) for initial use and later re-use.

Formal analysis – Application of statistical, mathematical, computational, or other formal techniques to analyze or synthesize study data.

Funding acquisition - Acquisition of the financial support for the project leading to this publication.

Investigation – Conducting a research and investigation process, specifically performing the experiments, or data/evidence collection.

Methodology – Development or design of methodology; creation of models.

Project administration – Management and coordination responsibility for the research activity planning and execution.

Resources – Provision of study materials, reagents, materials, patients, laboratory samples, animals, instrumentation, computing resources, or other analysis tools.

Software – Programming, software development; designing computer programs; implementation of the computer code and supporting algorithms; testing of existing code components.

Supervision – Oversight and leadership responsibility for the research activity planning and execution, including mentorship external to the core team.

Validation – Verification, whether as a part of the activity or separate, of the overall replication/reproducibility of results/experiments and other research outputs.

Visualization – Preparation, creation and/or presentation of the published work, specifically visualization/data presentation.

Writing – original draft – Preparation, creation and/or presentation of the published work, specifically writing the initial draft).

Writing – review & editing – Preparation, creation and/or presentation of the published work by those from the original research group, specifically critical review, commentary or revision – including pre- or post-publication stages.

LIST OF PUBLICATIONS

Publications related to this thesis:

Chapter 1

Wilde, M. (2020) Research Based Curriculum Resource Pack: Lipid Membrane Models in Biomedical Research. AccessEd. <https://www.access-ed.ngo/lipid-membrane-models-in-biomedical-research>

Chapter 3

Wilde, M., Wilde, C., Edwards-Gayle, C.J.C., Hamley, I.W., Wang, Z., Greco, F. and Green, R.J. (2021) pH and Methanol Responsive Conformational Changes of Poly(amidoamine) Dendrimers in Solution. ACS Applied Polymer Materials, Manuscript submitted

Chapter 4

Wilde, M., Green, R. J., Sanders, M. R. and Greco, F. (2017) Biophysical studies in polymer therapeutics: the interactions of anionic and cationic PAMAM dendrimers with lipid monolayers. Journal of Drug Targeting, 25 (9-10). pp. 910-918.

Chapter 5

Wilde, M., Florek, O.B., Clifton, L.A., Campana, M., Kabova, E., Greco, F. and Green, R.J. (2021) Binding of PAMAM dendrimers with DPPG lipid membrane models affected by solvent condition. Colloids And Surfaces B: Biointerfaces, Manuscript prepared

Publications not related to this thesis:

Florek, O. B., Clifton, L. A., **Wilde, M.**, Arnold, T., Green, R. J. and Frazier, R. (2018) Lipid composition in fungal membrane models: effect of lipid fluidity. Acta Crystallographica Section D: Biological Crystallography, 74.

Phillips, D. J., **Wilde, M.**, Greco, F. and Gibson, M. I. (2015) Enzymatically-triggered, isothermally responsive polymers: re-programming poly(oligoethylene glycols) to respond to phosphatase. Biomacromolecules, 16 (10). pp. 3256-3264.

Bajorat, R., **Wilde, M.**, Sellmann, T., Kirschstein, T. and Köhling, R. (2011) Seizure frequency in pilocarpine-treated rats is independent of circadian rhythm. Epilepsia, 52 (9). e118-e122.

RESEARCH EVENTS AND TRAINING

Conferences and Meetings

- 11th Apr 2019 Pharmacy PhD Showcase 2019, University of Reading, *Talk: From membrane models to biological membranes - relating lipid interactions of potential drug delivery systems to their biological activity*
- 12th Dec 2018 Faraday Division Chemistry, Software Tools Meeting, London
- 18th Jul 2018 APS Symposium: Nanomedicines for the Delivery of Biologics, Reading
- 4th – 7th Jun 2018 Biodendrimer 2018, Urbino (Italy), *Talk: Biophysical studies of PAMAM interactions with membrane models*, Travel Bursary: Macro Group, Graduate School
- 10th Apr 2018 Pharmacy PhD Showcase 2018, University of Reading
- 30th – 31st Oct 2017 ISIS Student Meeting 2017, Abingdon, *Poster and Gong Pitch: Exploring Interactions of PAMAM Dendrimers with Membrane Lipids – A Biophysical Approach*, Travel expenses: STFC/ ISIS
- 11th-13th Apr 2017 Faraday Joint Interest Group Conference 2017, Warwick, *Poster: Exploring Interactions of PAMAM Dendrimers with Membrane Lipids – A Biophysical Approach*
- 31st Mar 2017 Pharmacy PhD Showcase 2017, University of Reading, *Talk: A biophysical approach to study membrane binding behaviour of dendritic carrier molecules*
- 7th-8th Nov 2016 ISIS Student Meeting 2016, Abingdon, *Talk: Binding of PAMAM Dendrimers to Simple Biomembrane Models – Mechanistic Insights*, Travel expenses: STFC/ ISIS
- 12th -14th Sep 2016 Physics meets Biology 2016, Cambridge, *Poster: Binding of PAMAM Dendrimers to Simple Biomembrane Models – Mechanistic Insights*, Travel bursary: Biochemical Society, British Biophysical Society
- 23rd-25th May 2016 11th International Symposium Polymer Therapeutics (ISPT), Valencia (Spain), *Poster Presentation + Flash Talk: PAMAM Dendrimer Interactions at the Lipid Interface*, Travel Bursary: University of Reading Research Travel Grant, ISPT Travel Grant
- 5th May 2016 Future Applications of Small-Angle Scattering to Soft Matter, Swindon

14 th Apr 2016	Pharmacy PhD Showcase 2016, University of Reading, <i>Poster: Exploring Lipid Interactions of a Potential Drug and Gene Delivery System</i>
10 th Oct 2015	Royal Pharmaceutical Society, Pharmaceutical Science Poster Event 2015, London, <i>Poster: PAMAM Dendrimer Interactions with Model Membranes</i>
26 th – 29 th Jul 2015	CRS Annual Meeting, Edinburgh, <i>Poster: PAMAM Dendrimer Interactions with Model Membranes</i> , Travel Bursary: University of Reading Research Travel Grant
30 th Mar 2015	Pharmacy PhD Showcase 2015, University of Reading

Awarded Training Events

28 th Oct 2019	DMA Talents Creative Data Lab, London
16 th – 21 st Sep 2018	Diamond Synchrotron School, Harwell
19 th – 23 rd Mar 2018	Muon Training School 2018, STFC/ ISIS Muon and Neutron Source, Harwell
7 th – 18 th Sep 2015	14th Oxford School on Neutron Scattering, Oxford

Research Awards

2018	Undergraduate Summer Studentship (University of Reading)
2015 – 2018	11 days of project-related Neutron Beam Time (STFC/ ISIS)

CONTENTS

1	Introduction	2
1.1	Background and project motivation.....	2
1.2	Dendrimers - Poly(amidoamine) (PAMAM).....	5
1.2.1	Structure and activity of PAMAM dendrimers.....	5
1.2.2	Biomedical applications and limitations.....	6
1.3	Biological membranes	9
1.3.1	Membrane lipids.....	12
1.4	Overview of membrane models	15
1.4.1	Langmuir monolayer	16
1.4.2	(Planar) lipid bilayers.....	16
1.4.3	Lipid vesicles.....	17
1.5	Interactions between PAMAM dendrimers and (model) membranes	18
1.6	Thesis outline.....	19
1.6.1	Scientific rationale	21
1.7	References	22
2	Methodology.....	50
2.1	Materials	50
2.2	Surface pressure measurements.....	51
2.2.1	Preparation of the Langmuir trough.....	52

2.2.2	Preparation of lipid monolayers.....	53
2.2.3	Dendrimer addition.....	54
2.2.4	Data interpretation.....	55
2.3	Neutron reflectometry	56
2.3.1	Fabrication of lipid bilayers on to solid supports.....	56
2.3.2	Neutron reflectivity measurements.....	57
2.3.3	Simplified interpretation of neutron reflectivity data.....	59
2.4	General data analysis, drawing and figure synthesis.....	60
2.5	References	60
3	pH and Methanol Responsive Conformational Changes of Poly(amidoamine) Dendrimers in Solution.....	63
3.1	Introduction.....	65
3.2	Experimental setup	69
3.2.1	Sample preparation.....	69
3.2.2	Ultraviolet and visible spectroscopy (UV/Vis).....	69
3.2.3	Fluorescence spectrophotometry (fluorescence)	69
3.2.4	Small angle X-ray scattering (SAXS).....	70
3.2.5	Molecular dynamics (MD) simulations.....	71
3.2.6	Statistical analysis.....	73
3.3	Results.....	74
3.3.1	Effect of methanol	74

3.3.2	Effect of pH	80
3.4	Discussion	90
3.5	Conclusions	93
3.6	References	94
3.7	Supplementary information	103
3.7.1	Literature screening for studies using commercial PAMAM	103
3.7.2	Statistical comparison of UV/Vis and fluorescence data	104
3.7.3	SAXS fitting parameters Spherical Shell	108
3.7.4	Coarse-grained PAMAM dendrimer models.....	109
3.7.5	Overview of PAMAM G5 radii reported from computational and small angle scattering studies	112
3.7.6	References – Supplementary Information	114
4	Biophysical Studies in Polymer Therapeutics: The Interactions of Anionic and Cationic PAMAM Dendrimers with Lipid Monolayers	120
4.1	Introduction	122
4.2	Experimental.....	125
4.2.1	Materials.....	125
4.2.2	Surface pressure measurements	125
4.2.3	External reflection FTIR spectroscopy.....	126
4.3	Results.....	127
4.3.1	Effect of polymer charge on polymer-lipid interactions.....	127
4.3.2	Effect of polymer concentration on polymer-lipid interactions .	129

4.3.3	Effect of sodium chloride in the buffer subphase on polymer-lipid interactions.....	132
4.4	Discussion	133
4.5	Conclusions	137
4.6	References	138
5	Binding of PAMAM Dendrimers with DPPG Lipid Membrane Models Affected by Solvent Conditions	147
5.1	Introduction	149
5.2	Experimental.....	150
5.2.1	Materials.....	150
5.2.2	Methodology.....	151
5.3	Results and discussion	154
5.3.1	Interactions with lipid monolayers	154
5.3.2	Interactions with lipid bilayers – neutron reflectometry	158
5.4	Conclusions	164
5.5	References	165
5.6	Supplementary.....	172
5.6.1	Supplementary materials.....	172
5.6.2	Supplementary results.....	174
5.6.3	References supplementary	176
6	PAMAM Dendrimers Affect Gram-positive Bacterial Growth.....	178
6.1	Introduction	180

6.2	Experimental.....	187
6.2.1	Materials.....	187
6.2.2	Methods	187
6.3	Results and discussion	190
6.3.1	Screening of bacterial strains	190
6.3.2	Effect of PAMAM G5 on bacterial generation time	191
6.3.3	PAMAM effect on turbidity and bacterial survival	193
6.3.4	Linking PAMAM effect to membrane lipid composition	197
6.3.5	Conclusion	205
6.4	References	205
7	Discussion and Conclusion	216
7.1	Key findings	217
7.2	Significance to the wider research field	219
7.2.1	Membrane models and their translatability, a critical assessment 220	
7.2.2	Half-generation PAMAMs – an overlooked drug-delivery system? 222	
7.3	Conclusions and future development opportunities	225
7.4	References	228

LIST OF FIGURES

Figure 1-1 Dendrimers from synthesis to structure. Panel a) illustrates the differences between divergent and convergent approaches in dendrimer synthesis. The dashed lines on the final molecules denote the generations. In panel b) the symbols are aligned to the PAMAM dendrimers in the focus of this thesis, where ethylenediamine is the initiator core and the terminal generations are decorated with either with primary amines or carboxyl groups, for the full-generation or half-generation PAMAMs respectively. Panel c) shows the chemical structure of full-generation PAMAM G4 (64 terminal branches and surface groups), for clarity only a quarter of the molecule is fully drawn, and the repetitive unit indicated as R. Each generation is in a different color to help identification. The full PAMAM G4 structure was used to visualize the 3D arrangement in panel d) and to show solvent-accessible cavities in panel e). Structures in panels c – e were created in ChemOffice 2020. 7

Figure 1-2 Panel a) illustrates the asymmetric distribution of membrane lipids between inner and outer leaflet of the plasma membrane and arrangement of lipid raft domains (enriched in saturated phospholipids, sphingolipids, glycolipids, cholesterol, lipidated proteins and glycosylphosphatidylinositol (GPI)-anchored proteins). Interaction with actin is important for domain maintenance and remodelling. Panel b) Various raft-like and non-raft domains with distinct compositions and properties define the organization of membranes. Reprinted by permission from Nature Reviews Molecular Cell Biology, Sezgin et al 2017¹⁶⁶. Copyright 2017 Springer Nature. 10

Figure 1-3 Schematic illustration of the cell envelope of bacterial cells (not to scale). A typical example of gram-negative bacterium is *Escherichia coli*, an example gram-positive bacterium is *Staphylococcus aureus*. Illustration inspired by Berezin et al 2017¹⁷⁶. 12

Figure 1-4 Phospholipid composition of a human erythrocyte as an example for lipid asymmetry in membranes. Figure based on data from Virtanen et al 1998¹⁹⁶. CPL: Choline phospholipids, APL: Anionic phospholipids, PC: phosphatidylcholines, SM: sphingomyelin, LPC: lysophosphatidylcholine, PE: phosphatidylethanolamines, PS: phosphatidylserines, PI: phosphatidylinositols, PA: phosphatidic acids. 14

Figure 1-5 Schematic outline of the thesis concept and integration of the chapters 20

Figure 2-1 Wilhelmy plate submerged in subphase, where θ is the contact angle, t thickness, w width and l length of the plate. 52

Figure 2-2 Langmuir Blottgett trough setup. The instrument is shown in situ in panel a), with a close-up of the pressure sensor and the Wilhelmy plate in panel b). A simplified illustration of the setup and preparing the lipid monolayer is shown in panel c. 53

<i>Figure 2-3 Exemplary compression isotherms of DPPC (black) and DPPG (grey) monolayers at room temperature. At large areas per molecule, the monolayers exist in the gaseous state (G) and undergo a phase transition to the liquid-expanded state (LE) during compression. Upon further compression, the LE phase undergoes first a transition to the liquid-condensed state (LC); and finally, the monolayer reaches the solid state (S). The orientation of the molecules in the different phases is schematically illustrated. Arrows indicate lipid phase transitions. Illustration inspired by Oliveira et al 2017² and Maget-Dana 1999¹.....</i>	<i>54</i>
<i>Figure 2-4 Illustration of the experimental steps on the Langmuir trough, including lipid monolayer preparation and PAMAM addition.</i>	<i>55</i>
<i>Figure 2-5 Schematic adsorption and penetration of membrane-active molecules into lipid monolayers with related changes in surface pressure.</i>	<i>56</i>
<i>Figure 2-6 Preparation of a supported bilayer. First step is the Langmuir-Blodgett deposition of a lipid monolayer onto the silicon substrate. The second (outer) leaflet of the bilayer is created in Step 2 using the Langmuir-Schaefer deposition. Illustration inspired by Belegirinou et al 2010⁵.</i>	<i>57</i>
<i>Figure 2-7 Setup in the INTER Beamline. Panel a) shows the view into the beamline with the mirror and detector area highlighted by the red box. Panel b) and c) show the setup of the liquid flow cells on the movable stage and connection to the pump.</i>	<i>58</i>
<i>Figure 2-8 Simplified setup of the neutron experiment at INTER shown in Figure 2-7 panel c. .</i>	<i>58</i>
<i>Figure 2-9 Potential changes in the SLD profiles caused by membrane-active molecules.</i>	<i>59</i>
<i>Figure 3-1 UV/Vis absorbance spectra of PAMAM G5 and G4.5 in phosphate buffer pH 7 (0.04 M) with (2 % MeOH) and without residual methanol (0% MeOH). Panel a) compares the maximum absorption wavelength λ_{max} of 1 mg mL⁻¹ PAMAM solutions. Panel b) shows the resonance structures of the PAMAM dendrimers. The concentration-dependent absorbance with a linear fit is presented for G5 (panel c) and G4.5 (panel d). Data represent mean \pm SEM, n \geq 3. Error bars are hidden by the symbols when not visible. Panels e) and f) demonstrate example UV/Vis absorption spectra for G5 and G4.5, respectively. For clarity, data for 0.06 and 0.125 mg mL⁻¹ are not shown. Statistical difference, where applicable, is indicated as * for p < 0.05 and ** for p < 0.01.</i>	<i>75</i>
<i>Figure 3-2 Non-traditional intrinsic fluorescence of PAMAM G5 and G4.5 in phosphate buffer solution at pH 7 (0.04 M) under presence (2 %, filled symbols) and absence (0 %, clear symbols) of residual methanol. Data in panel a – d are presented in M \pm SEM, n \geq 3. Error bars are hidden by the symbols when not visible. Panels a) and b) compare the results of the emission search scan of the 1 mg mL⁻¹ PAMAM solution. The excitation wavelength causing the</i>	

highest emission intensity is referred to as λ_{ex} , whereas λ_{em} denotes the emission wavelength at the highest fluorescence. Panels c) and d) show the concentration – dependent emission intensity with linear fits for G5 (λ_{ex} 350 nm) and G4.5 (λ_{ex} 380 nm), respectively. Panels e) and f) present exemplary excitation and emission spectra of G5 and G4.5 at a solution concentration of 1 mg mL^{-1} , solid lines reflect 2 % methanol presence in the phosphate buffer solution, dashed lines absence of methanol (0 %). Statistical difference is indicated as ** for $p < 0.005$, in all other cases the difference was not significant. 77

Figure 3-3 Methanol effect on scattering of PAMAM dendrimers in solution. Spherical Shell form factor fitted SAXS profiles and Kratky plots (insets) of PAMAM G5 (panel a) and G4.5 (panel b) in sodium phosphate buffer pH 7 under the presence (filled symbols) and absence (clear symbols) of 1% methanol. 78

Figure 3-4 Charge and number of charged groups of PAMAM dendrimers. Charge calculations are based on the Henderson-Hasselbalch equation with pKa 6.7 for tertiary amines, pKa 9 for primary amines and pka 4.8 for carboxyl groups. The 128 surface groups of PAMAM G5 and G4.5 are primary amines and carboxyl groups, respectively, whereas tertiary amines represent the core functional groups of both dendrimer types. Total charged groups refer to the absolute number of all charged moieties of the molecule at any given pH irrespective if negative or positive, and the PAMAM Net Charge sums up the effective charge of the dendrimer. For G5, PAMAM Net Charge and Total Charged Groups are overlaid/ identical. 80

Figure 3-5 UV/Vis absorbance of PAMAM G4.5 and G5 in phosphate buffer solution of varying pH (pH 4, 7 and 10) without (0 %, clear columns) and with residual methanol (2 %, filled columns). Data are displayed as $M \pm SEM$, $n \geq 3$. Panels a) and b) represent the concentration – dependent maximum absorbance of G5 and G4.5, respectively. The λ_{max} were in the range of 270 – 278 nm for G5, and 287 – 289 for G4.5. Statistical difference is indicated as * for $p < 0.05$ and ** for $p < 0.005$ for the difference between pH 4 and pH 10, in all other cases the difference was not significant. 82

Figure 3-6 Fluorescence results of PAMAM G5 and PAMAM G4.5 in phosphate buffer solution of different pH (pH 4, 7, and 10) under presence (2 %, filled columns) and absence (0 %, clear columns) of residual methanol. Data are presented in $M \pm SEM$, $n \geq 3$. Error bars are hidden by the symbols when not visible. Panels a) and b) show the maximum emission fluorescence intensity for G5 (λ_{ex} 350 nm) and G4.5 (λ_{ex} 380 nm), respectively. The corresponding emission wavelengths varied between 428 – 453 nm for G5 and 458 – 464 nm for G4.5. Statistical difference is indicated as * for $p \leq 0.05$, ** for $p \leq 0.01$, *** for $p < 0.001$; in all other cases the difference is not significant. 82

Figure 3-7 Effect of solution pH on scattering of PAMAM dendrimers. SAXS data was fitted to a spherical shell form factor (lines). The fitted SAXS profiles (inset) and Kratky plots of 1 mg mL^{-1}

PAMAM dendrimer solutions under different pH conditions are shown for 1 % (panel a, b) and 0 % residual methanol (panel c, d)..... 84

Figure 3-8 MD simulation results of the radial number density distribution functions, $\rho(r)$, of all monomers and surface groups only for PAMAM G5 (a) and G4.5 (b); and of the counterions in the corresponding environments for PAMAM G5 (c) and G4.5 (d). For PAMAM G4.5, no anionic counterions were observed at pH 10 (d). The percentage of surface groups (outer groups) in all monomers, measured as the ratio between their radial number densities $\rho_{\text{outer}}(r)/\rho_{\text{all}}(r)$, is shown in (e). In (a-e) the radial distance r is measured from the centers of mass of the dendrimers. The pH-dependent radii of gyration, R_g , of the dendrimers are shown as filled symbols and the relative shape anisotropy κ^2 as clear symbols in panel (f). 86

Figure 3-9 Snapshots of (a) full-generation PAMAM G5 and (b) half-generation PAMAM G4.5 at pH 7 which show backfolding of outer generation groups and penetration of counterions into the molecular structure. The surface groups are represented by the red monomers. The lighter the red color the closer the monomer is located to the dendrimer core (depicted by two orange beads). The inner functional groups are either colored as cyan if they are cationic, or gray if they are neutral alongside the spacer units. The unbonded dark blue and green beads represent anionic and cationic counterions, respectively. 90

Figure 3-10 Literature screening for use of commercial PAMAM in studies with biological systems or biophysical model. Screening was performed for articles published up to 31/03/2019 103

Figure 4-1 Chemical structures of the lipids and the polymers used in this study. a) Chemical structure of i) 1,2-dipalmitoyl-sn-glycero-3-phosphocholine (DPPC); ii) 1,2-dipalmitoyl-sn-glycero-3-phospho-(1'-rac-glycerol) (sodium salt) (DPPG). b) Chemical Structure of linear polyethylene glycol (PEG). c) Chemical structure of poly(amidoamine) (PAMAM) dendrimer with ethylenediamine core; generations inset: i) PAMAM G4.5: R-group anionic in solution (pH 7), sodium carboxylate surface groups; ii) PAMAM G5: R-group cationic in solution (pH 7), amino surface groups..... 124

Figure 4-2 Selectivity of polymers towards different lipid monolayers. Changes in surface pressure for PEG 20,000 (panel a); PAMAM G5 (panel b); and PAMAM G4.5 (panel c) binding to DPPG (filled symbols) and DPPC (open symbols) monolayers were recorded over time. Experiments were carried out at pH 7, surface pressure was at $21 \pm 2 \text{ mN m}^{-1}$ immediately prior to polymer addition at concentration 0.061 mg mL^{-1} . Data show profiles for a single representative experiment from a set of at least 3 independent experiments ($n \geq 3$). Panel d shows comparison of maximum increase in surface pressure observed for the 3 polymers against DPPG (black) and DPPC (white), data show mean \pm SEM ($n \geq 3$). Statistical significance calculated via Student's t test, and set at $p \leq 0.05$. ns = non-significant. 128

Figure 4-3 Concentration-dependence of polymer interactions with lipid monolayers. Binding of PAMAM G5 (panel a); PAMAM G4.5 (panel b); and PEG 20,000 (panel c) to DPPG (filled symbols) and DPPC (open symbols) was studied at pH 7. Surface pressure was $21 \pm 2 \text{ mN m}^{-1}$ prior to polymer addition. Maximum surface pressure change data displayed indicate mean \pm SEM; error bars are hidden by the symbol when not visible. Statistical significance calculated via Student's t test, and set at $p \leq 0.05$. ns = non-significant. Comparisons carried out are highlighted with dashed line. 130

Figure 4-4 Concentration-dependent effect of PAMAM G5 dendrimers on the Amide I region of the FTIR spectrum. Changes in the peak area of the Amide I (panel a) were observed upon dendrimer binding to DPPG (filled symbols) and DPPC (open symbols) monolayers. The inset enlarges the data for interaction with DPPG only. Exemplary spectra focusing on the Amide I region (panel b) showing the addition of PAMAM G5 to a DPPG monolayer in the condensed phase. i) $0.0024 \text{ mg mL}^{-1}$; ii) $0.0125 \text{ mg mL}^{-1}$; iii) 0.018 mg mL^{-1} ; iv) 0.024 mg mL^{-1} . No visible changes were associated to the C = O stretch of the headgroup of the phospholipid. Reproducibility of the technique has been verified via experiments with a subset of PAMAM dendrimers of different generations. 132

Figure 5-1 PAMAM G5 and G4.5 in phosphate buffer ($I = 0.034 \text{ M}$) interacting with DPPG monolayers. Panel a) Effect of methanol and pH on maximum changes in surface pressure (SP_{max}). Panel b) Impact of initial pressure (IP) before PAMAM G5 introduction on surface pressure changes at different pH. SP30 and SP60 are surface pressure changes measured at 30 min and 60 min after starting the PAMAM interaction. Panel c) Representative excerpts of initial 30 min of surface pressure changes over time for PAMAM G4.5 in different buffer conditions. Panel d) Exemplary excerpts of initial 30 min of surface pressure changes over time for PAMAM G5 in different buffer conditions and varying initial surface pressure. Data in panel a) and b) shown as $M \pm \text{SEM}$, $n \geq 3$. Statistical Analysis performed with Anova and Bonferroni; * $p \leq 0.05$; *** $p \leq 0.005$; **** $p < 0.001$. (*) $p = 0.0512$ 155

Figure 5-2 Interaction of PAMAM G4.5 with an asymmetric, deuterated bilayer (dDPPC-hDPPG) in phosphate buffer pH 7 ($I = 0.039 \text{ M}$). Panel a) Neutron reflectivity profiles and fits of the bilayer before (grey) and after PAMAM (coloured) interaction at 0.06 mg mL^{-1} . Averaged data points and error bars from multiple counts. Panel b) Scattering length density profiles derived from fits of the reflectivity profiles in different contrasts. In both panels, the shaded area accounts for the 95 % confidence interval of the data fits. 160

Figure 5-3 Interaction of PAMAM G4.5 and G5 with an asymmetric, deuterated bilayer (hDPPC-dDPPG) in deuterated and hydrogenated phosphate buffer pH 4 ($I = 0.039 \text{ M}$). Neutron reflectivity profiles and fits of the bilayer before (light grey) and after PAMAM G4.5 (dark grey, panel a) and PAMAM G5 (panel c) interaction. Averaged data points and error bars from the scattering counts. Scattering length density profiles derived from fits of the reflectivity profiles in

different contrasts for PAMAM G4.5 (panel b) and PAMAM G5 (panel d). In all panels, the shaded area accounts for the 95 % confidence interval of the data fits 162

Figure 5-4 PAMAM dendrimer characteristics. a) Schematic representation of regular branching of PAMAM dendrimers. Number of surface groups/branches (Z) in each generation (G) can be calculated as follows: $Z = 4 \times 2^G$. b) Summary of key parameters of PAMAM dendrimers used in this study, chemical formula and molecular weight as provided by manufacturer..... 173

Figure 5-5 Representative profiles of 60 min of surface pressure changes over time under different experimental conditions for interactions of a) PAMAM G4.5 and b) PAMAM G5 with DPPG monolayers. IP stands for initial pressure and reflects the lipid monolayer surface pressure prior to PAMAM addition. 174

Figure 6-1 Effect of PAMAM G5 on the growth profile and generation time of *P. aeruginosa* ATCC 10145. Bacterial solutions were incubated for 20 h with PAMAM G5 and turbidity (optical density, OD) was measured every 15 min. The resulting growth profiles (panel a) were analyzed with an exponential fit which was used to calculate the generation times in panel b. As shown in panel a, the multiple phases for each growth curve were analyzed individually in segments and over the whole period of 255 min (I-III(IV))..... 193

Figure 6-2 Concentration effect of full-generation PAMAM G5 and half-generation PAMAM G4.5 on gram-positive *Staphylococcus* strains after 20 h of incubation. Data derive from the OD values at timepoint 20 h and are normalized to the LB control with 1 % methanol as co-solvent. Values shown reflect mean \pm standard error of the mean (SEM). 194

Figure 6-3 Effect of PAMAM dendrimers on the survival of *S. saprophyticus* after 20 h of incubation. Aliquots were incubated on LA plates for a minimum of 24 h before enumeration. Panel a) reflects the number of colony forming units (CFU) per 1 mL, the PAMAM-free control contained 1 % methanol. In panel, the absolute numbers of CFU / mL were normalized against the LB control (1 % methanol). For both panels, data reflect $M \pm SEM$, $n \geq 2$ 195

Figure 6-4 Concentration effect of full-generation PAMAM G5 and half-generation PAMAM G4.5 on common hospital pathogen strains after 20 h of incubation. Data derived from the OD values at timepoint 20 h and are normalized to the LB control with 1 % methanol as co-solvent. Values shown reflect mean \pm standard error of the mean (SEM). 196

Figure 6-5 Effect of 20 h incubation with PAMAM G5 on the survival of *P. aeruginosa* ATCC 10145 and *E. coli* ATCC 25922. Colony-forming units (CFU) derived from the PAMAM-treated test solutions were normalized against the bacterial CFU of the PAMAM-free LB control (containing 1 % methanol). Data are shown as mean \pm SEM, $n \geq 4$ 197

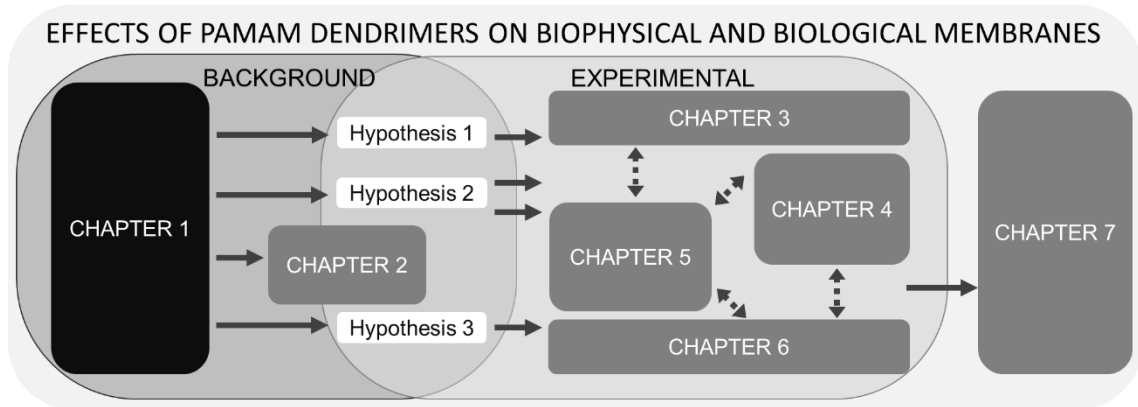
LIST OF TABLES

<i>Table 1-1 Overview of common polymer therapeutics platforms (not exhaustive)</i>	4
<i>Table 1-2 Impact of lipid shape on lipid self-assembly. Adapted from Gurr and Harwood 1991¹⁹⁷.</i>	14
<i>Table 1-3 Comparison of common model membranes for biophysical techniques^{221, 222}</i>	15
<i>Table 1-4 Simplistic comparison of lipid vesicle types²⁸⁰</i>	18
<i>Table 2-1 Final PAMAM concentrations used for membrane interaction studies.</i>	51
<i>Table 3-1 PAMAM applications using different strategies of chemical alterations. References are exemplary for the application, but not comprehensive.</i>	65
<i>Table 3-2 Common experimental variables that can affect the experimental endpoints and measured outputs. Examples are focused on PAMAM dendrimers.</i>	66
<i>Table 3-3 Comparison of radii* (Å) of PAMAM G5 and G4.5. Detailed fitting parameters are available in the Supplementary Information (Section 3.7.2, Table 3-10).</i>	79
<i>Table 3-4 Comparison of radii* (Å) of PAMAM G5 and G4.5 under different pH conditions. Detailed fitting parameters are available in the Supplementary Information (Section 3.7.2, Table 3-10).</i>	83
<i>Table 3-5 Overview of the 22 included articles from the literature screening (Figure 3-10).</i>	104
<i>Table 3-6 Summary of the parameters obtained from UV/Vis and fluorescence measurement. UV/Vis data reflect the maximum Absorbance measured at λ_{max}. Fluorescence parameters were obtained from emission search scans, whereby λ_{ex} is the wavelength with the maximum fluorescence at λ_{em}.</i>	106
<i>Table 3-7 Statistical comparison of the UV/Vis and fluorescence data of Table 3-6. Outcome of the ANOVA and Bonferroni's multiple comparison test are displayed as p value with indication of significance level and non-significant (n.s.) denotation where applicable.</i>	106
<i>Table 3-8 Summary of the parameters obtained from UV/Vis and fluorescence measurement. UV-Vis data reflect the maximum Absorbance measured at λ_{max}. Fluorescence parameters were obtained at fixed excitation wavelengths (G5 = 350 nm, G4.5 = 380 nm), whereby λ_{em} is the wavelength with the maximum fluorescence intensity.</i>	107

<i>Table 3-9 Statistical comparison of the UV/Vis and fluorescence data of Table 3-8. Outcome of the ANOVA and Bonferroni's multiple comparison test are displayed as p value with indication of significance level and non-significant (n.s.) denotation where applicable.</i>	107
<i>Table 3-10 SAXS fitting parameters obtained from fitting a Spherical Shell form factor.</i>	109
<i>Table 3-11 Total number of monomers and average numbers of charged monomers (ratio over all chargeable ones) in each PAMAM molecule at different pH values, as well as the number of counterions included to neutralize the system. Note that in cases of G4.5, counterions are included for both the negatively charged carboxyl and positively charged tertiary amine groups.</i>	110
<i>Table 3-12 Size information of PAMAM G5 studied with small angle scattering and computational techniques. The radius was mostly provided as radius of gyration (R_g) of the whole molecule, but R_N only considers the location of the primary nitrogen (terminal amine groups). Depending of the fit chosen for the experimental data, R_s refers to the radius of a sphere and R_f to the radius of a sphere with a fuzzy edge. For SANS experiments where the solvent is deuterium oxide, the acidity scale factor α refers to the molar ratio of acid to primary amine and is adjusted with deuterated acid.</i>	112
<i>Table 4-1 Characteristics of the PAMAM dendrimers used in the study.</i>	125
<i>Table 4-2 Effect of presence of sodium chloride in the phosphate buffer subphase (pH 7, 20 mM) on interaction of PAMAM G5 and G4.5 with DPPG and DPPC monolayers. Δ surface pressure data indicate mean \pm SEM. PAMAM dendrimer concentration for interacting with DPPG was 0.061 mg mL⁻¹; for interacting with DPPC 0.3 mg mL⁻¹.#.....</i>	133
<i>Table 5-1 Comparison of major fitting parameters in different PAMAM-lipid bilayer systems. Values in brackets reflect 95 % Confidence interval.</i>	164
<i>Table 5-2 Summary of Avanti Phospholipids used in this study and their properties as provided by the manufacturer.</i>	172
<i>Table 5-3 Neutron scattering length densities (ρ) of the components used to construct the layers for fitting the reflectivity data.</i>	175
<i>Table 5-4 Parameters derived from fitting incl. Bayesian error analysis. Values in brackets represent the 95 % confidence intervals.</i>	176
<i>Table 6-1 PAMAM-based systems in antibacterial research, mostly with amine-terminated PAMAM (exceptions are outlined in the footnotes). Bacteria used in this work are highlighted in grey.....</i>	182

<i>Table 6-2 Overview of bacterial strains screened in this work. Highlighted strains were further studied for the effect of PAMAM concentration on bacterial survival.</i>	<i>188</i>
<i>Table 6-3 Antibacterial activity after 20 h incubation with 1 mg mL⁻¹ PAMAM dendrimer solution based on turbidity (OD₅₉₅).</i>	<i>191</i>
<i>Table 6-4 Bacterial generation time for selected gram-positive and gram-negative bacterial strains affected by incubation with various concentrations of PAMAM G5.</i>	<i>192</i>
<i>Table 6-5 Membrane lipid composition (%) of selected bacteria relevant to this study.</i>	<i>198</i>
<i>Table 6-6 Literature-reported PAMAM effect on survival of gram-positive and gram-negative bacteria. Data with grey background derive from this study and are included for comparison. Concentrations are provided in µg mL⁻¹.</i>	<i>201</i>

CHAPTER 1: INTRODUCTION



This chapter provides a brief background on polymer therapeutics and how dendrimers, especially poly(amidoamine) (PAMAM), fit into the bigger picture. Furthermore, it presents an overview on biological and model membranes in general and presents up-to-date insights on PAMAM – lipid interactions.

1 INTRODUCTION

1.1 BACKGROUND AND PROJECT MOTIVATION

During the first 30 years after its first appearance in Otts's article in Science in 1930¹, the term polymer was rarely used in the title or abstract of publications. However, since the 1970s polymers have been studied for potential (bio)medical and pharmaceutical applications and the number of publications related to those applications increased vastly with nearly one million publications added to the PubMed Database (as of May 2021) alone during the last decade (reviews excluded).

Polymer therapeutics, including polymer-based drugs, are bioactive polymers used in an array of biomedical applications to enable/ improve targeted drug, protein or gene delivery. The most common types of polymer therapeutics are summarized in Table 1-1. They also belong to nanomedicines, which are defined as applied nanotechnology products (0.2 – 100 nm) for medical diagnostics, disease prevention or disease treatment². These systems have gained increasing interest globally with over 250 products approved for marketing as well as in clinical trials³. Most marketed nanomedicines are available for the treatment of cancer and blood disorders, and vaccines (Hepatitis A and B, Influenza, HPV)⁴.

Within the era of personalized and targeted medicine, the need for new and safer biomedical and pharmaceutical products is ever increasing. For *in vivo* diagnostic and therapeutic applications, good biocompatibility in combination with favorable biological activity is a big concern, and to meet requirements for a safe clinical use, an extensive knowledge of polymer properties, biological interactions, activity, and toxicity is key.

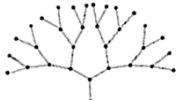
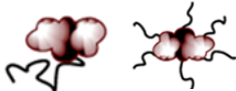
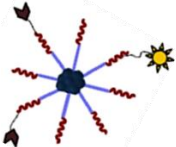
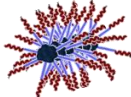
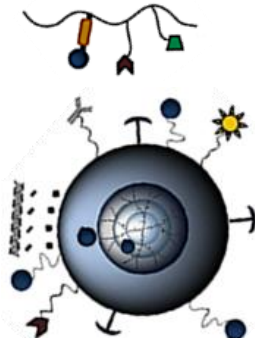
Results of *in vitro* assays are strongly influenced by the selected cell-type, incubation time and assay conditions (i.e., medium composition, pH, temperature)⁵. Some general polymers properties are identified to influence biological interactions, i.e., stealth, surface chemistry, smart ingredients, size,

concentration, polymer MW (and polydispersity), impurities (e.g., residual solvent), shape and aspect ratio, route of administration and stability⁵⁻⁷, however each polymer type has its own specific challenges.

Of special interest for this study are hyperbranched polymers with a radially-symmetric, tree-like structure illustrated in Table 1-1 – so called dendrimers (Greek: dendron – tree). For dendrimers in particular, the generation number, the chemistry and structure of dendrimer core and surface branches are influencing permeation across epithelial barriers and biological activity⁸⁻¹⁰. With their unique molecular architecture allowing guest molecules to be encapsulated within the core and conjugated to the terminal moieties, dendrimers are a promising platform for polymer therapeutics^{11, 12}. The mechanisms behind biological interactions are yet not fully understood and further research in that area is still required.

The goal of the thesis is to gain a fundamental understanding of how individual properties in an experimental system affect lipid membrane binding processes and how those processes correlate to reported *in vivo* activity and toxicity of poly(amidoamine) (PAMAM) – one of the first dendrimers to be commercialized. Therefore, background on PAMAM dendrimers and their current applications and limitations is summarized in section 1.2, whereas information on biological membranes and membrane lipids is given in section 1.3. An overview of membrane models, and specifically biophysical models relevant for this work, is provided in section 1.4, followed by a review PAMAM interactions with such models in section 1.5. and thesis outline in section 1.6.

Table 1-1 Overview of common polymer therapeutics platforms (not exhaustive).

Polymer therapeutic		Recent example application
Bioactive polymers – Polymeric drugs (10 – 20 nm)		
Linear		Antibacterial activity of linear oligoethyleneimine against carbapenem-resistant <i>Klebsiella pneumoniae</i> ¹³
Hyperbranched / dendron		PEG-dendrons to safeguard transplanted pancreatic islets from host immune response ¹⁴
Dendrimer		Polycationic phosphorus dendrimers as <i>in vivo</i> inhibitors of <i>Mycobacterium tuberculosis</i> ¹⁵
Polymer conjugates with biological macromolecules (10 – 20 nm)		
Polymer – protein conjugates		Polymeric hydrogels conjugated with target-specific peptides promoting osteochondral growth ¹⁶
Polymer – aptamer conjugates		Calorimetric biosensor for <i>Bacillus thuringiensis</i> spores ¹⁷
Polymer – antibody conjugates		Nanovaccine for cancer immunotherapy ¹⁸
Block copolymer micelles (50 – 200 nm)		
Polymer spherical micelle		Glutathione scavenging and reactive oxygen species (ROS) generating polymeric micelles for enhanced antitumor therapy ¹⁹
Polymer cylindrical micelle		Brush-shaped polymer micelles as nanocarriers for an anticancer drug ²⁰
Polymer – drug conjugates (5 – 25 nm)		
Linear delivery systems		pH-sensitive HPMA copolymer conjugate with doxorubicin ²¹
Dendrimer – based delivery systems		Phosphorus dendrimers / copper(II) complexes for ultrasound-enhanced tumor theranostics ²² Dendritic antibody conjugate as cocaine vaccine ²³

1.2 Dendrimers - Poly(amidoamine) (PAMAM)

Over 40 years ago, the first report on the concept of repetitive branch-like growth of molecules to create cavities was published²⁴. Shortly after, Tomalia *et al*²⁵ developed the first macromolecular synthesis of “true dendrimers” (PAMAM dendrimers) and Newkome *et al*²⁶ reported the synthesis of arborols (Latin: arbor – tree).

Since then, the group of dendritic polymers grew and encompasses now randomly hyperbranched polymers, dendrigrafts, dendrons, and dendrimers. Numerous surface modifications were applied to tune the dendrimer properties and functionalities such as solubility, miscibility and reactivity^{10, 27, 28}.

Generally, dendrimers are synthesized either via the divergent or convergent approach²⁹ as highlighted in Figure 1-1a, and are defined by radially joined interior layers (generations) of repetitive units (branches) that emerge from a focal point (or initiator core) and possess surface functionalities on the terminal branches that increase exponentially in number with the generation number (Figure 1-1b)^{25, 27, 30}. Typically, the nanosized molecules are theoretically monodisperse in size³¹, highly water-soluble³² and assume a more globular shape with increasing generation (> G4)^{28, 33, 34}.

1.2.1 Structure and activity of PAMAM dendrimers

The chemical structure of a PAMAM dendrimer generation 4 is drawn in Figure 1-1c. Commercially available PAMAMs that were used for this project, have an ethylenediamine (EDA) initiator core, 5 generations and carry primary amines as surface groups in case of the full-generation PAMAMs or carboxylic acid groups in the case of the half-generation PAMAMs. As shown in Figure 1-1 (panel d, e), medium-generation PAMAM assume a condensed three-dimensional conformation, and with the resulting cavities in the dendrimer core, and multivalent surface groups that can be easily conjugated, they are ideal carrier molecules as cargo can either be attached to the surface^{12, 31} or encapsulated in the interior. In particular, high-generation dendrimers have distinctively different nano-environments in their cores and periphery,³⁵ and this

core-shell architecture is suitable for encapsulation of molecules that are chemically sensitive or incompatible with the environment external to the dendrimers^{31, 36}. Furthermore, due to the chargeable moieties throughout the molecule, PAMAM dendrimers are pH-responsive^{37, 38}, which is a useful strategy for cargo release³⁹⁻⁴¹.

Particularly the charge of cationic surface groups of PAMAM dendrimers are associated to increased cytotoxicity⁴²⁻⁴⁵ which is not always a desired feature for their biomedical application, and surface modification with more biocompatible groups (i.e., pyrrolidone, lauroyl chains, L-cysteine) can help to overcome this problem⁴⁶⁻⁴⁸. On the other hand, amine-terminated PAMAMs have antibacterial⁴⁹⁻⁵¹ and antiviral^{52, 53} activity that could be utilized for therapeutic applications.

1.2.2 Biomedical applications and limitations

Due to their unique architecture and nanosize, PAMAM dendrimers are a promising polymeric platforms for drug⁵⁴⁻⁵⁶ and gene⁵⁷⁻⁵⁹ delivery and wider applications of dendrimers in nanomedicine was reviewed recently by Chis et al⁶⁰ and Dias et al⁶¹. PAMAM dendrimers have also been explored for immunosensor applications^{62, 63} and have already been commercialized as Stratus CS®, an *ex-vivo* sensor for cardiac biomarkers^{64, 65}. Another *in vitro* application of PAMAM dendrimers is the use as transfection agents, and already two PAMAM-based products are marketed as SuperFect® and Priofect®^{66, 67}.

The favorable properties of PAMAM dendrimers have led to a wide range of potential pharmaceutical applications. A pH-dependent complexation to medium – high generation PAMAM (\leq G5) improved significantly the solubility of hydrophobic drugs such as ketoprofen⁶⁸, indomethacin⁶⁹, and anticancer flavonoid analogues⁷⁰ and increased drug availability at the target cells *in vitro* up to 2.3-fold. Therefore, PAMAM-based systems were also probed for pH-responsive prolonged release applications^{41, 56, 71}.

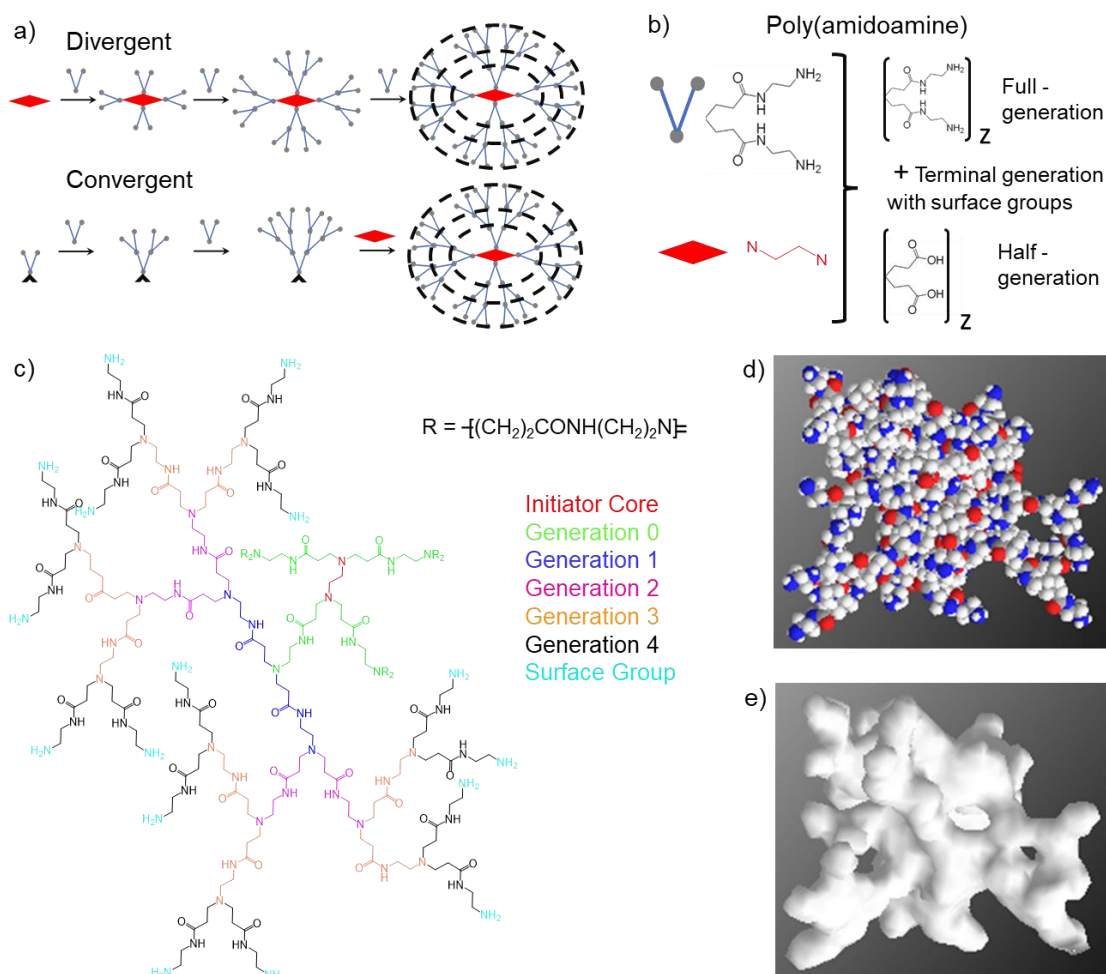


Figure 1-1 Dendrimers from synthesis to structure. Panel a) illustrates the differences between divergent and convergent approaches in dendrimer synthesis. The dashed lines on the final molecules denote the generations. In panel b) the symbols are aligned to the PAMAM dendrimers in the focus of this thesis, where ethylenediamine is the initiator core and the terminal generations are decorated with either with primary amines or carboxyl groups, for the full-generation or half-generation PAMAMs respectively. Panel c) shows the chemical structure of full-generation PAMAM G4 (64 terminal branches and surface groups), for clarity only a quarter of the molecule is fully drawn, and the repetitive unit indicated as R. Each generation is in a different color to help identification. The full PAMAM G4 structure was used to visualize the 3D arrangement in panel d) and to show solvent-accessible cavities in panel e). Structures in panels c – e were created in ChemOffice 2020.

The ability of the cationic surface groups of full-generation PAMAMs to complex nucleic acids⁷², drugs⁷³ and imaging agents⁷⁴ made them a popular delivery platform in anti-cancer research. Targeted drug delivery to the cancer cells was achieved by conjugation of targeting moieties (i.e. antibodies⁷⁵⁻⁷⁷, folic acid⁷⁸⁻⁸⁰) to the dendrimer surface, which also helped to reduce cytotoxicity and unwanted unspecific interactions caused by common cancer drugs (docetaxel⁷⁵,

⁷⁶, paclitaxel^{75, 76, 80}, methotrexate^{77, 78}, doxorubicin⁷⁹). An option to trace the PAMAM-mediated drug delivery to the target cell is the conjugation or encapsulation of imaging agents, i.e. metal-based magnetic resonance imaging (MRI) contrast agents^{81, 82} or positron emission tomography (PET) radionuclides^{83, 84}. Bioimaging is yet another application for PAMAMs, and combining targeting moieties with the intrinsic PAMAM fluorescence or fluorescent labels enabled visualization of the target cells in prostate cancer mouse model⁸⁵, breast cancer cell-line SK-BR-3⁸⁶ and central nervous system of zebrafish⁸⁷.

Initially, PAMAM dendrimers were primarily suggested for advanced treatments of cancer, but meanwhile their carrier potential and adjuvant effect on certain drugs has been explored for the treatment of neurological disorders (i.e. Alzheimer's^{88, 89}, Parkinson's^{90, 91}), inflammatory diseases (i.e. rheumatoid arthritis^{69, 92}, atherosclerosis^{93, 94}) and infectious diseases^{56, 95, 96}.

Overall, there are fewer reports on the biomedical applications of the carboxyl-terminated PAMAMs. So far, half-generation PAMAMs have been investigated for applications in dental regeneration^{97, 98}, in the delivery of cancer therapeutics⁹⁹⁻¹⁰², CNS-targeted drugs¹⁰³⁻¹⁰⁵ and inflammatory agents¹⁰⁶⁻¹⁰⁸. Furthermore, they have been suggested for potential applications in tissue repair and wound healing¹⁰⁹⁻¹¹¹. Anionic PAMAMs have shown some antimicrobial properties^{53, 112, 113} but less than PAMAMs with neutral or cationic surface groups¹¹⁴. However, amine-terminated PAMAMs are generally more effective in the outlined applications and the potential use of the half-generations PAMAMs as delivery system (i.e., for nucleic acids or proteins) is somewhat limited due to the anionic surface groups.

In general, anionic PAMAMs are exhibiting a favorable biocompatibility profile^{115, 116} with no *in vitro* cytotoxicity (e.g. Caco-2, Hep G2, SKOV3) or *in vivo* toxicity in zebrafish at high concentrations (≤ 1 mM) compared to the cationic counter parts¹¹⁷⁻¹¹⁹. This was shown in non-cancerous (HUVEC, hNPC)^{120, 121} and cancer cells (4T1, HepG2, DU145, SKOV3, MCF-7)^{116, 118, 119, 122}, tissue (intestine, lung)^{115, 123, 124}, zebrafish^{104, 118, 125} and mouse model^{116, 126},

¹²⁷. Carboxyl-terminated PAMAM also are associated with effective membrane translocation^{117, 128, 129} and good bioavailability^{100, 104, 126}.

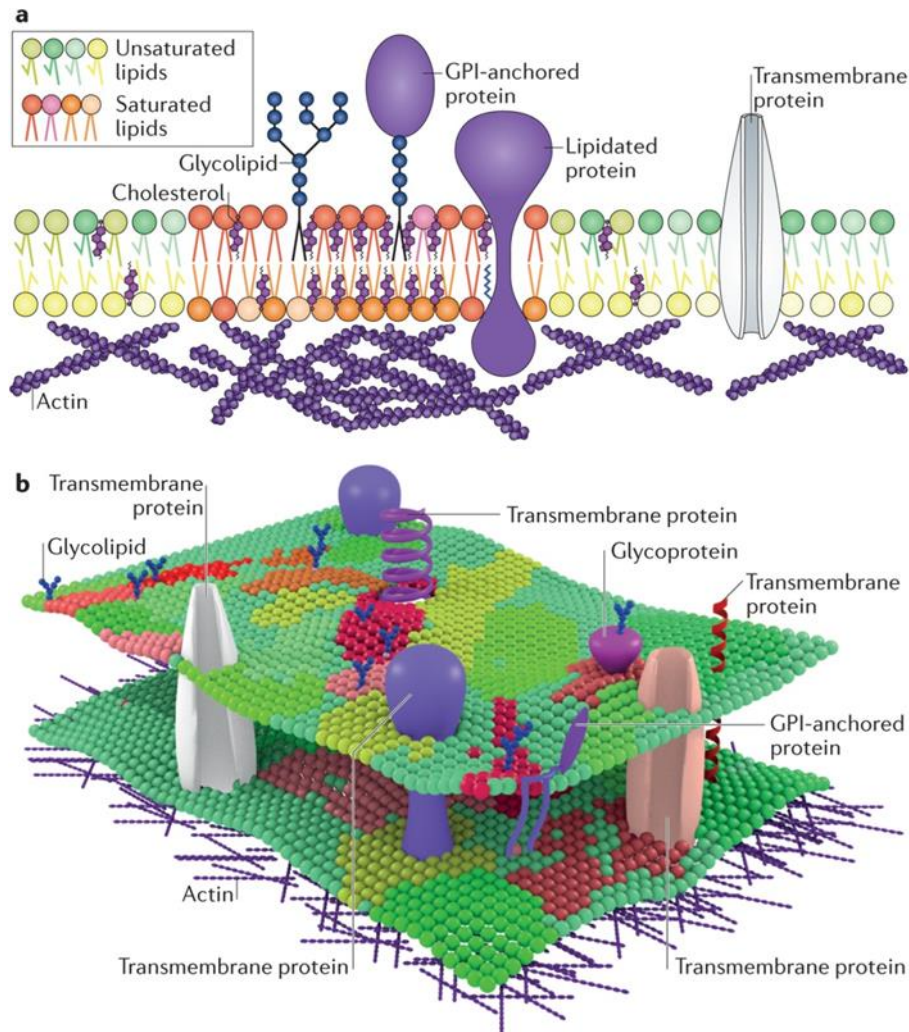
The cationic dendrimers on the other hand have been probed for a wide range of applications^{60, 61}, but to date, their less favorable toxicity profile is still limiting their clinical applicability^{8, 44, 130}. PAMAM toxicity was shown to be dependent on dendrimer properties^{42, 119, 121, 131} such concentration, generation, incubation-time, charge and type of surface groups, and membrane and membrane environment properties¹³²⁻¹³⁵ such as cell type, pH, uptake mechanism. Toxicity of PAMAM dendrimers is not limited to membrane toxicity, but also hemotoxicity^{42, 136, 137} and adverse interactions with serum or plasma proteins¹³⁸⁻¹⁴⁰. However, surface modifications (e.g. lauroyl chains, cysteine) can decrease toxicity and improve biocompatibility whilst still retaining the efficient cell permeation and molecule delivery properties⁴⁶⁻⁴⁸.

1.3 BIOLOGICAL MEMBRANES

In biological organisms, membranes surround cells and most of their intracellular organelles. Most commonly they are made of lipid bilayers; they are found in all eukaryotes, in most of prokaryotes. Bilayers are 30 – 50 Å thick depending on the layer composition and the lengths of the fatty acid tails^{141, 142}, which form the hydrophobic core of the lipid membrane. Monolayers are less common, but have been detected in some species of thermophilic single-cell microorganisms without nucleus (Archaea)¹⁴³.

Membranes are dynamic, selectively permeable lipid layers, complexed with proteins and carbohydrates. Their arrangement according to the fluid mosaic membrane model proposed by Singer and Nicolson in 1972¹⁴⁴ was widely accepted for decades. The discovery of lipid rafts^{145, 146}, forces and molecules that govern membrane deformation, curvature, compression and expansion¹⁴⁷⁻¹⁴⁹, asymmetric distributions of phospholipids between the outer and inner leaflet^{150, 151}, discovery of lipid transporters^{152, 153} various types of membrane proteins and membrane-associated proteins^{154, 155}, findings about cis and trans-membrane control of the mobility of membrane components¹⁵⁶⁻¹⁵⁸, consideration

of membrane-associated cytoskeletal and extracellular matrix interactions^{159, 160}; and protein-protein^{155, 159}, protein-lipid^{161, 162} and lipid-lipid^{163, 164} interactions led Nicolson¹⁶⁵ to update the fluid mosaic model with the new findings in 2014. Some of the new findings, such as lipid rafts, lipid asymmetry or cytoskeletal interactions are reflected in Figure 1-2.



Nature Reviews | Molecular Cell Biology

Figure 1-2 Panel a) illustrates the asymmetric distribution of membrane lipids between inner and outer leaflet of the plasma membrane and arrangement of lipid raft domains (enriched in saturated phospholipids, sphingolipids, glycolipids, cholesterol, lipidated proteins and glycosylphosphatidylinositol (GPI)-anchored proteins). Interaction with actin is important for domain maintenance and remodelling. Panel b) Various raft-like and non-raft domains with distinct compositions and properties define the organization of membranes. Reprinted by permission from Nature Reviews Molecular Cell Biology, Sezgin et al 2017¹⁶⁶. Copyright 2017 Springer Nature.

More recently there is a shift from the fluid mosaic to models that also consider numerous dynamic membrane processes. In the “picket-fence” model¹⁶⁷, certain transmembrane proteins are thought to be anchored to the actin-based cytoskeleton and as the actin mesh is relatively static, the immobilized proteins provide obstacles (“pickets”) to the diffusion of other molecules within the cytoplasm^{168, 169}. Another model that is predominantly based on thermodynamic equilibrium principles, proposes the membrane as a “patchwork quilt”¹⁷⁰ of multiple domains of proteins and lipids whereby not only various proteins are grouped with subsets of lipid species, but all membrane lipids are arranged in functional domains (patches)¹⁷¹.

Dependent on their composition and localization membranes have various functions, including compartmentalization, membrane potential and energy conversion/storage, signal transduction and molecular recognition, connection of the cytoskeleton and the extracellular matrix, selective barrier and transport of molecules¹⁷². The membrane- or membrane function- related barriers can be categorized into external (i.e. epithelia), *en-route* (i.e. blood, renal, hepatic and splenic clearance, blood-brain-barrier) and cellular barriers (cellular uptake, endo-/exocytosis)^{6, 173}.

In terms of structure and barrier function, the basic bacterial cell membrane differs from that of eukaryotic cells. In general, bacteria can be distinguished into gram-negative and gram-positive species according to the staining of their cell envelope, which is dependent on the structural configuration¹⁷⁴ as shown in Figure 1-3. All species have a lipid bilayer as cytoplasmic membrane. Gram-negative bacteria have a thinner peptidoglycan layer (1.5 – 15 nm) than gram-positive bacteria (30 – 100 nm)¹⁷⁵ but have another layer atop of it – the outer membrane. The peptidoglycan layer (and outer membrane) is also referred to as cell wall, which forms an additional barrier to the cytoplasmic membrane.

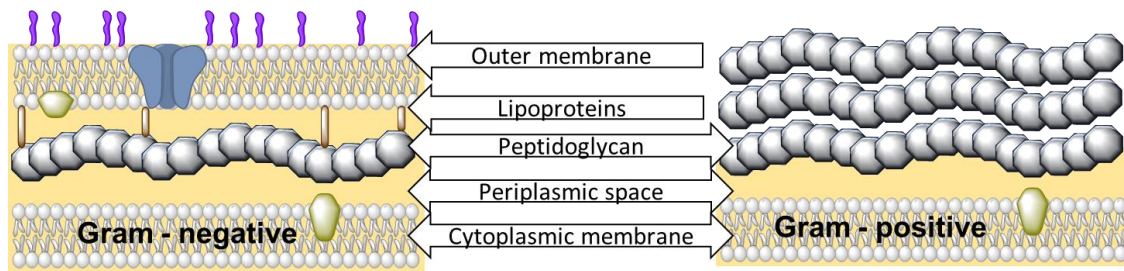


Figure 1-3 Schematic illustration of the cell envelope of bacterial cells (not to scale). A typical example of gram-negative bacterium is *Escherichia coli*, an example gram-positive bacterium is *Staphylococcus aureus*. Illustration inspired by Berezin et al 2017¹⁷⁶.

1.3.1 Membrane lipids

Most lipids have a polar head group and an apolar tail made of one or two fatty acid derivatives. Membrane fluidity mainly depends on the specific structure (length, saturation) of the fatty acid derivatives and temperature¹⁴¹. There are approximately 10,000 different lipids estimated to occur in prokaryotic and eukaryotic organisms¹⁷⁷ and the diversity is not only due to the head group variety but also to length and (un-) saturation of the hydrophobic lipid tails, and type of linkage of the of the lipid tails to the head group^{178, 179}.

Important membrane lipids are phospholipids, sphingolipids (major subgroups: sphingomyelin (SM) and glycosphingolipids) and the non-polar sterols (mainly cholesterol in mammals)¹⁸⁰. The planar structure of cholesterol and its high abundance in the membranes (around 30 %) have a strong impact on basic membrane properties such as viscosity or fluidity¹⁸¹. Furthermore, cholesterol is involved in cellular processes and signaling events when co-located with other membrane lipids in condensed microdomains called lipid rafts^{146, 182, 183} that also serve as anchor points for transmembrane and peripheral membrane proteins.

Most structural lipids are phospholipids, such as phosphatidylcholines (PC), phosphatidylethanolamines (PE), phosphatidylserines (PS), phosphatidylinositols (PI) and phosphatidic acids (PA) as shown in Fig 1-4 for a human erythrocyte. Major phospholipids of eukaryotic cell membrane are zwitterionic choline phospholipids (CPL)¹⁸⁰, whereas anionic

phosphatidylglycerols (PG) and cardiolipin (CL) lipids are predominant in prokaryotic membranes^{180, 184}. Examples of the lipid composition of several bacterial strains are available in Chapter 6, Table 6-5, which highlights the higher abundance of anionic lipids in gram-positive bacteria compared to gram-negative strains that also contain substantial amounts of zwitterionic PE. Furthermore, membranes of bacteria do not contain sterols but hopanoids that resemble steroids in structure and membrane functions^{185, 186}. Other bacteria – specific membrane lipids are lipopolysaccharides and phosphorus-free glycolipids, sulfolipids, homoserine-derived lipids, ornithine lipids that contribute to bacterial pathogenicity and adaption to environmental stress (i.e., extreme pH)¹⁸⁷⁻¹⁸⁹.

Membrane asymmetry describes the unequal distribution of lipids between the inner (facing the cytoplasm) and outer (facing the extracellular space) leaflet of membrane and influences mechanical properties¹⁹⁰ and physiological membrane functions, such as endocytosis¹⁵², vesicle budding and trafficking¹⁹¹ and signaltransduction¹⁹². The lipid asymmetry of the human erythrocyte is illustrated in Fig 1-4, and unilateral distribution of anionic lipids is a clear driver for the electric membrane potential^{193, 194}. The asymmetric lipid distribution also affects membrane structure and curvature^{148, 195} due to the different molecular shapes of the lipids as shown in Table 1-2.

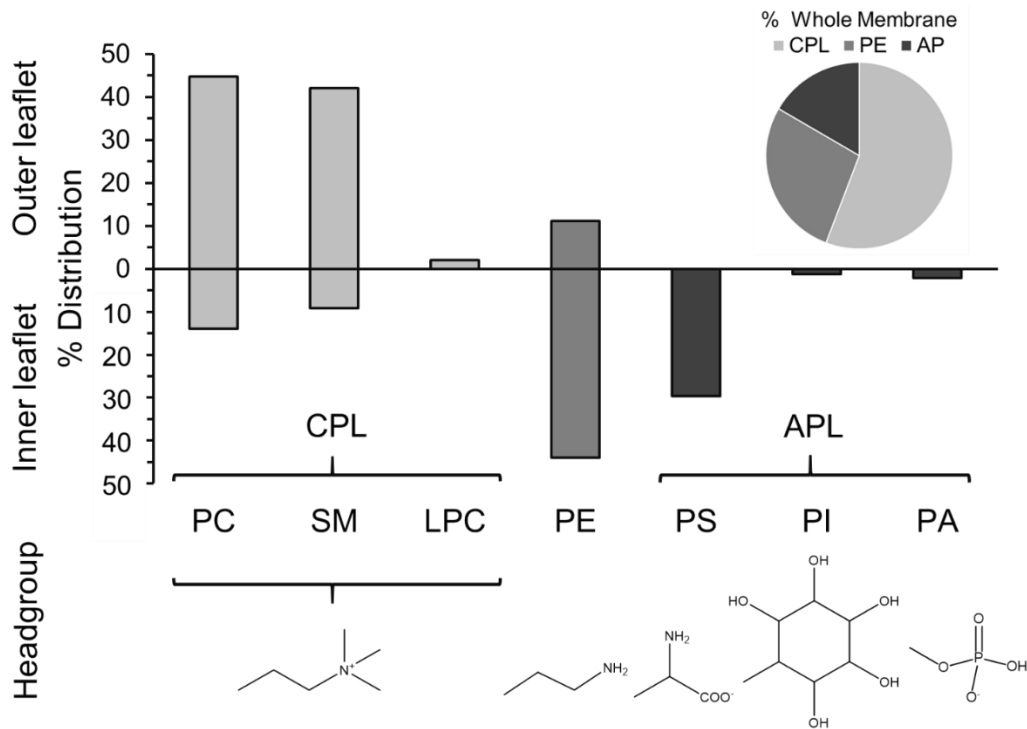
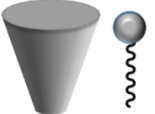
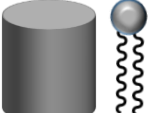


Figure 1-4 Phospholipid composition of a human erythrocyte as an example for lipid asymmetry in membranes. Figure based on data from Virtanen et al 1998¹⁹⁶. CPL: Choline phospholipids, APL: Anionic phospholipids, PC: phosphatidylcholines, SM: sphingomyelin, LPC: lysophosphatidylcholine, PE: phosphatidylethanolamines, PS: phosphatidylserines, PI: phosphatidylinositols, PA: phosphatidic acids.

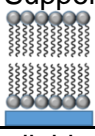
Table 1-2 Impact of lipid shape on lipid self-assembly. Adapted from Gurr and Harwood 1991¹⁹⁷.

Lipids	Membrane curvature and Phase behavior	Molecular Shape
Large headgroup, acyl chain(s) occupy smaller volume Lysophospholipids, Phosphoinositides (PIP ₂ , PIP ₃). Detergents	Positive membrane curvature Favor the assembly membranes into normal micelles or cubic structures	Inverted Conical 
Diameter of headgroup and acyl chains similar SM, PC, PS, PI, PG, PA	No membrane curvature Favor the assembly into lamellar structures or flat bilayers	Cylindrical 
Small headgroup, acyl chains occupy larger volume PE, PS at pH < 4, CL PA at pH < 3	Negative membrane curvature Favor assembly into tubular/ hexagonal or spherical inverted micelles	Conical 

1.4 OVERVIEW OF MEMBRANE MODELS

Interactions of polymers have been studied using a wide range of methods, ranging from physicochemical¹⁹⁸⁻²⁰⁰ over biological^{42, 201, 202} to computer-based approaches²⁰³⁻²⁰⁵. Biophysical model systems as simplified membrane representations are as varied as the techniques they are used with, and a comparison of the most common ones is provided in Table 1-7. Biological models are more complex and include red blood cells^{206, 207}, primary tissue culture or immortal cell lines to investigate toxicity²⁰⁸⁻²¹⁰, cellular internalization/uptake²¹¹⁻²¹³ and biological activity in general^{209, 210, 214}; whereas prokaryotic cultures are used to evaluate antimicrobial effects²¹⁵⁻²¹⁷, and at last, organs or whole animals for *in vivo* studies such as pharmacokinetics or long-term toxicity²¹⁸⁻²²⁰.

Table 1-3 Comparison of common model membranes for biophysical techniques^{221, 222}.

	Monolayers	Supported Bilayers	Vesicles
			
Controllable parameters	<ul style="list-style-type: none"> - lipid composition - lateral pressure 	<ul style="list-style-type: none"> - lipid composition - incorporation of integral proteins/ compounds - membrane curvature/ patterning 	<ul style="list-style-type: none"> - lipid composition - membrane curvature/ deformation - incorporation of proteins - lipid packing
	<ul style="list-style-type: none"> - defined geometry of lipid assembly - homogenous system - study of individual components possible 	<ul style="list-style-type: none"> - flat geometry - lipid asymmetry possible - accessibility of both leaflets - compatible with multiple techniques 	<ul style="list-style-type: none"> - simple preparation - free-standing membrane - compatible with multiple techniques, including microscopy
	<ul style="list-style-type: none"> - single leaflet not physiological - restricted to planar lipid monolayers (and mainly cylindrically shaped lipids) 	<ul style="list-style-type: none"> - restricted fluidity of lipids and non-physiological lipid distribution between the leaflets - possible defects 	<ul style="list-style-type: none"> - variability in terms of size and multi-lamellarity - size potentially below optical resolution - only outer leaflet accessible - no control of lipid distribution in a mix

1.4.1 Langmuir monolayer

Monolayers are simple artificial model for mimicking membrane leaflets and studying interactions with molecules²²³. Those films on the air/water interface, also referred as Langmuir monolayers, are prepared by spreading insoluble lipids on the surface of an aqueous subphase. To provide a more stable model system, they can be transferred onto a solid surface. Generally, monolayers systems are highly tunable in terms of the variety and packing of the lipid molecules and the subphase conditions (i.e. pH, ionic strength, temperature)²²⁴. There are several techniques to study monolayer behavior (i.e. lipid arrangements, lateral packing, curvature), such surface pressure measurements or tensiometry^{225, 226}, ER-FTIR^{227, 228}, neutron or X-ray reflectometry^{228, 229}, fluorescence correlation spectroscopy^{230, 231}, (Confocal) fluorescence microscopy^{232, 233}, atomic force microscopy (AFM)^{234, 235} and Brewster angle microscopy/ ellipsometry²³⁵⁻²³⁷ to name a few. Therefore, monolayer models are a versatile tool for characterization of drug-lipid, protein-lipid or lipid-lipid interactions at a molecular level^{223, 238, 239}.

1.4.2 (Planar) lipid bilayers

Planar lipid bilayers in general are a suitable system for investigating cellular surface chemistry and membrane processes such as cell signaling, ligand–receptor interactions or enzymatic reactions at the cell surface. Planar bilayers are more complex model membranes compared to lipid monolayers and can be divided into three kinds: black lipid membranes (BLM), supported lipid bilayers and tethered bilayer lipid membranes.

BLMs or suspended bilayers are self-assembled lipid membranes formed after spreading aqueous lipid suspension onto an aperture. The suspended lipid bilayers partition the aqueous solution and interfere with reflected light, which leads to a black appearance^{240, 241}. As a well-established model system in of ion channel research²⁴² they have been used study the membrane properties and membrane proteins²⁴³⁻²⁴⁷, membrane/ ion channel conductance²⁴⁸⁻²⁵⁰; and channel-active peptides²⁵¹⁻²⁵³ and molecules²⁵⁴⁻²⁵⁶.

More robust and stable than BLMs are supported lipid bilayers, which are deposited on a solid substrate such as metal, mica, glass or silicon oxide with a

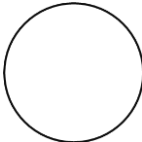
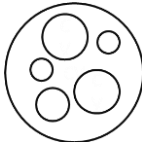
4 – 20 °Å layer of water trapped between^{257, 258}. Van der Waals, electrostatic, hydration and steric forces keep the bilayers in place, whilst membrane fluidity is still maintained²⁵⁹. The model system allows for surface-specific analytical techniques (i.e., AFM^{260, 261}, quartz crystal microbalance^{260, 262}, surface plasmon resonance^{262, 263}, vibrational sum frequency spectroscopy^{264, 265}, neutron reflectometry^{260, 266}). Supported bilayers have been applied to study membrane proteins^{267, 268} and lipid behaviour^{269, 270}, bio-sensors^{257, 271}; and membrane-active molecules^{222, 272}.

Tethered lipid bilayers or floating bilayers are decoupled from the solid substrate by a flexible spacer layer of peptides/ protein^{273, 274}, polymers^{275, 276} or lipopolymers^{277, 278}. The spacer layer allows for luminal domains of membrane proteins to be accommodated below the bilayer²⁷⁹ and prevents the lipid bilayer or membrane proteins interacting too strongly with the supporting substrate^{257, 273}. The applications for tethered lipid bilayers are similar to supported lipid bilayers but with the advantage on a higher membrane fluidity.

1.4.3 Lipid vesicles

Lipid vesicles or liposomes are produced from an aqueous dispersion of membrane lipids. Their arrangement is similar to a biological membrane, as they are composed of two lipid leaflets that encloses a small aqueous compartment. Depending on the method of preparation, different types and sizes of liposomes can be obtained²⁸⁰, for details refer to Table 1-4. Lipid vesicles are versatile model membranes commonly used for investigating membrane properties such as membrane dynamics²⁸¹⁻²⁸⁴, molecular recognition and cell adhesion²⁸⁵⁻²⁸⁷, membrane trafficking²⁸⁸⁻²⁹⁰ and interaction with membrane-active molecules²⁹¹⁻²⁹⁴. Furthermore, they are used as therapeutic platform for the transport of proteins, enzymes, DNA or drugs^{291, 295, 296}.

Table 1-4 Simplistic comparison of lipid vesicle types²⁸⁰

Small unilamellar vesicles (SUV)	Large unilamellar vesicles (LUV)	Giant unilamellar vesicles (GUV)	Multivesicular vesicles (MVV)	Large multilamellar vesicles (MLV)
				
20 nm – 100 nm	100 nm – 500 nm	> 1 μm	200 nm - ~3 μm	200 nm - ~3 μm

1.5 INTERACTIONS BETWEEN PAMAM DENDRIMERS AND (MODEL) MEMBRANES

To overcome the persisting issues with PAMAMs' biocompatibility and toxicity, it is vital to understand their effect on biomembranes and interactions with lipids as major membrane components (core topic of this PhD thesis), are of particular interest. So far, PAMAM effects were studied with several membrane model systems (biophysical and biological) and a range of *in silico*^{203, 204, 297, 298}, *in vitro*^{129, 198, 205} and *in vivo*^{114, 118, 126} techniques.

Some findings suggest that PAMAM dendrimers either adsorb onto lipid layers or form holes after membrane deformation depending on dendrimer concentration, generation, charge and type of surface groups^{198, 299-302}. For example, PAMAMs with cationic surface groups were shown to incorporate to a higher extent into zwitterionic PC bilayers than anionic PAMAMs causing a re-organization of the lipid bilayers²⁰⁰, and with increasing generation this leads to lipid desorption³⁰¹ up to the point where significant holes¹⁹⁸ are formed or the membrane is disrupted^{299, 300, 302} and leakage is measurable^{198, 205}. PAMAM G5 was also found to form sodium-selective ion channels in neuronal membranes²⁶⁴. PAMAMs were found to bind strongly to anionic lipids, such as PG, PI or PS, as seen in lipid monolayer and bilayer experiments^{265, 303, 304}, irrespective of the dendrimer surface charge which suggests an involvement of

the tertiary amines in the dendrimer core. A simulation study of PAMAM G4 on a negative mixed-lipid bilayer found increased dendrimer adsorption with decreasing pH that eventually led to hole formation and increased membrane asymmetry due to lipid flip-flop³⁰⁵.

In general, possible effects on lipid membranes include hydrophobic (mis)match effects, chain stretching of the lipids close to the site of interaction, changes in lipid packaging and lateral pressure, phase separation (domain formation), induced or suppressed membrane curvature and membrane thinning³⁰⁶⁻³⁰⁹. The diversity of membrane interactions not only depends on lipid layer properties (i.e. lipid types and phase)^{203, 204, 227}, but also on dendrimers characteristics^{204, 301, 308} and the surrounding environment (i.e. solvent conditions)^{227, 297, 305}. Thus far, most studies only focus on individual aspects rather than combined effects, therefore further research is required to gain a better understanding of the biological effects.

1.6 THESIS OUTLINE

The overall aim of this project is to systematically investigate PAMAM – membrane interactions, in view of understanding dendrimer-mediated processes in biological systems. This thesis aims to look at the interplay between various solvent conditions, PAMAM dendrimers with different physicochemical properties (generation, surface functionality and concentration) and membrane lipids and link it to PAMAMs biological activity and toxicity.

The following hypothesis are addressed in the experimental thesis chapters as outlined in Fig 1-5 by using biophysical and microbiological techniques, and model and bacterial membranes.

1) Depending on their functional groups, dendrimer structures are adaptive to environmental conditions, which eventually affects their behavior in solution (Chapter 3)

2) Full-generation and half-generation PAMAM interact differently with lipid membranes and the interaction can be altered by changing solution conditions (Chapter 4 and 5)

3) Lipid interactions are the driving force behind the PAMAM effect on biological membranes and determine nanotoxicity (Chapter 6)

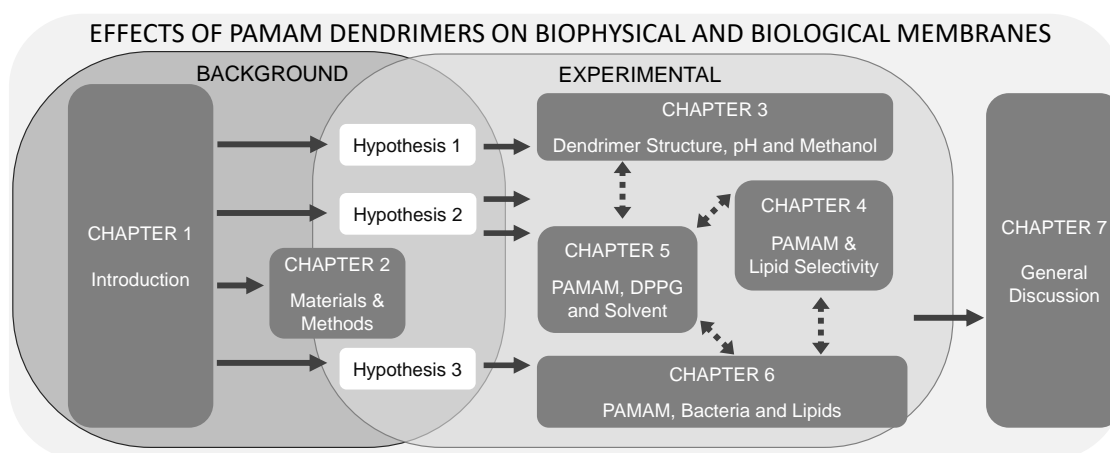


Figure 1-5 Schematic outline of the thesis concept and integration of the chapters

The main techniques used for the experimental chapters (surface pressure measurements and neutron reflectometry) are explained in Chapter 2, while chapter-specific methodology is reported in the relevant chapters.

Solution condition-dependent changes of PAMAM G4.5 and G5 dendrimers are characterized with spectroscopic techniques (UV/Vis and fluorescence), small-angle x-ray scattering (SAXS) and complementary molecular dynamics simulations in Chapter 3.

Chapter 4 explores the lipid affinity of both PAMAM dendrimer species to zwitterionic DPPC and anionic DPPG lipid monolayers at neutral solvent pH with surface pressure measurements and external reflection Fourier-transform infrared spectroscopy (ER-FTIR).

Changing solvent conditions (modulators of the PAMAM structure in Chapter 3) and the DPPG binding preference (observed in Chapter 4) are further explored with surface pressure measurements and neutron reflectivity (NR) on monolayer and bilayer models in Chapter 5.

In Chapter 6, the PAMAM effect on membranes is studied using the most complex anionic membrane model – living bacteria. Growth kinetics of gram-negative and gram-positive bacteria are monitored by absorbance readings and bacterial survival (determined by colony-forming units (CFU)), and the findings are linked to lipidomics reports in literature.

Finally, in Chapter 7 experimental findings are evaluated and considered in the wider context of research in this field, and potential lines of future work are indicated.

1.6.1 Scientific rationale

PAMAM dendrimers were selected for this project as they are promising candidates for drug-delivery solutions with widely researched potential applications (see section 1.2.2 for more details). In general, medium-generation PAMAM dendrimers, such as the selected G5, have better loading capacity as the low-generation dendrimer (i.e. G3 or lower) and a more favorable biocompatibility than the high-generation PAMAM (i.e. G7 or higher). However, there are still some knowledge gaps with regards to factors modulating observed toxicity; and much less is known for half-generation PAMAM, such as G4.5 used in this study, compared to full-generation PAMAM.

Lipid monolayer and supported bilayer are well established simplistic models for studying membrane-active molecules with a range of biophysical techniques (see section 1.4.1 and 1.4.2 for details). Components of these models are easily tunable and thereby modulating variables (i.e. pH, solvent, lipid type, lateral pressure) of membrane interactions can be assessed individually.

Bacterial membranes predominantly consist of PG lipids and whereas eukaryotic membranes are rich in choline phospholipids (refer to section 1.3.1 for details), therefore dipalmitoylphosphatidylglycerol (DPPG) and dipalmitoylphosphatidylcholine (DPPC) were selected as representative model lipids. Furthermore, these lipid species self-assemble into lamellar structures (flat layers) which makes them suitable for monolayer and supported bilayer membrane models.

1.7 REFERENCES

1. Ott, E., Determination of Polymerization of Some Polymer Formaldehydes by X-Ray Methods. *Science* **1930**, *71* (1844), 465-6.
2. Committee for medicinal products for human use, Reflection paper on nanotechnology-based medicinal products for human use. In *EMEA/CHMP/79769/2006*, European Medicines Agency: 2006.
3. Farjadian, F.; Ghasemi, A.; Gohari, O.; Roointan, A.; Karimi, M.; Hamblin, M. R., Nanopharmaceuticals and nanomedicines currently on the market: challenges and opportunities. *Nanomedicine : nanotechnology, biology, and medicine* **2019**, *14* (1), 93-126.
4. Gadekar, V.; Borade, Y.; Kannaujia, S.; Rajpoot, K.; Anup, N.; Tambe, V.; Kalia, K.; Tekade, R. K., Nanomedicines accessible in the market for clinical interventions. *Journal of Controlled Release* **2021**, *330*, 372-397.
5. Gaspar, R.; Duncan, R., Polymeric carriers: preclinical safety and the regulatory implications for design and development of polymer therapeutics. *Advanced drug delivery reviews* **2009**, *61* (13), 1220-31.
6. Elsabahy, M.; Wooley, K. L., Design of polymeric nanoparticles for biomedical delivery applications. *Chem. Soc. Rev.* **2012**, (41), 2545–2561.
7. Markovsky, E.; Baabur-Cohen, H.; Eldar-Boock, A.; Omer, L.; Tiram, G.; Ferber, S.; Ofek, P.; Polyak, D.; Scomparin, A.; Satchi-Fainaro, R., Administration, distribution, metabolism and elimination of polymer therapeutics. *Journal of controlled release : official journal of the Controlled Release Society* **2012**, *161* (2), 446-60.
8. Jain, K.; Kesharwani, P.; Gupta, U.; Jain, N. K., Dendrimer toxicity: Let's meet the challenge. *International journal of pharmaceutics* **2010**, *394* (1-2), 122-142.
9. Santos, A.; Veiga, F.; Figueiras, A., Dendrimers as Pharmaceutical Excipients: Synthesis, Properties, Toxicity and Biomedical Applications. *Materials* **2020**, *13* (1), 65.
10. Tomalia, D. A.; Nixon, L. S.; Hedstrand, D. M., The Role of Branch Cell Symmetry and Other Critical Nanoscale Design Parameters in the Determination of Dendrimer Encapsulation Properties. *Biomolecules* **2020**, *10* (4), 642.
11. Mignani, S.; Shi, X.; Rodrigues, J.; Tomas, H.; Karpus, A.; Majoral, J.-P., First-in-class and best-in-class dendrimer nanoplatfroms from concept to clinic: Lessons learned moving forward. *European journal of medicinal chemistry* **2021**, *219*, 113456.

12. Otto, D. P.; de Villiers, M. M., Poly(amidoamine) Dendrimers as a Pharmaceutical Excipient. Are We There yet? *Journal of pharmaceutical sciences* **2018**, *107* (1), 75-83.
13. Mil-Homens, D.; Martins, M.; Barbosa, J.; Serafim, G.; Sarmento, M. J.; Pires, R. F.; Rodrigues, V.; Bonifácio, V. D. B.; Pinto, S. N., Carbapenem-Resistant *Klebsiella pneumoniae* Clinical Isolates: In Vivo Virulence Assessment in *Galleria mellonella* and Potential Therapeutics by Polycationic Oligoethyleneimine. *Antibiotics* **2021**, *10* (1), 56.
14. Jeon, S. I.; Jeong, J.-H.; Kim, J. E.; Haque, M. R.; Kim, J.; Byun, Y.; Ahn, C.-H., Synthesis of PEG-dendron for surface modification of pancreatic islets and suppression of the immune response. *J Mater Chem B* **2021**, *9* (11), 2631-2640.
15. Mignani, S.; Tripathi, V. D.; Soam, D.; Tripathi, R. P.; Das, S.; Singh, S.; Gandikota, R.; Laurent, R.; Karpus, A.; Caminade, A.-M.; Steinmetz, A.; Dasgupta, A.; Srivastava, K. K.; Majoral, J.-P., Safe Polycationic Dendrimers as Potent Oral In Vivo Inhibitors of *Mycobacterium tuberculosis*: A New Therapy to Take Down Tuberculosis. *Biomacromolecules* **2021**.
16. Guo, J. L.; Kim, Y. S.; Koons, G. L.; Lam, J.; Navara, A. M.; Barrios, S.; Xie, V. Y.; Watson, E.; Smith, B. T.; Pearce, H. A.; Orchard, E. A.; van den Beucken, J. J. J. P.; Jansen, J. A.; Wong, M. E.; Mikos, A. G., Bilayered, peptide-biofunctionalized hydrogels for in vivo osteochondral tissue repair. *Acta Biomaterialia* **2021**.
17. Zhou, C.; You, T.; Jang, H.; Ryu, H.; Lee, E.-S.; Oh, M.-H.; Huh, Y. S.; Kim, S. M.; Jeon, T.-J., Aptamer-Conjugated Polydiacetylene Colorimetric Paper Chip for the Detection of *Bacillus thuringiensis* Spores. *Sensors* **2020**, *20* (11), 3124.
18. Gong, N.; Zhang, Y.; Teng, X.; Wang, Y.; Huo, S.; Qing, G.; Ni, Q.; Li, X.; Wang, J.; Ye, X.; Zhang, T.; Chen, S.; Wang, Y.; Yu, J.; Wang, P. C.; Gan, Y.; Zhang, J.; Mitchell, M. J.; Li, J.; Liang, X.-J., Proton-driven transformable nanovaccine for cancer immunotherapy. *Nature Nanotechnology* **2020**, *15* (12), 1053-1064.
19. Xia, H.; Liang, Y.; Chen, K.; Guo, C.; Wang, M.; Cao, J.; Han, S.; Ma, Q.; Sun, Y.; He, B., Reduction-sensitive polymeric micelles as amplifying oxidative stress vehicles for enhanced antitumor therapy. *Colloids and Surfaces B: Biointerfaces* **2021**, *203*, 111733.
20. Wang, D.; Wang, J.; Huang, H.; Zhao, Z.; Gunatillake, P. A.; Hao, X., Brush-shaped RAFT polymer micelles as nanocarriers for a ruthenium (II) complex photodynamic anticancer drug. *European Polymer Journal* **2019**, *113*, 267-275.
21. Randárová, E.; Nakamura, H.; Islam, R.; Studenovský, M.; Mamoru, H.; Fang, J.; Chytil, P.; Etrych, T., Highly effective anti-tumor nanomedicines based on HPMA copolymer conjugates with pirarubicin prepared by controlled RAFT polymerization. *Acta Biomaterialia* **2020**, *106*, 256-266.

22. Fan, Y.; Lin, L.; Yin, F.; Zhu, Y.; Shen, M.; Wang, H.; Du, L.; Mignani, S.; Majoral, J.-P.; Shi, X., Phosphorus dendrimer-based copper(II) complexes enable ultrasound-enhanced tumor theranostics. *Nano Today* **2020**, *33*, 100899.
23. Lowell, J. A.; Dikici, E.; Joshi, P. M.; Landgraf, R.; Lemmon, V. P.; Daunert, S.; Izenwasser, S.; Daftarian, P., Vaccination against cocaine using a modifiable dendrimer nanoparticle platform. *Vaccine* **2020**, *38* (50), 7989-7997.
24. Buhleier, E.; Wehner, W.; Vögtle, F., "Cascade"- and "Nonskid-Chain-like" Syntheses of Molecular Cavity Topologies. *Synthesis* **1978**, *1978* (02), 155-158.
25. Tomalia, D. A.; Baker, H.; Dewald, J.; Hall, M.; Kallos, G.; Martin, S.; Roeck, J.; Ryder, J.; Smith, P., A new class of polymers - Starburst-dendritic macromolecules. *Polym. J.* **1985**, *17* (1), 117-132.
26. Newkome, G.; Yao, Z.; Baker, G. R.; Gupta, V., Micelles. Part 1. Cascade molecules: a new approach to micelles. A [27]-arborol. *Journal of Organic Chemistry* **1985**, *16*, 2003-2004.
27. Fréchet, J. M., Functional polymers and dendrimers: reactivity, molecular architecture, and interfacial energy. *Science* **1994**, *263* (5154), 1710-5.
28. Tomalia, D. A.; Naylor, A. M.; Goddard, W. A., Starburst Dendrimers: Molecular-Level Control of Size, Shape, Surface Chemistry, Topology, and Flexibility from Atoms to Macroscopic Matter. *Angew. Chem., Int. Ed. Engl.* **1990**, *29* (2), 138-175.
29. Vögtle, F.; Richardt, G.; Werner, N.; Rackstraw, A., Dendrimer chemistry. *Strauss GmbH, Morlenbach* **2009**.
30. Liu, M.; Fréchet, J. M. J., Designing dendrimers for drug delivery. *Pharmaceutical Science & Technology Today* **1999**, *2* (10), 393-401.
31. Lee, C. C.; MacKay, J. A.; Fréchet, J. M. J.; Szoka, F. C., Designing dendrimers for biological applications. *Nature biotechnology* **2005**, *23* (12), 1517-1526.
32. Soto-Castro, D.; Cruz-Morales, J. A.; Ramírez Apan, M. T.; Guadarrama, P., Solubilization and anticancer-activity enhancement of Methotrexate by novel dendrimeric nanodevices synthesized in one-step reaction. *Bioorganic chemistry* **2012**, *41-42*, 13-21.
33. Zhong, T.; Ai, P.; Zhou, J., Structures and properties of PAMAM dendrimer: A multi-scale simulation study. *Fluid Phase Equilibria* **2011**, *302* (1), 43-47.
34. Maiti, P. K.; Çağın, T.; Wang, G.; Goddard, W. A., Structure of PAMAM Dendrimers: Generations 1 through 11. *Macromolecules* **2004**, *37* (16), 6236-6254.

35. Hecht, S.; Fréchet, J. M. J., Dendritic Encapsulation of Function: Applying Nature's Site Isolation Principle from Biomimetics to Materials Science. *Angewandte Chemie International Edition* **2001**, *40* (1), 74-91.
36. Shadrack, D. M.; Swai, H. S.; Munissi, J. J. E.; Mubofu, E. B.; Nyandoro, S. S., Polyamidoamine Dendrimers for Enhanced Solubility of Small Molecules and Other Desirable Properties for Site Specific Delivery: Insights from Experimental and Computational Studies. *Molecules* **2018**, *23* (6), 1419.
37. Liu, Y.; Bryantsev, V. S.; Diallo, M. S.; Goddard Iii, W. A., PAMAM Dendrimers Undergo pH Responsive Conformational Changes without Swelling. *Journal of the American Chemical Society* **2009**, *131* (8), 2798-2799.
38. Maiti, P. K.; Çağın, T.; Lin, S.-T.; Goddard, W. A., Effect of Solvent and pH on the Structure of PAMAM Dendrimers. *Macromolecules* **2005**, *38* (3), 979-991.
39. Devarakonda, B.; Otto, D. P.; Judefeind, A.; Hill, R. A.; de Villiers, M. M., Effect of pH on the solubility and release of furosemide from polyamidoamine (PAMAM) dendrimer complexes. *International journal of pharmaceuticals* **2007**, *345* (1-2), 142-53.
40. Chang, Y.; Meng, X.; Zhao, Y.; Li, K.; Zhao, B.; Zhu, M.; Li, Y.; Chen, X.; Wang, J., Novel water-soluble and pH-responsive anticancer drug nanocarriers: doxorubicin-PAMAM dendrimer conjugates attached to superparamagnetic iron oxide nanoparticles (IONPs). *J Colloid Interface Sci* **2011**, *363* (1), 403-9.
41. Maingi, V.; Kumar, M. V. S.; Maiti, P. K., PAMAM Dendrimer-Drug Interactions: Effect of pH on the Binding and Release Pattern. *The Journal of Physical Chemistry B* **2012**, *116* (14), 4370-4376.
42. Malik, N.; Wiwattanapatapee, R.; Klopsch, R.; Lorenz, K.; Frey, H.; Weener, J.; Meijer, E.; Paulus, W.; Duncan, R., Dendrimers: Relationship between structure and biocompatibility in vitro, and preliminary studies on the biodistribution of I-125-labelled polyamidoamine dendrimers in vivo. *Journal of Controlled Release* **2000**, *65* (1-2), 133-148.
43. Choi, Y. J.; Kang, S. J.; Kim, Y. J.; Lim, Y. B.; Chung, H. W., Comparative studies on the genotoxicity and cytotoxicity of polymeric gene carriers polyethylenimine (PEI) and polyamidoamine (PAMAM) dendrimer in Jurkat T-cells. *Drug and Chemical Toxicology (1977)* **2010**, *33* (4), 357-66.
44. Sadekar, S.; Ghandehari, H., Transepithelial transport and toxicity of PAMAM dendrimers: implications for oral drug delivery. *Advanced drug delivery reviews* **2012**, *64* (6), 571-88.
45. Thiagarajan, G.; Greish, K.; Ghandehari, H., Charge affects the oral toxicity of poly(amidoamine) dendrimers. *European journal of pharmaceuticals and biopharmaceutics : official journal of Arbeitsgemeinschaft fuer Pharmazeutische Verfahrenstechnik e.V* **2013**, *84* (2), 330-4.

46. Ciolkowski, M.; Petersen, J. F.; Ficker, M.; Janaszewska, A.; Christensen, J. B.; Klajnert, B.; Bryszewska, M., Surface modification of PAMAM dendrimer improves its biocompatibility. *Nanomedicine : nanotechnology, biology, and medicine* **2012**, *8* (6), 815-7.
47. Cui, Y. S.; Liang, B.; Wang, L. G.; Zhu, L. L.; Kang, J. X.; Sun, H. T.; Chen, S. F., Enhanced biocompatibility of PAMAM dendrimers benefiting from tuning their surface charges. *Mat Sci Eng C-Mater* **2018**, *93*, 332-340.
48. Saovapakhiran, A.; D'Emanuele, A.; Attwood, D.; Penny, J., Surface Modification of PAMAM Dendrimers Modulates the Mechanism of Cellular Internalization. *Bioconjugate chemistry* **2009**, *20* (4), 693-701.
49. Xue, X.; Chen, X.; Mao, X.; Hou, Z.; Zhou, Y.; Bai, H.; Meng, J.; Da, F.; Sang, G.; Wang, Y.; Luo, X., Amino-terminated generation 2 poly(amidoamine) dendrimer as a potential broad-spectrum, nonresistance-inducing antibacterial agent. *AAPS J* **2013**, *15* (1), 132-42.
50. Rastegar, A.; Nazari, S.; Allahabadi, A.; Falanji, F.; Akbari Dourbash, F. A. D.; Rezai, Z.; Alizadeh Matboo, S.; Hekmat-Shoar, R.; Mohseni, S. M.; Majidi, G., Antibacterial activity of amino- and amido- terminated poly (amidoamine)-G6 dendrimer on isolated bacteria from clinical specimens and standard strains. *Med J Islam Repub Iran* **2017**, *31*, 64.
51. Gholami, M.; Mohammadi, R.; Arzanlou, M.; Akbari Dourbash, F.; Kouhsari, E.; Majidi, G.; Mohseni, S. M.; Nazari, S., In vitro antibacterial activity of poly (amidoamine)-G7 dendrimer. *BMC Infect Dis* **2017**, *17* (1), 395.
52. Zhao, H.; Li, J.; Xi, F.; Jiang, L., Polyamidoamine dendrimers inhibit binding of Tat peptide to TAR RNA. *FEBS Letters* **2004**, *563* (1-3), 241-245.
53. Kandeel, M.; Al-Taher, A.; Park, B. K.; Kwon, H.-J.; Al-Nazawi, M., A pilot study of the antiviral activity of anionic and cationic polyamidoamine dendrimers against the Middle East respiratory syndrome coronavirus. *Journal of Medical Virology* **2020**, *92* (9), 1665-1670.
54. Vu, M. T.; Bach, L. G.; Nguyen, D. C.; Ho, M. N.; Nguyen, N. H.; Tran, N. Q.; Nguyen, D. H.; Nguyen, C. K.; Hoang Thi, T. T., Modified Carboxyl-Terminated PAMAM Dendrimers as Great Cytocompatible Nano-Based Drug Delivery System. *International journal of molecular sciences* **2019**, *20* (8), 2016.
55. Wang, G.; Fu, L.; Walker, A.; Chen, X.; Lovejoy, D. B.; Hao, M.; Lee, A.; Chung, R.; Rizos, H.; Irvine, M.; Zheng, M.; Liu, X.; Lu, Y.; Shi, B., Label-Free Fluorescent Poly(amidoamine) Dendrimer for Traceable and Controlled Drug Delivery. *Biomacromolecules* **2019**, *20* (5), 2148-2158.
56. Jose, J.; Charyulu, R. N., Prolonged drug delivery system of an antifungal drug by association with polyamidoamine dendrimers. *Int J Pharm Investig* **2018**, *6* (2), 123-7.

57. Abedi-Gaballu, F.; Dehghan, G.; Ghaffari, M.; Yekta, R.; Abbaspour-Ravasjani, S.; Baradaran, B.; Ezzati Nazhad Dolatabadi, J.; Hamblin, M. R., PAMAM dendrimers as efficient drug and gene delivery nanosystems for cancer therapy. *Applied Materials Today* **2018**, *12*, 177-190.
58. Tsai, Y. J.; Hu, C. C.; Chu, C. C.; Toyoko, I., Intrinsically Fluorescent PAMAM Dendrimer as Gene Carrier and Nanoprobe for Nucleic Acids Delivery: Bioimaging and Transfection Study. *Biomacromolecules* **2011**, *12* (12), 4283-4290.
59. Vaidyanathan, S.; Orr, B. G.; Banaszak Holl, M. M., Role of Cell Membrane-Vector Interactions in Successful Gene Delivery. *Accounts of Chemical Research* **2016**, *49* (8), 1486-1493.
60. Chis, A. A.; Dobrea, C.; Morgovan, C.; Arseniu, A. M.; Rus, L. L.; Butuca, A.; Juncan, A. M.; Totan, M.; Vonica-Tincu, A. L.; Cormos, G.; Muntean, A. C.; Muresan, M. L.; Gligor, F. G.; Frum, A., Applications and Limitations of Dendrimers in Biomedicine. *Molecules* **2020**, *25* (17), 3982.
61. Dias, A. P.; da Silva Santos, S.; da Silva, J. V.; Parise-Filho, R.; Igne Ferreira, E.; Seoud, O. E.; Giarolla, J., Dendrimers in the context of nanomedicine. *International journal of pharmaceutics* **2020**, *573*, 118814.
62. Congur, G.; Eksin, E.; Mese, F.; Erdem, A., Succinamic acid functionalized PAMAM dendrimer modified pencil graphite electrodes for voltammetric and impedimetric DNA analysis. *Sensors and Actuators B: Chemical* **2014**, *201*, 59-64.
63. Kavosi, B.; Hallaj, R.; Teymourian, H.; Salimi, A., Au nanoparticles/PAMAM dendrimer functionalized wired ethyleneamine-viologen as highly efficient interface for ultra-sensitive alpha-fetoprotein electrochemical immunosensor. *Biosensors & bioelectronics* **2014**, *59*, 389-96.
64. Singh, P.; Moll, F.; Lin, S. H.; Ferzli, C.; Yu, K. S.; Koski, R. K.; Saul, R. G.; Cronin, P., Starburst dendrimers: enhanced performance and flexibility for immunoassays. *Clinical Chemistry* **1994**, *40* (9), 1845-1849.
65. Singh, P., Dendrimers and their applications in immunoassays and clinical diagnostics. *Biotechnology and Applied Biochemistry* **2007**, *48*, 1-9.
66. Akhtar, S.; Al-Zaid, B.; El-Hashim, A. Z.; Chandrasekhar, B.; Attur, S.; Yousif, M. H. M.; Benter, I. F., Cationic Polyamidoamine Dendrimers as Modulators of EGFR Signaling In Vitro and In Vivo. *PLOS ONE* **2015**, *10* (7), e0132215.
67. Liu, H.; Wang, H.; Yang, W.; Cheng, Y., Disulfide Cross-Linked Low Generation Dendrimers with High Gene Transfection Efficacy, Low Cytotoxicity, and Low Cost. *Journal of the American Chemical Society* **2012**, *134* (42), 17680-17687.
68. Yiyun, C.; Tongwen, X.; Rongqiang, F., Polyamidoamine dendrimers used as solubility enhancers of ketoprofen. *European journal of medicinal chemistry* **2005**, *40* (12), 1390-1393.

69. Chauhan, A. S.; Jain, N. K.; Diwan, P. V.; Khopade, A. J., Solubility enhancement of indomethacin with poly(amidoamine) dendrimers and targeting to inflammatory regions of arthritic rats. *Journal of drug targeting* **2004**, *12* (9-10), 575-83.
70. Luong, D.; Kesharwani, P.; Killinger, B. A.; Moszczynska, A.; Sarkar, F. H.; Padhye, S.; Rishi, A. K.; Iyer, A. K., Solubility enhancement and targeted delivery of a potent anticancer flavonoid analogue to cancer cells using ligand decorated dendrimer nano-architectures. *J Colloid Interface Sci* **2016**, *484*, 33-43.
71. Buwalda, S. J.; Bethry, A.; Hunger, S.; Kandoussi, S.; Coudane, J.; Nottelet, B., Ultrafast in situ forming poly(ethylene glycol)-poly(amido amine) hydrogels with tunable drug release properties via controllable degradation rates. *European journal of pharmaceutics and biopharmaceutics : official journal of Arbeitsgemeinschaft fur Pharmazeutische Verfahrenstechnik e.V* **2019**, *139*, 232-239.
72. Palmerston Mendes, L.; Pan, J.; Torchilin, V. P., Dendrimers as Nanocarriers for Nucleic Acid and Drug Delivery in Cancer Therapy. *Molecules* **2017**, *22* (9), 1401.
73. Farshbaf, M.; Davaran, S.; Zarebkohan, A.; Annabi, N.; Akbarzadeh, A.; Salehi, R., Significant role of cationic polymers in drug delivery systems. *Artificial cells, nanomedicine, and biotechnology* **2018**, *46* (8), 1872-1891.
74. Qiao, Z.; Shi, X., Dendrimer-based molecular imaging contrast agents. *Progress in Polymer Science* **2015**, *44*, 1-27.
75. Marcinkowska, M.; Stanczyk, M.; Janaszewska, A.; Gajek, A.; Ksiezak, M.; Dzialak, P.; Klajnert-Maculewicz, B., Molecular Mechanisms of Antitumor Activity of PAMAM Dendrimer Conjugates with Anticancer Drugs and a Monoclonal Antibody. *Polymers* **2019**, *11* (9), 1422.
76. Marcinkowska, M.; Stanczyk, M.; Janaszewska, A.; Sobierajska, E.; Chworos, A.; Klajnert-Maculewicz, B., Multicomponent Conjugates of Anticancer Drugs and Monoclonal Antibody with PAMAM Dendrimers to Increase Efficacy of HER-2 Positive Breast Cancer Therapy. *Pharmaceutical research* **2019**, *36* (11), 154.
77. Shukla, R.; Thomas, T. P.; Desai, A. M.; Kotlyar, A.; Park, S. J.; Baker, J. R., HER2 specific delivery of methotrexate by dendrimer conjugated anti-HER2 mAb. *Nanotechnology* **2008**, *19* (29), 295102.
78. Majoros, I. J.; Thomas, T. P.; Mehta, C. B.; Baker, J. R., Jr., Poly(amidoamine) dendrimer-based multifunctional engineered nanodevice for cancer therapy. *Journal of medicinal chemistry* **2005**, *48* (19), 5892-9.
79. Wang, Y.; Cao, X.; Guo, R.; Shen, M.; Zhang, M.; Zhu, M.; Shi, X., Targeted delivery of doxorubicin into cancer cells using a folic acid-dendrimer conjugate. *Polymer Chemistry* **2011**, *2* (8), 1754-1760.

80. Majoros, I. J.; Myc, A.; Thomas, T.; Mehta, C. B.; Baker, J. R., PAMAM Dendrimer-Based Multifunctional Conjugate for Cancer Therapy: Synthesis, Characterization, and Functionality. *Biomacromolecules* **2006**, *7* (2), 572-579.
81. Liu, J.; Xiong, Z.; Zhang, J.; Peng, C.; Klajnert-Maculewicz, B.; Shen, M.; Shi, X., Zwitterionic Gadolinium(III)-Complexed Dendrimer-Entrapped Gold Nanoparticles for Enhanced Computed Tomography/Magnetic Resonance Imaging of Lung Cancer Metastasis. *ACS Appl. Mater. Interfaces* **2019**, *11* (17), 15212-15221.
82. Cao, Y.; Zu, G.; Kuang, Y.; He, Y.; Mao, Z.; Liu, M.; Xiong, D.; Pei, R., Biodegradable Nanoglobular Magnetic Resonance Imaging Contrast Agent Constructed with Host-Guest Self-Assembly for Tumor-Targeted Imaging. *ACS Appl Mater Interfaces* **2018**, *10* (32), 26906-26916.
83. Wei, X.; Liu, Z.; Zhao, Z., (68)Ga tagged dendrimers for molecular tumor imaging in animals. *Hell J Nucl Med* **2019**, *22* (1), 78-79.
84. Nabi, P. N.; Vahidfar, N.; Tohidkia, M. R.; Hamidi, A. A.; Omid, Y.; Aghanejad, A., Mucin-1 conjugated polyamidoamine-based nanoparticles for image-guided delivery of gefitinib to breast cancer. *International journal of biological macromolecules* **2021**, *174*, 185-197.
85. Lesniak, W. G.; Wu, Y.; Kang, J.; Boinapally, S.; Ray Banerjee, S.; Lisok, A.; Jablonska, A.; Boctor, E. M.; Pomper, M. G., Dual contrast agents for fluorescence and photoacoustic imaging: evaluation in a murine model of prostate cancer. *Nanoscale* **2021**.
86. Tanaka, S. I.; Wadati, H.; Sato, K.; Yasuda, H.; Niioka, H., Red-Fluorescent Pt Nanoclusters for Detecting and Imaging HER2 in Breast Cancer Cells. *ACS Omega* **2020**, *5* (37), 23718-23723.
87. Wang, G.; Zhao, X.; Wu, H.; Lovejoy, D. B.; Zheng, M.; Lee, A.; Fu, L.; Miao, K.; An, Y.; Sayyadi, N.; Ding, K.; Chung, R. S.; Lu, Y.; Li, J.; Morsch, M.; Shi, B., A Robust Intrinsically Green Fluorescent Poly(Amidoamine) Dendrimer for Imaging and Traceable Central Nervous System Delivery in Zebrafish. *Small* **2020**, *16* (39), e2003654.
88. Gothwal, A.; Singh, H.; Jain, S. K.; Dutta, A.; Borah, A.; Gupta, U., Behavioral and Biochemical Implications of Dendrimeric Rivastigmine in Memory-Deficit and Alzheimer's Induced Rodents. *ACS Chem Neurosci* **2019**, *10* (8), 3789-3795.
89. Igartúa, D. E.; Martinez, C. S.; Del, V. A. S.; Prieto, M. J., Combined Therapy for Alzheimer's Disease: Tacrine and PAMAM Dendrimers Co-Administration Reduces the Side Effects of the Drug without Modifying its Activity. *AAPS PharmSciTech* **2020**, *21* (3), 110.
90. Sun, H. J.; Wang, Y.; Hao, T.; Wang, C. Y.; Wang, Q. Y.; Jiang, X. X., Efficient GSH delivery using PAMAM-GSH into MPP-induced PC12 cellular model for Parkinson's disease. *Regen Biomater* **2016**, *3* (5), 299-307.

91. Rekas, A.; Lo, V.; Gadd, G. E.; Cappai, R.; Yun, S. I., PAMAM dendrimers as potential agents against fibrillation of alpha-synuclein, a Parkinson's disease-related protein. *Macromolecular bioscience* **2009**, *9* (3), 230-8.
92. Oliveira, I. M.; Gonçalves, C.; Oliveira, E. P.; Simón-Vázquez, R.; da Silva Morais, A.; González-Fernández, Á.; Reis, R. L.; Oliveira, J. M., PAMAM dendrimers functionalised with an anti-TNF α antibody and chondroitin sulphate for treatment of rheumatoid arthritis. *Mater Sci Eng C Mater Biol Appl* **2021**, *121*, 111845.
93. Duran-Lara, E.; Guzman, L.; John, A.; Fuentes, E.; Alarcon, M.; Palomo, I.; Santos, L. S., PAMAM dendrimer derivatives as a potential drug for antithrombotic therapy. *European journal of medicinal chemistry* **2013**, *69*, 601-8.
94. Spyropoulos-Antonakakis, N.; Sarantopoulou, E.; Trohopoulos, P. N.; Stefi, A. L.; Kollia, Z.; Gavriil, V. E.; Bourkoula, A.; Petrou, P. S.; Kakabakos, S.; Semashko, V. V.; Nizamutdinov, A. S.; Cefalas, A. C., Selective aggregation of PAMAM dendrimer nanocarriers and PAMAM/ZnPc nanodrugs on human atheromatous carotid tissues: a photodynamic therapy for atherosclerosis. *Nanoscale research letters* **2015**, *10*, 210.
95. Teo, I.; Toms, S. M.; Marteyn, B.; Barata, T. S.; Simpson, P.; Johnston, K. A.; Schnupf, P.; Puhar, A.; Bell, T.; Tang, C.; Zloh, M.; Matthews, S.; Rendle, P. M.; Sansonetti, P. J.; Shaunak, S., Preventing acute gut wall damage in infectious diarrhoeas with glycosylated dendrimers. *EMBO Mol Med* **2012**, *4* (9), 866-81.
96. Gao, Y.; Wang, J.; Chai, M.; Li, X.; Deng, Y.; Jin, Q.; Ji, J., Size and Charge Adaptive Clustered Nanoparticles Targeting the Biofilm Microenvironment for Chronic Lung Infection Management. *ACS Nano* **2020**, *14* (5), 5686-5699.
97. Chen, L.; Liang, K.; Li, J.; Wu, D.; Zhou, X.; Li, J., Regeneration of biomimetic hydroxyapatite on etched human enamel by anionic PAMAM template in vitro. *Archives of oral biology* **2013**, *58* (8), 975-80.
98. Fan, M.; Zhang, M.; Xu, H. H. K.; Tao, S.; Yu, Z.; Yang, J.; Yuan, H.; Zhou, X.; Liang, K.; Li, J., Remineralization effectiveness of the PAMAM dendrimer with different terminal groups on artificial initial enamel caries in vitro. *Dental Materials* **2020**, *36* (2), 210-220.
99. Kirkpatrick, G. J.; Plumb, J. A.; Sutcliffe, O. B.; Flint, D. J.; Wheate, N. J., Evaluation of anionic half generation 3.5-6.5 poly(amidoamine) dendrimers as delivery vehicles for the active component of the anticancer drug cisplatin. *Journal of inorganic biochemistry* **2011**, *105* (9), 1115-22.
100. Sadekar, S.; Thiagarajan, G.; Bartlett, K.; Hubbard, D.; Ray, A.; McGill, L. D.; Ghandehari, H., Poly(amido amine) dendrimers as absorption enhancers for oral delivery of camptothecin. *International journal of pharmaceutics* **2013**, *456* (1), 175-85.
101. Nishimoto, Y.; Nagashima, S.; Nakajima, K.; Ohira, T.; Sato, T.; Izawa, T.; Yamate, J.; Higashikawa, K.; Kuge, Y.; Ogawa, M.; Kojima, C., Carboxyl-, sulfonyl-,

and phosphate-terminal dendrimers as a nanoplatform with lymph node targeting. *International journal of pharmaceutics* **2020**, *576*, 119021.

102. Hanurry, E. Y.; Mekonnen, T. W.; Andrgie, A. T.; Darge, H. F.; Birhan, Y. S.; Hsu, W. H.; Chou, H. Y.; Cheng, C. C.; Lai, J. Y.; Tsai, H. C., Biotin-Decorated PAMAM G4.5 Dendrimer Nanoparticles to Enhance the Delivery, Anti-Proliferative, and Apoptotic Effects of Chemotherapeutic Drug in Cancer Cells. *Pharmaceutics* **2020**, *12* (5).

103. Prieto, M. J.; Temprana, C. F.; del Rio Zabala, N. E.; Marotta, C. H.; Alonso Sdel, V., Optimization and in vitro toxicity evaluation of G4 PAMAM dendrimer-risperidone complexes. *European journal of medicinal chemistry* **2011**, *46* (3), 845-50.

104. Prieto, M. J.; del Rio Zabala, N. E.; Marotta, C. H.; Carreño Gutierrez, H.; Arévalo Arévalo, R.; Chiaramoni, N. S.; del Valle Alonso, S., Optimization and in vivo toxicity evaluation of G4.5 PAMAM dendrimer-risperidone complexes. *PLoS One* **2014**, *9* (2), e90393.

105. Yuan, Q.; Fu, Y.; Kao, W. J.; Janigro, D.; Yang, H., Transbuccal Delivery of CNS Therapeutic Nanoparticles: Synthesis, Characterization, and In Vitro Permeation Studies. *ACS Chem Neurosci* **2011**, *2* (11), 676-683.

106. Souza, J. G.; Dias, K.; Silva, S. A. M.; de Rezende, L. C. D.; Rocha, E. M.; Emery, F. S.; Lopez, R. F. V., Transcorneal iontophoresis of dendrimers: PAMAM corneal penetration and dexamethasone delivery. *Journal of Controlled Release* **2015**, *200*, 115-124.

107. Wang, B.; Navath, R. S.; Romero, R.; Kannan, S.; Kannan, R., Anti-inflammatory and anti-oxidant activity of anionic dendrimer-N-acetyl cysteine conjugates in activated microglial cells. *International journal of pharmaceutics* **2009**, *377* (1-2), 159-68.

108. Yavuz, B.; Pehlivan, S. B.; Vural, İ.; Ünlü, N., *In Vitro/In Vivo* Evaluation of Dexamethasone—PAMAM Dendrimer Complexes for Retinal Drug Delivery. *Journal of Pharmaceutical Sciences* **2015**, *104* (11), 3814-3823.

109. Yang, H.; Kao, W. J., Synthesis and characterization of nanoscale dendritic RGD clusters for potential applications in tissue engineering and drug delivery. *International journal of nanomedicine* **2007**, *2* (1), 89-99.

110. Zhang, D.; Huang, Q., Encapsulation of Astragaloside with Matrix Metalloproteinase-2-Responsive Hyaluronic Acid End-Conjugated Polyamidoamine Dendrimers Improves Wound Healing in Diabetes. *J Biomed Nanotechnol* **2020**, *16* (8), 1229-1240.

111. Shah, A. H.; Djordjevic, I.; Steele, T. W. J., Tertiary blends of PAMAM/PEG/PEG tissue bioadhesives. *J Mech Behav Biomed Mater* **2020**, *101*, 103405.

112. Wang, B.; Navath, R. S.; Menjoge, A. R.; Balakrishnan, B.; Bellair, R.; Dai, H.; Romero, R.; Kannan, S.; Kannan, R. M., Inhibition of bacterial growth and intramniotic infection in a guinea pig model of chorioamnionitis using PAMAM dendrimers. *International Journal of Pharmaceutics (Amsterdam, Netherlands)* **2010**, *395* (1-2), 298-308.
113. Staneva, D.; Angelova, S.; Vasileva-Tonkova, E.; Grozdanov, P.; Nikolova, I.; Grabchev, I., Synthesis, photophysical characterisation and antimicrobial activity of a new anionic PAMAM dendrimer. *Journal of Photochemistry and Photobiology A: Chemistry* **2020**, *403*, 112878.
114. Holmes, A. M.; Heylings, J. R.; Wan, K. W.; Moss, G. P., Antimicrobial efficacy and mechanism of action of poly(amidoamine) (PAMAM) dendrimers against opportunistic pathogens. *Int J Antimicrob Agents* **2019**, *53* (4), 500-507.
115. Wiwattanapatapee, R.; Carreno-Gomez, B.; Malik, N.; Duncan, R., Anionic PAMAM dendrimers rapidly cross adult rat intestine in vitro: A potential oral delivery system? *Pharmaceutical research* **2000**, *17* (8), 991-998.
116. Oddone, N.; Lecot, N.; Fernandez, M.; Rodriguez-Haralambides, A.; Cabral, P.; Cerecetto, H.; Benech, J. C., In vitro and in vivo uptake studies of PAMAM G4.5 dendrimers in breast cancer. *J Nanobiotechnology* **2016**, *14* (1), 45.
117. Jevprasesphant, R.; Penny, J.; Attwood, D.; McKeown, N.; D'Emanuele, A., Engineering of dendrimer surfaces to enhance transepithelial transport and reduce cytotoxicity. *Pharmaceutical research* **2003**, *20* (10), 1543-1550.
118. Bodewein, L.; Schmelter, F.; Di Fiore, S.; Hollert, H.; Fischer, R.; Fenske, M., Differences in toxicity of anionic and cationic PAMAM and PPI dendrimers in zebrafish embryos and cancer cell lines. *Toxicology and applied pharmacology* **2016**, *305*, 83-92.
119. Janaszewska, A.; Mączyńska, K.; Matuszko, G.; Appelhans, D.; Voit, B.; Klajnert, B.; Bryszewska, M., Cytotoxicity of PAMAM, PPI and maltose modified PPI dendrimers in Chinese hamster ovary (CHO) and human ovarian carcinoma (SKOV3) cells. *New Journal of Chemistry* **2012**, *36* (2), 428-437.
120. Patel, M.; De Paoli, S. H.; Elhelu, O. K.; Farooq, S.; Simak, J., Cell membrane disintegration and extracellular vesicle release in a model of different size and charge PAMAM dendrimers effects on cultured endothelial cells. *Nanotoxicology* **2019**, *13* (5), 664-681.
121. Zeng, Y.; Kurokawa, Y.; Win-Shwe, T. T.; Zeng, Q.; Hirano, S.; Zhang, Z.; Sone, H., Effects of PAMAM dendrimers with various surface functional groups and multiple generations on cytotoxicity and neuronal differentiation using human neural progenitor cells. *J Toxicol Sci* **2016**, *41* (3), 351-70.
122. Zhang, J.; Li, M.; Wang, M.; Xu, H.; Wang, Z.; Li, Y.; Ding, B.; Gao, J., Effects of the surface charge of polyamidoamine dendrimers on cellular exocytosis and the

- exocytosis mechanism in multidrug-resistant breast cancer cells. *Journal of nanobiotechnology* **2021**, *19* (1), 135-135.
123. Morris, C. J.; Aljayyousi, G.; Mansour, O.; Griffiths, P.; Gumbleton, M., Endocytic Uptake, Transport and Macromolecular Interactions of Anionic PAMAM Dendrimers within Lung Tissue. *Pharmaceutical research* **2017**, *34* (12), 2517-2531.
124. Borowska, K.; Wolowiec, S.; Glowniak, K.; Sieniawska, E.; Radej, S., Transdermal delivery of 8-methoxypsoralene mediated by polyamidoamine dendrimer G2.5 and G3.5--in vitro and in vivo study. *International journal of pharmaceutics* **2012**, *436* (1-2), 764-70.
125. Pryor, J. B.; Harper, B. J.; Harper, S. L., Comparative toxicological assessment of PAMAM and thiophosphoryl dendrimers using embryonic zebrafish. *Int. J. Nanomed.* **2014**, *9*, 1947-56.
126. Thiagarajan, G.; Sadekar, S.; Greish, K.; Ray, A.; Ghandehari, H., Evidence of oral translocation of anionic G6.5 dendrimers in mice. *Molecular pharmaceutics* **2013**, *10* (3), 988-98.
127. Ghosh, S.; Roy, A.; Singhanian, A.; Chatterjee, S.; Swarnakar, S.; Fujita, D.; Bandyopadhyay, A., In-vivo & in-vitro toxicity test of molecularly engineered PCMS: A potential drug for wireless remote controlled treatment. *Toxicol Rep* **2018**, *5*, 1044-1052.
128. Kitchens, K.; Foraker, A.; Kolhatkar, R.; Swaan, P.; Ghandehari, H., Endocytosis and interaction of poly (amidoamine) dendrimers with Caco-2 cells. *Pharmaceutical research* **2007**, *24* (11), 2138-2145.
129. Lin, Y.-L.; Khanafer, K.; El-Sayed, M. E. H., Quantitative evaluation of the effect of poly(amidoamine) dendrimers on the porosity of epithelial monolayers. *Nanoscale* **2010**, *2* (5), 755-762.
130. Duncan, R.; Izzo, L., Dendrimer biocompatibility and toxicity. *Advanced drug delivery reviews* **2005**, *57* (15), 2215-2237.
131. Mukherjee, S. P.; Davoren, M.; Byrne, H. J., In vitro mammalian cytotoxicological study of PAMAM dendrimers - towards quantitative structure activity relationships. *Toxicology in vitro : an international journal published in association with BIBRA* **2010**, *24* (1), 169-77.
132. Halets, I.; Shcharbin, D.; Klajnert, B.; Bryszewska, M., Contribution of hydrophobicity, DNA and proteins to the cytotoxicity of cationic PAMAM dendrimers. *International Journal of Pharmaceutics (Amsterdam, Netherlands)* **2013**, *454* (1), 1-3.
133. Goldberg, D. S.; Ghandehari, H.; Swaan, P. W., Cellular entry of G3.5 poly (amido amine) dendrimers by clathrin- and dynamin-dependent endocytosis

- promotes tight junctional opening in intestinal epithelia. *Pharmaceutical research* **2010**, *27* (8), 1547-57.
134. Prevette, L. E.; Benish, N. C.; Schoenecker, A. R.; Braden, K. J., Cell-penetrating compounds preferentially bind glycosaminoglycans over plasma membrane lipids in a charge density- and stereochemistry-dependent manner. *Biophysical Chemistry* **2015**, *207*, 40-50.
135. Khandare, J.; Mohr, A.; Calderon, M.; Welker, P.; Licha, K.; Haag, R., Structure-biocompatibility relationship of dendritic polyglycerol derivatives. *Biomaterials* **2010**, *31* (15), 4268-77.
136. Ziemba, B.; Matuszko, G.; Bryszewska, M.; Klajnert, B., Influence of dendrimers on red blood cells. *Cellular & molecular biology letters* **2012**, *17* (1), 21-35.
137. Li, G.; Zhang, Y.; Tang, W.; Zheng, J., Comprehensive investigation of in vitro hemocompatibility of surface modified polyamidoamine nanocarrier. *Clin Hemorheol Microcirc* **2020**, *74* (3), 267-279.
138. Shcharbin, D.; Klajnert, B.; Bryszewska, M., The effect of PAMAM dendrimers on human and bovine serum albumin at different pH and NaCl concentrations. *Journal of Biomaterials Science, Polymer Edition* **2005**, *16* (9), 1081-1093.
139. Åkesson, A.; Cárdenas, M.; Elia, G.; Monopoli, M. P.; Dawson, K. A., The protein corona of dendrimers: PAMAM binds and activates complement proteins in human plasma in a generation dependent manner. *RSC Advances* **2012**, *2* (30), 11245-11248.
140. Chanphai, P.; Froehlich, E.; Mandeville, J. S.; Tajmir-Riahi, H. A., Protein conjugation with PAMAM nanoparticles: Microscopic and thermodynamic analysis. *Colloids and surfaces. B, Biointerfaces* **2017**, *150*, 168-174.
141. Dowhan, W.; Bogdanov, M.; Mileykovskaya, E., Chapter 1 – Functional roles of lipids in membranes. In *Biochemistry of Lipids, Lipoproteins and Membranes*, 5 ed.; Vance, D. E.; Vance, J. E., Eds. Elsevier B. V.: 2008; pp 1-37.
142. Nickels, J. D.; Chatterjee, S.; Stanley, C. B.; Qian, S.; Cheng, X.; Myles, D. A. A.; Standaert, R. F.; Elkins, J. G.; Katsaras, J., The in vivo structure of biological membranes and evidence for lipid domains. *PLOS Biology* **2017**, *15* (5), e2002214.
143. Sprott, G. D., Structures of archaebacterial membrane lipids. *J Bioenerg Biomembr* **1992**, *24* (6), 555-566.
144. Singer, S. J.; Nicolson, G. L., The fluid mosaic model of the structure of cell membranes. *Science* **1972**, *175* (4023), 720-31.
145. Simons, K.; Ikonen, E., Functional rafts in cell membranes. *Nature* **1997**, *387* (6633), 569-572.

146. Rajendran, L.; Simons, K., Lipid rafts and membrane dynamics. *Journal of Cell Science* **2005**, *118* (6), 1099-1102.
147. McMahon, H. T.; Gallop, J. L., Membrane curvature and mechanisms of dynamic cell membrane remodelling. *Nature* **2005**, *438* (7068), 590-596.
148. Chernomordik, L. V.; Kozlov, M. M., Protein-lipid interplay in fusion and fission of biological membranes. *Annual review of biochemistry* **2003**, *72*, 175-207.
149. Baumgart, T.; Capraro, B. R.; Zhu, C.; Das, S. L., Thermodynamics and mechanics of membrane curvature generation and sensing by proteins and lipids. *Annual review of physical chemistry* **2011**, *62*, 483-506.
150. Zimmerberg, J.; Gawrisch, K., The physical chemistry of biological membranes. *Nat Chem Biol* **2006**, *2* (11), 564-567.
151. Janmey, P. A.; Kinnunen, P. K., Biophysical properties of lipids and dynamic membranes. *Trends in cell biology* **2006**, *16* (10), 538-46.
152. Pomorski, T.; Hrafnisdottir, S.; Devaux, P. F.; van Meer, G., Lipid distribution and transport across cellular membranes. *Seminars in cell & developmental biology* **2001**, *12* (2), 139-48.
153. Sharom, F. J., Flipping and flopping--lipids on the move. *IUBMB life* **2011**, *63* (9), 736-46.
154. Cramer, W. A.; Engelman, D. M.; Von Heijne, G.; Rees, D. C., Forces involved in the assembly and stabilization of membrane proteins. *FASEB journal : official publication of the Federation of American Societies for Experimental Biology* **1992**, *6* (15), 3397-402.
155. von Heijne, G., Membrane-protein topology. *Nature reviews. Molecular cell biology* **2006**, *7* (12), 909-18.
156. Peterson, R. N.; Russell, L. D., The mammalian spermatozoon: A model for the study of regional specificity in plasma membrane organization and function. *Tissue and Cell* **1985**, *17* (6), 769-791.
157. Nicolson, G. L., Cis- and trans-membrane control of cell surface topography. *Journal of supramolecular structure* **1973**, *1* (4), 410-6.
158. Nicolson, G. L.; Yanagimachi, R., Mobility and the restriction of mobility of plasma membrane lectin binding components. *Science* **1974**, *184* (4143), 1294-6.
159. Geiger, B.; Bershadsky, A.; Pankov, R.; Yamada, K. M., Transmembrane crosstalk between the extracellular matrix--cytoskeleton crosstalk. *Nature reviews. Molecular cell biology* **2001**, *2* (11), 793-805.

160. Chichili, G. R.; Rodgers, W., Cytoskeleton-membrane interactions in membrane raft structure. *Cellular and molecular life sciences : CMLS* **2009**, *66* (14), 2319-28.
161. Marčelja, S., Lipid-mediated protein interaction in membranes. *Biochimica et Biophysica Acta (BBA) - Biomembranes* **1976**, *455* (1), 1-7.
162. Mouritsen, O. G.; Bloom, M., Mattress model of lipid-protein interactions in membranes. *Biophysical journal* **1984**, *46* (2), 141-53.
163. Ohvo-Rekila, H.; Ramstedt, B.; Leppimäki, P.; Peter Slotte, J., Cholesterol interactions with phospholipids in membranes. *Progress in Lipid Research* **2002**, *41* (1), 66-97.
164. van Meer, G.; Simons, K., Lipid polarity and sorting in epithelial cells. *Journal of cellular biochemistry* **1988**, *36* (1), 51-8.
165. Nicolson, G., The Fluid-Mosaic Model of Membrane Structure: Still relevant to understanding the structure, function and dynamics of biological membranes after more than 40 years. *Biochimica Et Biophysica Acta-Biomembranes* **2014**, *1838* (6), 1451-1466.
166. Sezgin, E.; Levental, I.; Mayor, S.; Eggeling, C., The mystery of membrane organization: composition, regulation and roles of lipid rafts. *Nature Reviews Molecular Cell Biology* **2017**, *18* (6), 361-374.
167. Bernardino de la Serna, J.; Schütz, G. J.; Eggeling, C.; Cebecauer, M., There Is No Simple Model of the Plasma Membrane Organization. *Frontiers in Cell and Developmental Biology* **2016**, *4* (106).
168. Kusumi, A.; Suzuki, K. G.; Kasai, R. S.; Ritchie, K.; Fujiwara, T. K., Hierarchical mesoscale domain organization of the plasma membrane. *Trends Biochem Sci* **2011**, *36* (11), 604-15.
169. Kusumi, A.; Nakada, C.; Ritchie, K.; Murase, K.; Suzuki, K.; Murakoshi, H.; Kasai, R. S.; Kondo, J.; Fujiwara, T., Paradigm shift of the plasma membrane concept from the two-dimensional continuum fluid to the partitioned fluid: high-speed single-molecule tracking of membrane molecules. *Annu Rev Biophys Biomol Struct* **2005**, *34*, 351-78.
170. Kalappurakkal, J. M.; Sil, P.; Mayor, S., Toward a new picture of the living plasma membrane. *Protein Science* **2020**, *29* (6), 1355-1365.
171. Spira, F.; Mueller, N. S.; Beck, G.; von Olshausen, P.; Beig, J.; Wedlich-Söldner, R., Patchwork organization of the yeast plasma membrane into numerous coexisting domains. *Nature Cell Biology* **2012**, *14* (6), 640-648.
172. Division of Life Sciences; Komaba Organization for Educational Excellence; Sciences, C. o. A. a. 5.3 Functions of Biological Membranes | Life Science | University of Tokyo. http://csls-text.c.u-tokyo.ac.jp/active/05_03.html (accessed 18.03.2015).

173. Pepić, I.; Lovrić, J.; Filipović-Grčić, J., How do polymeric micelles cross epithelial barriers? *European journal of pharmaceutical sciences : official journal of the European Federation for Pharmaceutical Sciences* **2013**, *50* (1), 42-55.
174. Silhavy, T. J.; Kahne, D.; Walker, S., The bacterial cell envelope. *Cold Spring Harb Perspect Biol* **2010**, *2* (5), a000414-a000414.
175. Vollmer, W.; Blanot, D.; De Pedro, M. A., Peptidoglycan structure and architecture. *FEMS Microbiology Reviews* **2008**, *32* (2), 149-167.
176. Berezin, S.; Aviv, Y.; Aviv, H.; Goldberg, E.; Tischler, Y. R., Replacing a Century Old Technique – Modern Spectroscopy Can Supplant Gram Staining. *Scientific Reports* **2017**, *7* (1), 3810.
177. Sud, M.; Fahy, E.; Cotter, D.; Brown, A.; Dennis, E. A.; Glass, C. K.; Merrill, A. H., Jr.; Murphy, R. C.; Raetz, C. R.; Russell, D. W.; Subramaniam, S., LMSD: LIPID MAPS structure database. *Nucleic Acids Res.* **2007**, *35* (Database issue), D527-532.
178. Symons, J. L.; Cho, K.-J.; Chang, J. T.; Du, G.; Waxham, M. N.; Hancock, J. F.; Levental, I.; Levental, K. R., Lipidomic atlas of mammalian cell membranes reveals hierarchical variation induced by culture conditions, subcellular membranes, and cell lineages. *Soft Matter* **2021**, *17* (2), 288-297.
179. Harayama, T.; Riezman, H., Understanding the diversity of membrane lipid composition. *Nature Reviews Molecular Cell Biology* **2018**, *19* (5), 281-296.
180. van Meer, G.; Voelker, D.; Feigenson, G., Membrane lipids: where they are and how they behave. *Nature Reviews Molecular Cell Biology* **2008**, *9* (2), 112-124.
181. Krause, M. R.; Regen, S. L., The Structural Role of Cholesterol in Cell Membranes: From Condensed Bilayers to Lipid Rafts. *Accounts of Chemical Research* **2014**, *47* (12), 3512-3521.
182. Munro, S., Lipid Rafts: Elusive or Illusive? *Cell* **2003**, *115* (4), 377-388.
183. Silvius, J. R., Role of cholesterol in lipid raft formation: lessons from lipid model systems. *Biochimica et Biophysica Acta (BBA) - Biomembranes* **2003**, *1610* (2), 174-183.
184. Epand, R. M.; Epand, R. F., Lipid domains in bacterial membranes and the action of antimicrobial agents. *Biochimica et Biophysica Acta, Biomembranes* **2009**, *1788* (1), 289-294.
185. Sáenz, J. P.; Grosser, D.; Bradley, A. S.; Lagny, T. J.; Lavrynenko, O.; Broda, M.; Simons, K., Hopanoids as functional analogues of cholesterol in bacterial membranes. *Proceedings of the National Academy of Sciences* **2015**, *112* (38), 11971-11976.
186. Welander, P. V.; Hunter, R. C.; Zhang, L.; Sessions, A. L.; Summons, R. E.; Newman, D. K., Hopanoids Play a Role in Membrane Integrity and pH Homeostasis

- in *Rhodopseudomonas palustris* TIE-1. *Journal of Bacteriology* **2009**, *191* (19), 6145-6156.
187. López-Lara, I. M.; Geiger, O., Bacterial lipid diversity. *Biochimica et Biophysica Acta (BBA) - Molecular and Cell Biology of Lipids* **2017**, *1862* (11), 1287-1299.
188. Vences-Guzmán, M. Á.; Geiger, O.; Sohlenkamp, C., Ornithine lipids and their structural modifications: from A to E and beyond. *FEMS Microbiology Letters* **2012**, *335* (1), 1-10.
189. Bertani, B.; Ruiz, N., Function and Biogenesis of Lipopolysaccharides. *EcoSal Plus* **2018**, *8* (1).
190. Elani, Y.; Purushothaman, S.; Booth, P. J.; Seddon, J. M.; Brooks, N. J.; Law, R. V.; Ces, O., Measurements of the effect of membrane asymmetry on the mechanical properties of lipid bilayers. *Chemical Communications* **2015**, *51* (32), 6976-6979.
191. Daleke, D. L., Phospholipid Flippases ^{		}. *Journal of Biological Chemistry* **2007**, *282* (2), 821-825.
192. Charalambous, K.; Booth, P. J.; Woscholski, R.; Seddon, J. M.; Templer, R. H.; Law, R. V.; Barter, L. M. C.; Ces, O., Engineering de Novo Membrane-Mediated Protein-Protein Communication Networks. *Journal of the American Chemical Society* **2012**, *134* (13), 5746-5749.
193. Khalili-Araghi, F.; Ziervogel, B.; Gumbart, J. C.; Roux, B., Molecular dynamics simulations of membrane proteins under asymmetric ionic concentrations. *Journal of General Physiology* **2013**, *142* (4), 465-475.
194. Xu, C.; Loew, L. M., The Effect of Asymmetric Surface Potentials on the Intramembrane Electric Field Measured with Voltage-Sensitive Dyes. *Biophysical journal* **2003**, *84* (4), 2768-2780.
195. Graham, T. R.; Kozlov, M. M., Interplay of proteins and lipids in generating membrane curvature. *Current Opinion in Cell Biology* **2010**, *22* (4), 430-436.
196. Virtanen, J. A.; Cheng, K. H.; Somerharju, P., Phospholipid composition of the mammalian red cell membrane can be rationalized by a superlattice model. *Proceedings of the National Academy of Sciences* **1998**, *95* (9), 4964-4969.
197. Gurr, M. I.; Harwood, J. L., Lipids in cellular structures. In *Lipid Biochemistry: An Introduction*, Gurr, M. I.; Harwood, J. L., Eds. Springer US: Boston, MA, 1991; pp 244-294.
198. Hong, S.; Leroueil, P.; Janus, E.; Peters, J.; Kober, M.; Islam, M.; Orr, B.; Baker, J.; Holl, M., Interaction of polycationic polymers with supported lipid bilayers and cells: Nanoscale hole formation and enhanced membrane permeability. *Bioconjugate chemistry* **2006**, *17* (3), 728-734.

199. Gabellieri, E.; Strambini, G. B.; Shcharbin, D.; Klajnert, B.; Bryszewska, M., Dendrimer-protein interactions studied by tryptophan room temperature phosphorescence. *Biochimica et biophysica acta* **2006**, *1764* (11), 1750-1756.
200. Gardikis, K.; Hatziantoniou, S.; Viras, K.; Wagner, M.; Demetzos, C., A DSC and Raman spectroscopy study on the effect of PAMAM dendrimer on DPPC model lipid membranes. *International journal of pharmaceutics* **2006**, *318* (1-2), 118-123.
201. Domanski, D. M.; Klajnert, B.; Bryszewska, M., Influence of PAMAM dendrimers on human red blood cells. *Bioelectrochemistry* **2004**, *63* (1-2), 189-191.
202. Roberts, J. C.; Bhalgat, M. K.; Zera, R. T., Preliminary biological evaluation of polyamidoamine (PAMAM) Starburst dendrimers. *J. Biomed. Mater. Res.* **1996**, *30* (1), 53-65.
203. Kim, Y.; Kwak, Y.; Chang, R., Free energy of PAMAM dendrimer adsorption onto model biological membranes. *Journal of Physical Chemistry B* **2014**, *118* (24), 6792-6802.
204. Kelly, C. V.; Leroueil, P. R.; Orr, B. G.; Banaszak Holl, M. M.; Andricioaei, I., Poly(amidoamine) dendrimers on lipid bilayers II: Effects of bilayer phase and dendrimer termination. *Journal of Physical Chemistry B* **2008**, *112* (31), 9346-9353.
205. Evans, K.; Laszlo, J.; Compton, D., Carboxyl-terminated PAMAM dendrimer interaction with 1-palmitoyl-2-oleoyl phosphocholine bilayers. *Biochimica Et Biophysica Acta-Biomembranes* **2014**, *1838* (1), 445-455.
206. Pretini, V.; Koenen, M. H.; Kaestner, L.; Fens, M. H. A. M.; Schiffelers, R. M.; Bartels, M.; Van Wijk, R., Red Blood Cells: Chasing Interactions. *Frontiers in Physiology* **2019**, *10* (945).
207. Jeong, H.; Hwang, J.; Lee, H.; Hammond, P. T.; Choi, J.; Hong, J., In vitro blood cell viability profiling of polymers used in molecular assembly. *Scientific Reports* **2017**, *7* (1), 9481.
208. Bapat, R. A.; Parolia, A.; Chaubal, T.; Dharamadhikari, S.; Abdulla, A. M.; Sakkir, N.; Arora, S.; Bapat, P.; Sindi, A. M.; Kesharwani, P., Recent update on potential cytotoxicity, biocompatibility and preventive measures of biomaterials used in dentistry. *Biomaterials Science* **2021**, *9* (9), 3244-3283.
209. Park, Y.; Huh, K. M.; Kang, S.-W., Applications of Biomaterials in 3D Cell Culture and Contributions of 3D Cell Culture to Drug Development and Basic Biomedical Research. *International journal of molecular sciences* **2021**, *22* (5), 2491.
210. Belfiore, L.; Aghaei, B.; Law, A. M. K.; Dobrowolski, J. C.; Raftery, L. J.; Tjandra, A. D.; Yee, C.; Piloni, A.; Volkerling, A.; Ferris, C. J.; Engel, M., Generation and Analysis of 3D Cell Culture Models for Drug Discovery. *European Journal of Pharmaceutical Sciences* **2021**, 105876.

211. Méndez-Ardoy, A.; Lostalé-Seijo, I.; Montenegro, J., Where in the Cell Is our Cargo? Methods Currently Used To Study Intracellular Cytosolic Localisation. *ChemBioChem* **2019**, *20* (4), 488-498.
212. Mushtaq, A.; Li, L.; A., A.; Grøndahl, L., Chitosan Nanomedicine in Cancer Therapy: Targeted Delivery and Cellular Uptake. *Macromolecular bioscience* **2021**, *21* (5), 2100005.
213. Deprey, K.; Batistatou, N.; Kritzer, J. A., A critical analysis of methods used to investigate the cellular uptake and subcellular localization of RNA therapeutics. *Nucleic Acids Res.* **2020**, *48* (14), 7623-7639.
214. Mohan, A.; Raj R., R.; Mohan, G.; K. P., P.; Thomas Maliekal, T., Reporters of Cancer Stem Cells as a Tool for Drug Discovery. *Frontiers in Oncology* **2021**, *11* (1270).
215. Subhash, N.; Sundaramurthy, V., Advances in host-based screening for compounds with intracellular anti-mycobacterial activity. *Cellular Microbiology n/a* (n/a), e13337.
216. Benítez-Chao, D. F.; León-Buitimea, A.; Lerma-Escalera, J. A.; Morones-Ramírez, J. R., Bacteriocins: An Overview of Antimicrobial, Toxicity, and Biosafety Assessment by in vivo Models. *Frontiers in Microbiology* **2021**, *12* (677).
217. Schäfer, A.-B.; Wenzel, M., A How-To Guide for Mode of Action Analysis of Antimicrobial Peptides. *Frontiers in Cellular and Infection Microbiology* **2020**, *10* (610).
218. Xu, Y.; Shrestha, N.; Préat, V.; Beloqui, A., An overview of in vitro, ex vivo and in vivo models for studying the transport of drugs across intestinal barriers. *Advanced drug delivery reviews* **2021**.
219. Lima, A.; Maddalo, D., SEMMs: Somatically Engineered Mouse Models. A New Tool for In Vivo Disease Modeling for Basic and Translational Research. *Frontiers in Oncology* **2021**, *11* (1177).
220. Rae, C.; Amato, F.; Braconi, C., Patient-Derived Organoids as a Model for Cancer Drug Discovery. *International journal of molecular sciences* **2021**, *22* (7), 3483.
221. Knobloch, J.; Suhendro, D. K.; Zieleniecki, J. L.; Shapter, J. G.; Köper, I., Membrane–drug interactions studied using model membrane systems. *Saudi Journal of Biological Sciences* **2015**, *22* (6), 714-718.
222. Sarkis, J.; Vié, V., Biomimetic Models to Investigate Membrane Biophysics Affecting Lipid–Protein Interaction. *Frontiers in Bioengineering and Biotechnology* **2020**, *8* (270).
223. Maget-Dana, R., The monolayer technique: a potent tool for studying the interfacial properties of antimicrobial and membrane-lytic peptides and their

- interactions with lipid membranes. *Biochimica Et Biophysica Acta-Biomembranes* **1999**, *1462* (1-2), 109-140.
224. Eeman, M.; Deleu, M., From biological membranes to biomimetic model membranes. *Biotechnologie, Agronomie, Société et Environnement* **2010**, *14* (4), 719-736.
225. Tripp, B. C.; Magda, J. J.; Andrade, J. D., Adsorption of Globular Proteins at the Air/Water Interface as Measured via Dynamic Surface Tension: Concentration Dependence, Mass-Transfer Considerations, and Adsorption Kinetics. *J. Colloid Interface Sci.* **1995**, *173* (1), 16-27.
226. Lad, M. D.; Birembaut, F.; Clifton, L. A.; Frazier, R. A.; Webster, J. R.; Green, R. J., Antimicrobial peptide-lipid binding interactions and binding selectivity. *Biophys. J.* **2007**, *92* (10), 3575-86.
227. Wilde, M.; Green, R. J.; Sanders, M. R.; Greco, F., Biophysical studies in polymer therapeutics: the interactions of anionic and cationic PAMAM dendrimers with lipid monolayers. *Journal of drug targeting* **2017**, *25* (9-10), 910-918.
228. Sanders, M. R.; Clifton, L. A.; Neylon, C.; Frazier, R. A.; Green, R. J., Selected wheat seed defense proteins exhibit competitive binding to model microbial lipid interfaces. *Journal of Agricultural and Food Chemistry* **2013**, *61* (28), 6890-900.
229. Phan, M. D.; Korotych, O. I.; Brady, N. G.; Davis, M. M.; Satija, S. K.; Ankner, J. F.; Bruce, B. D., X-ray and Neutron Reflectivity Studies of Styrene-Maleic Acid Copolymer Interactions with Galactolipid-Containing Monolayers. *Langmuir : the ACS journal of surfaces and colloids* **2020**, *36* (14), 3970-3980.
230. Auerswald, J.; Ebenhan, J.; Schwieger, C.; Scrima, A.; Meister, A.; Bacia, K., Measuring protein insertion areas in lipid monolayers by fluorescence correlation spectroscopy. *Biophysical journal* **2021**, *120* (8), 1333-1342.
231. Gudmand, M.; Fidorra, M.; Bjørnholm, T.; Heimburg, T., Diffusion and Partitioning of Fluorescent Lipid Probes in Phospholipid Monolayers. *Biophysical journal* **2009**, *96* (11), 4598-4609.
232. Shieh, I. C.; Zasadzinski, J. A., Visualizing monolayers with a water-soluble fluorophore to quantify adsorption, desorption, and the double layer. *Proceedings of the National Academy of Sciences* **2015**, *112* (8), E826-E835.
233. Langeveld, S. A. G.; Schwieger, C.; Beekers, I.; Blaffert, J.; van Rooij, T.; Blume, A.; Kooiman, K., Ligand Distribution and Lipid Phase Behavior in Phospholipid-Coated Microbubbles and Monolayers. *Langmuir : the ACS journal of surfaces and colloids* **2020**, *36* (12), 3221-3233.
234. Deleu, M.; Nott, K.; Brasseur, R.; Jacques, P.; Thonart, P.; Dufrêne, Y. F., Imaging mixed lipid monolayers by dynamic atomic force microscopy. *Biochimica et Biophysica Acta (BBA) - Biomembranes* **2001**, *1513* (1), 55-62.

235. Lima, L. M. C.; Fu, W.; Jiang, L.; Kros, A.; Schneider, G. F., Graphene-stabilized lipid monolayer heterostructures: a novel biomembrane superstructure. *Nanoscale* **2016**, *8* (44), 18646-18653.
236. Sanders, M. R.; Clifton, L. A.; Frazier, R. A.; Green, R. J., Role of Lipid Composition on the Interaction between a Tryptophan-Rich Protein and Model Bacterial Membranes. *Langmuir : the ACS journal of surfaces and colloids* **2016**, *32* (8), 2050-2057.
237. Kita-Tokarczyk, K.; Itel, F.; Grzelakowski, M.; Egli, S.; Rossbach, P.; Meier, W., Monolayer Interactions between Lipids and Amphiphilic Block Copolymers. *Langmuir : the ACS journal of surfaces and colloids* **2009**, *25* (17), 9847-9856.
238. Beddoes, C. M.; Case, C. P.; Briscoe, W. H., Understanding nanoparticle cellular entry: A physicochemical perspective. *Advances in colloid and interface science* **2015**, *218*, 48-68.
239. Stefaniu, C.; Brezesinski, G.; Möhwald, H., Langmuir monolayers as models to study processes at membrane surfaces. *Advances in colloid and interface science* **2014**, *208*, 197-213.
240. Andersson, J.; Köper, I., 3.03 - Biomimetic Membranes. In *Comprehensive Nanoscience and Nanotechnology (Second Edition)*, Andrews, D. L.; Lipson, R. H.; Nann, T., Eds. Academic Press: Oxford, 2019; pp 49-64.
241. Mueller, P.; Rudin, D. O.; Ti Tien, H.; Wescott, W. C., Reconstitution of Cell Membrane Structure in vitro and its Transformation into an Excitable System. *Nature* **1962**, *194* (4832), 979-980.
242. Winterhalter, M., Black lipid membranes. *Current Opinion in Colloid & Interface Science* **2000**, *5* (3), 250-255.
243. Ries, R. S.; Choi, H.; Blunck, R.; Bezanilla, F.; Heath, J. R., Black Lipid Membranes: Visualizing the Structure, Dynamics, and Substrate Dependence of Membranes. *The Journal of Physical Chemistry B* **2004**, *108* (41), 16040-16049.
244. Grewer, C.; Gameiro, A.; Mager, T.; Fendler, K., Electrophysiological Characterization of Membrane Transport Proteins. *Annual Review of Biophysics* **2013**, *42* (1), 95-120.
245. Block, S., Brownian Motion at Lipid Membranes: A Comparison of Hydrodynamic Models Describing and Experiments Quantifying Diffusion within Lipid Bilayers. *Biomolecules* **2018**, *8* (2), 30.
246. Simon, A.; Gounou, C.; Tan, S.; Tiefenauer, L.; Di Berardino, M.; Brisson, A. R., Free-standing lipid films stabilized by Annexin-A5. *Biochimica et Biophysica Acta (BBA)-Biomembranes* **2013**, *1828* (11), 2739-2744.

247. Mey, I.; Stephan, M.; Schmitt, E. K.; Müller, M. M.; Ben Amar, M.; Steinem, C.; Janshoff, A., Local Membrane Mechanics of Pore-Spanning Bilayers. *Journal of the American Chemical Society* **2009**, *131* (20), 7031-7039.
248. Zhou, Y.; Bright, L. K.; Shi, W.; Aspinwall, C. A.; Baker, L. A., Ion Channel Probes for Scanning Ion Conductance Microscopy. *Langmuir : the ACS journal of surfaces and colloids* **2014**, *30* (50), 15351-15355.
249. Kataoka-Hamai, C.; Miyahara, Y., Field-effect detection using phospholipid membranes. *Sci Technol Adv Mater* **2010**, *11* (3), 033001-033001.
250. White, R. J.; Zhang, B.; Daniel, S.; Tang, J. M.; Ervin, E. N.; Cremer, P. S.; White, H. S., Ionic Conductivity of the Aqueous Layer Separating a Lipid Bilayer Membrane and a Glass Support. *Langmuir : the ACS journal of surfaces and colloids* **2006**, *22* (25), 10777-10783.
251. Kepplinger, C.; Höfer, I.; Steinem, C., Impedance analysis of valinomycin activity in nano-BLMs. *Chemistry and physics of lipids* **2009**, *160* (2), 109-113.
252. Osaki, T.; Suzuki, H.; Le Pioufle, B.; Takeuchi, S., Multichannel Simultaneous Measurements of Single-Molecule Translocation in α -Hemolysin Nanopore Array. *Analytical Chemistry* **2009**, *81* (24), 9866-9870.
253. Han, X.; Studer, A.; Sehr, H.; Geissbühler, I.; Di Berardino, M.; Winkler, F. K.; Tiefenauer, L. X., Nanopore Arrays for Stable and Functional Free-Standing Lipid Bilayers. *Advanced Materials* **2007**, *19* (24), 4466-4470.
254. Wodzinska, K.; Blicher, A.; Heimburg, T., The thermodynamics of lipid ion channel formation in the absence and presence of anesthetics. BLM experiments and simulations. *Soft Matter* **2009**, *5* (17), 3319-3330.
255. Aminipour, Z.; Khorshid, M.; Keshvari, H.; Bonakdar, S.; Wagner, P.; Van der Bruggen, B., Passive permeability assay of doxorubicin through model cell membranes under cancerous and normal membrane potential conditions. *European Journal of Pharmaceutics and Biopharmaceutics* **2020**, *146*, 133-142.
256. Toca-Herrera, J. L.; Krasteva, N.; Müller, H.-J.; Krastev, R., Interactions in lipid stabilised foam films. *Advances in colloid and interface science* **2014**, *207*, 93-106.
257. Castellana, E. T.; Cremer, P. S., Solid supported lipid bilayers: From biophysical studies to sensor design. *Surface Science Reports* **2006**, *61* (10), 429-444.
258. Wacklin, H. P., Composition and Asymmetry in Supported Membranes Formed by Vesicle Fusion. *Langmuir* **2011**, *27* (12), 7698-7707.
259. Cremer, P. S.; Boxer, S. G., Formation and Spreading of Lipid Bilayers on Planar Glass Supports. *The Journal of Physical Chemistry B* **1999**, *103* (13), 2554-2559.

260. Luchini, A.; Nzulumike, A. N. O.; Lind, T. K.; Nylander, T.; Barker, R.; Arleth, L.; Mortensen, K.; Cárdenas, M., Towards biomimics of cell membranes: Structural effect of phosphatidylinositol triphosphate (PIP3) on a lipid bilayer. *Colloids and Surfaces B: Biointerfaces* **2019**, *173*, 202-209.
261. Meredith, S. A.; Yoneda, T.; Hancock, A. M.; Connell, S. D.; Evans, S. D.; Morigaki, K.; Adams, P. G., Model Lipid Membranes Assembled from Natural Plant Thylakoids into 2D Microarray Patterns as a Platform to Assess the Organization and Photophysics of Light-Harvesting Proteins. *Small* **2021**, *17* (14), 2006608.
262. Parkkila, P.; Elderdfi, M.; Bunker, A.; Viitala, T., Biophysical Characterization of Supported Lipid Bilayers Using Parallel Dual-Wavelength Surface Plasmon Resonance and Quartz Crystal Microbalance Measurements. *Langmuir : the ACS journal of surfaces and colloids* **2018**, *34* (27), 8081-8091.
263. Stahelin, R. V., Surface plasmon resonance: a useful technique for cell biologists to characterize biomolecular interactions. *Molecular Biology of the Cell* **2013**, *24* (7), 883-886.
264. Nyitrai, G.; Keszthelyi, T.; Bota, A.; Simon, A.; Toke, O.; Horvath, G.; Pal, I.; Kardos, J.; Heja, L., Sodium selective ion channel formation in living cell membranes by polyamidoamine dendrimer. *Biochim. Biophys. Acta* **2013**, *1828* (8), 1873-80.
265. Keszthelyi, T.; Hollo, G.; Nyitrai, G.; Kardos, J.; Heja, L., Bilayer Charge Reversal and Modification of Lipid Organization by Dendrimers as Observed by Sum-Frequency Vibrational Spectroscopy. *Langmuir : the ACS journal of surfaces and colloids* **2015**, *31* (28), 7815-25.
266. Rondelli, V.; Brocca, P.; Tranquilli, N.; Fragneto, G.; Del Favero, E.; Cantù, L., Building a biomimetic membrane for neutron reflectivity investigation: Complexity, asymmetry and contrast. *Biophysical Chemistry* **2017**, *229*, 135-141.
267. Andersson, J.; Bilotto, P.; Mears, L. L. E.; Fossati, S.; Ramach, U.; Köper, I.; Valtiner, M.; Knoll, W., Solid-supported lipid bilayers – A versatile tool for the structural and functional characterization of membrane proteins. *Methods* **2020**, *180*, 56-68.
268. Castillo-Sánchez, J. C.; Cruz, A.; Pérez-Gil, J., Structural hallmarks of lung surfactant: Lipid-protein interactions, membrane structure and future challenges. *Archives of Biochemistry and Biophysics* **2021**, *703*, 108850.
269. Richter, R. P.; Bérat, R.; Brisson, A. R., Formation of Solid-Supported Lipid Bilayers: An Integrated View. *Langmuir : the ACS journal of surfaces and colloids* **2006**, *22* (8), 3497-3505.
270. Zhang, L.; Granick, S., Lipid diffusion compared in outer and inner leaflets of planar supported bilayers. *The Journal of chemical physics* **2005**, *123* (21), 211104.

271. Mazur, F.; Bally, M.; Städler, B.; Chandrawati, R., Liposomes and lipid bilayers in biosensors. *Advances in colloid and interface science* **2017**, *249*, 88-99.
272. Deleu, M.; Crowet, J. M.; Nasir, M. N.; Lins, L., Complementary biophysical tools to investigate lipid specificity in the interaction between bioactive molecules and the plasma membrane: A review. *Biochimica et biophysica acta* **2014**, *1838* (12), 3171-3190.
273. Knoll, W.; Köper, I.; Naumann, R.; Sinner, E.-K., Tethered bimolecular lipid membranes—A novel model membrane platform. *Electrochimica Acta* **2008**, *53* (23), 6680-6689.
274. Rossi, C.; Doumiati, S.; Lazzairelli, C.; Davi, M.; Meddar, F.; Ladant, D.; Chopineau, J., A Tethered Bilayer Assembled on Top of Immobilized Calmodulin to Mimic Cellular Compartmentalization. *PLOS ONE* **2011**, *6* (4), e19101.
275. Junghans, A.; Köper, I., Structural Analysis of Tethered Bilayer Lipid Membranes. *Langmuir : the ACS journal of surfaces and colloids* **2010**, *26* (13), 11035-11040.
276. Tanaka, M.; Sackmann, E., Polymer-supported membranes as models of the cell surface. *Nature* **2005**, *437* (7059), 656-663.
277. Lin, Y.-H.; Minner, D. E.; Herring, V. L.; Naumann, C. A., Physisorbed Polymer-Tethered Lipid Bilayer with Lipopolymer Gradient. *Materials* **2012**, *5* (11), 2243-2257.
278. Förting, A.; Jordan, R.; Graf, K.; Schiavon, G.; Purrucker, O.; Tanaka, M. In *Solid-supported biomimetic membranes with tailored lipopolymer tethers*, Macromolecular Symposia, Wiley Online Library: 2004; pp 329-338.
279. Knoll, W.; Frank, C. W.; Heibel, C.; Naumann, R.; Offenhäusser, A.; Rühle, J.; Schmidt, E. K.; Shen, W. W.; Sinner, A., Functional tethered lipid bilayers. *Reviews in Molecular Biotechnology* **2000**, *74* (3), 137-158.
280. Gregoriadis, G.; Perrie, Y., Liposomes. In *Encyclopedia of Life Sciences (ELS)*, John Wiley & Sons, Ltd: Chichester, 2010.
281. Shi, L.; Howan, K.; Shen, Q.-T.; Wang, Y. J.; Rothman, J. E.; Pincet, F., Preparation and characterization of SNARE-containing nanodiscs and direct study of cargo release through fusion pores. *Nature Protocols* **2013**, *8* (5), 935-948.
282. Pinot, M.; Vanni, S.; Pagnotta, S.; Lacas-Gervais, S.; Payet, L.-A.; Ferreira, T.; Gautier, R.; Goud, B.; Antonny, B.; Barelli, H., Polyunsaturated phospholipids facilitate membrane deformation and fission by endocytic proteins. *Science* **2014**, *345* (6197), 693-697.
283. Przybylo, M.; Sýkora, J.; Humpolíčková, J.; Benda, A.; Zan, A.; Hof, M., Lipid diffusion in giant unilamellar vesicles is more than 2 times faster than in supported

phospholipid bilayers under identical conditions. *Langmuir : the ACS journal of surfaces and colloids* **2006**, 22 (22), 9096-9099.

284. Morlot, S.; Roux, A., Mechanics of dynamin-mediated membrane fission. *Annual review of biophysics* **2013**, 42, 629-649.

285. Sideratou, Z.; Tsiourvas, D.; Paleos, C. M.; Tsortos, A.; Nounesis, G., Molecular Recognition of Complementary Liposomes: The Enhancing Role of Cholesterol. *Langmuir : the ACS journal of surfaces and colloids* **2000**, 16, 9186-9191.

286. Pantos, A.; Tsiourvas, D.; Paleos, C.; Nounesis, G., Enhanced drug transport from unilamellar to multilamellar liposomes induced by molecular recognition of their lipid membranes. *Langmuir : the ACS journal of surfaces and colloids* **2005**, 21 (15), 6696-6702.

287. Đtimac, A.; Cvitba, J. T. j.; Frkanec, L.; Vugrek, O.; Frkanec, R. a. In *Molecular recognition of ConA and mannose on liposome surface*, 2015.

288. Conrard, L.; Tyteca, D., Regulation of Membrane Calcium Transport Proteins by the Surrounding Lipid Environment. *Biomolecules* **2019**, 9 (10), 513.

289. Pollock, S.; Antrobus, R.; Newton, L.; Kampa, B.; Rossa, J.; Latham, S.; Nichita, N. B.; Dwek, R. A.; Zitzmann, N., Uptake and trafficking of liposomes to the endoplasmic reticulum. *The FASEB Journal* **2010**, 24 (6), 1866-1878.

290. Tomori, Y.; Iijima, N.; Hinuma, S.; Ishii, H.; Takumi, K.; Takai, S.; Ozawa, H., Morphological Analysis of Trafficking and Processing of Anionic and Cationic Liposomes in Cultured Cells. *Acta Histochem Cytochem* **2018**, 51 (2), 81-92.

291. Voskuhl, J.; Ravoo, B. J., Molecular recognition of bilayer vesicles. *Chemical Society reviews* **2009**, 38 (2), 495-505.

292. Pantos, A.; Tsiourvas, D.; Nounesis, G.; Paleos, C., Interaction of functional dendrimers with multilamellar liposomes: Design of a model system for studying drug delivery. *Langmuir : the ACS journal of surfaces and colloids* **2005**, 21 (16), 7483-7490.

293. Pinheiro, M.; Magalhães, J.; Reis, S., Antibiotic interactions using liposomes as model lipid membranes. *Chemistry and physics of lipids* **2019**, 222, 36-46.

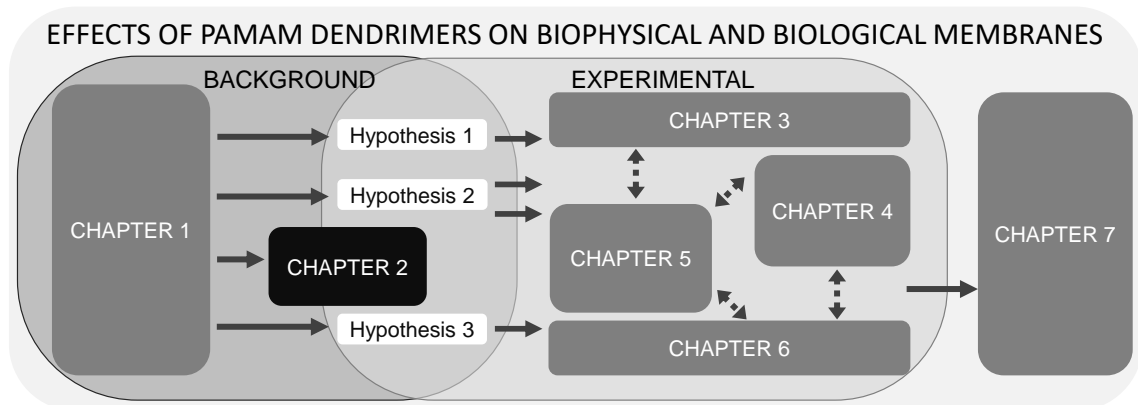
294. Hasan, M.; Yamazaki, M., Elementary Processes and Mechanisms of Interactions of Antimicrobial Peptides with Membranes-Single Giant Unilamellar Vesicle Studies. *Adv Exp Med Biol* **2019**, 1117, 17-32.

295. Pattni, B. S.; Chupin, V. V.; Torchilin, V. P., New Developments in Liposomal Drug Delivery. *Chemical Reviews* **2015**, 115 (19), 10938-10966.

296. Al-Jamal, W. T.; Kostarelos, K., Liposomes: From a Clinically Established Drug Delivery System to a Nanoparticle Platform for Theranostic Nanomedicine. *Accounts of Chemical Research* **2011**, *44* (10), 1094-1104.
297. Kanchi, S.; Gosika, M.; Ayappa, K. G.; Maiti, P. K., Dendrimer Interactions with Lipid Bilayer: Comparison of Force Field and Effect of Implicit vs Explicit Solvation. *Journal of Chemical Theory and Computation* **2018**, *14* (7), 3825-3839.
298. Jafari, M.; Mehrnejad, F.; Talandashti, R.; Doustdar, F.; Reza Vakili, M.; Lavasanifar, A., Effect of the lipid composition and cholesterol on the membrane selectivity of low generations PAMAM dendrimers: A molecular dynamics simulation study. *Applied Surface Science* **2021**, *540*, 148274.
299. Mecke, A.; Uppuluri, S.; Sassanella, T. M.; Lee, D. K.; Ramamoorthy, A.; Baker, J. R., Jr.; Orr, B. G.; Banaszak Holl, M. M., Direct observation of lipid bilayer disruption by poly(amidoamine) dendrimers. *Chemistry and physics of lipids* **2004**, *132* (1), 3-14.
300. Shcharbin, D.; Drapeza, A.; Loban, V.; Lisichenok, A.; Bryszewska, M., The breakdown of bilayer lipid membranes by dendrimers. *Cellular & molecular biology letters* **2006**, *11* (2), 242-8.
301. Parimi, S.; Barnes, T.; Prestidge, C., PAMAM Dendrimer Interactions with Supported Lipid Bilayers: A Kinetic and Mechanistic Investigation. *Langmuir : the ACS journal of surfaces and colloids* **2008**, *24* (23), 13532-13539.
302. Berenyi, S.; Mihaly, J.; Wacha, A.; Toke, O.; Bota, A., A mechanistic view of lipid membrane disrupting effect of PAMAM dendrimers. *Colloids and Surfaces, B: Biointerfaces* **2014**, *118*, 164-71.
303. Akesson, A.; Lind, T. K.; Barker, R.; Hughes, A.; Cardenas, M., Unraveling dendrimer translocation across cell membrane mimics. *Langmuir : the ACS journal of surfaces and colloids* **2012**, *28* (36), 13025-33.
304. Tiriveedhi, V.; Kitchens, K. M.; Nevels, K. J.; Ghandehari, H.; Butko, P., Kinetic analysis of the interaction between poly(amidoamine) dendrimers and model lipid membranes. *Biochimica et Biophysica Acta (BBA) - Biomembranes* **2011**, *1808* (1), 209-218.
305. Tian, W.-d.; Ma, Y.-q., pH-responsive dendrimers interacting with lipid membranes. *Soft Matter* **2012**, *8* (9), 2627-2632.
306. Tribet, C.; Vial, F., Flexible macromolecules attached to lipid bilayers: impact on fluidity, curvature, permeability and stability of the membranes. *Soft Matter* **2008**, *4* (1), 68-81.
307. Fox, L. J.; Matthews, L.; Stockdale, H.; Pichai, S.; Snow, T.; Richardson, R. M.; Briscoe, W. H., Structural changes in lipid mesophases due to intercalation of dendritic polymer nanoparticles: Swollen lamellae, suppressed curvature, and augmented structural disorder. *Acta Biomater* **2020**, *104*, 198-209.

308. Fox, L. J.; Slastanova, A.; Taylor, N.; Wlodek, M.; Bikondoa, O.; Richardson, R. M.; Briscoe, W. H., Interactions between PAMAM dendrimers and DOPC lipid multilayers: Membrane thinning and structural disorder. *Biochimica et Biophysica Acta (BBA) - General Subjects* **2021**, *1865* (4), 129542.
309. Sezgin, E.; Schwille, P., Model membrane platforms to study protein-membrane interactions. *Molecular Membrane Biology* **2012**, *29* (5), 144-154.

CHAPTER 2: METHODOLOGY



This chapter aims to provide more information on the experimental techniques Surface Pressure Measurements and Neutron Reflectometry and a general indication on how to interpret results generated from those techniques.

2 METHODOLOGY

2.1 MATERIALS

Salts, solvents, and deuterium oxide (D₂O) for buffers were obtained from Sigma Aldrich (UK) and Fisher Scientific (UK.) Ultrapure (UHQ grade, 18.2 mΩ) water was produced in-house by an ELGA water purifier. Phosphate buffers (I = 0.034 M) at pH 4, pH 7 and pH 10 were prepared in either UHQ grade water or D₂O. D₂O-buffers were used for neutron reflectometry and external reflection FTIR only whereas aqueous phosphate buffers were used for all other techniques. Enriched salt buffer was prepared adding 144 mM sodium chloride to phosphate buffer pH 7.

1,2-dipalmitoyl-*sn*-glycero-3-phosphocholine (hydrogenated, h-DPPC, 734 g mol⁻¹); 1,2-dipalmitoyl-d62-*sn*-glycero-3-phosphocholine (deuterated, d-DPPC, 796 g mol⁻¹); 1,2-dipalmitoyl-*sn*-glycero-3-phospho-(1'-*rac*-glycerol) (sodium salt) (hydrogenated, h-DPPG, 744 g mol⁻¹) were purchased from Avanti Polar Lipids Inc (USA) and used without further purification. The powdered phospholipids were dissolved in chloroform to lipid stocks of a concentration of 0.5 – 1 mg mL⁻¹. DPPG required up to 10% methanol as solubility enhancer. The chemical structures of the lipids are shown in the Supplementary section 5.6.1 in Table 5-2.

Methanol solutions of amine-terminated PAMAM G5 (28,826 g mol⁻¹), and G3 (6,909 g mol⁻¹), and carboxyl-terminated PAMAM G4.5 (26,258 g mol⁻¹) and G2.5 (6,267 g mol⁻¹) were obtained from Sigma-Aldrich (UK). Dilutions in phosphate buffer were made with and without prior methanol removal (depending on the type of experiment) and the final PAMAM concentrations for each model system are summarized in Table 2-1. Structural information of PAMAM dendrimers can be retrieved in Section 1.1.1, Figure 1-1.

Table 2-1 Final PAMAM concentrations used for membrane interaction studies.

Experimental model system	PAMAM G5	PAMAM G4.5	PAMAM G3	PAMAM G2.5
Lipid Monolayers	0.3; 0.12; 0.06; 0.024; 0.018; 0.012; 0.0024 mg mL ⁻¹	0.3; 0.18; 0.12; 0.06; 0.012 mg mL ⁻¹	N/A	N/A
Supported Lipid Bilayers	0.3; 0.06 mg mL ⁻¹	0.06 mg mL ⁻¹	N/A	N/A
Bacterial Strains	1, 0.1; 0.01; 0.001 mg mL ⁻¹ ;	1, 0.1; 0.01; 0.001 mg mL ⁻¹	1 mg mL ⁻¹	1 mg mL ⁻¹

2.2 SURFACE PRESSURE MEASUREMENTS

The method was used to measure changes in surface pressure of a lipid monolayer at the air/liquid interface upon the adsorption of polymer from the sub phase and to aid the preparation of phospholipid monolayers stable in the condensed phase¹. The Langmuir trough and surface pressure measurements were also used to prepare monolayers for use with other analytical techniques.

Surface pressure (π) is equal to the surface tension of a clean water interface (γ_0) subtracted by the surface tension measured (γ) by the pressure sensor (Wilhelmy plate).

$$\pi = \gamma_0 - \gamma$$

The force due to the surface tension (γ) on the Wilhelmy plate, when partially immersed into the subphase, is measured. The force is converted to surface tension only with knowledge of the plate dimension (length, width).

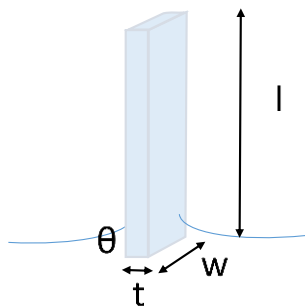


Figure 2-1 Wilhelmy plate submerged in subphase, where θ is the contact angle, t thickness, w width and l length of the plate.

The Wilhelmy plate consists of a small strip of chromatography paper, used to maintain the contact angle at 0° . The weight of the plate is set to zero before each surface pressure reading. Surface tension is determined as shown as follows

$$\gamma = \frac{\text{force}}{2(w + t)}$$

2.2.1 Preparation of the Langmuir trough

For the surface pressure measurements a small Langmuir-Blodgett Trough (Nima Type 611)(Figure 2-2a) with two moveable Teflon barriers was used. The Wilhelmy plate was made of filter paper.

Prior to each experiment, the trough and barriers were cleaned thoroughly with repeated washing steps involving ethanol and UHQ grade water. After the cleaning procedure the surfaces were wiped with pure chloroform to remove any residual contaminations, and then filled with 80 mL of phosphate buffer.

Impurities (i.e. dust particles) were removed from the surface by aspiration, and cleanliness of the surface checked through compression on the bare subphase. The presence of impurities could then be observed by an increase in the surface pressure. Compression and aspiration of the bare subphase was repeated until no increase in surface pressure ($< 0.2 \text{ mN m}^{-1}$) was observed. Once the surface was prepared the barriers were placed in the open position in preparation for lipid layer formation.

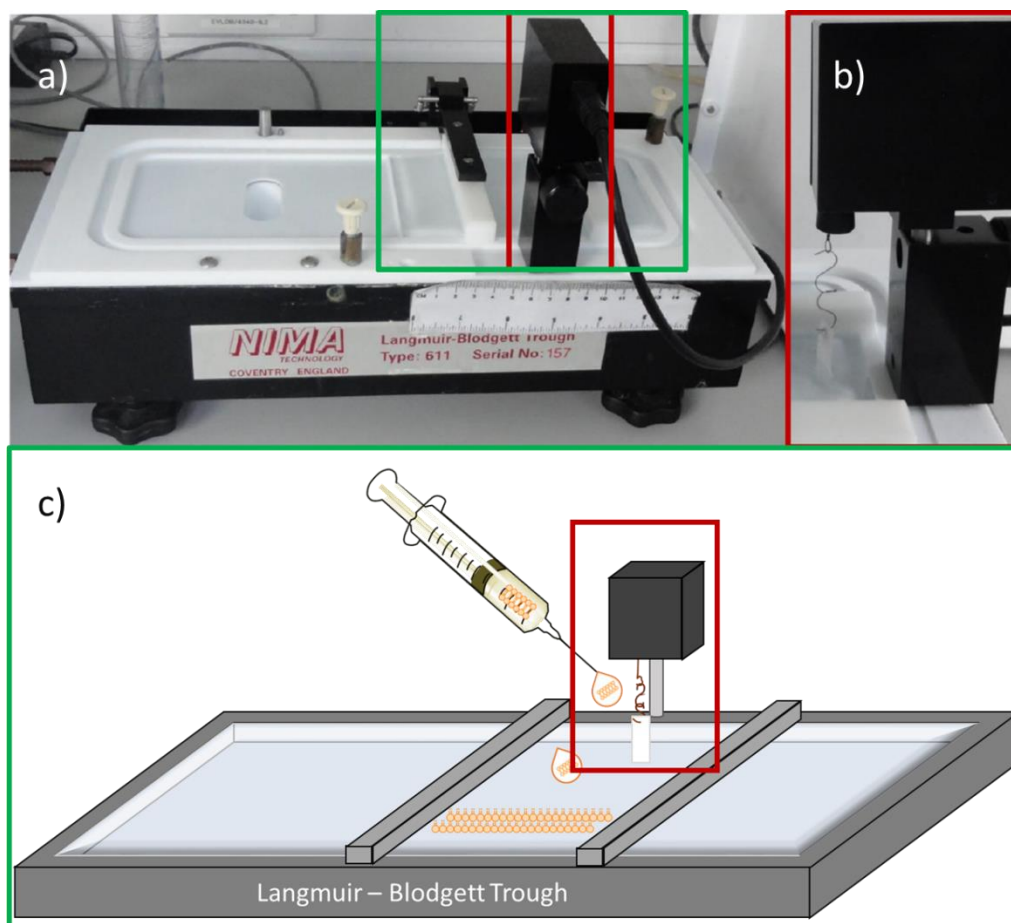


Figure 2-2 Langmuir Blodgett trough setup. The instrument is shown in situ in panel a), with a close-up of the pressure sensor and the Wilhelmy plate in panel b). A simplified illustration of the setup and preparing the lipid monolayer is shown in panel c).

2.2.2 Preparation of lipid monolayers

Depending on lipid type, the powder lipids were dissolved in chloroform or chloroform-methanol mixture and small quantities (μl range) of this stock solution were spread dropwise onto the subphase. Time was allowed for the chloroform to evaporate, which was indicated by the lipid surface pressure stabilizing near the baseline.

Surface pressure (π) – area per molecule (\AA^2) isotherms of the lipid monolayers were recorded to ensure verify their quality and stability, but also to observe the phase transitions and ensure the monolayers are in the solid state at the chosen pressure for sample addition. Exemplary compression isotherms of DPPC and DPPG monolayers are shown in *Figure 2-3*, prominent phase transitions from the liquid-expanded (LE) to the liquid-condensed (LC) state and

from the LC to the solid (S) state could be demonstrated indicating high quality monolayers.

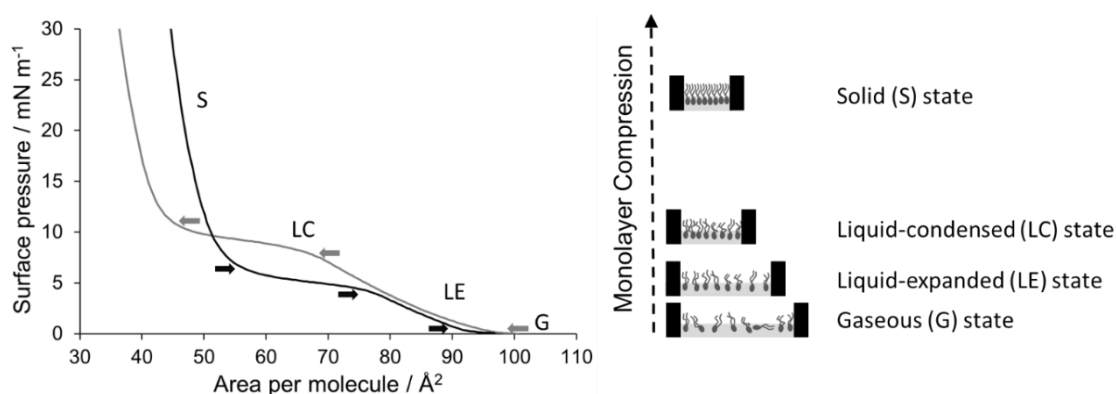


Figure 2-3 Exemplary compression isotherms of DPPC (black) and DPPG (grey) monolayers at room temperature. At large areas per molecule, the monolayers exist in the gaseous state (G) and undergo a phase transition to the liquid-expanded state (LE) during compression. Upon further compression, the LE phase undergoes first a transition to the liquid-condensed state (LC); and finally, the monolayer reaches the solid state (S). The orientation of the molecules in the different phases is schematically illustrated. Arrows indicate lipid phase transitions. Illustration inspired by Oliveira et al 2017² and Maget-Dana 1999¹.

The surface area was held constant by barriers allow for the lipid layer stabilization (lipids in solid state) around the target initial pressure.

2.2.3 Dendrimer addition

Once the lipid monolayer was stable, 2mL of concentrated dendrimer solution (in buffer) was carefully added into the phosphate buffer subphase with a custom-made needle. The changes in surface pressure were monitored for at least 60 min. The maximum value of change in surface pressure (Δ) was determined and used for further analysis. An illustration of the complete process provided in Figure 2-4.

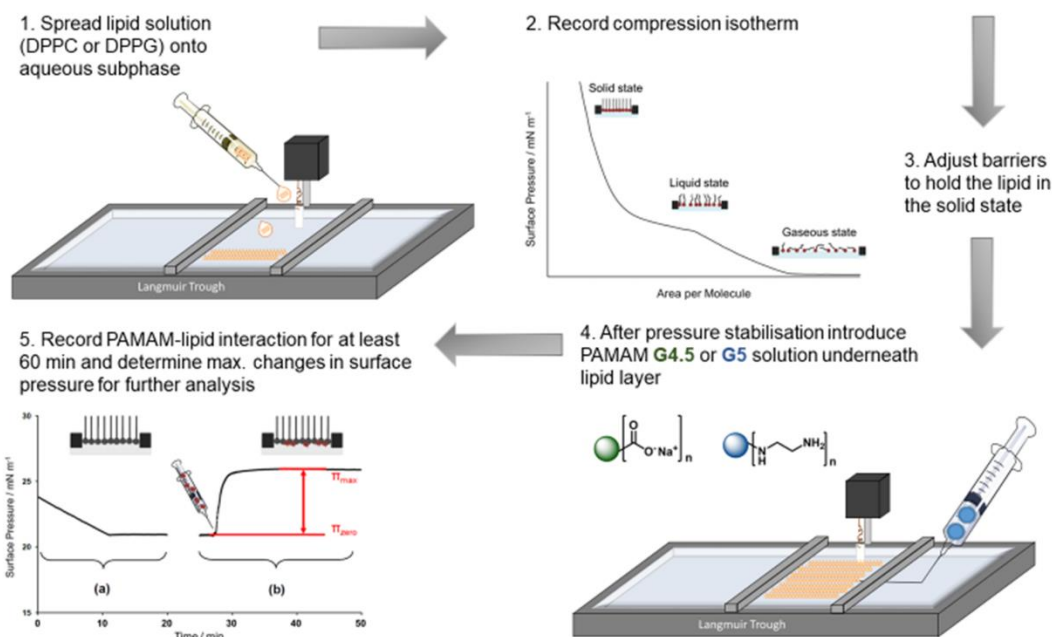


Figure 2-4 Illustration of the experimental steps on the Langmuir trough, including lipid monolayer preparation and PAMAM addition.

2.2.4 Data interpretation

This technique is sensitive to changes in surface pressure, and these are caused when the lipid monolayer is disturbed and changes in lateral packing occur. Therefore, the changes are most likely related to penetration of molecules into the lipid layer or changes to the lipid layer itself (i.e. bending). Membrane-active molecules either adsorb below lipid head area or penetrate into the lipid layer and intercalate between the lipid molecules and in the worst case destroy the lipid layer (surface pressure decrease). In Figure 2-5 the adsorption and penetration mechanism are simplified and the resulting changes in surface pressure parameters indicated.

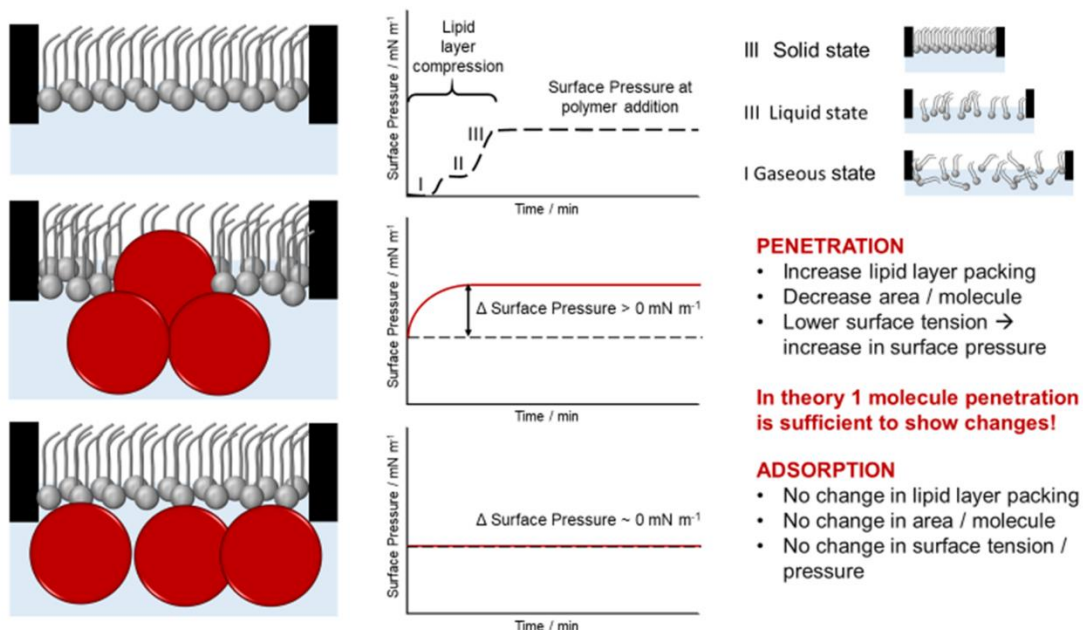


Figure 2-5 Schematic adsorption and penetration of membrane-active molecules into lipid monolayers with related changes in surface pressure.

2.3 NEUTRON REFLECTOMETRY

2.3.1 Fabrication of lipid bilayers on to solid supports

Lipid monolayers were created according to the techniques described in Section 2.1.2 with the difference that a cooled, nonbuffered water subphase containing 5 mM CaCl_2 was used. Prior to monolayer deposition, the lipids were compressed to a surface pressure of $> 35 \text{ mN m}^{-1}$.

The lipid bilayers were deposited onto polished silicon crystals utilizing a purpose-built LB trough (KSV-Nima, Biolin Scientific, Finland)³. The inner leaflet of the membrane was fabricated by LB deposition of either tail-hydrogenated h-DPPC or tail-deuterated d-DPPC onto the silicon surface. Thereby, the silicon block is immersed into the subphase prior to creating the lipid film on the surface. Langmuir–Schaeffer (LS) deposition of h-DPPC or h-DDPG was used for the outer leaflet⁴ as shown in Figure 2-6, in that step the lipid film is created first and the crystal with the already deposited inner leaflet is “pushed” onto the second monolayer to create the bilayer. The crystal with the deposited bilayer was then placed in a purpose-built liquid flow cell for analysis of the silicon-liquid interface.

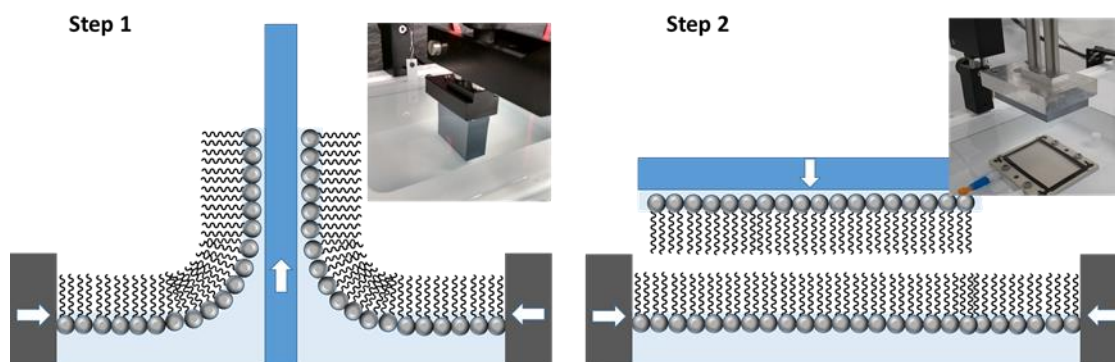


Figure 2-6 Preparation of a supported bilayer. First step is the Langmuir-Blodgett deposition of a lipid monolayer onto the silicon substrate. The second (outer) leaflet of the bilayer is created in Step 2 using the Langmuir-Schaefer deposition. Illustration inspired by Belegriou et al 2010⁵.

2.3.2 Neutron reflectivity measurements

Measurements were performed on the specular INTER⁶ and SURF reflectometer at the Rutherford Appleton Laboratory (Oxfordshire, UK), using a neutron spectrum with wavelengths from 1 to 16 Å. The reflection intensity was recorded at angles of 0.7° and 2.3° to cover a momentum transfer range Q_z of 0.01 – 0.5 Å⁻¹ ($Q_z = (4\pi \sin \theta)/\lambda$; λ = wavelength; θ = incident angle). The liquid flow cells containing the deposited bilayer were placed on a variable angle stage in the beamline and connected to the pump to enable automatic change of solution contrasts. The setup of the liquid flow cells and part of the INTER beamline is shown in Figure 2-7 and 2-8.

For experiment we used a chain-deuterated and chain-hydrogenated lipid bilayer. The isotopic solutions contrasts were H₂O and D₂O-based phosphate buffers and silicon-matched water (SMW; 38% D₂O: 62% H₂O), both as buffer-only and PAMAM-containing contrast. The lipid bilayers were first characterized with all contrasts on their own to check the quality of the layer and generate baseline data. Then, the bilayers were studied again under the addition of the PAMAM solutions. Therefore, up to 12 reflectivity contrasts were generated in each PAMAM system.

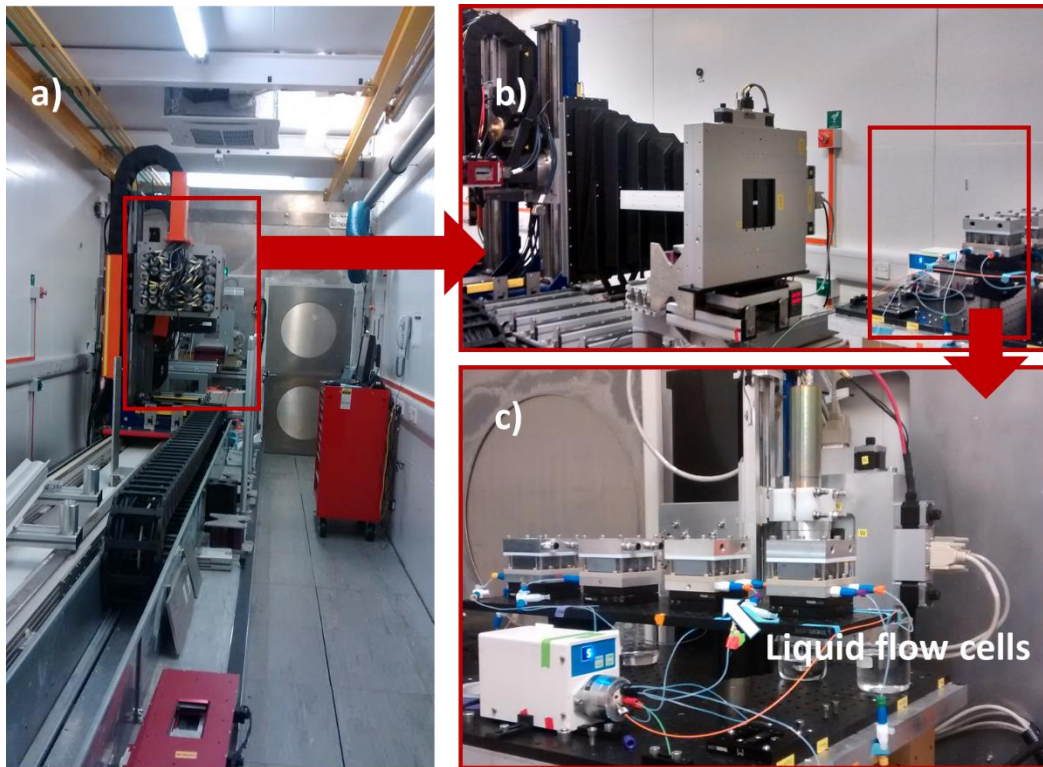


Figure 2-7 Setup in the INTER Beamline. Panel a) shows the view into the beamline with the mirror and detector area highlighted by the red box. Panel b) and c) show the setup of the liquid flow cells on the movable stage and connection to the pump.

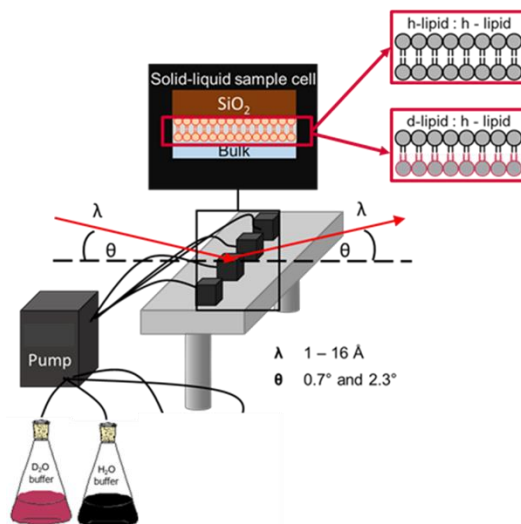


Figure 2-8 Simplified setup of the neutron experiment at INTER shown in Figure 2-7 panel c.

2.3.3 Simplified interpretation of neutron reflectivity data

The reflectivity raw data were fitted with Rascal⁷, the STFC/ ISIS own analysis software. Models could be customized to the available solution contrasts and lipid systems used. Here, we used a five-layer slab model, that accounts for the silicon subphase, inner leaflet lipid headgroups, inner leaflet lipid tails, outer leaflet lipid tails and outer leaflet headgroups. The bulk solution contrast (including PAMAMs) was also fitted. Fitting the reflectivity data resulted in scattering length densities (SLD) profiles, that could then indicate any changes to one of the layers. A simplistic overview on those changes caused by membrane-active molecules is given in Figure 2-9. It should be noted that neutron scattering dependent on the atomistic composition of the studied materials and differences between the material and the solution contrasts. Therefore, the changes visible will be most pronounced when the material SLD is distinctively different from the solution contrast SLD, i.e. hydrogenated tails in D₂O contrast or deuterated tails in H₂O contrast.

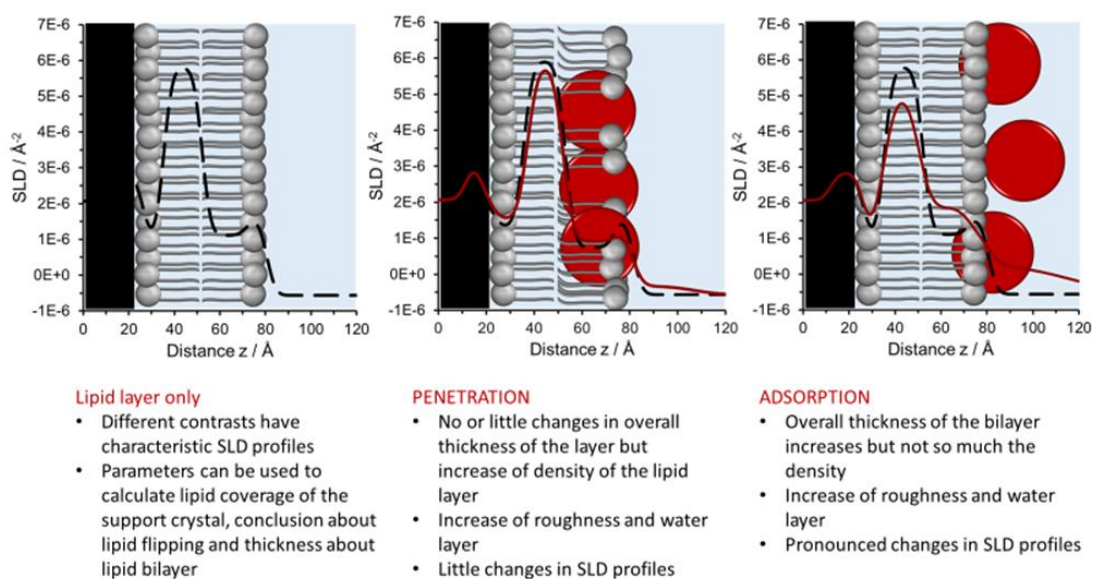


Figure 2-9 Potential changes in the SLD profiles caused by membrane-active molecules.

2.4 GENERAL DATA ANALYSIS, DRAWING AND FIGURE SYNTHESIS

Where no instrument-specific software was required, data wrangling and general data analysis was conducted in Microsoft Excel (Microsoft 365).

Final statistical analysis was performed with GraphPad Prism 8.4.1. ChemDraw and Chem3D (ChemOffice 20.0) were used for structural drawing and visualization of scientific objects.

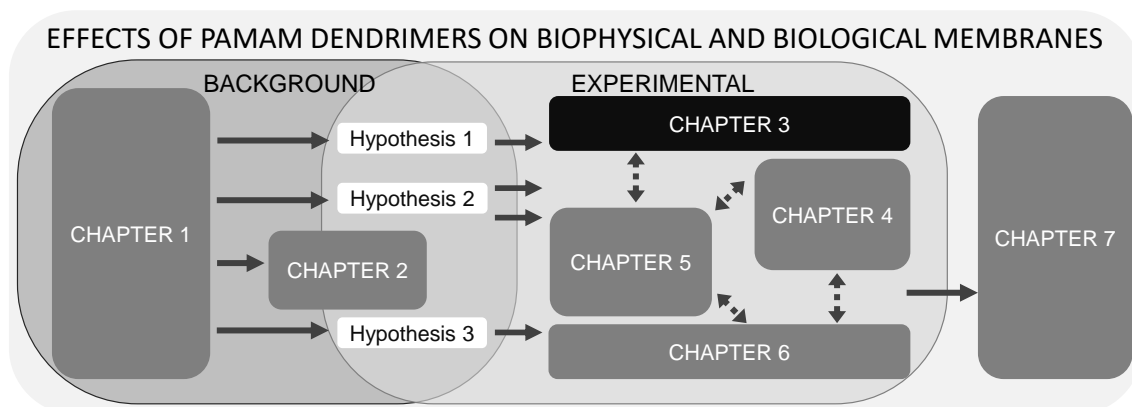
Unless stated otherwise, illustrations were created by the PhD candidate based on the knowledge and ideas of the candidate that were derived from broad reading of textbooks and research articles in the field. Complex figures and illustrations were synthesized in Microsoft Powerpoint, in combination with elements from ChemDraw, own Microsoft Excel graphs and photographs.

2.5 REFERENCES

1. Maget-Dana, R., The monolayer technique: a potent tool for studying the interfacial properties of antimicrobial and membrane-lytic peptides and their interactions with lipid membranes. *Biochimica Et Biophysica Acta-Biomembranes* **1999**, *1462* (1-2), 109-140.
2. de Oliveira, R. F.; de Barros, A.; Ferreira, M., 4 - Nanostructured Films: Langmuir–Blodgett (LB) and Layer-by-Layer (LbL) Techniques. In *Nanostructures*, Da Róz, A. L.; Ferreira, M.; de Lima Leite, F.; Oliveira, O. N., Eds. William Andrew Publishing: 2017; pp 105-123.
3. Hughes, A. V.; Howse, J. R.; Dabkowska, A.; Jones, R. A.; Lawrence, M. J.; Roser, S. J., Floating lipid bilayers deposited on chemically grafted phosphatidylcholine surfaces. *Langmuir : the ACS journal of surfaces and colloids* **2008**, *24* (5), 1989-1999.
4. Tamm, L. K.; McConnell, H. M., Supported phospholipid bilayers. *Biophysical journal* **1985**, *47* (1), 105-113.
5. Belegriou, S.; Dorn, J.; Kreiter, M.; Kita-Tokarczyk, K.; Sinner, E.-K.; Meier, W., Biomimetic supported membranes from amphiphilic block copolymers. *Soft Matter* **2010**, *6* (1), 179-186.
6. Webster, J.; Holt, S.; Dalgliesh, R., INTER the chemical interfaces reflectometer on target station 2 at ISIS. *Phys. B. (Amsterdam, Netherlands)* **2006**, *385-386*, 1164-1166.

7. Hughes, A. V. *RasCal*, 2014 Beta; ISIS Spallation Neutron Source (Rutherford Appleton Laboratory): <http://sourceforge.net/projects/rscl/>, 2014.

CHAPTER 3: PH AND METHANOL RESPONSIVE CONFORMATIONAL CHANGES OF POLY(AMIDOAMINE) DENDRIMERS IN SOLUTION



This chapter on the solution behavior of PAMAM G4.5 and G5 represents a collaborative work with the Department of Mathematics and Statistics, Department of Chemistry and Diamond Light Source. It was submitted to the Scientific Journal ACS Applied Polymer Materials and is currently under review.

The estimated contribution of the candidate to the work described in this chapter is 70 %.

MW: Conceptualization, Data curation, Formal analysis, Investigation, Project administration, Validation, Visualization, Writing – original draft

FG: Conceptualization, Funding acquisition, Supervision, Writing – review & editing

RJG: Conceptualization, Funding acquisition, Supervision, Writing – review & editing

Collaboration: Molecular Simulations

CW: Data curation, Software, Formal analysis, Investigation, Methodology, Validation, Visualization, Writing – original draft Simulation part

ZW: Conceptualization, Funding acquisition, Methodology, Resources, Software, Supervision, Writing – review & editing

Collaboration: SAXS

CJCEG: Data curation, Formal analysis, Funding acquisition, Investigation, Validation, Writing – review & editing

IWH: Resources, Funding acquisition, Supervision, Writing – review & editing

3 PH AND METHANOL RESPONSIVE CONFORMATIONAL CHANGES OF POLY(AMIDOAMINE) DENDRIMERS IN SOLUTION

Marleen Wilde^a, Christopher Wilde^b, Charlotte J.C. Edwards-Gayle^c, Ian W. Hamley^d, Zouwei Wang^b, Francesca Greco^a, Rebecca R. Green^a

^a University of Reading, Department of Pharmacy, RG6 6AD

^b University of Reading, Department of Mathematics and Statistics, RG6 6AX

^c Diamond Light Source, Harwell Science and Innovation Campus, OX11 0DE

^d University of Reading, Department of Chemistry, RG6 6AD, UK

KEYWORDS:

PAMAM, methanol, fluorescence, SAXS, Molecular Dynamics, pH

ABBREVIATIONS

PAMAM, poly(amidoamine); UV/VIS, ultraviolet/ visible light; SAXS, small angle X-ray scattering; MD, molecular dynamics; CG, coarse-grained; CoM, center of mass.

ACKNOWLEDGMENT / FUNDING

We are grateful to Diamond Light Source for the award to IWH (SM217118) and CJCEG (SM26698-1) of SAXS beam time on beamline B21.

ABSTRACT

Poly(amidoamine) (PAMAM) dendrimers potentially have a wide range of biomedical applications and therefore it is important to understand their behavior in physiological solutions. This work studied solutions of full-generation PAMAM G5 (-NH₂) and half-generation PAMAM G4.5 (-COOH) in phosphate buffer of different pH, and with and without residual methanol as a co-solvent. The effect of the various solvent conditions was experimentally evaluated by using spectroscopic (UV/Vis, fluorescence) and scattering (SAXS) techniques, and computational simulations (coarse-grained MD with implicit solvent). Taken together the results showed that the molecular structure was affected by the presence of methanol and pH, highlighting the importance of experimental parameters when interpreting data from PAMAM systems. Changing pH was also shown to alter PAMAM three-dimensional structure. Differences between the behavior of the full and half generation PAMAMs are attributed to the changes in molecular charge under the different solution conditions used.

3.1 INTRODUCTION

Dendrimers, specifically poly(amidoamines) (PAMAMs), first described by Tomalia and co-workers¹, display a symmetric, well-defined molecular architecture with very low polydispersity² and functionalized surface groups which allow tuning of properties such as solubility, miscibility and reactivity.³ Their general structure consists of three distinct domains: (i) an initiator core, (ii) radially joined layers (generations) of repeating units, and (iii) an exterior surface functionality whereby the number of exterior surface groups doubles with each generation number.

Dendrimers are available commercially in generations G0 to G10 with a range of different cores and functional surface groups. Given their numerous modifications deriving from research, their diversity allows a variety of applications, not only in the biomedical field (summarized in Table 3-1).

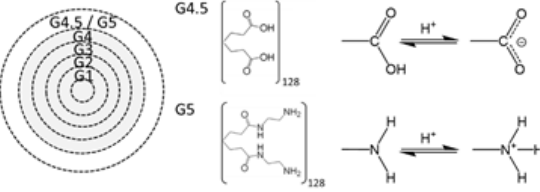
Table 3-1 PAMAM applications using different strategies of chemical alterations. References are exemplary for the application, but not comprehensive.

	Native or Surface-modified	Non-covalent (Complexed or Encapsulated)	Covalent (Conjugated)
Therapeutic	API ⁴ , Active Scaffold for Dental Remineralisation ⁵	Hydrophobic Drugs ⁶ , Nucleic Acids ⁷ , Proteins ⁸	Drugs ⁹ , Peptides ¹⁰ , Antibodies ¹¹ , Folate ¹²
Diagnostic / Imaging	Fluorescent Tags ¹³ , Intrinsic Fluorescence ¹⁴	Contrast/ Imaging Agents ^{15, 16}	Metals ¹⁷ , Imaging Agents ¹⁸ , Antibodies ¹⁹
Theranostic	N.A.	Imaging Agent + Cancer Drug ²⁰	Fluorescent Tag+ Peptide ²¹
Other / Ex-vivo	Biosensor ²² , Biomaterial ²³	Catalyst ²⁴ , Semiconductor ²⁵	Bioadhesive ²⁶ , Optical Sensing ²⁷

Since PAMAM dendrimers are promising candidates in therapeutic and diagnostic applications, they require increased efforts to elucidate their structure and properties at (sub-) cellular levels. To date, the toxic effects of the cationic surface groups of the dendrimers are still limiting their clinical use²⁸⁻³⁰. In comparison, PAMAMs with carboxyl or hydroxyl surface groups are considerably less or even non-toxic to eukaryotic organisms^{31, 32}, but fewer studies have focused on their interactions and potential applications. Recently, half-generation PAMAMs (carboxyl surface groups) have been investigated for applications in dental regeneration,³³ delivery of cancer therapeutics³⁴⁻³⁶ and inflammatory agents^{37, 38}.

Biological experiments involving PAMAM dendrimers typically involve applying the dendrimer onto a biological model (e.g. mammalian cells) and then measure an experimental output (e.g. fluorescence, UV/Vis etc.). Physico-chemical parameters including pH, solvent type, temperature, or sample concentration are known to have a significant effect on the conformation and behavior of the dendrimers (see Table 3-2), however some aspects are not always controlled when investigating biological interactions. For example, numerous research groups use commercially available PAMAM as is supplied in methanol solution, and often simply dilute with a biologically friendly solvent (i.e., culture medium, phosphate buffer) depending on the purpose of the study³⁹⁻⁴² (summarized in Table 3-2). The presence of a small amount of residual methanol is often considered acceptable if kept low (≤ 1 %). However, biophysical studies have shown that methanol lowers the surface tension of water⁴³ and affects the structure of lipid bilayers^{44, 45}. Therefore, aqueous cell culture medium containing even traces of methanol might impact on culturing, toxicity, or uptake studies more than anticipated. Whilst studies have reported considerably high tolerance levels of various cell types,^{46, 47} an effect on human biochemical pathways can be already observed at methanol concentrations as low as 0.08 %.⁴⁸

Table 3-2 Common experimental variables that can affect the experimental endpoints and measured outputs. Examples are focused on PAMAM dendrimers.

Typical Experimental Variables	Selected variables in the focus of this article relevant to PAMAM dendrimers	Potentially Affected Experimental Endpoints/ Outputs
<p>pH</p> <ul style="list-style-type: none"> • Solution pH • Physiological pH • pH of cell organelles <p>Solvent</p> <ul style="list-style-type: none"> • Type • Purity • Mixture • Residuals • Temperature <p>Other</p> <ul style="list-style-type: none"> • Body vs. room temperature • Solubility • Concentration • Humidity • Lighting • Vibration 	<p>Protonation of surface groups</p>  <p>Residual methanol in experiments using commercial unmodified PAMAM^a</p> <p>□ MeOH removed ■ MeOH present / not stated</p> 	<p>UV/Vis spectra, fluorescence, scattering profiles, size, shape, aggregation, cellular uptake, toxicity etc.</p>

^a Screening of recent 200 publications showed that 22 research articles matched our inclusion criteria and used commercial PAMAMs. Of these, only 5 stated that methanol was removed prior to biological or biophysical experiments (see supplementary information, Table 3-5).

The chemical structure of PAMAM dendrimers does not contain typical fluorophores, however, the phenomenon of blue emission was first reported in 1991 by Larson and Tucker⁴⁹ for half-generation PAMAM. Since then, it was also observed for dendrimers with other surface moieties or structural modifications and was termed *non-traditional intrinsic fluorescence* (NTIF)⁵⁰⁻⁵³. A better understanding of the NTIF of PAMAM dendrimers is important for developing applications such as sensing^{54, 55} or label-free, traceable drug or gene delivery.^{14, 56, 57} Whilst the cause of the blue intrinsic fluorescence is not fully explained yet, however, it is assumed to mainly originate from the dendrimer core (tertiary amines, resonance structures)^{51, 58} with an indirect impact of the surface groups. Additionally, it can be affected by oxygen-doping and aging of the dendrimers in solution^{52, 59} and by solvent-dependent non-covalent aggregation of solvent and dendrimer⁵³. Some studies indicated a pH-dependency of the fluorescence intensity with higher emissions at acidic conditions compared to basic conditions,^{50, 51} however, other researchers observed the opposite behavior^{60, 61}.

Finally, for biomedical applications, it is important to understand the solution properties of an active molecule and factors potentially affecting those properties. Solution scattering techniques such as small angle scattering with either X-rays (SAXS) or neutrons (SANS) are well-established for characterization of macromolecules in solution⁶² and are often complemented with computational techniques to gain conformational information^{63, 64}. However, such experiments are mostly performed in non-physiological solvents and therefore are limited in their relevance to biological systems. To date, PAMAM behavior in solution has not been studied in complex, physiological-like solvents such as phosphate buffer. The chosen dendrimer solvent for SAXS was mostly pure methanol⁶⁵ or deionized water,⁶⁶ whereas for SANS the preferred solvent is based on D₂O⁶⁷. Also amino-terminated PAMAM dendrimers^{68, 69} have been studied more frequently than their carboxyl-terminated counterparts^{66, 70}.

Molecular dynamics simulations have mainly focused on the structural behavior (size, shape) of amine-terminated PAMAM dendrimers, either in the gas phase,⁷¹ with implicit⁷² or explicit water,⁷³ and with methanol,⁷⁴ whereas only very few studies have involved half-generation PAMAM-COOH dendrimers^{75, 76}. Studies revealed the effect of counter ions,⁷⁷ surface modification,⁷⁸ solvent type,⁷⁴ pH⁷³ or intramolecular interactions with water,⁷⁹ and very few studied the pH-dependent interaction with a model bilayer membrane⁸⁰.

The overall aim of this study was to assess how experimental parameters using commercial PAMAM dendrimers affected physico-chemical and structural properties, and consequently how those changes might impact on interactions in biological studies and/or their interpretation. We provide an in-depth study investigating how properties of PAMAM G5 and G4.5 dendrimers vary under different conditions, namely in phosphate buffers at pH 4, 7 and 10 with the presence and absence of residual methanol. Specifically, we first used the experimental techniques of spectroscopy (UV/Vis, fluorescence) and small-angle scattering (SAXS). These findings were then complemented with computational studies based on a coarse-grained (CG) bead-spring model.

3.2 EXPERIMENTAL SETUP

PAMAM dendrimers solutions in methanol of generation 4.5 (COOH surface groups, MW ~ 26.3 kDa) and 5 (NH₂ surface groups, MW ~ 28.8 kDa); solvents and sodium phosphate salts were purchased from Sigma Aldrich (UK). Ultrapure (UHQ-grade) water was obtained *in house* from a TripleRed Alto UHQ water machine (TripleRed, UK).

3.2.1 Sample preparation

Phosphate buffers of pH 4, 7 and 10 were prepared *in house* with sodium phosphate salts and UHQ-grade water to an ionic strength of 0.04 M. For UV/Vis and fluorescence, PAMAM dendrimers were either used as supplied in methanol and directly diluted in phosphate buffer (2 % residual methanol) or the methanol was evaporated (min. 24 h in desiccator) and the film was rehydrated to a maximum PAMAM concentration of 1 mg mL⁻¹ which was then further diluted (range 0.5 – 0.0625 mg mL⁻¹).

The PAMAM samples were freshly prepared, stored at room temperature and used within 3 days of preparation.

3.2.2 Ultraviolet and visible spectroscopy (UV/Vis)

The UV/vis measurements were carried out on a Varian Cary 300 UV-Visible double-beam spectrometer, using an automatic cell changer. For the measurements, a scanning rate of 600 nm min⁻¹, data interval of 1 nm and an averaging time of 0.1 s was set, and the samples were scanned in the range of 450 - 250 nm. Subtraction of the phosphate buffer background was done manually.

3.2.3 Fluorescence spectrophotometry (fluorescence)

A Varian Eclipse Fluorescence spectrophotometer was used for the fluorescence spectra measurements. The slit width was 5 nm, with a scanning rate of 600 nm min⁻¹, data interval of 1 nm and an averaging time of 0.1 s. The

PMT voltage was set to 'Medium', the excitation filter to 'Auto' and the emission filter to 'Open'. Background subtraction was done manually.

Initially, a search scan (10 nm steps) for the emission and excitation was performed with 1 mg mL⁻¹ PAMAM solution to determine the optimum emission and excitation wavelength for each PAMAM species and pH. Following this, single emission wavelength scans at fixed excitation wavelength were run for all sample concentrations.

3.2.4 Small angle X-ray scattering (SAXS)

Data Collection. Solution small-angle X-ray scattering (SAXS) was performed on the bioSAXS beamline B21 at Diamond Light Source (Harwell, UK)⁸¹. PAMAM sample solutions with 1% and 0 % methanol were prepared at 1 mg mL⁻¹ in pH 4, 7 and pH 10 phosphate buffer and were loaded into PCR tubes in an automated sample changer. Samples (30 µL) were then delivered into a temperature-controlled quartz capillary and exposed for 15 s, collecting 18 frames at 20°C. Data was collected using a Pilatus Dectris 2M detector, each sample spectrum was collected once.

Data Analysis. Background was manually subtracted using SCATTER⁸², an open-source software for basic SAXS analysis that includes the Guinier approximation. Form and structure factor modeling was carried out using SAS fit (version 0.94.11)⁸³. The quantitative analysis of particle size and shape was initiated with the generalized Guinier approximation, which provided the radius of gyration (R_g), characteristic of the overall dimensions of the molecule, by model-independent fitting of the scattering in the low q -region. The radius of gyration for a sphere is obtained from the Guinier equation⁸⁴

$$I(q) = I_0 \exp\left(-\frac{1}{3}q^2 R_g^2\right)$$

where I is the scattered intensity (I_0 is the intensity at $q = 0$) and q is the momentum transfer:

$$q = 4\pi \sin \frac{\theta}{\lambda}$$

Here λ is the wavelength ($\lambda = 0.89 - 1.3 \text{ \AA}$ on Diamond B21) and 2θ is the scattering angle.

For the PAMAM concentrations of 1 mg mL^{-1} a spherical shell form factor was found to best fit the data. This model uses as parameters the outer (shell) radius R_1 and inner (core) radius R_2 , the scattering contrast of the shell $\Delta\eta$ and the scattering contrast relative to the matrix of the core $\mu\Delta\eta$.

The scattered intensity I_{shell} can be described as

$$I_{shell}(Q, R_1, R_2, \Delta\eta, \mu) = [K(Q, R_1, \Delta\eta) - K(Q, R_2, \Delta\eta(1 - \mu))]^2$$

with K defined as

$$K(Q, R, \Delta\eta) = \frac{4}{3}\pi R^3 \Delta\eta \frac{\sin QR - QR \cos QR}{(QR)^3}$$

The forward scattering for $q = 0$ is given by

$$\lim_{Q=0} I_{shell}(Q, R_1, R_2, \Delta\eta, \mu) = \left(\frac{4}{3}\pi\Delta\eta[R_1^3 - R_2^3(1 - \mu)]\right)^2$$

3.2.5 Molecular dynamics (MD) simulations

The structural properties of PAMAM dendrimers and their dependence on pH values have been previously studied using molecular simulations at the atomistic level with chemical details. Most published works are either focused on the full-^{72, 74, 78} or half- generation dendrimers,⁷⁶ but seldom both. In this work, we chose to perform molecular dynamics simulations of G5 and G4.5 PAMAM dendrimers using a coarse-grained (CG) bead-spring model with implicit solvent. The use of CG dendrimer model is not only computationally efficient to render simulation results with good statistics, but also allows for

convenient separation of the excluded volume and electrostatic interaction contributions to determine the dendrimer structures. Moreover, simulating both full- and half-generation dendrimers under the same simulation framework facilitates direct comparison of their structural properties and enables an understanding at a molecular level of the effects of charged group distributions and their interactions with counterions.

In the CG PAMAM dendrimer model, each of the chemical groups or monomers, including the primary and tertiary amine, carboxyl, amide, and methylene groups, is represented by one spherical particle or monomer, either charged or neutral depending on the nature of the represented group and the pH value in the system. Apart from the central bond, each branch in the dendrimer consists of three neutral monomers or spacers and two functional monomers, one at each end. The total numbers of monomers in each type of dendrimers and the numbers of monomers representing chargeable groups are given in Table 3-11 (Supplementary Information). Details of the CG MD simulation method and system setup can be found in Section 3.7.4 (Supplementary Information).

In correspondence with our experimental studies, three pH values, namely 4, 7 and 10, are studied in MD simulations. The average numbers of positively and/or negatively charged monomers in a PAMAM dendrimer (G5 or G4.5) at a given pH are determined by the Henderson-Hasselbalch equation. These numbers, together with the corresponding average numbers of counterions, are listed in Table VII in the SI. In each simulation system, the required numbers of positive and/or negative charges are randomly assigned to the monomers representing the amine and/or carboxyl groups. For each given dendrimer type, 25 individual simulation runs with different charge allocations are carried out at each pH to ensure good statistics of the simulation results.

The structural properties of a dendrimer with N monomers can be characterized by calculating its gyration tensor S which has three principal moments $\lambda_1 \geq \lambda_2 \geq \lambda_3$ (see Section 3.7.4 of the Supplementary Information). The squared radius of gyration of the dendrimer is given by⁸⁵

$$R_g^2 = Tr(S) = \lambda_1 + \lambda_2 + \lambda_3,$$

where $Tr(S)$ is the trace of S , and its relative shape anisotropy is

$$\kappa^2 = 1 - 3 \frac{\lambda_1\lambda_2 + \lambda_2\lambda_3 + \lambda_3\lambda_1}{(Tr(S))^2}$$

with $0 \leq \kappa^2 \leq 1$. κ^2 equals to one for a molecule of perfectly linear conformation but approaches zero for a molecule of spherical shape. Another type of descriptors of the molecular geometric shape are the aspect ratios between the principal moments λ_1/λ_2 , λ_1/λ_3 and λ_2/λ_3 , which all equal unity for a perfect spherical shape but are larger than unity for elongated shapes.

Information about the spatial distributions of the monomers and counterions can be obtained from their radial number density distribution functions defined as

$$\rho(r) = \frac{\langle n(r) \rangle}{V(r, \delta r)}$$

where $n(r)$ is the number of certain type of particles in a spherical shell of thickness δr at a distance r away from the center of mass (CoM) of the dendrimer and $V(r, \delta r)$ is the volume of the shell. For branched molecules like star polymers and dendrimers, $\rho(r)$ typically shows a sharp peak at very small r due to dividing a finite number of central or core monomers by a small volume.

3.2.6 Statistical analysis

All experiments were repeated at least three times unless otherwise stated, and basic analyses and background subtractions were carried out in Microsoft® Excel. One-way Analysis of Variance (ANOVA) followed by Bonferroni's multiple comparisons test was carried out in GraphPad Prism version 8.4.1 for Windows), GraphPad Software, USA. Statistical comparison tables can be viewed in the Supplementary Information (section 3.7.2).

3.3 RESULTS

3.3.1 Effect of methanol

Using commercially available PAMAM (5 % v/v in methanol), we have investigated the effect of the residual methanol on solution properties of PAMAM G5 and G4.5 that have been diluted in pH 7 phosphate buffer.

Figure 3-1 fully defines the UV/Vis spectra of PAMAM G5 and G4.5 solutions containing no methanol and 2% methanol. The methanol did not affect the λ_{\max} of either species (PAMAM G4.5 ~ 288 nm, G5 ~ 276 nm) (Figure 3-1a). The PAMAM molecules do not have an obvious chromophore and the absorbance between 270 – 290 nm can be attributed to the carbonyl groups (C=O) of the amides in the dendrimer interior (transitions between non-bonding orbitals (n) and π orbital ($n \rightarrow \pi^*$ transition))⁸⁶. The differences between the λ_{\max} of G5 and G4.5 are due to the presence of the different surface groups (Table 3-2).

Figure 3-1c and 3-1d show a linear, concentration-dependent absorbance for both PAMAM species, which was unaffected by the residual methanol for G5. Whereas, for G4.5 the absorbance was higher than seen for G5 (0.3-0.4 AU compared to 0.15-0.2 AU) and the methanol-containing samples had lower absorbance compared to the methanol free sample.

For the PAMAM G5 UV/Vis data, we observed little to no effect of the addition of methanol. However, the residual methanol depressed the UV/vis absorbance of PAMAM G4.5. This might be a result of interactions between the solvent, where the polarity changes in the presence of methanol, and the COO⁻ surface groups of PAMAM G4.5⁸⁷.

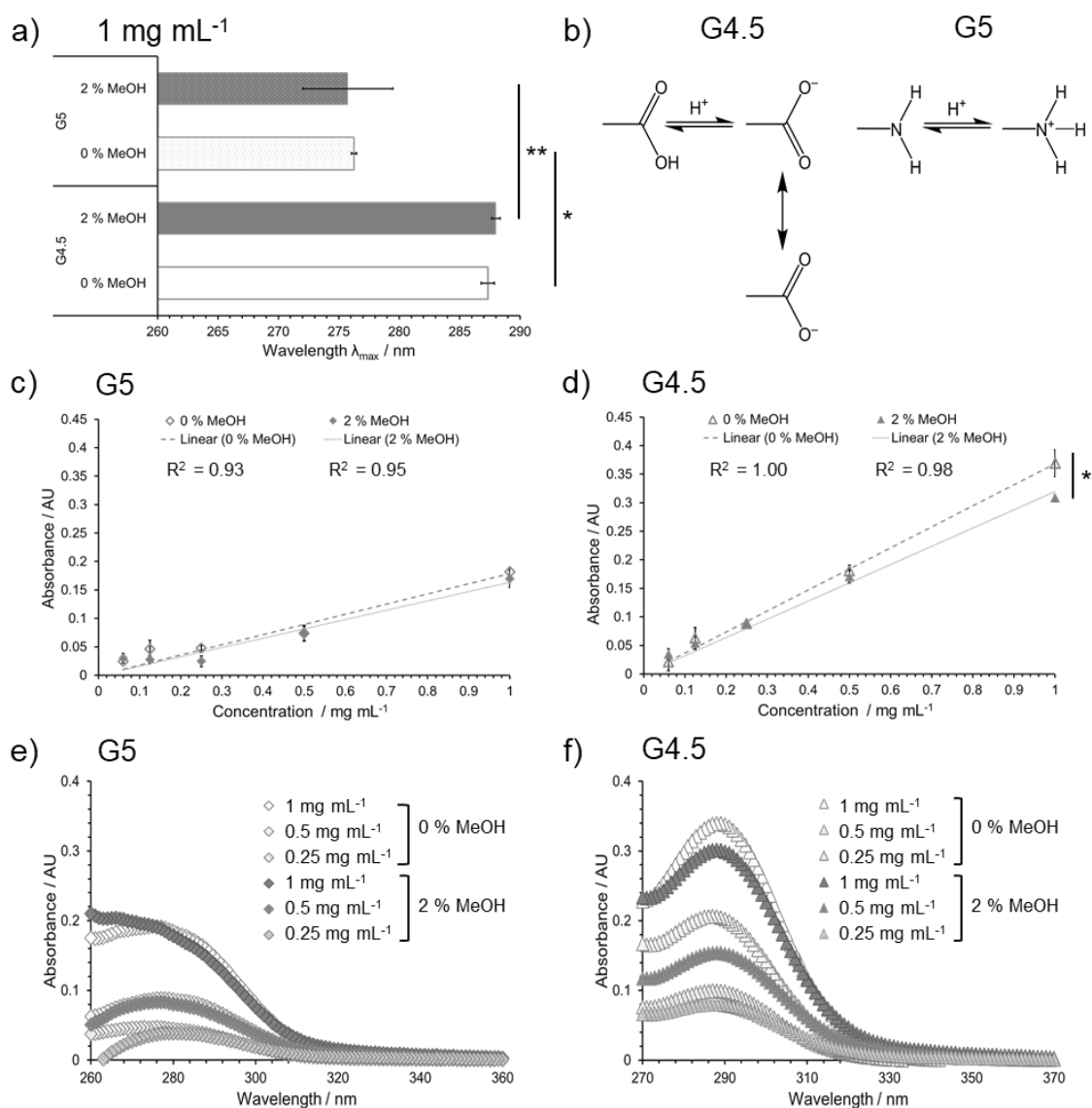


Figure 3-1 UV/Vis absorbance spectra of PAMAM G5 and G4.5 in phosphate buffer pH 7 (0.04 M) with (2 % MeOH) and without residual methanol (0% MeOH). Panel a) compares the maximum absorption wavelength λ_{max} of 1 mg mL⁻¹ PAMAM solutions. Panel b) shows the resonance structures of the PAMAM dendrimers. The concentration-dependent absorbance with a linear fit is presented for G5 (panel c) and G4.5 (panel d). Data represent mean \pm SEM, $n \geq 3$. Error bars are hidden by the symbols when not visible. Panels e) and f) demonstrate example UV/Vis absorption spectra for G5 and G4.5, respectively. For clarity, data for 0.06 and 0.125 mg mL⁻¹ are not shown. Statistical difference, where applicable, is indicated as * for $p < 0.05$ and ** for $p < 0.01$.

Fluorescence profiles of both PAMAM dendrimers are presented in Figure 3-2. As with UV/Vis, addition of methanol did not affect the wavelength of the maximum emission (λ_{em}) nor the excitation wavelength causing the emission (λ_{ex}) (see Figure 3-2 a and b). A red-shift for both, λ_{ex} and λ_{em} , of approximately

20 – 40 nm was seen for PAMAM G4.5 compared to G5 that can be attributed to the difference in surface groups.

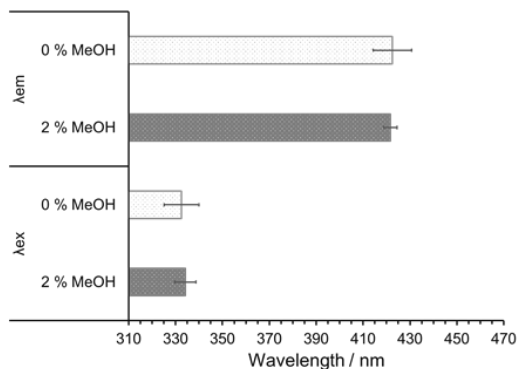
Low intensities of *non-traditional intrinsic fluorescence* were recorded for full-generation G5, at values that are under the noise threshold for fluorescence spectra, and up to 10-fold higher intensities for the half-generation PAMAM G4.5 at the highest concentration (Figure 3-2c and d). For both PAMAM species, the fluorescence intensity was shown to be concentration-dependent under all conditions. Interestingly, and in agreement with UV/Vis spectroscopy, methanol affected the fluorescence emission intensity for G4.5, where solutions with 2 % residual methanol resulted in a significantly higher fluorescence intensity compared to 0 % residual methanol ($p = 0.0013$). This is further illustrated by the example excitation and emission spectra of PAMAM G5 and G4.5 at 1 mg mL^{-1} (Figure 3-2e and f). Overall, the emission peaks for both PAMAM species appeared to be broad, which may be due to structural fluctuations of the solvation shell surrounding the dendrimer molecule and consequential variation in the local electric field⁸⁸.

Several factors are known to affect fluorescence emission spectra, including solvent polarity, internal charge transfer, probe-probe interactions, or conformational changes of the probe^{89, 90}. This data set focusses on the effect of residual methanol within the aqueous phosphate buffer solvent. The dielectric properties of the solvent are reduced with the presence of methanol although it should be noted that the concentration of methanol is low. The methanol may have the ability to preferentially interact with the PAMAM, and this could be driven by hydrophobic interactions or hydrogen bonding.

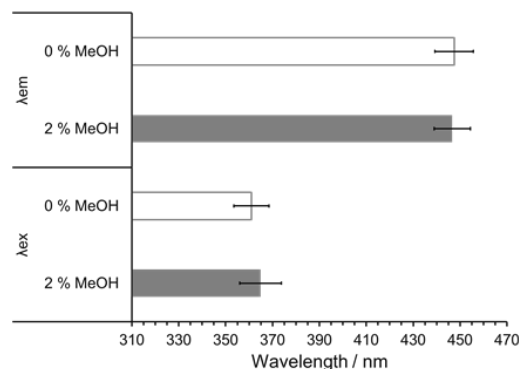
The higher emission intensity observed for PAMAM G4.5 in the methanol containing phosphate buffer could be caused by the lower polarity of the mixed solvent and therefore smaller quenching effects⁸⁹. The difference in behavior of the two PAMAM molecules is likely to be due to the different net charge of the molecules at pH 7. At pH 7, most of the carboxyl surface groups of PAMAM G4.5 will be deprotonated (pK_a 4.8) and the inner tertiary amines partially

protonated (pKa 6.7)⁹¹, creating a zwitterionic, polar molecule accessible to emission–inducing solvent interactions.

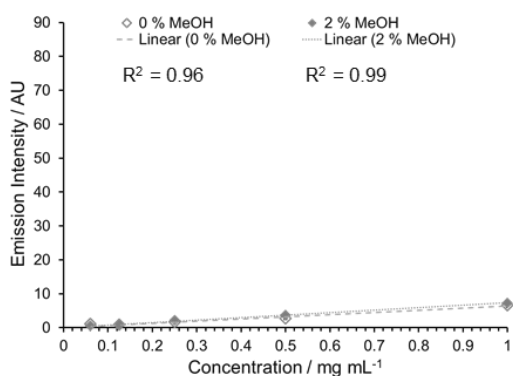
a) G5 1 mg mL⁻¹



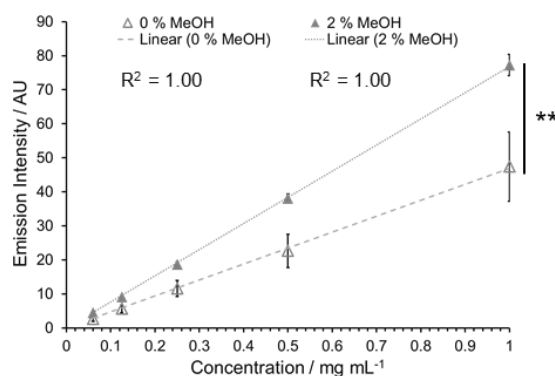
b) G4.5 1 mg mL⁻¹



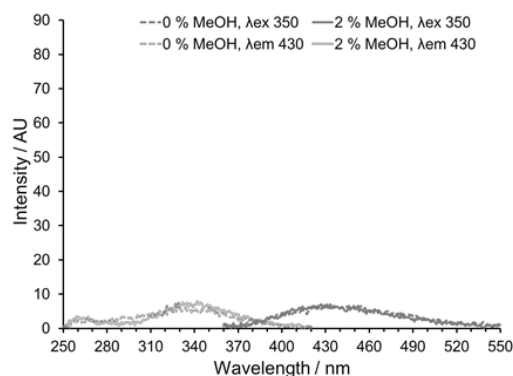
c) G5 λ_{ex} 350



d) G4.5 λ_{ex} 380



e) G5 1 mg mL⁻¹



f) G4.5 1 mg mL⁻¹

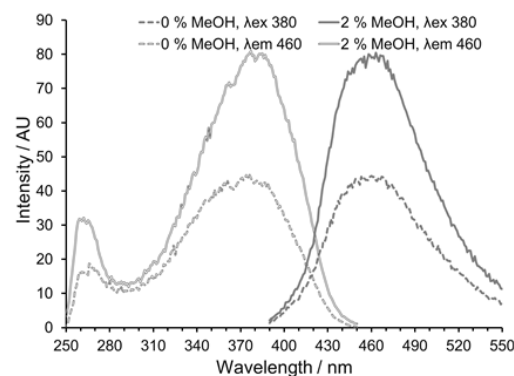


Figure 3-2 Non-traditional intrinsic fluorescence of PAMAM G5 and G4.5 in phosphate buffer solution at pH 7 (0.04 M) under presence (2 %, filled symbols) and absence (0 %, clear symbols) of residual methanol. Data in panel a – d are presented in $M \pm SEM$, $n \geq 3$. Error bars are hidden by the symbols when not visible. Panels a) and b) compare the results of the emission search scan of the 1 mg mL⁻¹ PAMAM solution. The excitation wavelength causing the highest emission intensity is referred to as λ_{ex} , whereas λ_{em} denotes the emission wavelength at the highest fluorescence. Panels c) and d) show the concentration – dependent emission intensity with linear fits

for G5 (λ_{ex} 350 nm) and G4.5 (λ_{ex} 380 nm), respectively. Panels e) and f) present exemplary excitation and emission spectra of G5 and G4.5 at a solution concentration of 1 mg mL^{-1} , solid lines reflect 2 % methanol presence in the phosphate buffer solution, dashed lines absence of methanol (0 %). Statistical difference is indicated as ** for $p < 0.005$, in all other cases the difference was not significant.

Small Angle X-ray Scattering (SAXS) experiments were carried out to investigate the effect of the residual methanol on the size and shape of the PAMAM (1 mg mL^{-1}), dendrimers. SAXS data was fitted to a spherical shell form factor (Figure 3-3) with the derived outer radii (R_1) and R_g of the Guinier approximation compared in Table 3-3, and detailed fitting parameters provided in the Supporting Information (Section 3.7.3, Table 3-10).

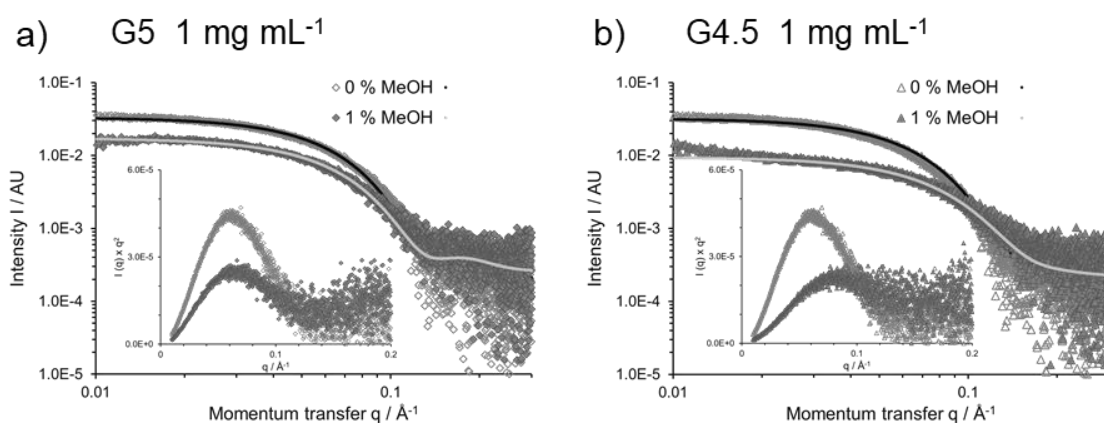


Figure 3-3 Methanol effect on scattering of PAMAM dendrimers in solution. Spherical Shell form factor fitted SAXS profiles and Kratky plots (insets) of PAMAM G5 (panel a) and G4.5 (panel b) in sodium phosphate buffer pH 7 under the presence (filled symbols) and absence (clear symbols) of 1% methanol.

In all cases, the R_g were larger than the outer radii from the spherical shell model (form factor fit). The outer shell radii R_1 as well as the R_g suggest a methanol (1 %) impact on the conformation and size of both dendrimers in solution although changes to G5 were very subtle. Generally, the methanol effect was more pronounced for PAMAM G4.5 where a decrease of 17.7 % in R_1 and 5.3% in R_g was observed, and this could be attributed to the zwitterionic charge state of the molecules and resulting solvent interactions at pH 7. It is known that phosphate ions penetrate PAMAM molecules affecting the PAMAM radii⁹². Our data suggests that methanol as co-solvent shields this effect.

Generally, the radii of PAMAM G4.5 were smaller than those of PAMAM G5, with the outer radius from the form factor fit showing the largest difference under the presence of 1 % methanol (29.3 % smaller). Given that the mass (molecular weight) of PAMAM G4.5 is only 8.7% smaller than G5, this difference in radius implies that the G4.5 dendrimer has a denser molecular structure compared to G5.

Table 3-3 Comparison of radii (Å) of PAMAM G5 and G4.5. Detailed fitting parameters are available in the Supplementary Information (Section 3.7.2, Table 3-10).*

(a) Change in PAMAM radii (Å) due to presence of methanol					
		0%	1%	Change (Å)	Change (%)
PAMAM G5	R _g	29.9	29.3	0.6	2.0
	Outer	28.6	27.0	1.6	5.6
PAMAM G4.5	R _g	24.4	23.1	1.3	5.3
	Outer	23.2	19.1	4.1	17.7

(b) Change in PAMAM radii (Å) due to PAMAM generation					
		G5	G4.5	Change (Å)	Change (%)
0% MeOH	R _g	29.9	24.4	5.5	18.4
	Outer	28.6	23.2	5.4	18.9
1% MeOH	R _g	29.3	23.1	6.2	21.2
	Outer	27.0	19.1	7.9	29.3

* Radii are given as the outer radius, obtained from the form factor fits (Spherical Shell), and the radius of gyration (R_g), calculated using Guinier approximation of the low q region only.

Kratky plots of SAXS data are used to obtain information about shape and flexibility^{93, 94}. Here, the bell-shape plots reveal that the full-generation PAMAM G5 (Figure 3-3a, inset) assumed a globular, compact conformation under both solvent conditions, however, in methanol-containing buffer, the maximum is less pronounced suggesting slightly less rigidity. In comparison, the Kratky profile of PAMAM G4.5 (Figure 3-3b, inset) in methanol-free phosphate buffer is similar to that of G5, but the peak for the methanol-containing environment is not only flatter and shifted but shows a plateau in the high-q region. This indicates partial folding of the dendrimer branches and a more flexible conformation under methanol presence compared to the more compact condition without residual methanol.

3.3.2 Effect of pH

To illustrate the effect of pH on the ionizable groups of the PAMAM dendrimers, their theoretical charges (pH 1-14) were calculated for the whole molecule as well as for the surface groups only (Figure 3-4). Whilst PAMAM dendrimers are often referred to as cationic or anionic dendrimers according to their surface functionalities (NH_2 or COOH), these terms are inadequate considering their net charge and ionization state over the full pH range.

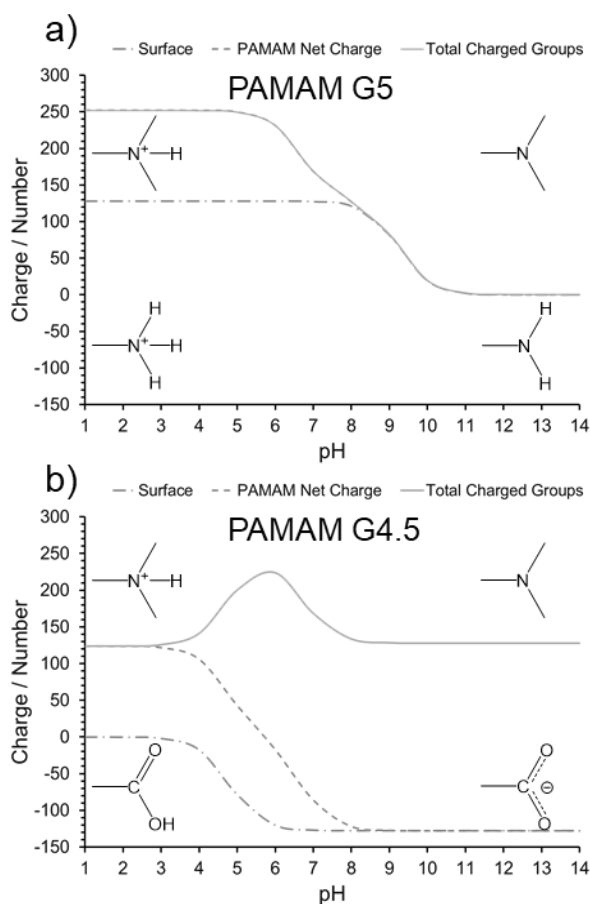


Figure 3-4 Charge and number of charged groups of PAMAM dendrimers. Charge calculations are based on the Henderson-Hasselbalch equation with pK_a 6.7 for tertiary amines, pK_a 9 for primary amines and pK_a 4.8 for carboxyl groups. The 128 surface groups of PAMAM G5 and G4.5 are primary amines and carboxyl groups, respectively, whereas tertiary amines represent the core functional groups of both dendrimer types. Total charged groups refer to the absolute number of all charged moieties of the molecule at any given pH irrespective if negative or positive, and the PAMAM Net Charge sums up the effective charge of the dendrimer. For G5, PAMAM Net Charge and Total Charged Groups are overlaid/ identical.

The full-generation PAMAM G5 exhibits a cationic charge over a wide pH range including physiological pH range up to pH 8, but with increasing pH the net charge diminishes until it becomes zero. For the half-generation PAMAM G4.5, the effect of the pH on the net charge is more complicated due to its zwitterionic properties. At low pH it exhibits a cationic charge as the tertiary amines of the dendrimer core are all protonated, whereas with increasing pH the amines and carboxyl groups become more deprotonated, and the overall charge is dominated by the anionic surface groups. As the pKa values of carboxyl and tertiary amine groups are relatively close to each other, there is a high number of oppositely charged groups between pH 5 and pH 8 causing intramolecular interactions that are absent for PAMAM G5. Note that the values calculated for the tertiary amines in the core should be taken with caution. Considering the spatial conformation of the PAMAM molecules under different pH conditions, it can be assumed that not all chargeable groups are accessible by the surrounding solution and ions, and therefore the real charge of the core amines is likely lower than the theoretical charge value and will in turn affect the PAMAM behavior.

The UV/Vis absorbance of PAMAM solution samples in Figure 3-5 was concentration-dependent across all pH conditions, and for pH 7 and pH 10 significantly higher for PAMAM G4.5 than for G5 ($p < 0.0001$). Whilst the maximum absorbance of PAMAM G5 did not indicate a pH-dependence, absorbance was increased for G4.5 with elevating pH, and generally higher for the methanol-free phosphate buffer than the one with 2 % residual methanol (see Figure 3-5).

Fluorescence was recorded at fixed excitation wavelengths λ_{ex} 350 nm for PAMAM G5 and 380 nm for PAMAM G4.5 as they yielded on average the highest emission intensity during the search scans. A concentration-dependent emission intensity of the PAMAM solution samples was observed across all pH conditions (see Figure 3-6) and it was significantly higher for PAMAM G4.5 than for G5 ($p < 0.001$).

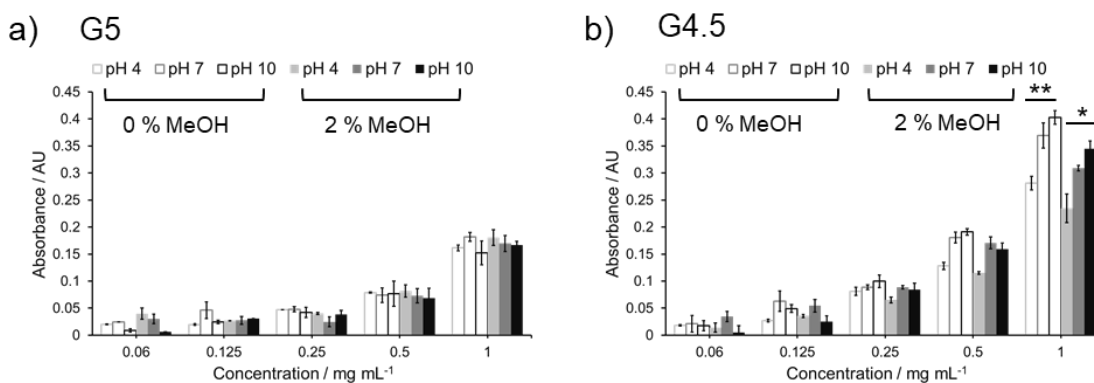


Figure 3-5 UV/Vis absorbance of PAMAM G4.5 and G5 in phosphate buffer solution of varying pH (pH 4, 7 and 10) without (0 %, clear columns) and with residual methanol (2 %, filled columns). Data are displayed as $M \pm SEM$, $n \geq 3$. Panels a) and b) represent the concentration – dependent maximum absorbance of G5 and G4.5, respectively. The λ_{max} were in the range of 270 – 278 nm for G5, and 287 – 289 for G4.5. Statistical difference is indicated as * for $p < 0.05$ and ** for $p < 0.005$ for the difference between pH 4 and pH 10, in all other cases the difference was not significant.

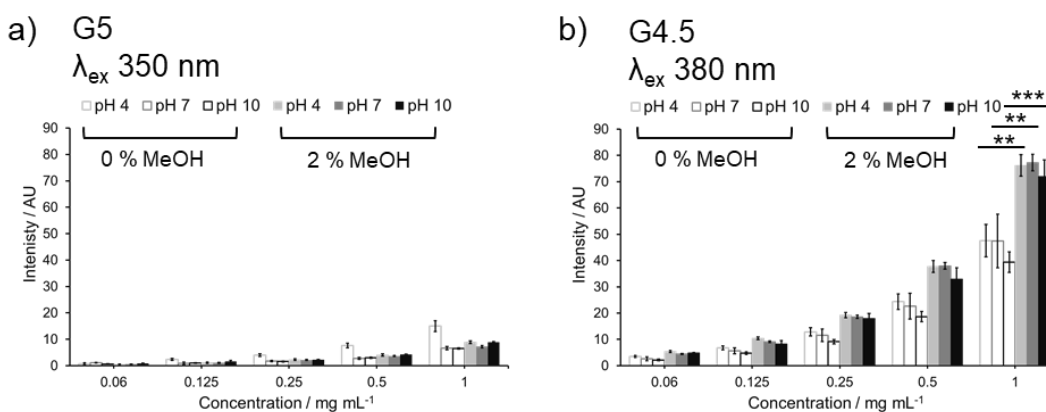


Figure 3-6 Fluorescence results of PAMAM G5 and PAMAM G4.5 in phosphate buffer solution of different pH (pH 4, 7, and 10) under presence (2 %, filled columns) and absence (0 %, clear columns) of residual methanol. Data are presented in $M \pm SEM$, $n \geq 3$. Error bars are hidden by the symbols when not visible. Panels a) and b) show the maximum emission fluorescence intensity for G5 (λ_{ex} 350 nm) and G4.5 (λ_{ex} 380 nm), respectively. The corresponding emission wavelengths varied between 428 – 453 nm for G5 and 458 – 464 nm for G4.5. Statistical difference is indicated as * for $p \leq 0.05$, ** for $p \leq 0.01$, *** for $p < 0.001$; in all other cases the difference is not significant.

The intensity trend for PAMAM G4.5 hints toward a decrease with increasing pH, but too subtle to achieve statistical significance and the fluorescence emission of PAMAM G5 was too low (< 10 AU) for all conditions to draw meaningful conclusions. However, across the pH range there was a significant methanol effect on the PAMAM G4.5 emission ($p < 0.005$) resulting in ~ 30 – 40

AU higher intensity for the samples containing 2 % methanol, as seen already for pH 7 in Figure 3-2.

SAXS scattering profiles were fitted to a spherical shell form factor across the pH range. As was seen previously for pH 7 data in Table 3-3, PAMAM G5 and G4.5 radii in methanol-free buffer were generally larger than in the methanol-containing buffer solution. Table 3-4 also shows that R_g values exhibited only modest changes for the different pH and methanol conditions for both PAMAMs.

Table 3-4 Comparison of radii (\AA) of PAMAM G5 and G4.5 under different pH conditions. Detailed fitting parameters are available in the Supplementary Information (Section 3.7.2, Table 3-10).*

(a) Change in PAMAM radii (\AA) due to pH (0 % MeOH)						
		pH 4	pH 7	pH 10	Change pH 4 to 7	Change pH 7 to 10
PAMAM G5	R_g	30.1	29.9	29.3	<1	<1
	outer	28.8	28.6	23.5	<1	↓5.1 (17.8%)
PAMAM G4.5	R_g	23.0	24.4	24.8	↑1.4 (6.1%)	<1
	outer	21.1	23.2	20.4	↑2.1 (10.0%)	↓2.8 (12.1%)

(b) Change in PAMAM radii (\AA) due to pH (1% MeOH)						
		pH 4	pH 7	pH 10	Change pH 4 to 7	Change pH 7 to 10
PAMAM G5	R_g	29.9	29.3	28.1	<1	↓1.2 (4.1%)
	outer	26.8	27.0	23.6	<1	↓3.4 (12.6%)
PAMAM G4.5	R_g	23.0	23.1	23.0	<1	<1
	outer	19.9	19.1	18.4	<1	<1

* Radii are given as the outer radius, obtained from the form factor fits (Spherical Shell) and the radius of gyration (R_g), calculated using Guinier approximation of the low q region only.

For PAMAM G5, a decrease ($\sim 4 \text{ \AA}$) in radius between pH 7 and pH 10 was observed with 0 % and 1% methanol as co-solvent which might be significant and could relate to the deprotonation of the dendrimers. The radius was likely dominated by the surface branches as primary amines are fully protonated at pH 4 and 7.

SAXS scattering profiles with respective form factor fits (Spherical Shell) in Figure 3-7 show that at pH 4, G5 had the highest scattering intensity, $I(0)$. This could be explained by the high charge state of the G5 at pH 4 (see Figure 3-4) since the scattering intensity correlates with the electron density and spatial

distribution of electrons of a molecule. In the Kratky plots (insets in Figure 3-7a and c), the pH differences were more pronounced, but did not seem to affect the globular shape of the dendrimers.

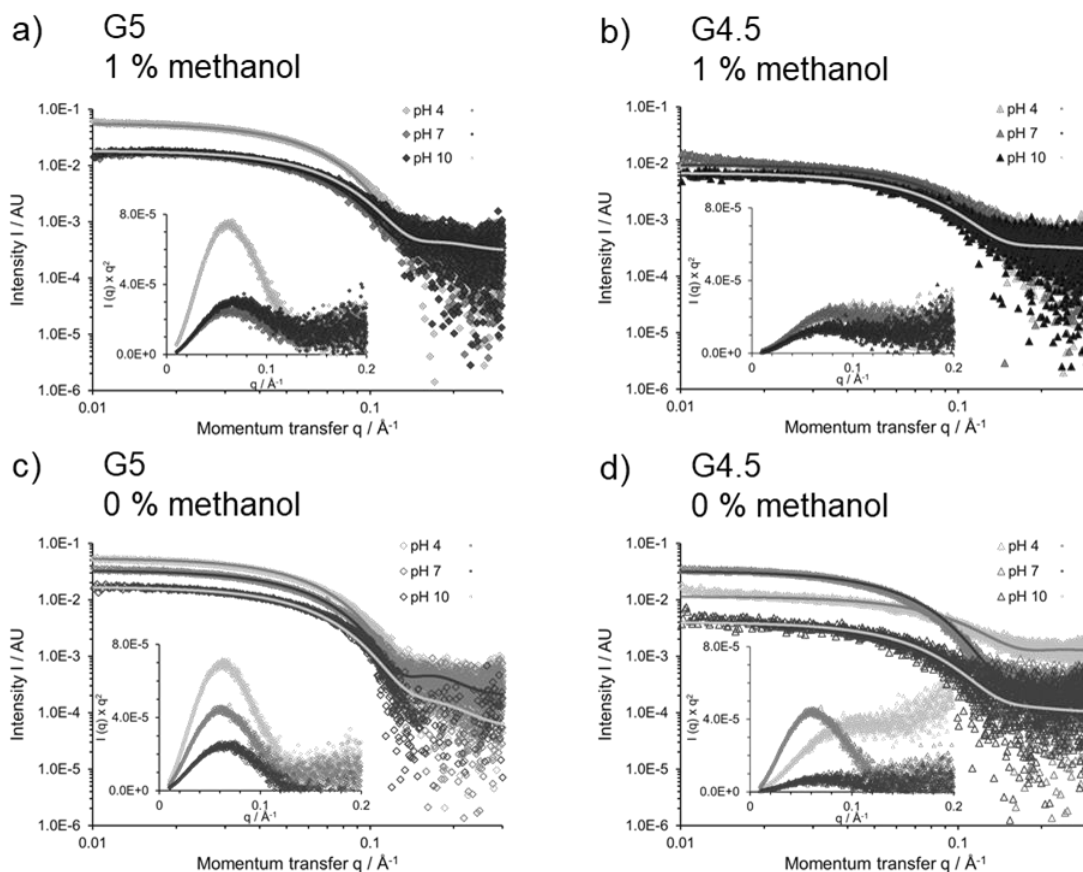


Figure 3-7 Effect of solution pH on scattering of PAMAM dendrimers. SAXS data was fitted to a spherical shell form factor (lines). The fitted SAXS profiles (inset) and Kratky plots of 1 mg mL⁻¹ PAMAM dendrimer solutions under different pH conditions are shown for 1 % (panel a, b) and 0 % residual methanol (panel c, d).

PAMAM G4.5 was affected differently by the varying pH conditions. The outer radii R_1 showed no obvious trend in PAMAM size and varied by ~ 2.5 Å across the different pH conditions. The scattering profiles and Kratky plots of PAMAM G4.5 in methanol-containing phosphate buffer showed similar trends in scattering intensity as well as shape across all pH conditions (Figure 3-7b) and implied a degree of flexibility in the dendrimer conformation. There were distinctively different scattering intensities and slope patterns for the methanol-free buffer conditions (Figure 3-7d). Whilst the spherical shell model was a suitable fit for all three pH conditions, the Kratky plot (inset Figure 3-7d)

revealed pH-dependent conformational changes. At pH 7, when the carboxyl groups were fully deprotonated and the tertiary amines were still partially protonated, the dendrimer assumed a globular, more rigid shape which could be aided by intramolecular charge interactions. Assuming the deprotonated, outer branches stretched mainly outwards and the partially charged inner groups were accessible to the buffering ions, the dendrimer molecules could have been subject to swelling⁹⁵ which in turn would explain the largest radius. At pH 10 the lowest scattering intensity was observed as only the carboxyl groups on the surface groups were deprotonated and the shallow Kratky plot suggests a disordered arrangement of the dendrimer with clusters of back-folded branches, which could be enabled by the deprotonated amine core. In comparison, the scattering intensity was considerably higher at pH 4 and the Kratky profile indicates the branches behaving as Gaussian chains driven by the nearly fully protonated tertiary amines. Charge repulsion together with stretching of the molecule from the core could occur, whereas the surface-neutral outer generation could arrange itself randomly causing disorder and cross-linkage.

The structural features of PAMAM G5 and G4.5 in different pH environments were modelled with coarse-grained molecular dynamics (CG-MD) simulations and the results are summarized in Figure 3-8. Benefiting from the coarse-grained model without explicit solvent, we can directly relate the pH-dependent behavior of the dendrimer size to the electrostatic interactions among the charged monomers and counterions. Figure 3-8 (a) and (b) show the radial number densities of functional groups with respect to the centers of mass (CoMs) of PAMAM G5 and G4.5 at pH 4, 7 and 10. The distribution of counterions within the PAMAM structures are shown in Figure 3-8(c) and (d).

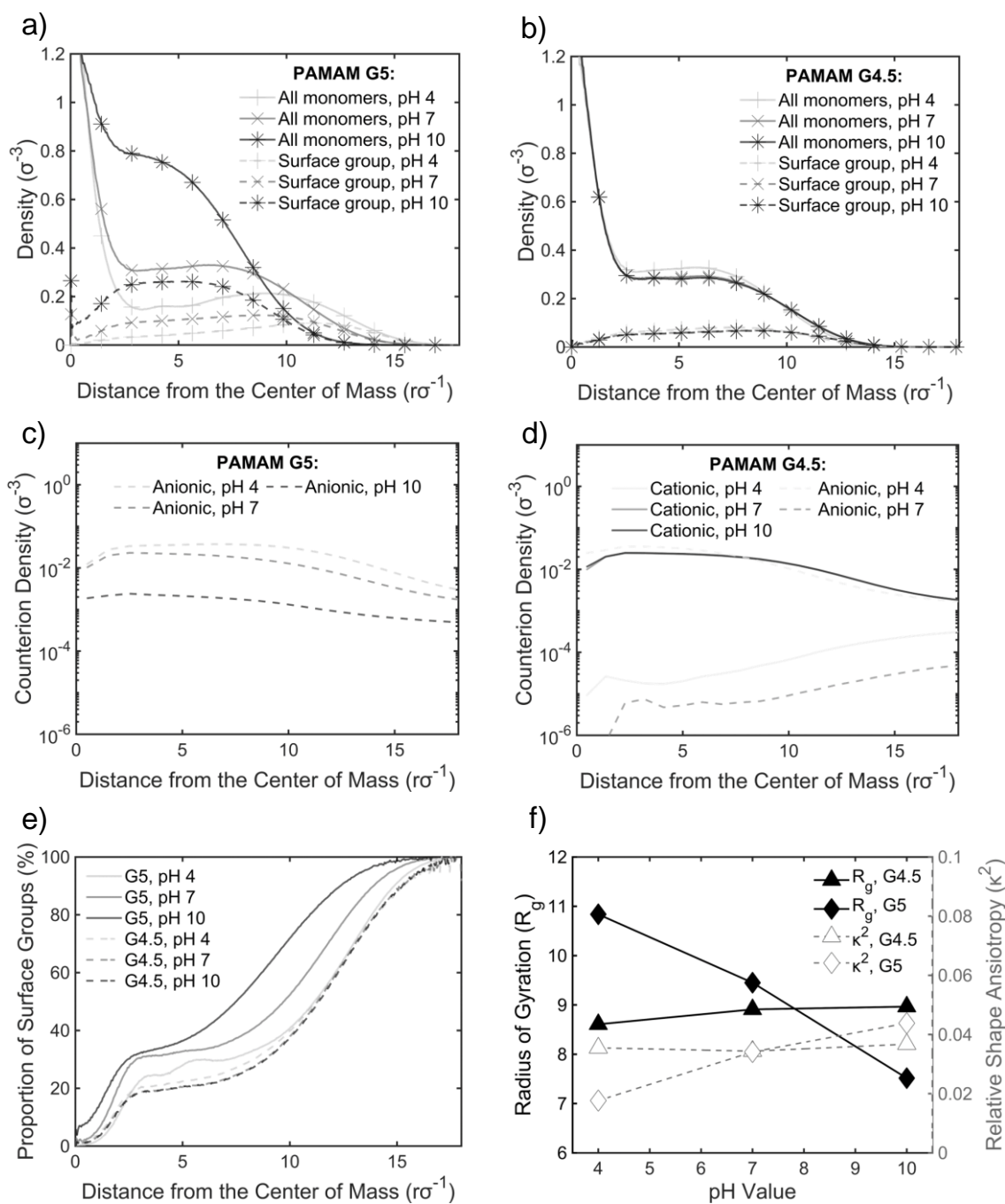


Figure 3-8 MD simulation results of the radial number density distribution functions, $\rho(r)$, of all monomers and surface groups only for PAMAM G5 (a) and G4.5 (b); and of the counterions in the corresponding environments for PAMAM G5 (c) and G4.5 (d). For PAMAM G4.5, no anionic counterions were observed at pH 10 (d). The percentage of surface groups (outer groups) in all monomers, measured as the ratio between their radial number densities $\rho_{\text{outer}}(r)/\rho_{\text{all}}(r)$, is shown in (e). In (a-e) the radial distance r is measured from the centers of mass of the dendrimers. The pH-dependent radii of gyration, R_g , of the dendrimers are shown as filled symbols and the relative shape anisotropy κ^2 as clear symbols in panel (f).

For PAMAM G5, the molecular structure demonstrates strong changes with pH. In Figure 3-8(a) the highest radial number density of all groups is found at pH 10 within distance $r/\sigma \leq 8$ from the dendrimer CoM, because only a small fraction of primary amine groups is charged (see Figure 3-4, and Table 3-11 in the Supporting Information) and the dendrimer behaves like neutral molecules with more flexible branch conformations. We can also see the increased backfolding of the outer branches with increasing pH from the high density of the outer surface groups (primary amine) within the molecular structure at pH 10. The backfolding behavior is further illustrated by Figure 3-8(e) where the surface group distribution throughout the molecule is shown as a percentage of all groups at each distance away from the CoM. This percentage value increases with increasing pH at distances close to the CoM. The PAMAM G5 thus takes more compact conformation and consequently a smaller R_g at higher pH.

On the other hand, at low pH values (e.g., pH 4), nearly all the primary and tertiary amines are protonated. The electrostatic repulsions between these positively charged monomers lead to stretching of the branches, like polyelectrolyte chains, and accordingly an overall swelling of the dendrimer. This can be seen in Figure 3-8(a) from the broader ranges, but lower values, of the radial density distributions of all monomers (solid lines) and surface groups (dashed lines) at distances close to the CoM of PAMAM G5 at pH 4. But they both show broadened peaks far away from the CoM. Moreover, the high number of charged monomers generates a strong electrostatic field which attracts counterions into the molecular structure, as shown in Figure 3-8(c) from the higher density profile of counterions at distances close to the CoM at pH 4 than those at higher pH. The counterion-induced osmotic pressure also drives the dendrimer to swell. These attracted counterions will also alter the local electric field distribution inside the dendrimer and so potentially could affect its fluorescence profile.

Our results also show that highly charged dendrimers at low pH take more symmetric or spherical shapes than the nearly neutral ones at high pH. For example, we found that the maximum aspect ratio l_1/l_3 is about 1.53 at pH 4 but

increases to about 1.97 at pH 7. This can be understood as being due to the strong electrostatic repulsions among charged amines at low pH that lead to nearly uniform swelling of the dendrimers. At neutral pH, thermal fluctuations of the branches become predominant and so allow for larger fluctuations and more anisotropic shapes of these molecules at higher pH. This can also be seen from the increment of the relative shape anisotropy from $k^2 \approx 0.0177$ at pH=4 to 0.0438 at pH=10 (Figure 3-8d). These small k^2 values indicate that the PAMAM G5 dendrimers are generally taking globular shapes over the pH range we studied, which agrees with our SAXS results. Figure 3-8(f) presents the simulation results for the radii of gyration, R_g , of PAMAM G5 and G4.5 dendrimers at different pH values. For PAMAM G5, R_g demonstrates a clear decrease with increasing pH due to the strong backfolding at high pH and swelling at low pH, which is qualitatively consistent with the SAXS data in Table 3-4. We note that R_g of the full-generation PAMAM G5 obtained in our CG simulations decreases by 30.7% from 10.84s, 9.45□ to 7.51s as the pH increasing from 4, 7 to 10, which is significantly larger than the 2.7-6 % drop for R_g (or 13-18 % reduction for R_1) in the SAXS data presented in Table 3-4. Previous simulation studies on PAMAM G5 using atomistic models have shown large magnitude of decrease in R_g by 31.9-51.9 % over the same range of pH in systems with implicit solvents (mimicking water^{72, 74} and methanol⁷⁴), but much smaller decrement in systems with explicit solvents (about 16.5% drop in water⁷³ and 6% in methanol⁷⁴). The inclusion of explicit solvent molecules has been shown to cause swelling of the less charged dendrimers at high and medium pH due to excluded volume effects, but more compact conformations of highly charged dendrimers at low pH due to shielding electrostatic repulsions between charged amines⁷⁴. This can well explain the much weaker pH dependence of dendrimer size observed in the SAXS experiments (with explicit solvents) than in the CG MD simulations with implicit solvents.

For PAMAM G4.5, the zwitterionic nature of the molecule means that there are charged groups at all pH studied. The radial number densities of all monomers and only the surface (carboxyl) groups presented in Figure 3-8(b) are relatively insensitive to the change in pH. They reflect that the backfolding

level in PAMAM G4.5 does not vary significantly with pH, as manifested in Figure 3-8(e). The radius of gyration of the half-generation PAMAM G4.5 thus has a qualitatively different pH-dependence from that of the full-generation PAMAM G5, see Figure 3-8(f). It marginally increases from low to medium pH (e.g., $R_g \approx 8.61\sigma$ at pH 4 and 8.91σ at pH 7), and levels off between pH 7 and 10. This behavior is similar to the SAXS data in Table 3-4. The nearly invariant R_g in the medium to high pH region can be understood from the deprotonation of all carboxyl groups. The electrostatic repulsions among these negatively charged outer groups drive themselves and the connected branches move away from the dendrimer CoM. In this pH region the tertiary amines are deprotonated and so the inner branches behave as neutral chains subject to pulling forces from the outer groups. The backfolding level of the outer branches in PAMAM G4.5 at pH 7 and 10 is weaker than that of the nearly neutral PAMAM G5 at pH 10 but is close to that in PAMAM G5 at pH 7, as evidenced in Figure 3-8(a) and (b) by the similar radial density profiles of outer functional groups in these cases. The backfolding phenomenon can be clearly visualized in Figure 9 from the snapshots of the dendrimers at pH 7. At this pH, both PAMAM G5 and G4.5 have fully charged surface groups and nearly fully deprotonated tertiary amines. Penetration of counterions into the molecular structures can also be seen in Figure 3-9. Since we do not reach a PAMAM G4.5 system that is fully uncharged, counterions can be found in the molecular structure at all pH, as shown in Figure 3-8(d).

At pH 4 the tertiary amines in PAMAM 4.5 are fully protonated. The electrostatic repulsions between these positively charged monomers lead to outwards stretching of the inner branches, together with the osmotic pressure contributions from the negatively charged counterions. On the other hand, a fraction of surface carboxyl groups is deprotonated at this pH, giving the half-generation dendrimer distinctive zwitterionic features. These negatively charged terminal groups tend to move deeply into the core region to stay closely to as many positively charged amines as possible to reduce the total electrostatic energy of the system. Other outer generation branches with protonated surface groups behave as flexible neutral chains and can fold back freely under

requirement of conformation entropy. The interplay between the different effects results in a slightly more compact conformation and so smaller R_g of the zwitterionic dendrimer at pH 4 than that at pH 7 and 10. The overall geometric shape of the half-generation PAMAM G4.5 is insensitive to the change in pH with the aspect ratios close to those of the full-generation PAMAM G5 at pH 7. Their relative shape anisotropy stays at $k^2 = 0.035 \pm 0.010$, which corresponds to an overall spherical shape, as also found in an atomistic simulation with implicit solvent⁷⁶.

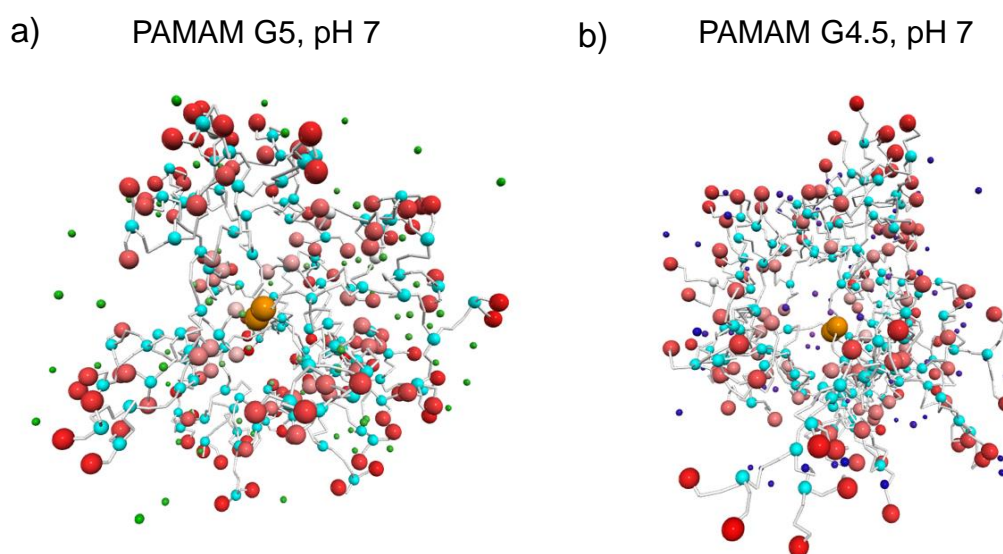


Figure 3-9 Snapshots of (a) full-generation PAMAM G5 and (b) half-generation PAMAM G4.5 at pH 7 which show backfolding of outer generation groups and penetration of counterions into the molecular structure. The surface groups are represented by the red monomers. The lighter the red color the closer the monomer is located to the dendrimer core (depicted by two orange beads). The inner functional groups are either colored as cyan if they are cationic, or gray if they are neutral alongside the spacer units. The unbonded dark blue and green beads represent anionic and cationic counterions, respectively.

3.4 DISCUSSION

The focus of this work was to research the impact of the solvent environment (pH and residual methanol) on typical experimental end points of PAMAM studies, thereby highlighting physico-chemical changes that might affect observation and interpretation of dendrimer interactions in biological systems. We chose to study the dendrimers in phosphate buffer as this is widely used in

biological and biophysical studies, and currently available conformational data of PAMAM dendrimers is largely derived from studies in pure water or non-physiological solvents such as methanol. Within the wide range of potential biomedical applications, it is vital to be fully aware of potential solvent effects and thus interference on the experimental outcomes when designing experimental studies with PAMAM dendrimers. This is particularly pertinent since PAMAM is supplied commercially in methanol and there is often residual methanol in the samples used in biological studies (Figure 3-1).

We investigated the role that methanol has on spectroscopic data and molecular size for G5 and G4.5. Methanol is a common co-solvent that is present in many biological and biophysical experiments where potential medical and pharmaceutical applications for the use of PAMAM are investigated³⁹⁻⁴¹. In our studies we found that the presence of methanol (2%) increased fluorescence of PAMAM G4.5 by almost 70 % at pH 7. However, intrinsic fluorescence in G5 was minimal under all experimental conditions which is not in line with several studies in the literature^{50, 96, 97} and suggests quenching of the electron-rich amines may have occurred. This agrees with observations that ionic interactions affect the mechanism of intrinsic fluorescence of PAMAM dendrimers^{53, 55}. Thus, we see further evidence that experimental conditions can make interpretation of spectroscopic data difficult. We observed fluorescence emission wavelengths in line with values reported in the literature for PAMAM dendrimers^{49, 97, 98}. However, we detected little to no fluorescence for PAMAM G5. The literature shows a wider variety of results for PAMAM in terms of fluorescence emission^{49, 50, 53, 54, 97, 99, 100}.

The presence of methanol was found to increase the overall compactness of the PAMAM molecule reducing molecular size. Differences in molecular size between G4.5 and G5 were amplified by the presence of methanol. For example, our SAXS fits showed that the outer radii for G4.5 was 19 % smaller than G5 when no methanol present and 29 % smaller than G5 in the presence of methanol (see Table 3-3). In terms of molecular weight, G4.5 is only 9 % smaller. We can therefore conclude that G4.5 has a denser conformation (and

thus less solvation) than G5 and the molecular dimensions decrease further when methanol is a co-solvent.

The changes in structural behaviour of the PAMAM molecules in systems with methanol as a co-solvent have the potential to affect molecular interactions within *in vitro* biological systems. It is likely that the methanol preferentially associates with the PAMAM resulting in changes of the dielectric properties of the solvent and electrostatic interaction within the PAMAM structure. Indeed, G4.5 was shown to have a higher density (volume/molecular weight) compared to G5 at pH 7 even without the presence of methanol and this was shown to be due to differences in net charge of the molecules. This difference was amplified by the presence of methanol allowing the molecules to contract in size further.

Previous SAXS studies of PAMAM dendrimers were conducted either in pure methanol or deionised water but never in phosphate buffer, and to our knowledge there is only one research group that studied PAMAM, specifically G3.5 and G3, in both methanol and deionised water^{66, 101-103}. They found the radius of dendrimer solutions in methanol smaller than in deionised water which is in line with the trend we have seen in our studies.

We were also interested in exploring further the differences in behaviour due to changes in net charge of PAMAM G5 and G4.5 because of changing the pH (Figure 3-4). For PAMAM G5, increasing pH reduces the charge of amine groups throughout the molecule whereas for PAMAM G4.5 the amine charge decreases but the carboxyl group deprotonates leading to a negative charge at high pH. Interestingly, in our studies the larger impact of pH was seen for PAMAM G5 than for G4.5 and showed that G5 had a more extended conformation with a larger radius than G4.5 at all pH.

For PAMAM G5 the size of the molecule decreased between pH 7 and 10 as observed by our SAXS and MD data, and Figure 3-8(e) showed that the concentration of counterions incorporated within the molecular structure also decreased. In addition, we saw increased backfolding of the outer generations (surface groups) for pH 10. This means that at pH 10 the PAMAM G5 structure was more compact and our MD results showed that G5 incorporated less

counterions within its structure. This is because the molecule has no charge at this pH and the surface groups did not dominate the surface properties of the dendrimer in the way that they did at pH 4 and 7. MD simulation by Opitz and Wagner⁷⁴ studied the impact of the solution pH on the molecular structure of amine-terminated PAMAM dendrimers G2-G5. They also found an effect of solvent conditions and observed a decrease in dendrimer radii with increasing pH.

For G4.5, the zwitterionic nature of the molecule meant that there remained charged moieties within the molecule across all solution pH leading to no significant changes in size. Our MD studies showed that there was some backfolding across the whole pH range, which resembled the arrangement of surface groups and size seen for PAMAM G5 at pH 7. Our SAXS data, obtained under more complex buffer conditions than modelled in the CG-MD simulations, showed evidence of a more disordered arrangement for PAMAM G4.5 at pH 10 compared to pH 4 and 7 and showed a lower scattering intensity at pH 10.

3.5 CONCLUSIONS

We report a comprehensive investigation of the impact of pH and solvent composition on the spectroscopic (UV/Vis and fluorescence) and structural (SAXS and MD) properties of PAMAM dendrimers. We gained new insights into the pH-dependent conformational behavior of half-generation PAMAM G4.5 and the effect of methanol as co-solvent for both PAMAM G4.5 and G5. The effect of pH and methanol differs between the dendrimers but can be explained with the charge behavior of the internal and external functional groups that facilitate solvent interactions and resulting conformational changes in the PAMAM structure. For full-generation PAMAM, the amount of protonation of tertiary and primary amines and electrostatic interactions are the main drivers of the effects seen. In contrast, half-generation PAMAM G4.5 is a more complex amphiphile with both cationic and anionic functional groups that provide a wider range of possible molecular interactions with the surrounding solvent and the dendrimer branches themselves affecting charge localization and electron orbits. Our research provides insights on effects of solvent composition and pH using a

more physiological solvent than previous reports and indicate that particular care is needed in the interpretation of biological data from PAMAMs, particularly in more complex, multi-environment systems (e.g., different pHs in different cell organelles).

3.6 REFERENCES

1. Tomalia, D. A.; Baker, H.; Dewald, J.; Hall, M.; Kallos, G.; Martin, S.; Roeck, J.; Ryder, J.; Smith, P., A new class of polymers - Starburst-dendritic macromolecules. *Polym. J.* **1985**, *17* (1), 117-132.
2. Tomalia, D. A.; Naylor, A. M.; Goddard, W. A., Starburst Dendrimers: Molecular-Level Control of Size, Shape, Surface Chemistry, Topology, and Flexibility from Atoms to Macroscopic Matter. *Angew. Chem., Int. Ed. Engl.* **1990**, *29* (2), 138-175.
3. Fréchet, J. M., Functional polymers and dendrimers: reactivity, molecular architecture, and interfacial energy. *Science* **1994**, *263* (5154), 1710-5.
4. Akhtar, S.; Chandrasekhar, B.; Yousif, M. H.; Renno, W.; Benter, I. F.; El-Hashim, A. Z., Chronic administration of nano-sized PAMAM dendrimers in vivo inhibits EGRF-ERK1/2-ROCK signaling pathway and attenuates diabetes-induced vascular remodeling and dysfunction. *Nanomedicine : nanotechnology, biology, and medicine* **2019**, *18*, 78-89.
5. Fan, M.; Zhang, M.; Xu, H. H. K.; Tao, S.; Yu, Z.; Yang, J.; Yuan, H.; Zhou, X.; Liang, K.; Li, J., Remineralization effectiveness of the PAMAM dendrimer with different terminal groups on artificial initial enamel caries in vitro. *Dental Materials* **2020**, *36* (2), 210-220.
6. Singh, M. K.; Kuncha, M.; Nayak, V. L.; Sarma, A. V. S.; Kumar, M. J. M.; Chauhan, A. S.; Sistla, R., An innovative in situ method of creating hybrid dendrimer nano-assembly: An efficient next generation dendritic platform for drug delivery. *Nanomedicine : nanotechnology, biology, and medicine* **2019**, *21*, 102043.
7. Jain, A.; Mahira, S.; Majoral, J. P.; Bryszewska, M.; Khan, W.; Ionov, M., Dendrimer mediated targeting of siRNA against polo-like kinase for the treatment of triple negative breast cancer. *Journal of biomedical materials research. Part A* **2019**, *107* (9), 1933-1944.
8. Tao, L.; Geng, J.; Chen, G.; Xu, Y.; Ladmiral, V.; Mantovani, G.; Haddleton, D. M., Bioconjugation of biotinylated PAMAM dendrons to avidin. *Chemical Communications* **2007**, (33), 3441-3443.
9. Marcinkowska, M.; Sobierajska, E.; Stanczyk, M.; Janaszewska, A.; Chworos, A.; Klajnert-Maculewicz, B., Conjugate of PAMAM Dendrimer,

Doxorubicin and Monoclonal Antibody—Trastuzumab: The New Approach of a Well-Known Strategy. *Polymers* **2018**, *10* (2), 187.

10. Yang, B. S.; Mallick, S.; Kwon, Y.-E.; Kim, Y.-J.; Kim, G. H.; Choi, J. S., PAMAM Dendrimer Conjugated with Cell-penetrating Peptide-derived Oligopeptides for Enhanced Cell Uptake and Gene Delivery. *Bulletin of the Korean Chemical Society* **2015**, *36* (10), 2477-2483.
11. Xie, J.; Wang, J.; Chen, H.; Shen, W.; Sinko, P. J.; Dong, H.; Zhao, R.; Lu, Y.; Zhu, Y.; Jia, L., Multivalent Conjugation of Antibody to Dendrimers for the Enhanced Capture and Regulation on Colon Cancer Cells. *Scientific Reports* **2015**, *5* (1), 9445.
12. Chanphai, P.; Tajmir-Riahi, H. A., Characterization of folic acid-PAMAM conjugates: drug loading efficacy and dendrimer morphology. *Journal of Biomolecular Structure and Dynamics* **2018**, *36* (7), 1918-1924.
13. Cui, Y. S.; Liang, B.; Wang, L. G.; Zhu, L. L.; Kang, J. X.; Sun, H. T.; Chen, S. F., Enhanced biocompatibility of PAMAM dendrimers benefiting from tuning their surface charges. *Materials Science & Engineering C - Materials for Biological Applications* **2018**, *93*, 332-340.
14. Wang, G.; Fu, L.; Walker, A.; Chen, X.; Lovejoy, D. B.; Hao, M.; Lee, A.; Chung, R.; Rizos, H.; Irvine, M.; Zheng, M.; Liu, X.; Lu, Y.; Shi, B., Label-Free Fluorescent Poly(amidoamine) Dendrimer for Traceable and Controlled Drug Delivery. *Biomacromolecules* **2019**, *20* (5), 2148-2158.
15. Mekuria, S. L.; Debele, T. A.; Tsai, H.-C., Encapsulation of Gadolinium Oxide Nanoparticle (Gd₂O₃) Contrasting Agents in PAMAM Dendrimer Templates for Enhanced Magnetic Resonance Imaging in Vivo. *ACS applied materials & interfaces* **2017**, *9* (8), 6782-6795.
16. Mekonnen, T. W.; Birhan, Y. S.; Andrgie, A. T.; Hanurry, E. Y.; Darge, H. F.; Chou, H.-Y.; Lai, J.-Y.; Tsai, H.-C.; Yang, J. M.; Chang, Y.-H., Encapsulation of gadolinium ferrite nanoparticle in generation 4.5 poly(amidoamine) dendrimer for cancer theranostics applications using low frequency alternating magnetic field. *Colloids and Surfaces B: Biointerfaces* **2019**, *184*, 110531.
17. Kobayashi, H.; Brechbiel, M. W., Dendrimer-based Macromolecular MRI Contrast Agents: Characteristics and Application. *Molecular Imaging* **2003**, *2* (1), 1-10.
18. Yang, R.; Xia, S.; Ye, T.; Yao, J.; Zhang, R.; Wang, S.; Wang, S., Synthesis of a novel polyamidoamine dendrimer conjugating with alkali blue as a lymphatic tracer and study on the lymphatic targeting in vivo. *Drug Delivery* **2016**, *23* (7), 2298-2308.
19. Otis, J. B.; Zong, H.; Kotylar, A.; Yin, A.; Bhattacharjee, S.; Wang, H.; Jr, J. R. B.; Wang, S. H., Dendrimer antibody conjugate to target and image HER-2 overexpressing cancer cells. *Oncotarget* **2016**, *7* (24), 36002-36013.

20. Cao, Y.; Zu, G.; Kuang, Y.; He, Y.; Mao, Z.; Liu, M.; Xiong, D.; Pei, R., Biodegradable Nanoglobular Magnetic Resonance Imaging Contrast Agent Constructed with Host-Guest Self-Assembly for Tumor-Targeted Imaging. *ACS applied materials & interfaces* **2018**, *10* (32), 26906-26916.
21. Cao, J.; Ge, R.; Zhang, M.; Xia, J.; Han, S.; Lu, W.; Liang, Y.; Zhang, T.; Sun, Y., A triple modality BSA-coated dendritic nanoplatform for NIR imaging, enhanced tumor penetration and anticancer therapy. *Nanoscale* **2018**, *10* (19), 9021-9037.
22. Şenel, M.; Nergiz, C.; Çevik, E., Novel reagentless glucose biosensor based on ferrocene cored asymmetric PAMAM dendrimers. *Sensors and Actuators B: Chemical* **2013**, *176*, 299-306.
23. Staehlke, S.; Lehnfeld, J.; Schneider, A.; Nebe, J. B.; Muller, R., Terminal chemical functions of polyamidoamine dendrimer surfaces and its impact on bone cell growth. *Material Science and Engineering: C* **2019**, *101*, 190-203.
24. Borkowski, T.; Subik, P.; Trzeciak, A. M.; Wołowiec, S., Palladium(0) Deposited on PAMAM Dendrimers as a Catalyst for C-C Cross Coupling Reactions. *Molecules* **2011**, *16* (1), 427-441.
25. Lemon, B. I.; Crooks, R. M., Preparation and Characterization of Dendrimer-Encapsulated CdS Semiconductor Quantum Dots. *Journal of the American Chemical Society* **2000**, *122* (51), 12886-12887.
26. Gao, F.; Djordjevic, I.; Pokhonenko, O.; Zhang, H.; Zhang, J.; Steele, T. W. J., On-Demand Bioadhesive Dendrimers with Reduced Cytotoxicity. *Molecules* **2018**, *23* (4), 796.
27. Mustapha Kamil, Y.; Al-Rekabi, S. H.; Yaacob, M. H.; Syahir, A.; Chee, H. Y.; Mahdi, M. A.; Abu Bakar, M. H., Detection of dengue using PAMAM dendrimer integrated tapered optical fiber sensor. *Scientific Reports* **2019**, *9* (1), 13483.
28. Sadekar, S.; Ghandehari, H., Transepithelial transport and toxicity of PAMAM dendrimers: implications for oral drug delivery. *Advanced drug delivery reviews* **2012**, *64* (6), 571-88.
29. Jain, K.; Kesharwani, P.; Gupta, U.; Jain, N. K., Dendrimer toxicity: Let's meet the challenge. *International journal of pharmaceutics* **2010**, *394* (1-2), 122-142.
30. Duncan, R.; Izzo, L., Dendrimer biocompatibility and toxicity. *Advanced drug delivery reviews* **2005**, *57* (15), 2215-2237.
31. Wiwattanapatapee, R.; Carreno-Gomez, B.; Malik, N.; Duncan, R., Anionic PAMAM dendrimers rapidly cross adult rat intestine in vitro: A potential oral delivery system? *Pharmaceutical research* **2000**, *17* (8), 991-998.
32. Roberts, J. C.; Bhalgat, M. K.; Zera, R. T., Preliminary biological evaluation of polyamidoamine (PAMAM) Starburst dendrimers. *Journal of Biomedical Materials Research* **1996**, *30* (1), 53-65.

33. Chen, L.; Liang, K.; Li, J.; Wu, D.; Zhou, X.; Li, J., Regeneration of biomimetic hydroxyapatite on etched human enamel by anionic PAMAM template in vitro. *Archives of oral biology* **2013**, *58* (8), 975-80.
34. Kirkpatrick, G. J.; Plumb, J. A.; Sutcliffe, O. B.; Flint, D. J.; Wheate, N. J., Evaluation of anionic half generation 3.5-6.5 poly(amidoamine) dendrimers as delivery vehicles for the active component of the anticancer drug cisplatin. *Journal of inorganic biochemistry* **2011**, *105* (9), 1115-22.
35. Sadekar, S.; Thiagarajan, G.; Bartlett, K.; Hubbard, D.; Ray, A.; McGill, L. D.; Ghandehari, H., Poly(amido amine) dendrimers as absorption enhancers for oral delivery of camptothecin. *International Journal of Pharmaceutics* **2013**, *456* (1), 175-85.
36. Prieto, M. J.; del Rio Zabala, N. E.; Marotta, C. H.; Carreño Gutierrez, H.; Arévalo Arévalo, R.; Chiaramoni, N. S.; del Valle Alonso, S., Optimization and in vivo toxicity evaluation of G4.5 PAMAM dendrimer-risperidone complexes. *PLoS One* **2014**, *9* (2), e90393.
37. Souza, J. G.; Dias, K.; Silva, S. A.; de Rezende, L. C.; Rocha, E. M.; Emery, F. S.; Lopez, R. F., Transcorneal iontophoresis of dendrimers: PAMAM corneal penetration and dexamethasone delivery. *Journal of Controlled Release* **2015**, *200*, 115-24.
38. Wang, B.; Navath, R. S.; Romero, R.; Kannan, S.; Kannan, R., Anti-inflammatory and anti-oxidant activity of anionic dendrimer-N-acetyl cysteine conjugates in activated microglial cells. *International Journal of Pharmaceutics* **2009**, *377* (1-2), 159-68.
39. Lombardo, D.; Calandra, P.; Magazu, S.; Wanderlingh, U.; Barreca, D.; Pasqua, L.; Kiselev, M. A., Soft nanoparticles charge expression within lipid membranes: The case of amino terminated dendrimers in bilayers vesicles. *Colloids and Surfaces B-Biointerfaces* **2018**, *170*, 609-616.
40. He, L.; Wu, D.; Tong, M., The influence of different charged poly (amido amine) dendrimer on the transport and deposition of bacteria in porous media. *Water Res* **2019**, *161*, 364-371.
41. Markowicz-Piasecka, M.; Sadkowska, A.; Podsiedlik, M.; Mikiciuk-Olasik, E.; Sikora, J., Generation 2 (G2) - Generation 4 (G4) PAMAM dendrimers disrupt key plasma coagulation parameters. *Toxicol In Vitro* **2019**, *59*, 87-99.
42. Wilde, M.; Green, R. J.; Sanders, M. R.; Greco, F., Biophysical studies in polymer therapeutics: the interactions of anionic and cationic PAMAM dendrimers with lipid monolayers. *Journal of drug targeting* **2017**, *25* (9-10), 910-918.
43. Vazquez, G.; Alvarez, E.; Navaza, J. M., Surface Tension of Alcohol Water + Water from 20 to 50 .degree.C. *Journal of Chemical & Engineering Data* **1995**, *40* (3), 611-614.

44. Patra, M.; Salonen, E.; Terama, E.; Vattulainen, I.; Faller, R.; Lee, B. W.; Holopainen, J.; Karttunen, M., Under the Influence of Alcohol: The Effect of Ethanol and Methanol on Lipid Bilayers. *Biophysical Journal* **2006**, *90* (4), 1121-1135.
45. Joo, H.-J.; Ahn, S.-H.; Lee, H.-R.; Jung, S.-W.; Choi, C.-W.; Kim, M.-S.; Bae, M.-K.; Chung, I.-K.; Bae, S.-K.; Jang, H.-O.; Yun, I., The Effect of Methanol on the Structural Parameters of Neuronal Membrane Lipid Bilayers. *Korean Journal of Physiology & Pharmacology* **2012**, *16* (4), 255-264.
46. Oyama, Y.; Sakai, H.; Arata, T.; Okano, Y.; Akaike, N.; Sakai, K.; Noda, K., Cytotoxic effects of methanol, formaldehyde, and formate on dissociated rat thymocytes: A possibility of aspartame toxicity. *Cell Biology and Toxicology* **2002**, *18* (1), 43.
47. Jover, R.; Ponsoda, X.; Castell, J. V.; Gómez-Lechón, M. J., Evaluation of the cytotoxicity of ten chemicals on human cultured hepatocytes: Predictability of human toxicity and comparison with rodent cell culture systems. *Toxicology in Vitro* **1992**, *6* (1), 47-52.
48. Désy, O.; Carignan, D.; Caruso, M.; de Campos-Lima, P. O., Methanol Induces a Discrete Transcriptional Dysregulation that Leads to Cytokine Overproduction in Activated Lymphocytes. *Toxicological Sciences* **2010**, *117* (2), 303-313.
49. Larson, C. L.; Tucker, S. A., Intrinsic fluorescence of carboxylate-terminated polyamido amine dendrimers. *Appl Spectrosc* **2001**, *55* (6), 679-683.
50. Wang, D.; Imae, T., Fluorescence emission from dendrimers and its pH dependence. *Journal of the American Chemical Society* **2004**, *126* (41), 13204-13205.
51. Wang, D.; Imae, T.; Miki, M., Fluorescence emission from PAMAM and PPI dendrimers. *Journal of colloid and interface science* **2007**, *306* (2), 222-227.
52. Saravanan, G.; Imae, T., Visual Observation and Characterization of Fluorescent Poly(amido amine) Dendrimer in Film State. *Journal of Nanoscience and Nanotechnology* **2011**, *11* (6), 4838-4845.
53. Jasmine, M. J.; Kavitha, M.; Prasad, E., Effect of solvent-controlled aggregation on the intrinsic emission properties of PAMAM dendrimers. *Journal of Luminescence* **2009**, *129* (5), 506-513.
54. Yamaji, D.; Takaguchi, Y., A Novel Fluorescent Fluoride Chemosensor Based on Unmodified Poly(amidoamine) Dendrimer. *Polym. J.* **2009**, *41* (4), 293-296.
55. Staneva, D.; Bosch, P.; Asiri, A. M.; Taib, L. A.; Grabchev, I., Studying pH dependence of the photophysical properties of a blue emitting fluorescent PAMAM dendrimer and evaluation of its sensor potential. *Dyes and Pigments* **2014**, *105*, 114-120.

56. Tsai, Y. J.; Hu, C. C.; Chu, C. C.; Toyoko, I., Intrinsically Fluorescent PAMAM Dendrimer as Gene Carrier and Nanoprobe for Nucleic Acids Delivery: Bioimaging and Transfection Study. *Biomacromolecules* **2011**, *12* (12), 4283-4290.
57. Khosroshahi, M. E.; Tajabadi, M., Characterization and Cellular Fluorescence Microscopy of Superparamagnetic Nanoparticles Functionalized with Third Generation Nanomolecular Dendrimers: In-vitro Cytotoxicity and Uptake study. *Journal of Nanomaterials & Molecular Nanotechnology* **2016**, *05* (03).
58. Ji, Y.; Qian, Y., A study using quantum chemical theory methods on the intrinsic fluorescence emission and the possible emission mechanisms of PAMAM. *Rsc Advances* **2014**, *4* (102), 58788-58794.
59. Lee, W. I.; Bae, Y.; Bard, A. J., Strong Blue Photoluminescence and ECL from OH-Terminated PAMAM Dendrimers in the Absence of Gold Nanoparticles. *Journal of the American Chemical Society* **2004**, *126* (27), 8358-8359.
60. Onoshima, D.; Imae, T., Dendritic nano- and microhydrogels fabricated by triethoxysilyl focal dendrons. *Soft Matter* **2006**, *2* (2), 141-148.
61. Ji, Y.; Qian, Y., pH dependent one-/two-photon fluorescence emission properties and mechanism of the dendrimer PAMAM triphenylamine imine. *RSC Advances* **2015**, *5* (91), 74940-74946.
62. Hamley, I. W., Applications and Specifics of SAXS. In *Small-Angle Scattering*, 2021; pp 137-195.
63. Chen, P.-c.; Shevchuk, R.; Strnad, F. M.; Lorenz, C.; Karge, L.; Gilles, R.; Stadler, A. M.; Hennig, J.; Hub, J. S., Combined Small-Angle X-ray and Neutron Scattering Restraints in Molecular Dynamics Simulations. *Journal of Chemical Theory and Computation* **2019**, *15* (8), 4687-4698.
64. Hub, J. S., Interpreting solution X-ray scattering data using molecular simulations. *Current Opinion in Structural Biology* **2018**, *49*, 18-26.
65. Prosa, T. J.; Bauer, B. J.; Amis, E. J., From Stars to Spheres: A SAXS Analysis of Dilute Dendrimer Solutions. *Macromolecules* **2001**, *34* (14), 4897-4906.
66. Lombardo, D., Liquid-like Ordering of Negatively Charged Poly(amidoamine) (PAMAM) Dendrimers in Solution. *Langmuir : the ACS journal of surfaces and colloids* **2009**, *25* (5), 3271-3275.
67. Hong, K.; Liu, Y.; Porcar, L.; Liu, D.; Gao, C. Y.; Smith, G. S.; Herwig, K. W.; Cai, S.; Li, X.; Wu, B.; Chen, W.-R.; Liu, L., Structural response of polyelectrolyte dendrimer towards molecular protonation: the inconsistency revealed by SANS and NMR. *Journal of Physics: Condensed Matter* **2012**, *24* (6), 064116.
68. Prosa, T. J.; Bauer, B. J.; Amis, E. J.; Tomalia, D. A.; Scherrenberg, R., A SAXS study of the internal structure of dendritic polymer systems. *Journal of Polymer Science Part B: Polymer Physics* **1997**, *35* (17), 2913-2924.

69. Rathgeber, S.; Pakula, T.; Urban, V., Structure of star-burst dendrimers: A comparison between small angle x-ray scattering and computer simulation results. *The Journal of Chemical Physics* **2004**, *121* (8), 3840-3853.
70. Pilkington, G. A.; Pedersen, J. S.; Briscoe, W. H., Dendrimer Nanofluids in the Concentrated Regime: From Polymer Melts to Soft Spheres. *Langmuir : the ACS journal of surfaces and colloids* **2015**, *31* (11), 3333-3342.
71. Çagin, T.; Wang, G.; Martin, R.; Breen, N.; Goddard, W. A., Molecular modelling of dendrimers for nanoscale applications. *Nanotechnology* **2000**, *11* (2), 77-84.
72. Lee, I.; Athey, B. D.; Wetzel, A. W.; Meixner, W.; Baker, J. R., Structural Molecular Dynamics Studies on Polyamidoamine Dendrimers for a Therapeutic Application: Effects of pH and Generation. *Macromolecules* **2002**, *35* (11), 4510-4520.
73. Maiti, P. K.; Çağın, T.; Lin, S.-T.; Goddard, W. A., Effect of Solvent and pH on the Structure of PAMAM Dendrimers. *Macromolecules* **2005**, *38* (3), 979-991.
74. Opitz, A. W.; Wagner, N. J., Structural investigations of poly(amido amine) dendrimers in methanol using molecular dynamics. *Journal of Polymer Science Part B: Polymer Physics* **2006**, *44* (21), 3062-3077.
75. Wang, B.; Sun, Y.; Davis, T. P.; Ke, P. C.; Wu, Y.; Ding, F., Understanding Effects of PAMAM Dendrimer Size and Surface Chemistry on Serum Protein Binding with Discrete Molecular Dynamics Simulations. *Sustainable Chemistry & Engineering* **2018**, *6* (9), 11704-11715.
76. Paulo, P. M. R.; Lopes, J. N. C.; Costa, S. M. B., Molecular Dynamics Simulations of Charged Dendrimers: Low-to-Intermediate Half-Generation PAMAMs. *The Journal of Physical Chemistry B* **2007**, *111* (36), 10651-10664.
77. Liu, Y.; Porcar, L.; Hong, K.; Shew, C.-Y.; Li, X.; Liu, E.; Butler, P. D.; Herwig, K. W.; Smith, G. S.; Chen, W.-R., Effect of counterion valence on the pH responsiveness of polyamidoamine dendrimer structure. *The Journal of Chemical Physics* **2010**, *132* (12), 124901.
78. Lee, H.; Baker, J. R.; Larson, R. G., Molecular Dynamics Studies of the Size, Shape, and Internal Structure of 0% and 90% Acetylated Fifth-Generation Polyamidoamine Dendrimers in Water and Methanol. *The Journal of Physical Chemistry B* **2006**, *110* (9), 4014-4019.
79. Lin, S.-T.; Maiti, P. K.; Goddard, W. A., Dynamics and Thermodynamics of Water in PAMAM Dendrimers at Subnanosecond Time Scales. *The Journal of Physical Chemistry B* **2005**, *109* (18), 8663-8672.
80. Tian, W.-d.; Ma, Y.-q., pH-responsive dendrimers interacting with lipid membranes. *Soft Matter* **2012**, *8* (9), 2627-2632.

81. Cowieson, N. P.; Edwards-Gayle, C. J. C.; Inoue, K.; Khunti, N. S.; Douth, J.; Williams, E.; Daniels, S.; Preece, G.; Krumpa, N. A.; Sutter, J. P.; Tully, M. D.; Terrill, N. J.; Rambo, R. P., Beamline B21: high-throughput small-angle X-ray scattering at Diamond Light Source. *J Synchrotron Radiat* **2020**, *27* (Pt 5), 1438-1446.
82. Rambo, R. P. *About Scatter*, IV.E; Bioisis.net: online - Open Source, 2020.
83. Bressler, I.; Kohlbrecher, J.; Thunemann, A. F., SASfit: a tool for small-angle scattering data analysis using a library of analytical expressions. *Journal of Applied Crystallography* **2015**, *48* (5), 1587-1598.
84. Guinier, A.; Fournet, G.; Walker, C. B.; Yudowitch, K. L., *Small-angle Scattering of X-rays*. Wiley: 1955.
85. Arkin, H.; Janke, W., Gyration tensor based analysis of the shapes of polymer chains in an attractive spherical cage. *The Journal of chemical physics* **2013**, *138* (5), 054904.
86. Sahariah, B.; Sarma, B. K., Relative orientation of the carbonyl groups determines the nature of orbital interactions in carbonyl-carbonyl short contacts. *Chemical Science* **2019**, *10* (3), 909-917.
87. Pavlovich, V. S., Solvatochromism and Nonradiative Decay of Intramolecular Charge-Transfer Excited States: Bands-of-Energy Model, Thermodynamics, and Self-Organization. *ChemPhysChem* **2012**, *13* (18), 4081-4093.
88. Nemkovich, N. A.; Rubinov, A. N.; Tomin, V. I., Inhomogeneous Broadening of Electronic Spectra of Dye Molecules in Solutions. In *Topics in Fluorescence Spectroscopy*, J.R., L., Ed. Springer: Boston, MA, 2002; Vol. 2, pp 367-428.
89. Hrdlovic, P.; Donovalova, J.; Stankovicova, H.; Gaplovsky, A., Influence of polarity of solvents on the spectral properties of bichromophoric coumarins. *Molecules* **2010**, *15* (12), 8915-32.
90. Solvent and Environmental Effects. In *Principles of Fluorescence Spectroscopy*, J.R., L., Ed. Springer: Boston, MA, 2006; pp 205-235.
91. Cakara, D.; Borkovec, M., Microscopic protonation mechanism of branched polyamines: Poly(amidoamine) versus poly(propyleneimine) dendrimers. *Croat. Chem. Acta* **2007**, *80* (3-4), 421-428.
92. Kéri, M.; Nagy, Z.; Novák, L.; Szarvas, E.; Balogh, L. P.; Bányai, I., Beware of phosphate: evidence of specific dendrimer-phosphate interactions. *Physical Chemistry Chemical Physics* **2017**, *19* (18), 11540-11548.
93. Kratky, O., Die Berechnung der Mizelldimensionen von Faserstoffen aus den unter kleinsten Winkeln abgebeugten Interferenzen. *Naturwissenschaften* **1938**, *26* (6), 94-94.

94. Walenta, E., Small angle x-ray scattering. Von O. GLATTER und O. KRATKY. London: Academic Press Inc. Ltd. 1982. ISBN 0-12-286280-5. X, 515 Seiten, geb. £ 43,60; US \$ 81.00. *Acta Polymerica* **1985**, 36 (5), 296-296.
95. Liu, Y.; Chen, C.-Y.; Chen, H.-L.; Hong, K.; Shew, C.-Y.; Li, X.; Liu, L.; Melnichenko, Y. B.; Smith, G. S.; Herwig, K. W.; Porcar, L.; Chen, W.-R., Electrostatic Swelling and Conformational Variation Observed in High-Generation Polyelectrolyte Dendrimers. *The Journal of Physical Chemistry Letters* **2010**, 1 (13), 2020-2024.
96. Pande, S.; Crooks, R. M., Analysis of poly(amidoamine) dendrimer structure by UV-vis spectroscopy. *Langmuir : the ACS journal of surfaces and colloids* **2011**, 27 (15), 9609-13.
97. Chu, C. C.; Imae, T., Fluorescence Investigations of Oxygen-Doped Simple Amine Compared with Fluorescent PAMAM Dendrimer. *Macromolecular rapid communications* **2009**, 30 (2), 89-93.
98. Wang, D.; Imae, T., Fluorescence emission from dendrimers and its pH dependence. *J Am Chem Soc* **2004**, 126 (41), 13204-5.
99. Konopka, M.; Janaszewska, A.; Klajnert-Maculewicz, B., Intrinsic Fluorescence of PAMAM Dendrimers-Quenching Studies. *Polymers (Basel)* **2018**, 10 (5).
100. Zhang, Z.; Rong, F.; Niu, S.; Xie, Y.; Wang, Y.; Yang, H.; Fu, D., Investigation the effects of nano golds on the fluorescence properties of the sectorial poly(amidoamine) (PAMAM) dendrimers. *Applied Surface Science* **2010**, 256 (23), 7194-7199.
101. Mallamace, F.; Lesieur, P.; Lombardo, D.; Micali, N.; Scolaro, L. M.; Romeo, A.; Romeo, E. In *Small-angle X-ray scattering structural investigations of starburst dendrimers in solution*, Trends in Colloid and Interface Science XIII, Berlin, Heidelberg, 1999//; Težak, D.; Martinis, M., Eds. Springer Berlin Heidelberg: Berlin, Heidelberg, 1999; pp 152-156.
102. Micali, N.; Scolaro, L. M.; Romeo, A.; Lombardo, D.; Lesieur, P.; Mallamace, F., Structural properties of methanol-polyamidoamine dendrimer solutions. *Physical Review E* **1998**, 58 (5), 6229-6235.
103. Lombardo, D.; Calandra, P.; Bellocco, E.; Lagana, G.; Barreca, D.; Magazu, S.; Wanderlingh, U.; Kiselev, M. A., Effect of anionic and cationic polyamidoamine (PAMAM) dendrimers on a model lipid membrane. *Biochimica et biophysica acta* **2016**, 1858 (11), 2769-2777.

3.7 SUPPLEMENTARY INFORMATION

3.7.1 Literature screening for studies using commercial PAMAM

Recent research articles have been screened according to the flow outlined in Figure 3-10 and the information of included articles (Table 3-5) was used to create the piechart assessing the presence of methanol in studies using commercial PAMAM dendrimers (main article, Table 3-2).

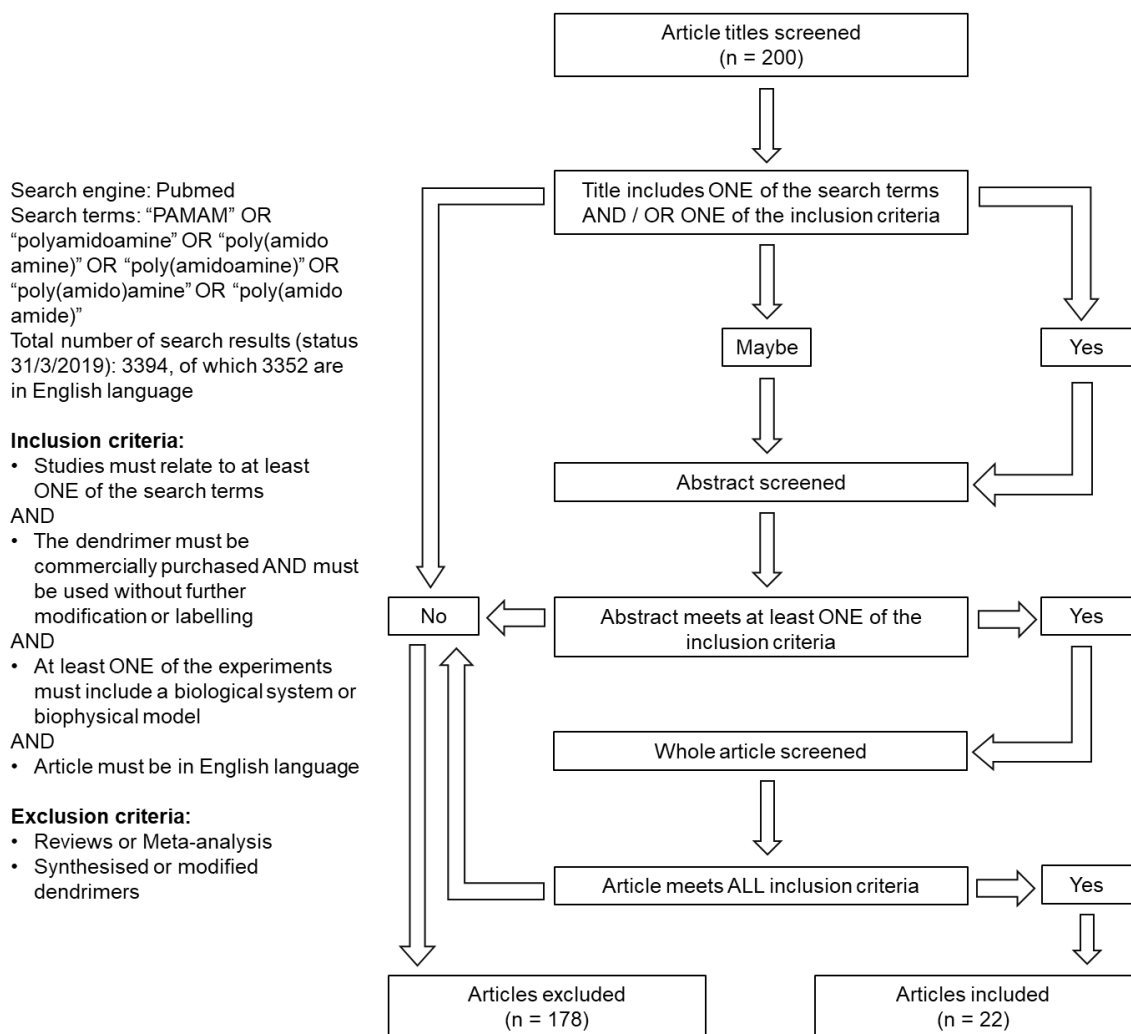


Figure 3-10 Literature screening for use of commercial PAMAM in studies with biological systems or biophysical model. Screening was performed for articles published up to 31/03/2019

Table 3-5 Overview of the 22 included articles from the literature screening (Figure 3-10).

Residual Methanol	Supplier	Broad Research Field	Ref
Removed or absent	Chenyuan Dendrimer Tech.	Dentistry	1
	Sigma	Topical Drug Delivery	2
	Sigma	siRNA Delivery	3
	Sigma	Microbiology	4
	Sigma	Biomaterials/ Implants	5
Present	Sigma	Microbiology	6
	Sigma	Nanotoxicity	7
	Sigma	Liposomal Drug Delivery	8
	Sigma	Nanotoxicity	9
	Sigma	Microbiology	10
	Sigma	Nanotoxicity/ Membrane Interactions	11
No info provided, but assumed to be present	NanoSynthons	Topical Drug Delivery	12
	Sigma	Nanotoxicity/ Surface Chemistry	13
	NanoSynthons	Drug Delivery	14
	Sigma	Nanotoxicity/ Protein Interactions	15
	Sigma	Neurotherapy	16
	Dendritech	Pulmonary Drug Delivery	17
	Dendritech	Nanotoxicity/ Membrane Interactions	18
	Sigma	Gene delivery	19
	Sigma	Nanotoxicity	20
	Sigma	Diabetes Therapy	21
	Sigma	Drug Delivery	22

3.7.2 Statistical comparison of UV/Vis and fluorescence data

One-way Analysis of Variance (ANOVA) followed by Bonferroni's multiple comparisons test was carried out in GraphPad Prim version 8.4.1. for Windows), GraphPad Software, USA.

3.7.2.1 Effect of methanol

Impact of methanol was probed for PAMAM samples (1 mg mL⁻¹) in phosphate buffer solution at pH 7. Results from UV/Vis absorption and

fluorescence of PAMAM G4.5 and G5 was compared for methanol-free buffer and phosphate buffer containing 2 % methanol.

Table 3-6 illustrates the UV/Vis and fluorescence data from the individual conditions at pH 7, whereas the Table 3-7 shows the outcomes and p-values of the statistical comparison.

3.7.2.2 Effect of pH

Impact of pH was probed for PAMAM samples (1 mg m^{-1}) in phosphate buffer solution at pH 4, 7 and 10 under presence and absence methanol within the solution. Results from UV/Vis absorption and fluorescence of PAMAM G4.5 and G5 was compared across all pH for methanol-free buffer and phosphate buffer containing 2 % methanol.

Table 3-8 illustrates the UV/Vis and fluorescence data from the individual conditions across the pH range, whereas Table 3-9 shows the outcomes and p-values of the statistical comparison.

Table 3-6 Summary of the parameters obtained from UV/Vis and fluorescence measurement. UV/Vis data reflect the maximum Absorbance measured at λ_{max} . Fluorescence parameters were obtained from emission search scans, whereby λ_{ex} is the wavelength with the maximum fluorescence at λ_{em} .

ID	PAMAM	MeOH	Absorbance / AU M \pm SEM	Wavelength λ_{max} / nm M \pm SEM	Emission Intensity M \pm SEM	Wavelength λ_{ex} / nm M \pm SEM	Wavelength λ_{em} / nm M \pm SEM
A	G4.5	2 %	0.31 \pm 0.01	288.0 \pm 0.3	77.24 \pm 3.63	380.1 \pm 1.8	460.0 \pm 0
B	G4.5	0 %	0.37 \pm 0.02	287.3 \pm 0.5	47.42 \pm 12.47	363.3 \pm 9.5	443.3 \pm 9.8
C	G5	2 %	0.17 \pm 0.01	275.8 \pm 3.7	7.22 \pm 0.46	339.8 \pm 1.4	425.0 \pm 2.5
D	G5	0 %	0.18 \pm 0.01	276.3 \pm 0.2	6.93 \pm 0.79	340.7 \pm 3.0	426.7 \pm 9.8

Table 3-7 Statistical comparison of the UV/Vis and fluorescence data of Table 3-6. Outcome of the ANOVA and Bonferroni's multiple comparison test are displayed as p value with indication of significance level and non-significant (n.s.) denotation where applicable.

Comparison	P value Absorbance	P value Wavelength λ_{max}	P value Emission Intensity	P value Wavelength λ_{ex}	P value Wavelength λ_{em}
A x B	0.0390 *	> 0.9999 n.s.	0.0013 **	0.2863 n.s.	0.2903 n.s.
A x C	< 0.0001 ****	0.0043 **	< 0.0001 ****	< 0.0001 ****	0.0004 ***
C x D	> 0.9999 n.s.	> 0.9999 n.s.	> 0.9999 n.s.	> 0.9999 n.s.	> 0.9999 n.s.
B x D	< 0.0001 ****	0.0145 *	< 0.0001 ****	0.0793 n.s.	0.3894 n.s.

Table 3-8 Summary of the parameters obtained from UV/Vis and fluorescence measurement. UV-Vis data reflect the maximum Absorbance measured at λ_{max} . Fluorescence parameters were obtained at fixed excitation wavelengths (G5 = 350 nm, G4.5 = 380 nm), whereby λ_{em} is the wavelength with the maximum fluorescence intensity.

ID	PAMAM	pH	MeOH	Absorbance / AU M \pm SEM	Wavelength λ_{max} / nm M \pm SEM	Emission Intensity M \pm SEM	Wavelength λ_{em} / nm M \pm SEM
A	G4.5	4	0 %	0.28 \pm 0.02	288.7 \pm 0.3	47.55 \pm 7.59	460.3 \pm 0.9
B	G4.5	7		0.37 \pm 0.03	287.3 \pm 0.7	47.42 \pm 12.47	458.0 \pm 2.5
C	G4.5	10		0.40 \pm 0.01	288.0 \pm 0.4	39.43 \pm 4.50	463.2 \pm 0.5
D	G5	4		0.18 \pm 0.02	275.7 \pm 0.9	15.0 \pm 2.54	452.7 \pm 7.1
E	G5	7		0.18 \pm 0.01	276.3 \pm 0.3	6.93 \pm 0.79	438.5 \pm 4.9
F	G5	10		0.15 \pm 0.02	278.0 \pm 1.5	6.57 \pm 0.28	427.8 \pm 2.0
G	G4.5	4	2 %	0.23 \pm 0.03	287.3 \pm 0.9	76.21 \pm 5.04	461.6 \pm 2.7
H	G4.5	7		0.30 \pm 0.01	288.0 \pm 0.4	77.24 \pm 3.63	461.0 \pm 1.4
I	G4.5	10		0.36 \pm 0.02	288.7 \pm 0.3	71.97 \pm 7.77	463.3 \pm 2.0
J	G5	4		0.18 \pm 0.02	273.5 \pm 2.5	8.89 \pm 0.61	440.8 \pm 3.3
K	G5	7		0.17 \pm 0.01	275.8 \pm 4.3	7.22 \pm 0.46	430.2 \pm 2.4
L	G5	10		0.17 \pm 0.01	269.8 \pm 2.1	8.93 \pm 0.25	431.8 \pm 1.1

Table 3-9 Statistical comparison of the UV/Vis and fluorescence data of Table 3-8. Outcome of the ANOVA and Bonferroni's multiple comparison test are displayed as p value with indication of significance level and non-significant (n.s.) denotation where applicable.

Comparison	P value Absorbance	P value Wavelength λ_{max}	P value Emission Intensity	P value Wavelength λ_{em}
A \times B	0.1047 n.s.	> 0.9999 n.s.	> 0.9999 n.s.	> 0.9999 n.s.
A \times C	> 0.9999 n.s.	> 0.9999 n.s.	> 0.9999 n.s.	> 0.9999 n.s.
B \times C	0.0018 **	> 0.9999 n.s.	> 0.9999 n.s.	> 0.9999 n.s.
D \times E	> 0.9999 n.s.	> 0.9999 n.s.	> 0.9999 n.s.	0.0596 n.s.
E \times F	> 0.9999 n.s.	> 0.9999 n.s.	> 0.9999 n.s.	0.1973 n.s.
D \times F	> 0.9999 n.s.	> 0.9999 n.s.	> 0.9999 n.s.	< 0.0001 ****
G \times H	0.2176 n.s.	> 0.9999 n.s.	> 0.9999 n.s.	> 0.9999 n.s.

H × I	> 0.9999 n.s.	> 0.9999 n.s.	> 0.9999 n.s.	> 0.9999 n.s.
G × I	0.0121*	> 0.9999 n.s.	> 0.9999 n.s.	> 0.9999 n.s.
J × K	> 0.9999 n.s.	> 0.9999 n.s.	> 0.9999 n.s.	0.3093 n.s.
K × L	> 0.9999 n.s.	0.6001 n.s.	> 0.9999 n.s.	> 0.9999 n.s.
J × L	> 0.9999 n.s.	> 0.9999 n.s.	> 0.9999 n.s.	0.7624 n.s.
<hr/>				
A × G	> 0.9999 n.s.	> 0.9999 n.s.	0.0050 **	> 0.9999 n.s.
A × D	0.0171 *	0.0026 **	0.0010 ***	> 0.9999 n.s.
D × J	> 0.9999 n.s.	> 0.9999 n.s.	> 0.9999 n.s.	0.2278 n.s.
G × J	> 0.9999 n.s.	0.0005 ***	> 0.9999 n.s.	0.0008 ***
<hr/>				
B × H	0.7564 n.s.	> 0.9999 n.s.	0.0013 **	> 0.9999 n.s.
B × E	< 0.0001 ****	0.0079 **	< 0.0001 ****	0.0020 **
E × K	> 0.9999 n.s.	> 0.9999 n.s.	> 0.9999 n.s.	> 0.9999 n.s.
H × K	< 0.0001 ****	0.0008 ***	< 0.0001 ****	< 0.0001 ****
<hr/>				
C × I	0.9317 n.s.	> 0.9999 n.s.	0.0004 ***	> 0.9999 n.s.
C × F	< 0.0001 ****	0.0058 **	< 0.0001 ****	< 0.0001 ****
F × L	> 0.9999 n.s.	0.0428 *	> 0.9999 n.s.	> 0.9999 n.s.
I × L	< 0.0001 ****	< 0.0001 ****	< 0.0001 ****	< 0.0001 ****

3.7.3 SAXS fitting parameters Spherical Shell

All SAXS data for PAMAM G5 and G4.5 were fitted to a Spherical Shell form factor, where the core and shell contribution are reflected by an overall outer radius (R_1), with an associated degree of polydispersity σ , an inner radius of the core (R_2), a scattering length difference between shell and surrounding matrix ($\Delta\eta$), and a scattering length density difference between core and matrix relative to the shell contrast ($\mu\Delta\eta$)²³. Additional parameters used for fitting were the scale factor N and the background Intensity.

Table 3-10 SAXS fitting parameters obtained from fitting a Spherical Shell form factor.

	pH	MeOH	N	Polydispersity (σ) / Å	Outer	Inner	Ncore ($\mu\Delta\eta$)	Nshell ($\Delta\eta$)	Background
					Radius / Å (R_1)	Radius / Å (R_2)			
PAMAMG5	4		1	6.6	26.8	8.005	0.26	1.78E-07	0.0005
	7	1 %	1	6	26.99	12.05	0.26	1.21E-06	0.0003
	10		1	6.6	23.57	10.28	0.26	1.16E-06	0.0003
	4		1	6.6	28.76	9.104	0.26	1.71E-06	0.0002
	7	0 %	1	6.6	28.58	11.74	0.26	1.45E-06	0.0001
	10		1	8.1	23.52	10.37	0.26	1.31E-06	0.0001
PAMAMG4.5	4		1	5.55	19.90	6.81	0.21	1.92E-06	0.0003
	7	1 %	1	6	19.13	7.85	0.21	2.02E-06	0.0002
	10		1	6	18.42	6.38	0.21	1.69E-06	0.0003
	4		1	4.96	21.12	8.81	0.21	1.95E-06	0.0001
	7	0 %	1	7.32	23.16	9.91	0.26	2.09E-06	0.0001
	10		1	7.51	20.35	7.45	0.21	9.09E-07	0.0001

3.7.4 Coarse-grained PAMAM dendrimer models

In our coarse-grained dendrimer model, each chemical group is represented by a spherical particle or monomer. The total number of monomers in the full-generation case is calculated by

$$N_{\text{full}} = 2 + (S + 1)(f + 1) \sum_{i=0}^{\text{gen}} (f - 1)^i$$

whereas, that for the half-generational case is given by

$$N_{\text{half}} = 2 + S(f + 1)(f - 1)^{\text{gen}} + (S + 1)(f + 1) \sum_{i=0}^{\text{gen}-1} (f - 1)^i$$

where the functionality $f=3$, the maximum generation index gen is 5, and the number of neutral spacers (methylene groups) in each branch is $S=3$.

Table 3-11 lists the average numbers of different types of monomers in PAMAM dendrimers with generations 5 and 4.5, as well as the corresponding numbers of counterions.

Table 3-11 Total number of monomers and average numbers of charged monomers (ratio over all chargeable ones) in each PAMAM molecule at different pH values, as well as the number of counterions included to neutralize the system. Note that in cases of G4.5, counterions are included for both the negatively charged carboxyl and positively charged tertiary amine groups.

	pH	Ratio of charged surface groups *	Ratio of charged Tertiary Amines (core)	Total number of Monomers	Total number of Counterions
PAMAM G5	4	128 / 128	120 / 124	1010	248
	7	128 / 128	3 / 124	1010	131
	10	30 / 128	0 / 124	1010	30
PAMAM G4.5	4	17 / 128	120 / 124	754	137
	7	128 / 128	3 / 124	754	131
	10	128 / 128	0 / 124	754	128

* Surface (outer functional) groups for PAMAM G5 = primary Amines; for PAMAM G4.5 = carboxyl groups

In each of our simulation system, a single dendrimer is introduced in the cubic simulation box with periodic boundary conditions applied in all three directions. Counterions are added to maintain charge neutrality in the system. All dendrimer monomers and counterions are taken to be of the same diameter σ . The excluded volume effects of these particles are modelled by the pairwise Lennard-Jones (LJ) interaction potential

$$U_{LJ}(r_{ij}) = 4\epsilon \left[\left(\frac{\sigma}{r_{ij}} \right)^{12} - \left(\frac{\sigma}{r_{ij}} \right)^6 \right]$$

where r_{ij} is the center-to-center distance between particles i and j . The particles are embedded in a dielectric continuum solvent at Θ -condition with no explicit solvent molecules. The LJ parameter ϵ is set to be $0.34k_B T$, where k_B is the Boltzmann constant and T is the temperature, and the cut-off distance of the LJ interaction forces is $R_c = 2.5\sigma$.^{24,25} All charged monomers and counterions carry monovalent charges. Their electrostatic interaction strength is measured by the Bjerrum length $l_B = e^2 / \epsilon k_B T$ which is defined as the distance at which the electrostatic interaction energy between two elementary charges e equals

thermal energy $k_B T$. Additionally, ϵ is the dielectric constant of the solvent. In this work, we take $l_B = 1\sigma$. There is thus no Manning condensation effect for dendrimers with relatively low charge density. The long-range electrostatic interaction forces in the periodic systems are calculated using the particle-particle-mesh (P3M) algorithm^{26,27} with the optimal splitting parameters²⁸.

The simulations are performed in the canonical ensemble where the constant temperature is obtained by coupling the system to a Langevin thermostat. The equations of motion of the particles are then given by^{24,25}

$$m\ddot{\mathbf{r}}_i(t) = -\zeta\dot{\mathbf{r}}_i(t) - \nabla_i U(\{\mathbf{r}(t)\}) + \mathbf{\Gamma}_i(t)$$

where m and \mathbf{r}_i are the mass and Cartesian coordinate of particle i . The friction coefficient takes the value of $\zeta = (mk_B T)^{1/2}/\sigma$, and the stochastic force $\mathbf{\Gamma}_i$ is a Gaussian white noise.

The equations of motion are solved numerically using the velocity-Verlet method with time step size $\Delta t = 10^{-3}\tau$ where $\tau = (m\sigma^2/k_B T)^{1/2}$ is the LJ time unit. The covalent bond lengths between adjacent monomers are constrained to a fixed value of $l = 1\sigma$ using the RATTLE algorithm²⁶ with tolerance of 10^{-7} . Our simulation model has been tested for the neutral and charged dendrimers with trifunctional groups as studied by Lyulin *et al.* using Brownian dynamics simulations and similar coarse-grained model²⁹. Good agreement has been found between our simulation results and those reported in their work on the radii of gyration, R_g , and monomer radial density distribution functions for dendrimers up to generation 5.

The number density of monomers in the central simulation box is fixed to $\rho = 8 \times 10^{-3}\sigma^{-3}$ which is low enough to avoid physical contact of the dendrimer with its periodic images, but sufficiently high for investigating the counterion-dendrimer interactions. In each simulation run, the system is first equilibrated for a period of $10^3\tau$ as neutral dendrimers and then another $5 \times 10^2\tau$ with charges switched on. Analysis data on the structural properties are then collected and

averaged over a further simulation period of $10^4\tau$. All simulation data reported in this work are results averaged over an ensemble of 25 independent runs.

The structural properties of a dendrimer with N monomers can be first characterized by calculating its gyration tensor S defined as

$$S_{\alpha,\beta} = \frac{1}{N} \sum_{i=1}^N (r_i^{(\alpha)} - r_{cm}^{(\alpha)})(r_i^{(\beta)} - r_{cm}^{(\beta)})$$

where $r_i^{(\alpha)}$ is the α^{th} Cartesian coordinate of the position vector r_i of monomer i , and $r_{cm}^{(\alpha)}$ is that of the position vector r_{cm} of the center of mass of the whole dendrimer. Diagonalizing the gyration tensor by transforming it to the principal axis system yields $S = \text{diag}(\lambda_1, \lambda_2, \lambda_3)$ with the three-tuple of principal moments $\lambda_1 \geq \lambda_2 \geq \lambda_3$. The trace (first invariant) of such a diagonalized tensor gives the squared radius of gyration³⁰, R_g , and the second invariant yields the relative shape anisotropy κ^2 (see more details in the Methods Section 3.2.5). The simulation results on R_g of PAMAM G5 and G4.5 at different pH are presented in Figure 8(f), and those for their aspect ratios and κ^2 are given in Section 3.7.2.2.

3.7.5 Overview of PAMAM G5 radii reported from computational and small angle scattering studies

Table 3-12 Size information of PAMAM G5 studied with small angle scattering and computational techniques. The radius was mostly provided as radius of gyration (R_g) of the whole molecule, but R_N only considers the location of the primary nitrogen (terminal amine groups). Depending of the fit chosen for the experimental data, R_S refers to the radius of a sphere and R_f to the radius of a sphere with a fuzzy edge. For SANS experiments where the solvent is deuterium oxide, the acidity scale factor a refers to the molar ratio of acid to primary amine and is adjusted with deuterated acid.

Method	Condition	Radius / Å	Fit / Approach
SAXS ³¹	Methanol	R_g 24.1	Sphere
		R_g 25.3	Guinier
		R_g 31.0	Zimm
SAXS ³²	Methanol	R_g 21.9	Polydisperse Sphere
		R_g 22.0	Ellipsoid of Revolution
SAXS ³³	Methanol	R_g 23.07 ± 0.03	Indirect Fourier Transform

		$R_s 29.95 \pm 0.08$	Polydisperse Sphere
		$R_g 22.76 \pm 0.09$	Rotational Ellipsoid
		$R_f 24.37 \pm 0.04$	Fuzzy Edge
SANS ³⁴	Bulk	$R_g 16.4 \pm 0.6$	Guinier
	$0 \leq x_s \leq 0.4$ <i>xs: mix of (methanol)/ (acetone)</i>	$R_g 22.1 \pm 0.2^a$	
		$R_g 22.9 \pm 0.2^b$	
SANS ³⁵	$\alpha = 0$	$R_g 26.2 \pm 0.53$	(1) S(Q): numerical solution of the Ornstein-Zernike integral equation (OZ) with the hypernetted chain closure (HNC), (2) P(Q): modified fuzzy ball model with diffuse edges
	$\alpha = 1$	$R_g 26.5 \pm 0.95^c$; 26.9 ± 0.30^d	
	$\alpha = 2$	$R_g 26.5 \pm 1.10^c$; 26.8 ± 0.25^d	
SANS ³⁶	$\alpha = 0; 0.23; 0.89; 1.60$ (respective pD of 10.38; 9.12; 6.79; 4.70)	$R_g 25.8648 + 0.5631\alpha^d$	(1) S(Q): OZ-HNC, (2) P(Q): modified fuzzy ball model with diffuse edges
Simulation ³⁷	Gas phase	$R_g 16.001$	Molecular Dynamics with atomistic configurations derived from continuous configurational Boltzmann biased direct Monte Carlo (CCBB-MC)
Simulation ³⁸	High pH (> 10)	$R_g 18.3 \pm 0.3$	MD with atomistic configurations derived from Insight II software package
	Neutral pH (~ 7)	$R_g 32.8 \pm 0.7$	
	Low pH (< 4) (Implicit water)	$R_g 38.0 \pm 0.1$	
Simulation ³⁹	Gas phase	$R_g 18.34 \pm 0.37$; $R_N 20.26 \pm 0.68$	MD with atomistic configurations derived from CCBB-MC
	High pH	$R_g 20.67 \pm 0.09$; $R_N 22.71 \pm 0.47$	
	Neutral pH	$R_g 22.19 \pm 0.14$; $R_N 24.43 \pm 0.07$	
	Low pH (explicit water with Cl ⁻ counter ions)	$R_g 24.76 \pm 0.14$; $R_N 27.38 \pm 0.18$	
Simulation ⁴⁰	Water with Cl ⁻ counter ions	$R_g 25.1 \pm 0.001$	MD with atomistic configurations derived from Insight II software Package

Simulation ⁴¹	Vacuum high pH	R _g 17.04 ± 0.09	MD with atomistic configurations derived from Insight II software Package
	Implicit water		
	High pH	R _g 18.02 ± 0.15	
	Neutral pH	R _g 20.78 ± 0.30	
	Low pH	R _g 26.47 ± 0.44	
	Implicit methanol		
	High pH	R _g 18.02 ± 0.15	
	Neutral pH	R _g 20.70 ± 0.37	
	Low pH	R _g 28.93 ± 0.32	
	Explicit methanol		
	High pH	R _g 21.01 ± 0.17	
	Neutral pH	R _g 22.38 ± 0.09	
Low pH	R _g 22.36 ± 0.09		
Simulation ³⁰	High pH	R _g 20.57	MD with atomistic configurations derived from CCBB-MC
	Low pH	R _g 26.1	
	(water with Cl ⁻ counter ions)		
Simulation ⁴²	Gas phase	R _g 18.15	MD of a coarse-grained (CG) model based on atomistic configurations from CCBB-MC
Simulation ⁴³	CG1	R _g 17.82	MD of three CG models and all-atoms model with atomistic configurations derived from Materials Studio software package
	CG2	R _g 14.31	
	CG3	R _g 18.05	
	All Atoms	R _g 18.03	
	(no water)		
Simulation ⁴⁴	High pH	R _g 19.00 ± 0.06	MD with atomistic configurations derived from Dendrimer Builder Toolkit
	Low pH	R _g 25.32 ± 0.22	
	(water with counter ions)		

^a at 20 °C

^b at 50 °C

^c α adjusted with D₂SO₄

^d α adjusted with DCl

3.7.6 References – Supplementary Information

1. Liang, K.; Gao, Y.; Xiao, S.; Tay, F. R.; Weir, M. D.; Zhou, X.; Oates, T. W.; Zhou, C.; Li, J.; Xu, H. H. K., Poly(amido amine) and rechargeable adhesive containing calcium phosphate nanoparticles for long-term dentin remineralization. *Journal of dentistry* **2019**, *85*, 47-56.
2. Buwalda, S. J.; Bethry, A.; Hunger, S.; Kandoussi, S.; Coudane, J.; Nottelet, B., Ultrafast in situ forming poly(ethylene glycol)-poly(amido amine) hydrogels

with tunable drug release properties via controllable degradation rates. *European journal of pharmaceuticals and biopharmaceutics : official journal of Arbeitsgemeinschaft fur Pharmazeutische Verfahrenstechnik e.V* **2019**, *139*, 232-239.

3. Jain, A.; Mahira, S.; Majoral, J. P.; Bryszewska, M.; Khan, W.; Ionov, M., Dendrimer mediated targeting of siRNA against polo-like kinase for the treatment of triple negative breast cancer. *Journal of biomedical materials research. Part A* **2019**, *107* (9), 1933-1944.
4. Serri, A.; Mahboubi, A.; Zarghi, A.; Moghimi, H. R., PAMAM-dendrimer Enhanced Antibacterial Effect of Vancomycin Hydrochloride Against Gram-Negative Bacteria. *J Pharm Pharm Sci* **2018**, *22* (1), 10-21.
5. Staehlke, S.; Lehnfeld, J.; Schneider, A.; Nebe, J. B.; Muller, R., Terminal chemical functions of polyamidoamine dendrimer surfaces and its impact on bone cell growth. *Material Science and Engineering: C* **2019**, *101*, 190-203.
6. He, L.; Wu, D.; Tong, M., The influence of different charged poly (amido amine) dendrimer on the transport and deposition of bacteria in porous media. *Water Res* **2019**, *161*, 364-371.
7. Mohammadpour, R.; Yazdimamaghani, M.; Reilly, C. A.; Ghandehari, H., Transient Receptor Potential Ion Channel-Dependent Toxicity of Silica Nanoparticles and Poly(amido amine) Dendrimers. *J Pharmacol Exp Ther* **2019**, *370* (3), 751-760.
8. Roy, B.; Guha, P.; Nahak, P.; Karmakar, G.; Maiti, S.; Mandal, A. K.; Bykov, A. G.; Akentiev, A. V.; Noskov, B. A.; Tsuchiya, K.; Torigoe, K.; Panda, A. K., Biophysical Correlates on the Composition, Functionality, and Structure of Dendrimer-Liposome Aggregates. *ACS Omega* **2018**, *3* (9), 12235-12245.
9. Markowicz-Piasecka, M.; Sadkowska, A.; Podsiedlik, M.; Mikiciuk-Olasik, E.; Sikora, J., Generation 2 (G2) - Generation 4 (G4) PAMAM dendrimers disrupt key plasma coagulation parameters. *Toxicol In Vitro* **2019**, *59*, 87-99.
10. Holmes, A. M.; Heylings, J. R.; Wan, K. W.; Moss, G. P., Antimicrobial efficacy and mechanism of action of poly(amidoamine) (PAMAM) dendrimers against opportunistic pathogens. *Int J Antimicrob Agents* **2019**, *53* (4), 500-507.
11. Lombardo, D.; Calandra, P.; Magazu, S.; Wanderlingh, U.; Barreca, D.; Pasqua, L.; Kiselev, M. A., Soft nanoparticles charge expression within lipid membranes: The case of amino terminated dendrimers in bilayers vesicles. *Colloids and Surfaces B-Biointerfaces* **2018**, *170*, 609-616.
12. Tripathi, P. K.; Gorain, B.; Choudhury, H.; Srivastava, A.; Kesharwani, P., Dendrimer entrapped micro sponge gel of dithranol for effective topical treatment. *Heliyon* **2019**, *5* (3), e01343.

13. Cui, Y. S.; Liang, B.; Wang, L. G.; Zhu, L. L.; Kang, J. X.; Sun, H. T.; Chen, S. F., Enhanced biocompatibility of PAMAM dendrimers benefiting from tuning their surface charges. *Materials Science & Engineering C - Materials for Biological Applications* **2018**, *93*, 332-340.
14. Singh, M. K.; Kuncha, M.; Nayak, V. L.; Sarma, A. V. S.; Kumar, M. J. M.; Chauhan, A. S.; Sistla, R., An innovative in situ method of creating hybrid dendrimer nano-assembly: An efficient next generation dendritic platform for drug delivery. *Nanomedicine : nanotechnology, biology, and medicine* **2019**, *21*, 102043.
15. Serchenya, T.; Shcharbin, D.; Shyrochyna, I.; Sviridov, O.; Terekhova, M.; Dzmitruk, V.; Abashkin, V.; Apartsin, E.; Mignani, S.; Majoral, J. P.; Ionov, M.; Bryszewska, M., Immunoreactivity changes of human serum albumin and alpha-1-microglobulin induced by their interaction with dendrimers. *Colloids and Surfaces B-Biointerfaces* **2019**, *179*, 226-232.
16. Inoue, M.; Ueda, M.; Higashi, T.; Anno, T.; Fujisawa, K.; Motoyama, K.; Mizuguchi, M.; Ando, Y.; Jono, H.; Arima, H., Therapeutic Potential of Polyamidoamine Dendrimer for Amyloidogenic Transthyretin Amyloidosis. *ACS Chem Neurosci* **2019**, *10* (5), 2584-2590.
17. Tian, F. J.; Lin, X.; Valle, R. P.; Zuo, Y. Y.; Gu, N., Poly(amidoamine) Dendrimer as a Respiratory Nanocarrier: Insights from Experiments and Molecular Dynamics Simulations. *Langmuir : the ACS journal of surfaces and colloids* **2019**, *35* (15), 5364-5371.
18. Patel, M.; De Paoli, S. H.; Elhelu, O. K.; Farooq, S.; Simak, J., Cell membrane disintegration and extracellular vesicle release in a model of different size and charge PAMAM dendrimers effects on cultured endothelial cells. *Nanotoxicology* **2019**, *13* (5), 664-681.
19. Tariq, I.; Pinnapireddy, S. R.; Duse, L.; Ali, M. Y.; Ali, S.; Amin, M. U.; Goergen, N.; Jedelska, J.; Schafer, J.; Bakowsky, U., Lipodendriplexes: A promising nanocarrier for enhanced gene delivery with minimal cytotoxicity. *European journal of pharmaceuticals and biopharmaceutics : official journal of Arbeitsgemeinschaft fur Pharmazeutische Verfahrenstechnik e.V* **2019**, *135*, 72-82.
20. Czarnomysy, R.; Bielawska, A.; Bielawski, K., Effect of 2nd and 3rd generation PAMAM dendrimers on proliferation, differentiation, and pro-inflammatory cytokines in human keratinocytes and fibroblasts. *International journal of nanomedicine* **2019**, *14*, 7123-7139.
21. Akhtar, S.; Chandrasekhar, B.; Yousif, M. H.; Renno, W.; Benter, I. F.; El-Hashim, A. Z., Chronic administration of nano-sized PAMAM dendrimers in vivo inhibits EGRF-ERK1/2-ROCK signaling pathway and attenuates diabetes-induced vascular remodeling and dysfunction. *Nanomedicine : nanotechnology, biology, and medicine* **2019**, *18*, 78-89.

22. Wang, G.; Fu, L.; Walker, A.; Chen, X.; Lovejoy, D. B.; Hao, M.; Lee, A.; Chung, R.; Rizos, H.; Irvine, M.; Zheng, M.; Liu, X.; Lu, Y.; Shi, B., Label-Free Fluorescent Poly(amidoamine) Dendrimer for Traceable and Controlled Drug Delivery. *Biomacromolecules* **2019**, *20* (5), 2148-2158.
23. Pedersen, J. S., Analysis of small-angle scattering data from colloids and polymer solutions: modeling and least-squares fitting. *Advances in colloid and interface science* **1997**, *70*, 171-210.
24. Micka, U.; Holm, C.; Kremer, K., Strongly Charged, Flexible Polyelectrolytes in Poor Solvents: Molecular Dynamics Simulations. *Langmuir : the ACS journal of surfaces and colloids* **1999**, *15* (12), 4033-4044.
25. Wang, Z.; Rubinstein, M., Regimes of conformational transitions of a diblock polyampholyte. *Macromolecules* **2006**, *39*, 5897-5912.
26. Hockney, R. W.; Eastwood, J. W., *Computer Simulation Using Particles*. 2021.
27. Luty, B. A.; van Gunsteren, W. F., Calculating Electrostatic Interactions Using the Particle-Particle Particle-Mesh Method with Nonperiodic Long-Range Interactions. *The Journal of Physical Chemistry* **1996**, *100* (7), 2581-2587.
28. Deserno, M.; Holm, C., How to mesh up Ewald sums. I. A theoretical and numerical comparison of various particle mesh routines. *The Journal of chemical physics* **1998**, *109* (18), 7678-7693.
29. Lyulin, S. V.; Lyulin, A. V.; Darinski, A. A., Brownian dynamics simulation of charged dendrimers. *Polymer Science. Series A* **2004**, *46* (2), 196 - 206.
30. Maiti, P. K.; Bagchi, B., Diffusion of flexible, charged, nanoscopic molecules in solution: Size and pH dependence for PAMAM dendrimer. *The Journal of chemical physics* **2009**, *131* (21), 214901.
31. Prosa, T. J.; Bauer, B. J.; Amis, E. J.; Tomalia, D. A.; Scherrenberg, R., A SAXS study of the internal structure of dendritic polymer systems. *Journal of Polymer Science Part B: Polymer Physics* **1997**, *35* (17), 2913-2924.
32. Prosa, T. J.; Bauer, B. J.; Amis, E. J., From Stars to Spheres: A SAXS Analysis of Dilute Dendrimer Solutions. *Macromolecules* **2001**, *34* (14), 4897-4906.
33. Rathgeber, S.; Monkenbusch, M.; Kreitschmann, M.; Urban, V.; Brulet, A., Dynamics of star-burst dendrimers in solution in relation to their structural properties. *The Journal of Chemical Physics* **2002**, *117* (8), 4047-4062.
34. Topp, A.; Bauer, B. J.; Tomalia, D. A.; Amis, E. J., Effect of Solvent Quality on the Molecular Dimensions of PAMAM Dendrimers. *Macromolecules* **1999**, *32* (21), 7232-7237.
35. Hong, K.; Liu, Y.; Porcar, L.; Liu, D.; Gao, C. Y.; Smith, G. S.; Herwig, K. W.; Cai, S.; Li, X.; Wu, B.; Chen, W.-R.; Liu, L., Structural response of polyelectrolyte

dendrimer towards molecular protonation: the inconsistency revealed by SANS and NMR. *Journal of Physics: Condensed Matter* **2012**, *24* (6), 064116.

36. Porcar, L.; Liu, Y.; Verduzco, R.; Hong, K.; Butler, P. D.; Magid, L. J.; Smith, G. S.; Chen, W.-R., Structural Investigation of PAMAM Dendrimers in Aqueous Solutions Using Small-Angle Neutron Scattering: Effect of Generation. *The Journal of Physical Chemistry B* **2008**, *112* (47), 14772-14778.

37. Çagin, T.; Wang, G.; Martin, R.; Breen, N.; Goddard, W. A., Molecular modelling of dendrimers for nanoscale applications. *Nanotechnology* **2000**, *11* (2), 77-84.

38. Lee, I.; Athey, B. D.; Wetzel, A. W.; Meixner, W.; Baker, J. R., Structural Molecular Dynamics Studies on Polyamidoamine Dendrimers for a Therapeutic Application: Effects of pH and Generation. *Macromolecules* **2002**, *35* (11), 4510-4520.

39. Maiti, P. K.; Çağın, T.; Lin, S.-T.; Goddard, W. A., Effect of Solvent and pH on the Structure of PAMAM Dendrimers. *Macromolecules* **2005**, *38* (3), 979-991.

40. Lee, H.; Baker, J. R.; Larson, R. G., Molecular Dynamics Studies of the Size, Shape, and Internal Structure of 0% and 90% Acetylated Fifth-Generation Polyamidoamine Dendrimers in Water and Methanol. *The Journal of Physical Chemistry B* **2006**, *110* (9), 4014-4019.

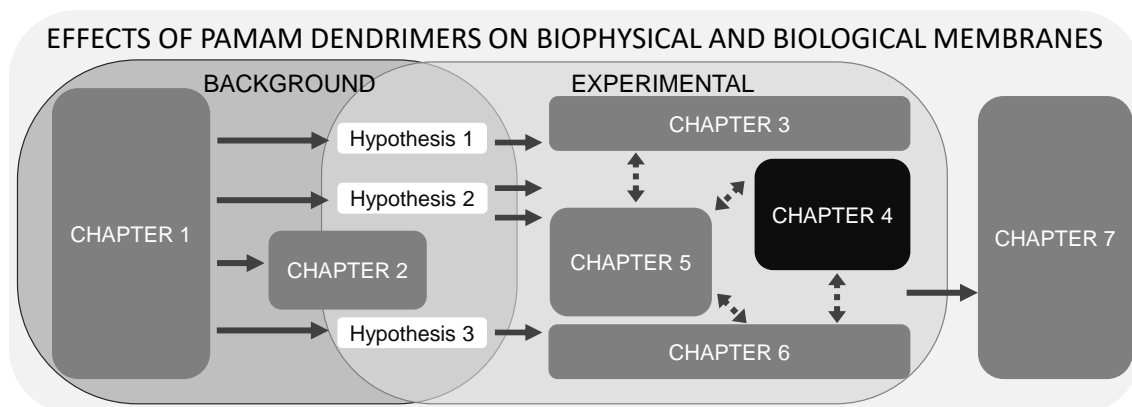
41. Opitz, A. W.; Wagner, N. J., Structural investigations of poly(amido amine) dendrimers in methanol using molecular dynamics. *Journal of Polymer Science Part B: Polymer Physics* **2006**, *44* (21), 3062-3077.

42. Maiti, P. K.; Li, Y.; Cagin, T.; III, W. A. G., Structure of polyamidoamide dendrimers up to limiting generations: A mesoscale description. *The Journal of Chemical Physics* **2009**, *130* (14), 144902.

43. Zhong, T.; Ai, P.; Zhou, J., Structures and properties of PAMAM dendrimer: A multi-scale simulation study. *Fluid Phase Equilibria* **2011**, *302* (1-2), 43-47.

44. Maingi, V.; Jain, V.; Bharatam, P. V.; Maiti, P. K., Dendrimer building toolkit: Model building and characterization of various dendrimer architectures. *Journal of Computational Chemistry* **2012**, *33* (25), 1997-2011.

CHAPTER 4: BIOPHYSICAL STUDIES IN POLYMER THERAPEUTICS: THE INTERACTIONS OF ANIONIC AND CATIONIC PAMAM DENDRIMERS WITH LIPID MONOLAYERS



Wilde, M., Green, R. J., Sanders, M. R. and Greco, F. (2017) Biophysical studies in polymer therapeutics: the interactions of anionic and cationic PAMAM dendrimers with lipid monolayers. *Journal of Drug Targeting*, 25 (910). pp. 910-918. <https://doi.org/10.1080/1061186X.2017.1365877>

This chapter is the reproduction of the 'Accepted Manuscript' (permission of the publisher granted). It shows how lipid monolayers under simplified physiological conditions and biophysical techniques can be used as tool to study molecule-membrane interactions. Here, we used PAMAM dendrimers with anionic (G4.5) and cationic (G5) surface groups and zwitterionic DPPC and anionic DPPG as mono-lipid membrane models.

The estimated contribution of the candidate to the work described in this chapter is 80 %, whereby data on PEG and preliminary PAMAM results were generated during MW's Master thesis (~20 %).

MW: Conceptualization, Data curation, Investigation, Formal analysis, Validation, Visualization, Writing – original draft

MRS: Data curation, Investigation, Formal analysis, Validation, and Visualization, Writing – review & editing

FG: Conceptualization, Funding acquisition, Project administration Supervision, Writing – review & editing

RJG: Conceptualization, Funding acquisition, Project administration, Supervision, Writing – review & editing

4 BIOPHYSICAL STUDIES IN POLYMER THERAPEUTICS: THE INTERACTIONS OF ANIONIC AND CATIONIC PAMAM DENDRIMERS WITH LIPID MONOLAYERS

Marleen Wilde^a, Rebecca J. Green^a, Michael R. Sanders^{ab} and Francesca Greco^a

^aSchool of Pharmacy, University of Reading, Whiteknights, Reading, RG6 6AD, United Kingdom.

^bCurrent address: Department of Chemistry, King's College London, Britannia House, 7 Trinity Street, London, SE1 1DB, United Kingdom.

KEYWORDS

PAMAM dendrimers; anionic; lipid monolayer; surface pressure; FTIR

ACKNOWLEDGEMENTS

The authors thank the Erasmus program and University of Reading for funding of the project and students involved. Hannah Burnhams and Josh Howgego are also acknowledged for carrying out preliminary investigations.

ABSTRACT

Understanding how polymers interact with biological membranes is important for the development of polymer based therapeutics and wider biomedical applications. Here, biophysical methods (surface pressure measurements, external reflection FTIR) have been used to investigate the interaction between PAMAM dendrimers (Generation 5 or 4.5) and anionic (DPPG) or zwitterionic (DPPC) model membranes. We observed a concentration-dependent binding behaviour of both PAMAM species to both model membranes; however, equivalent levels of penetration into DPPC monolayers required approximately 10-fold higher dendrimer concentrations than for penetration into DPPG monolayers. Overall, the anionic PAMAM G4.5 showed a slightly better penetration ability which could be caused by repulsive forces towards the lipid layers. In comparison, increasing concentration of cationic PAMAM G5 leads to saturation of adsorption at the anionic lipid surface before penetration into the lipid layer likely driven by electrostatic attraction. Our studies also showed that physiologically relevant concentrations of sodium chloride (144 mM) decreased PAMAM penetration into DPPG monolayers but did not significantly affect the dendrimer-DPPC interaction. These results provide an insight into the mechanism of interaction between charged dendritic polymers with a lipid interface and show that the nature of such interactions are affected by lipid headgroup, dendrimer charge and solution salinity.

4.1 INTRODUCTION

Poly (amidoamine) (PAMAM) dendrimers are monodispersed polymeric systems characterised by a well-defined molecular architecture ^{1,2}. In the context of polymer therapeutics, PAMAM dendrimers have been explored for multiple purposes: as drug/gene carriers ³⁻⁵ and as biologically active polymers *per se*. In particular, full generation PAMAM dendrimers have been investigated for use in gene delivery ⁶ as the positive charges conferred by the primary amino groups on the surface of the dendrimer make them ideal for complexing with negatively charged DNA ^{7,8}.

While PAMAM dendrimers have proved to be efficient gene transfer agents, their transition into medical products is somewhat limited by their toxicity, previously reported to be concentration-, generation-, and charge-dependent ⁹⁻¹¹. Therefore, studies have investigated PAMAM dendrimer - cell membrane (or model membrane) interactions, to determine: (a) the mechanisms of gene transfer ^{7,12,13}, (b) the mechanism of toxicity ¹⁴⁻¹⁶, and, most importantly, (c) physico-chemical factors affecting PAMAM toxicity ¹⁷⁻¹⁹, in view of tailoring the chemical structure to produce more optimised systems. Moreover, PAMAM dendrimers have displayed antibacterial properties ²⁰⁻²³, which makes them potentially interesting candidates as drugs, *per se*.

Biophysical and *in vitro* biological studies have been carried out to elucidate PAMAM-membrane interactions, primarily using cells ^{24,25}, vesicles ²⁶⁻²⁸, and lipid bilayers ^{27,29-31}. For studies investigating the impact of lipid composition and solution properties on polymer binding to model membranes, lipid monolayers at the air/water interface are well-established physico-chemical models. Lipid monolayers have been used extensively to investigate lipid layer phase states ³², protein/peptide binding to lipid surfaces ^{33,34}, and DNA adsorption ^{35,36}. Their simplicity does not reflect the complexity of biological scenarios, but in turn, it does allow an excellent control over individual features and, as a result, it allows assessment of the individual contribution of different factors. In contrast to other model systems, lipid monolayers allow the lipid composition and lipid density to be selected and modified without restriction. Lipid monolayers have proved to be

good models to understand interactions of antimicrobial peptides^{37, 38} with bacterial membranes. In general, results obtained from monolayer-based experiments are in accordance with observations on other membrane models^{29,37,39}.

Herein, we present a systematic study looking at PAMAM dendrimers in lipid monolayers as a simple and tuneable model system to assess polymer – biological membrane interactions. We have investigated the impact of polymer charge and concentration on its interactions with a zwitterionic and an anionic model membrane. Specifically, to produce the model membranes two saturated phospholipids were selected with differently charged head groups; 1,2-dipalmitoyl-*sn*-glycero-3-phosphocholine (DPPC, zwitterionic) and 1,2-dipalmitoyl-*sn*-glycero-3-phospho-(1'-*rac*-glycerol) (sodium salt) (DPPG, anionic) (Figure 1), which are predominant polar lipids in eukaryotic and prokaryotic membranes, respectively^{40, 41}. Due to their simplistic structure, they are well-established model lipids to study membrane interactions under a wide range of conditions. As unsaturated phospholipids tend to create disorder in the hydrophobic region and hinder formation of the condensed phase in which the interaction experiments are to be carried out, the saturated 1,2-dipalmitoyl- phospholipids have been chosen for this study.

Surface pressure measurements were employed to determine penetration of polymers (details in Table 4-1, Figure 4-1) into lipid monolayer surfaces and to assess polymer selectivity towards different lipids. To measure the impact of polymer concentration and charge, studies were carried out on PAMAM dendrimers generation 5 (G5, cationic) and generation 4.5 (G4.5, anionic). Both dendrimers carrying 128 functional surface groups and are of a similar size. Linear polyethylene glycol (PEG) of a similar size (20,000 g mol⁻¹) was used as a negative control; as a model of a non-ionic, non-toxic polymer. Further, as most PEGylated products on the market contain linear PEG, it was decided that linear PEG would be a clinically relevant comparator. FTIR studies were carried out to complement and clarify the findings from surface pressure measurements.

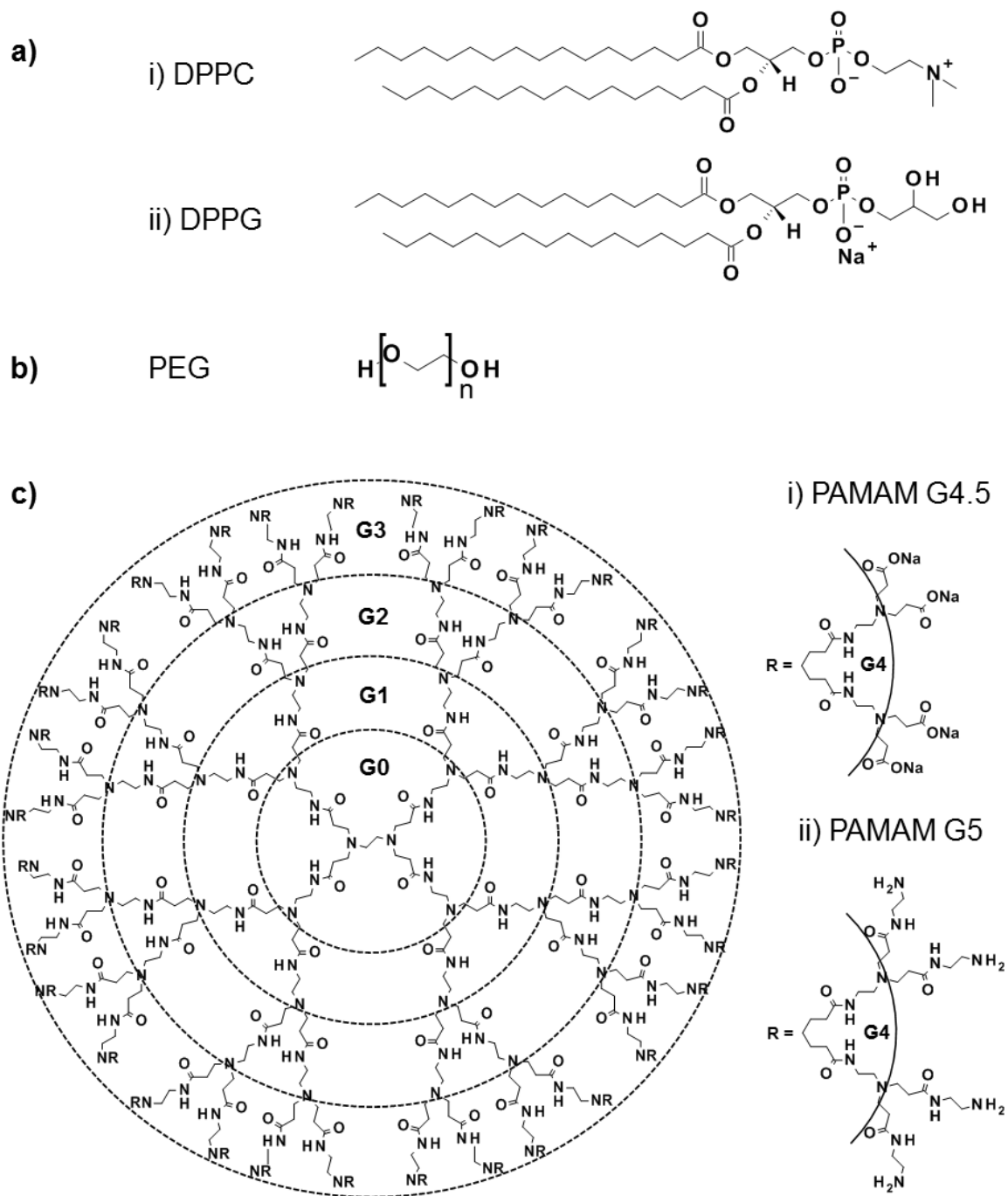


Figure 4-1 Chemical structures of the lipids and the polymers used in this study. a) Chemical structure of i) 1,2-dipalmitoyl-*sn*-glycero-3-phosphocholine (DPPC); ii) 1,2-dipalmitoyl-*sn*-glycero-3-phospho-(1'-*rac*-glycerol) (sodium salt) (DPPG). b) Chemical Structure of linear polyethylene glycol (PEG). c) Chemical structure of poly(amidoamine) (PAMAM) dendrimer with ethylenediamine core; generations inset: i) PAMAM G4.5: R-group anionic in solution (pH 7), sodium carboxylate surface groups; ii) PAMAM G5: R-group cationic in solution (pH 7), amino surface groups.

Table 4-1 Characteristics of the PAMAM dendrimers used in the study.

PAMAM (Poly(amidoamine))		
Generation	G4.5	G5
Molecular Weight (g mol ⁻¹) ^a	26,251.86	28,824.81
Charge (in methanol)	Anionic	Cationic
Charge density: ratio of number of amino groups to MW ^b	0.0048	0.0088 (0.0044) ^c

a As determined by the manufacturer

b Theoretical values

c Considering only surface amino groups

4.2 EXPERIMENTAL

4.2.1 Materials

Lipids were obtained from Avanti Polar Lipids, Inc (AL, USA). The solutions of 1,2-dipalmitoyl-*sn*-glycero-3-phosphocholine (DPPC; synthetic purity >99%, 734 g mol⁻¹) and 1,2-dipalmitoyl-*sn*-glycero-3-phospho-(1'-*rac*-glycerol) (sodium salt) (DPPG; synthetic purity >99%, 745 g mol⁻¹) were prepared in chloroform (Sigma Aldrich UK, 99%+) to a concentration of 0.5 mg mL⁻¹. PAMAM G5 (~28,800 g mol⁻¹, ethylenediamine core), PAMAM G4.5 (~26,300 g mol⁻¹, ethylenediamine core) and Polyethylene glycol (PEG, 20,000 g mol⁻¹), the phosphate salts and solvents were obtained from Sigma Aldrich (Dorset, UK). Sodium chloride was obtained from Fisher Scientific UK Ltd (Loughborough, UK). Aqueous Phosphate buffer solution (20 mM) at pH 7 was prepared in house with UHQ water at 18.2 mΩ (ELGA purelab). Enriched salt buffer was prepared adding 144 mM sodium chloride to phosphate buffer pH 7.

4.2.2 Surface pressure measurements

Experiments were performed on a Langmuir-Blodgett trough (model 611, Nima Technology Ltd, Coventry, UK) equipped with barriers used for monolayer compression. Lipid monolayers were created at the air/liquid interface and surface pressure measurements were carried out using the Wilhelmy plate method as previously described^{34, 38}. The trough was filled with 80 mL of phosphate buffer,

onto which 25 μL of a 0.5 mg mL^{-1} lipid solution was spread on the surface. After allowing up to 15 min for the chloroform to evaporate, surface pressure versus area per molecule isotherms were recorded; and the lipid layer was compressed and held in the condensed phase at $21 \pm 2 \text{ mN m}^{-1}$. Two millilitres of concentrated polymer solution (0.1 - 25 mg mL^{-1} in phosphate buffer) were then introduced into the buffer subphase with a custom-made needle to obtain concentrations ranges from 0.0024 – 0.6 mg mL^{-1} . The polymer-lipid interaction was recorded as a function of surface pressure versus time until equilibration and the maximum change in surface pressure determined.

4.2.3 External reflection FTIR spectroscopy

ER-FTIR spectra were recorded using a ThermoNicolet Nexus instrument (Madison, WI, USA) fitted with a monolayer/grazing angle accessory (Specac 19650 series, Kent, UK). The instrument was also fitted with a mercury cadmium telluride (MCT) detector and connected to an air dryer to purge the instrument of water and carbon dioxide. A small PTFE trough was used to control lipid compression and allow studies at the air/water interface to be carried out. The grazing angle accessory was set to a grazing incident angle of 55° from the surface of the trough. Polymer-lipid interactions were analysed using external reflectance as described by Lad et al³⁸.

All FTIR spectra were collected at a resolution 4 cm^{-1} where 256 interferograms were collected, co-added and ratioed against a background spectrum of D_2O buffer solution. In each experiment, 9.5 mL of 20 mM sodium phosphate buffer (pD 7.0) were placed in the trough and a background single beam spectra recorded. The lipid solution (5 μL of 0.5 mg mL^{-1}) was spread onto the surface of the buffer and compressed to $21 \pm 2 \text{ mN m}^{-1}$ predefined using surface pressure measurements, as described previously³⁸. After collection of the lipid spectra, 500 μL of PAMAM solution was introduced into the phosphate buffer subphase in stages to allow for measurements of binding at different polymer concentrations of 0.0024, 0.0125, 0.018 and 0.024 mg mL^{-1} for binding to a DPPG monolayer and 0.02, 0.06, 0.12 and 0.3 mg mL^{-1} for binding to DPPC monolayer. These different ranges of concentrations were selected based on the concentrations that had

shown a similar response (similar Δ surface pressure) in the previous experiments (Figure 4-3). Spectra were collected continually for the first 30 min after polymer injection, and one spectrum every 15 min for a total of 2 h until the next polymer addition.

The interaction of the polymer with the lipid monolayer was observed by monitoring the amide region, 1,700 – 1,550 cm^{-1} , and the CH_2 asymmetric and symmetric stretching frequencies (2,850 – 2,930 cm^{-1}). To correct for any water vapor present, H_2O and HOD spectra were scaled and subtracted against dendrimer adsorbed spectra, the degree of subtraction was dependent on the adsorption time as well as the amount of H/D exchange. No further processing was performed.

4.3 RESULTS

4.3.1 Effect of polymer charge on polymer-lipid interactions

In this initial study, we selected two PAMAM dendrimers (G4.5 and G5) and PEG. The polymers had very similar molecular weights (approx. 30,000 Da, see Table 4-1), but differed in charge. While at neutral pH the full-generation PAMAM dendrimers (including G5) have the primary amines of their surface groups protonated and therefore carry a cationic charge^{42, 43}, the carboxylate surface groups of their half-generation counterparts (e.g. G4.5) are deprotonated and account for the anionic charge of these dendrimers. Considering the charge difference of the otherwise structurally similar PAMAM dendrimer molecules, we studied their interaction with differently charged lipid monolayers and compared the results to those of linear, non-charged PEG 20,000. Aqueous solutions of these three polymers were exposed to DPPC and DPPG monolayer, as mimics of eukaryotic and procaryotic membranes. Surface pressure changes over time were recorded for PAMAM G5 and G4.5 and for PEG (all at 0.061 mg mL^{-1}) interacting with DPPC and DPPG monolayers compressed to the condensed phase (Figure 4-2). This technique records changes in surface pressure, indicative of a penetration of the molecules into the lipid monolayer. The addition of both PAMAM dendrimer types at 0.061 mg mL^{-1} produced distinctively different interaction

profiles for DPPG suggesting a different interaction mechanism and showed similar profiles with significantly less interaction for DPPC monolayers.

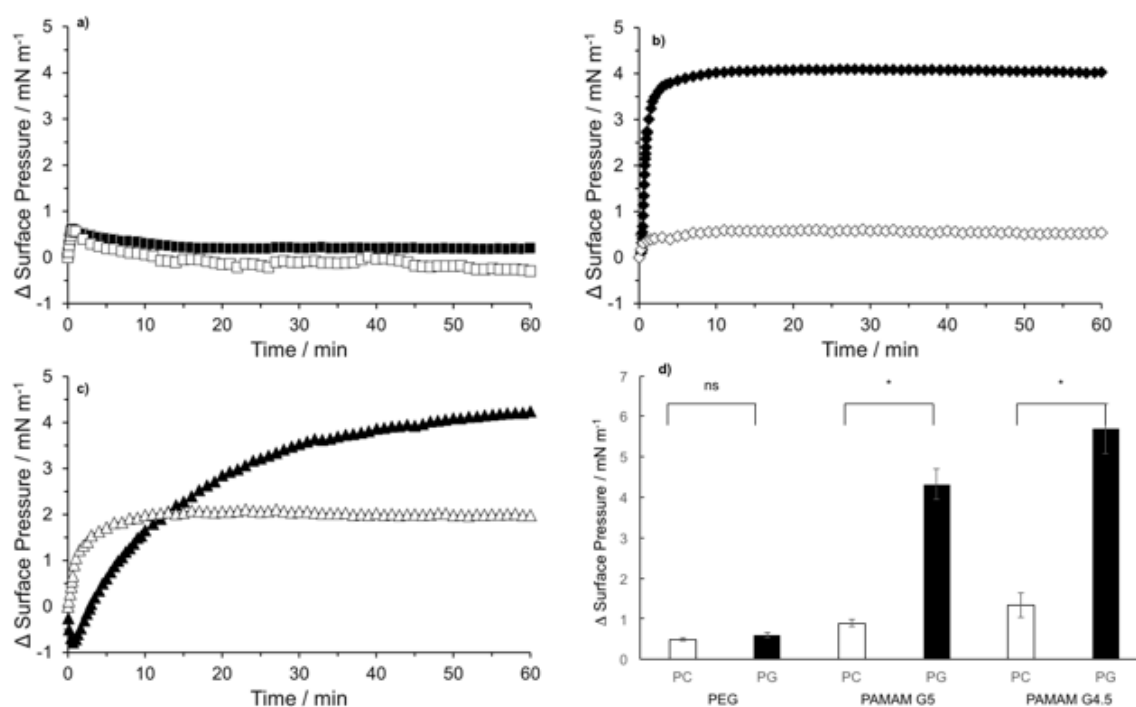


Figure 4-2 Selectivity of polymers towards different lipid monolayers. Changes in surface pressure for PEG 20,000 (panel a); PAMAM G5 (panel b); and PAMAM G4.5 (panel c) binding to DPPG (filled symbols) and DPPC (open symbols) monolayers were recorded over time. Experiments were carried out at pH 7, surface pressure was at $21 \pm 2 \text{ mN m}^{-1}$ immediately prior to polymer addition at concentration 0.061 mg mL^{-1} . Data show profiles for a single representative experiment from a set of at least 3 independent experiments ($n \geq 3$). Panel d shows comparison of maximum increase in surface pressure observed for the 3 polymers against DPPG (black) and DPPC (white), data show mean \pm SEM ($n \geq 3$). Statistical significance calculated via Student's *t* test, and set at $p \leq 0.05$. ns = non-significant.

More specifically, PAMAM G5 interaction with DPPG monolayers resulted in a fast increase reaching its maximum surface pressure within 10 min and remaining in equilibrium at this level; whereas in comparison PAMAM G4.5 first induced a small decrease in surface pressure prior to a slow but steady increase reaching its maximum surface pressure within 60 – 120 minutes of the observation period. The interaction of both dendrimers with DPPG monolayers resulted in a similar magnitude of change in surface pressure ($4.32 \pm 0.33 \text{ mN m}^{-1}$ and $5.69 \pm 0.58 \text{ mN m}^{-1}$ PAMAM G5 and PAMAM G4.5 respectively, Fig. 4-2d), which indicates that both dendrimers were able to penetrate the DPPG monolayer to a similar extent.

Conversely, little to no penetration of PAMAM dendrimers into the zwitterionic DPPC monolayer occurred at the dendrimer concentration of 0.061 mg mL^{-1} (Figure 4-2b and c, open symbols). Only minor increases in surface pressure were observed for dendrimer interaction with DPPC; $0.84 \pm 0.08 \text{ mN m}^{-1}$ and $1.34 \pm 0.25 \text{ mN m}^{-1}$ for PAMAM G5 and PAMAM G4.5 respectively (Figure 4-2d). This was probably because of the net-neutral charge of the DPPC headgroups did not offer sufficient electrostatic attraction to facilitate adsorption and penetration of the PAMAM dendrimers at this concentration.

In comparison, the non-charged PEG 20,000 displayed a different behaviour, showing no significant increase in surface pressure for interaction with either DPPG or DPPC (Figure 4-2a), indicating that the polymer was unable to penetrate either monolayer. The interaction profiles showed a small increase in surface pressure ($< 1 \text{ mN m}^{-1}$) relating to the injection process within the first two minutes and then the surface pressure remained in equilibrium. The lack of interaction of PEG was somewhat expected as this polymer, a clinically relevant comparator, is well known for its biocompatibility.

4.3.2 Effect of polymer concentration on polymer-lipid interactions

4.3.2.1 Surface pressure measurements

Upon observing a difference in PAMAM dendrimer binding to anionic DPPG and zwitterionic DPPC, the effect of polymer concentration on penetration into the lipid layers was investigated using surface pressure measurements. The changes in surface pressure with increasing polymer concentration are compared in Figure 4-3; for PAMAM G5 (4-3a), PAMAM G4.5 (4-3b) and PEG 20,000 (4-3c) interacting with DPPG (filled symbols) and DPPC (open symbols) monolayers respectively.

Both PAMAM species showed a concentration-dependent surface pressure increase related to greater penetration when more dendrimer molecules were present in the phosphate buffer subphase. Furthermore, the interaction profiles with the lipid monolayers described above for the PAMAM concentration of 0.06 mg mL^{-1} were observed over the whole concentration range studied.

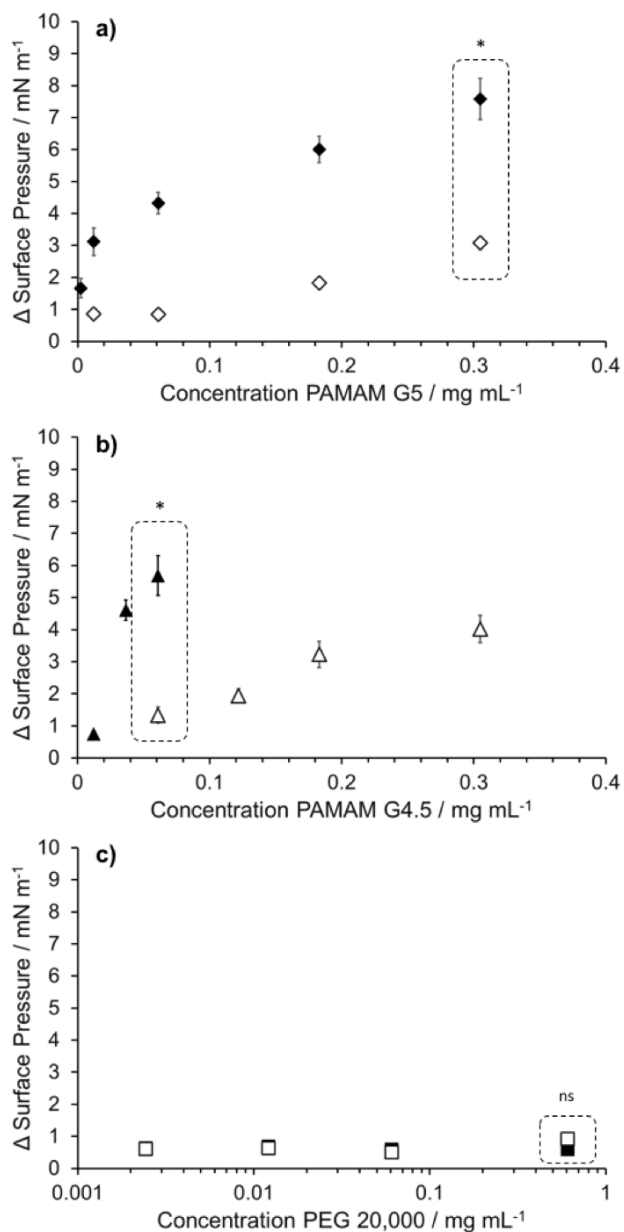


*Figure 4-3 Concentration-dependence of polymer interactions with lipid monolayers. Binding of PAMAM G5 (panel a); PAMAM G4.5 (panel b); and PEG 20,000 (panel c) to DPPG (filled symbols) and DPPC (open symbols) was studied at pH 7. Surface pressure was $21 \pm 2 \text{ mN m}^{-1}$ prior to polymer addition. Maximum surface pressure change data displayed indicate mean \pm SEM; error bars are hidden by the symbol when not visible. Statistical significance calculated via Student's *t* test, and set at $p \leq 0.05$. ns = non-significant. Comparisons carried out are highlighted with dashed line.*

The concentration-dependent changes in surface pressure for PAMAM G5 are displayed in Figure 4-3a. For the interaction with DPPG, the surface pressure change observed increased from approximately 1.7 to 7.6 mN m^{-1} at concentrations of 0.0024 to 0.3 mg mL^{-1} . Interestingly, for concentrations above

0.18 mg mL⁻¹, penetration into DPPC monolayers was also observed (which had not been detected at lower concentrations), inducing a maximum change in surface pressure of approximately 3.1 mN m⁻¹ for the highest concentration of 0.3 mg mL⁻¹.

The results of the study of PAMAM G4.5 are depicted in Figure 4-3b. The surface pressure change observed for interaction with DPPG increased from approximately 0.8 to 5.7 mN m⁻¹ at concentrations of 0.012 to 0.06 mg mL⁻¹. Furthermore, similarly to what observed for PAMAM G5, the surface pressure change observed for interaction with DPPC monolayers increased with higher concentrations (from approximately 1.3 to 4.0 mN m⁻¹ for concentrations from 0.06 – 0.3 mg mL⁻¹) indicating dendrimer penetration at all concentrations studied.

Interaction of PEG 20,000 with DPPG and DPPC monolayers was investigated over a wide concentration range (0.0024 – 0.6 mg mL⁻¹) (Figure 4-3c) and the interaction profile described earlier (i.e. no penetration) remained the same for all concentrations studied. This observation could be explained with PEG being a non-charged polymer and therefore not involved in electrostatic interactions.

4.3.2.2 External reflection FTIR spectroscopy

As surface pressure measurements are sensitive to polymer penetration into the lipid layer, but not total adsorbed amount, external reflection FTIR spectroscopy was used to investigate adsorption of PAMAM G5 to the lipid interface. This method provided a measure of total mass of polymer at the lipid/water interface through measurement of the peak area around the Amide I peak (1,700-1,550 cm⁻¹) associated with the peptide bond.

Figure 4-4 shows Amide I peak area plotted against polymer concentration for PAMAM G5 binding to DPPC and DPPG monolayers. The presence of an increasing peak area around the Amide I peak confirms the presence of PAMAM G5 at the lipid interface. However, PAMAM G5 adsorption to the different lipid surfaces varies considerably. A visible amount of dendrimer was adsorbing at very low concentrations (0.0024 mg mL⁻¹) with an observed equilibrium peak area starting at 0.05 for binding to DPPG. In comparison, when the interaction with

DPPC was investigated less dendrimer adsorption was observed with a peak area maximum of 0.015. The peak area maximum for DPPC occurred at a concentration that was a magnitude larger than the maximum peak area observed for DPPG.

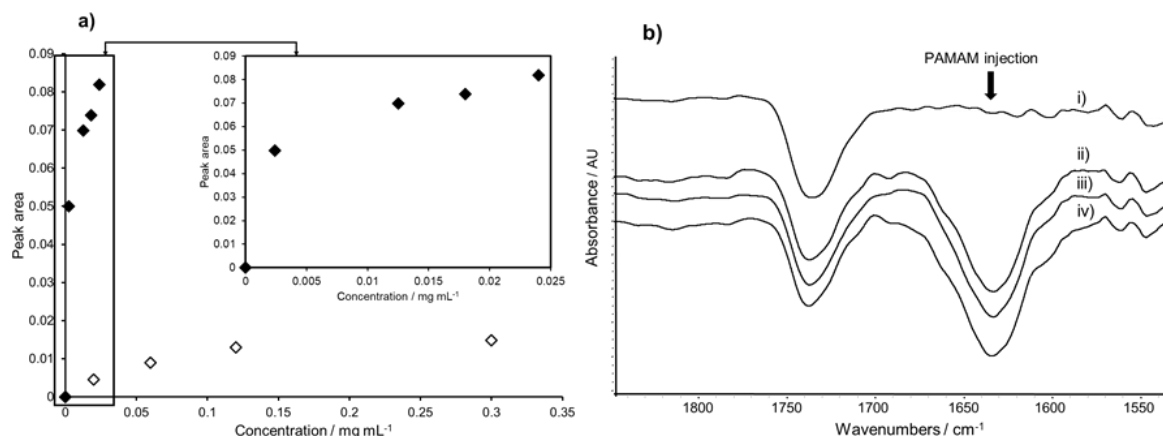


Figure 4-4 Concentration-dependent effect of PAMAM G5 dendrimers on the Amide I region of the FTIR spectrum. Changes in the peak area of the Amide I (panel a) were observed upon dendrimer binding to DPPG (filled symbols) and DPPC (open symbols) monolayers. The inset enlarges the data for interaction with DPPG only. Exemplary spectra focusing on the Amide I region (panel b) showing the addition of PAMAM G5 to a DPPG monolayer in the condensed phase. i) 0.0024 mg mL⁻¹; ii) 0.0125 mg mL⁻¹; iii) 0.018 mg mL⁻¹; iv) 0.024 mg mL⁻¹. No visible changes were associated to the C = O stretch of the headgroup of the phospholipid. Reproducibility of the technique has been verified via experiments with a subset of PAMAM dendrimers of different generations.

For PAMAM G5 adsorption to DPPG, the lipid surface appeared to become saturated by the dendrimer towards the maximum concentration tested (peak area at 0.0125 mg mL⁻¹ equalled 83% of that observed for 0.025 mg mL⁻¹). In contrast, measurements of penetration by surface pressure showed no evidence of saturation even at much higher concentrations of PAMAM G5 (maximum concentration 0.3 mg mL⁻¹). The comparison of results from the two techniques suggests that dendrimer accumulation at the surface of the lipid occurs before penetration into the monolayer.

4.3.3 Effect of sodium chloride in the buffer subphase on polymer-lipid interactions

Sodium chloride is an important component of biological systems. Concentrations of sodium chloride observed in biological systems are different in

different cellular environments. As PAMAM dendrimers carry charges, their interaction with the lipid monolayer are likely to be influenced by these charges, and, as such, by the presence of sodium chloride. We studied PAMAM interaction with DPPG and DPPC monolayers in presence of sodium chloride (144 mM) in the phosphate buffer subphase. The interactions were studied at a PAMAM concentration of 0.06 mg mL⁻¹ for DPPG and 0.3 mg mL⁻¹ for DPPC; these concentrations selected as they corresponded to equivalent surface pressure changes without addition of salt (see Figure 4-3). The results are summarised in Table 4-2.

Table 4-2 Effect of presence of sodium chloride in the phosphate buffer subphase (pH 7, 20 mM) on interaction of PAMAM G5 and G4.5 with DPPG and DPPC monolayers. Δ surface pressure data indicate mean \pm SEM. PAMAM dendrimer concentration for interacting with DPPG was 0.061 mg mL⁻¹; for interacting with DPPC 0.3 mg mL⁻¹.#

Δ Surface Pressure / mN m ⁻¹				
	PAMAM G5		PAMAM G4.5	
	DPPG	DPPC	DPPG	DPPC
0 mM NaCl	4.3 \pm 0.3	3.1 \pm 0.2	5.7 \pm 0.6	4.0 \pm 0.4
144 mM NaCl	3.1 \pm 0.4 ns	3.8 \pm 0.8 ns	1.6 \pm 0.2*	3.6 \pm 0.3*

#Statistical significance (Student's t test 144 vs 0 mM); ns = non-significant, * p \leq 0.05

The sodium chloride addition to the phosphate buffer resulted in a smaller increase in surface pressure for both PAMAM species binding to DPPG compared to the non-salt results, but only for PAMAM G4.5 this effect reached statistical significance (1.6 mN m⁻¹ compared to 5.7 mN m⁻¹ without the salt addition, p < 0.05). The decrease in penetration ability might be explained by sodium ions screening the anionic lipid heads and anionic surface groups of the PAMAM G4.5 and therefore reducing the electrostatic forces involved in the lipid layer penetration.

4.4 DISCUSSION

We used two related biophysical techniques to study the binding behaviour of anionic PAMAM G4.5 and cationic PAMAM G5 to zwitterionic DPPC and anionic DPPG monolayers. To our knowledge, existing membrane studies of PAMAM

dendrimers have been mainly focussing on cationic dendrimers^{26, 27, 29} as due to their charge they have been proven good agents for drug^{3, 4} and gene delivery^{7, 8}. Interestingly, fewer studies have been carried out using anionic dendrimers despite their lower cytotoxicity^{25, 44}, antimicrobial activity^{21, 45} and suitability as potential drug delivery agents^{46, 47}. Just recently, their advantages over the cationic counterparts have started to attract more interest in the research community and membrane interactions *in vitro* were studied with the view of their potential as an anionic drug carrier^{48, 49}. However, the molecular processes underlying their interactions with biomembranes and their lower cytotoxicity are still not understood and very few studies have been focussing on elucidating anionic PAMAM's interaction mechanism with model lipid membranes^{50, 51} or proteins^{52, 53} so far.

As indicated previously, surface pressure measurements are particularly sensitive to monolayer penetration by molecules^{33, 54, 55}. This is used to our advantage since this technique is able to selectively probe interactions that lead to lipid penetration rather than those that result in significant adsorption of material below the lipid layer. It is not a quantitative measure of adsorbed amount, and measurements have shown that interactions where adsorption of molecules is below a lipid monolayer with little or no lipid penetration lead to negligible changes in surface pressure⁵⁶.

It has been observed previously that polycations, including PAMAM G5, are toxic towards eukaryotic cells at concentrations that depend on cell line and exposure time^{11, 25}. Our monolayer studies show evidence of concentration-dependent penetration for both anionic PAMAM G4.5 and cationic PAMAM G5 to a DPPC monolayer selected as a simplified eukaryotic model membrane. The penetration at higher concentrations ($> 0.18 \text{ mg mL}^{-1}$) seem to match (and could potentially explain) the toxicity reported for cationic PAMAMs and, in fact, evidence of membrane disruption and pore formation has been observed previously using different membranes models^{26, 31, 57-59}. Those studies and simulation studies⁶⁰⁻⁶² concluded that such mechanisms are dependent on concentration and size of the cationic dendrimers. However, those studies do not explain our results observed for the anionic, better-tolerated PAMAM G4.5 which displayed similar penetration

levels into our model as the cationic counterpart. It has been previously suggested that anionic PAMAM either induce membrane defects and leakage (G1.5) or prevent those by increased lipid packing and local swelling (G4.5) of amphiphilic POPC bilayers⁶³. Another study directly compared anionic PAMAM G2.5 and cationic PAMAM G3 binding to DPPC bilayers provides similar conclusions about their different membrane interaction behaviour⁵⁰.

Those observations from the PAMAM interactions are supported by other studies that investigated diverse mechanisms of interaction for the binding of anionic and cationic polymers to zwitterionic lipids; specifically the PC head group, and revealed that anionic nanoparticles reduce fluidity of lipid surfaces^{64, 65}. Wang et al.⁶⁶ suggested that the charge of the approaching polymer affects the tilt angle of the zwitterionic PC head group as a result of the positions of the N⁺ and P⁻ charges on the lipid. Considering the molecular weight of PAMAM G4.5 dendrimers, only a small number of molecular contacts are required to deeply penetrate the lipid monolayer to reach the hydrophobic region and for an observable change in surface pressure to occur^{34, 54}.

It is also interesting to consider the behaviour of PAMAM dendrimers to these simple lipid surfaces in the context of their selectivity between bacterial and eukaryotic membranes (Figure 4-2a and b). For example, other studies have shown that full-generation PAMAM G5 and G3 dendrimers are toxic against prokaryotes (i.e. *Pseudomonas Aeruginosa*; *Staphylococcus Aureus*) and that higher concentrations were required to observe toxicity against eukaryotic cells (human corneal epithelial cells; human bone mesenchymal stem cells)^{20, 22, 23}. Studies involving anionic PAMAM species confirmed a similar toxic effect towards bacterial membranes, however at higher concentrations compared to their cationic counterparts^{21, 45}. Interestingly, there are only few studies on eukaryotic membranes assessing anionic PAMAM dendrimers, but all reports indicate no or little toxicity even at concentrations up to 1 mg mL⁻¹ (human corneal epithelial cells; human glioma cells)^{49, 67}. The different interaction kinetics of PAMAM G5 and PAMAM G4.5 observed in our study indicate different modes of penetration into the DPPG and DPPC lipid monolayers, which might be related to the

distinctive toxicity behaviour of both PAMAM species reported in some of the studies mentioned above, and might be due to the lipid model used.

Our observations of the comparator polymer PEG 20,000 Da showing no penetration in the investigated model membranes can be attributed to its physico-chemical characteristics (non-charged, with a flexible, linear geometry) and support PEG's previously reviewed biocompatibility and non-toxic behaviour towards eukaryotic and prokaryotic cells^{68, 69}. In fact, PEGylation of PAMAM dendrimers has been used previously as a strategy to decrease cationic PAMAMs toxicity^{20,22,25}. However, findings of some other groups suggest that low molecular weight PEG (6000, 8000 g mol⁻¹) could cause defects and leakage of zwitterionic lipid vesicles (i.e. DPPC; DMPC; POPC)^{70, 71}. The use of a higher molecular weight PEG in our study (20,000 g mol⁻¹) could be potentially responsible for this difference observed, as the impact of the terminal OH would not be as significant as in lower molecular weight derivatives.

Another reported factor influencing polymer-membrane interaction is the salt content of the surrounding media^{62, 72, 73} and this is also of biological relevance considering the different salts regulating physiological processes in the human body^{74, 75}. Therefore, we decided to investigate the effect of addition of 144 mM of sodium chloride to the phosphate buffer subphase as this concentration corresponds roughly to the physiological sodium concentration found extracellularly (e.g. blood plasma). We found that the sodium chloride addition to the buffer solution did not affect the interaction of both PAMAM G4.5 and G5 with zwitterionic DPPC monolayers but seemed to decrease the interaction with anionic DPPG. Lee and Larson⁶² showed in simulation studies with DPPC and PAMAM G5 addition of higher salt concentrations (500 mM) decreased interaction of the dendrimer with the lipid bilayer, probably due to the electrolyte weakening electrostatic forces. The significantly lower interaction of anionic PAMAM G4.5 with DPPG under sodium chloride addition could probably be explained by a study by Böhme et al.⁴², where they found counterions reducing the effective charge of PAMAM dendrimers. These results are further supported by findings of Zhao et al.⁷⁶ where POPG bilayer showed strong attractive interactions between lipid molecules and dense lipid packing driven interlipid counterion bridges in the

bilayers and strong intra- and intermolecular hydrogen bonding that increased even further under sodium ion addition and led to complexation of PG molecules. Considering sodium as a counterion for the carboxylate surface groups and the anionic headgroup of DPPG, the excessive amount available after sodium chloride addition to the buffer is likely to screen and bind to the anionic groups and therefore drastically reduce the charge density driven interaction. The small decrease observed for PAMAM G5 against DPPG in the presence of NaCl would be consistent with electrostatic interactions (this was however shown to not be statistically significant ($P > 0.05$, Table 4-2)). It should be noted that variations in ionic strength could affect other parameters in addition to charge interactions, most notably they could potentially affect the size of the dendrimers. However, although PAMAM dendrimers are polyelectrolytes, their size has been reported to be independent from ionic strength⁷⁸, and as such, our discussion on this aspect has focussed on the effect on charge.

4.5 CONCLUSIONS

In this study, the interactions of the dendrimers PAMAM G5 and G4.5 with DPPC and DPPG monolayers have been investigated, with a view to providing an insight into how the polymer, lipid and solution properties can influence polymer binding to biological membranes. To our knowledge, we are the first to report comparative cationic/anionic PAMAM-membrane interaction studies utilising lipid monolayers. Both, PAMAM G4.5 and G5 were able to differentiate between the zwitterionic and anionic lipid layers, however their interaction profiles suggest different mechanisms of dendrimer binding. The strong electrostatic attraction between PAMAM G5 surface groups and the DPPG head group allowed for adsorption and penetration of the polymer into the lipid layer. Interestingly, the anionic polymer PAMAM G4.5 showed evidence of strong penetration into DPPG monolayers. We hypothesise that this process is driven by DPPG head repulsion and interaction with lipid tails and intercalating into the hydrophobic areas of the lipid monolayer. Both PAMAM species interact in a concentration-dependent manner with the zwitterionic DPPC monolayers, however, much higher concentrations than for DPPG monolayers are required to induce significant increase in surface pressure, which is characteristic for membrane penetration.

Addition of sodium chloride to the buffer solution decreased the interaction with anionic DPPG monolayers for both PAMAM G4.5 and G5, but did not affect their interaction with DPPC.

To confirm this hypothesis, further experiments would need to be carried out that enable the position of the polymer within the lipid layer to be quantitatively determined. Further proof of our hypothesis could be achieved by studying the polymer-membrane interactions in more complex model systems, such as mixed lipid systems or cell culture. Taken together, our results provide an insight into the mechanism of interaction between charged dendritic polymers and a lipid membrane surface. We have identified that binding and lipid penetration can occur via different mechanisms where both electrostatic and hydrophobic interactions appear to play a role.

4.6 REFERENCES

1. Svenson, S., Dendrimers as versatile platform in drug delivery applications. *European Journal of Pharmaceutics and Biopharmaceutics : official journal of Arbeitsgemeinschaft fuer Pharmazeutische Verfahrenstechnik e.V.* **2009**, 71 (3), 445-462.
2. Tomalia, D. A.; Naylor, A. M.; Goddard, W. A., Starburst Dendrimers: Molecular-Level Control of Size, Shape, Surface Chemistry, Topology, and Flexibility from Atoms to Macroscopic Matter. *Angew. Chem., Int. Ed. Engl.* **1990**, 29 (2), 138-175.
3. Jedrych, M.; Borowska, K.; Galus, R.; Jodlowska-Jedrych, B., The evaluation of the biomedical effectiveness of poly(amido)amine dendrimers generation 4.0 as a drug and as drug carriers: a systematic review and meta-analysis. *International Journal of Pharmaceutics (Amsterdam, Netherlands)* **2014**, 462 (1-2), 38-43.
4. Yabbarov, N. G.; Posypanova, G. A.; Vorontsov, E. A.; Popova, O. N.; Severin, E. S., Targeted delivery of doxorubicin: drug delivery system based on PAMAM dendrimers. *Biochemistry (Mosc.)* **2013**, 78 (8), 884-94.
5. Gajbhiye, V.; Palanirajan, V. K.; Tekade, R. K.; Jain, N. K., Dendrimers as therapeutic agents: a systematic review. *Journal of Pharmacy and Pharmacology* **2009**, 61 (8), 989-1003.
6. Shcharbin, D.; Shakhbazau, A.; Bryszewska, M., Poly(amidoamine) dendrimer complexes as a platform for gene delivery. *Expert Opin Drug Del* **2013**, 10 (12), 1687-98.

7. Yu, S.; Li, M.-H.; Choi, S. K.; Baker, J. R., Jr. ; Larson, R. G., DNA Condensation by Partially Acetylated Poly(amido amine) Dendrimers: Effects of Dendrimer Charge Density on Complex Formation. *Molecules* **2013**, *18*, 10707-10720.
8. Zhong, H.; He, Z.-G.; Li, Z.; Li, G.-Y.; Shen, S.-R.; Li, X.-L., Studies on polyamidoamine dendrimers as efficient gene delivery vector. *Journal of biomaterials applications* **2008**, *22* (6), 527-44.
9. Sadekar, S.; Ghandehari, H., Transepithelial transport and toxicity of PAMAM dendrimers: implications for oral drug delivery. *Advanced drug delivery reviews* **2012**, *64* (6), 571-88.
10. Mukherjee, S. P.; Davoren, M.; Byrne, H. J., In vitro mammalian cytotoxicological study of PAMAM dendrimers - towards quantitative structure activity relationships. *Toxicology in vitro : an international journal published in association with BIBRA* **2010**, *24* (1), 169-77.
11. Duncan, R.; Izzo, L., Dendrimer biocompatibility and toxicity. *Advanced drug delivery reviews* **2005**, *57* (15), 2215-2237.
12. Kumar, A.; Yellepeddi, V. K.; Davies, G. E.; Strychar, K. B.; Palakurthi, S., Enhanced gene transfection efficiency by polyamidoamine (PAMAM) dendrimers modified with ornithine residues. *International Journal of Pharmaceutics (Amsterdam, Netherlands)* **2010**, *392* (1-2), 294-303.
13. Albertazzi, L. A.; Serresi, M.; Albanese, A.; Beltram, F., Dendrimer Internalization and Intracellular Trafficking in Living Cells. *Mol. Pharmaceutics* **2010**, *7* (3), 680-688.
14. Wang, S.; Li, Y.; Fan, J.; Wang, Z.; Zeng, X.; Sun, Y.; Song, P.; Ju, D., The role of autophagy in the neurotoxicity of cationic PAMAM dendrimers. *Biomaterials* **2014**, *35* (26), 7588-97.
15. Mukherjee, S. P.; Byrne, H. J., Polyamidoamine dendrimer nanoparticle cytotoxicity, oxidative stress, caspase activation and inflammatory response: experimental observation and numerical simulation. *Nanomedicine : nanotechnology, biology, and medicine* **2013**, *9* (2), 202-11.
16. Akhtar, S.; Chandrasekhar, B.; Attur, S.; Yousif, M. H.; Benter, I. F., On the nanotoxicity of PAMAM dendrimers: Superfect® stimulates the EGFR-ERK1/2 signal transduction pathway via an oxidative stress-dependent mechanism in HEK 293 cells. *International Journal of Pharmaceutics (Amsterdam, Netherlands)* **2013**, *448* (1), 239-46.
17. Pryor, J. B.; Harper, B. J.; Harper, S. L., Comparative toxicological assessment of PAMAM and thiophosphoryl dendrimers using embryonic zebrafish. *Int. J. Nanomed.* **2014**, *9*, 1947-56.

18. Halets, I.; Shcharbin, D.; Klajnert, B.; Bryszewska, M., Contribution of hydrophobicity, DNA and proteins to the cytotoxicity of cationic PAMAM dendrimers. *International Journal of Pharmaceutics (Amsterdam, Netherlands)* **2013**, *454* (1), 1-3.
19. Thiagarajan, G.; Greish, K.; Ghandehari, H., Charge affects the oral toxicity of poly(amidoamine) dendrimers. *European journal of pharmaceutics and biopharmaceutics : official journal of Arbeitsgemeinschaft fuer Pharmazeutische Verfahrenstechnik e.V* **2013**, *84* (2), 330-4.
20. Wang, L.; Erasquin, U. J.; Zhao, M.; Ren, L.; Zhang, M. Y.; Cheng, G. J.; Wang, Y.; Cai, C., Stability, antimicrobial activity, and cytotoxicity of poly(amidoamine) dendrimers on titanium substrates. *ACS Appl. Mater. Interfaces* **2011**, *3* (8), 2885-94.
21. Wang, B.; Navath, R. S.; Menjoge, A. R.; Balakrishnan, B.; Bellair, R.; Dai, H.; Romero, R.; Kannan, S.; Kannan, R. M., Inhibition of bacterial growth and intramniotic infection in a guinea pig model of chorioamnionitis using PAMAM dendrimers. *International Journal of Pharmaceutics (Amsterdam, Netherlands)* **2010**, *395* (1-2), 298-308.
22. Lopez, A. I.; Reins, R. Y.; McDermott, A. M.; Trautner, B. W.; Cai, C., Antibacterial activity and cytotoxicity of PEGylated poly(amidoamine) dendrimers. *Molecular bioSystems* **2009**, *5* (10), 1148-56.
23. Calabretta, M.; Kumar, A.; McDermott, A.; Cai, C., Antibacterial activities of poly(amidoamine) dendrimers terminated with amino and poly(ethylene glycol) groups. *Biomacromolecules* **2007**, *8* (6), 1807-1811.
24. Choi, Y. J.; Kang, S. J.; Kim, Y. J.; Lim, Y. B.; Chung, H. W., Comparative studies on the genotoxicity and cytotoxicity of polymeric gene carriers polyethylenimine (PEI) and polyamidoamine (PAMAM) dendrimer in Jurkat T-cells. *Drug and Chemical Toxicology (1977)* **2010**, *33* (4), 357-66.
25. Jevprasesphant, R.; Penny, J.; Jalal, R.; Attwood, D.; McKeown, N.; D'Emanuele, A., The influence of surface modification on the cytotoxicity of PAMAM dendrimers. *International Journal of Pharmaceutics (Amsterdam, Netherlands)* **2003**, *252* (1-2), 263-266.
26. Berenyi, S.; Mihaly, J.; Wacha, A.; Toke, O.; Bota, A., A mechanistic view of lipid membrane disrupting effect of PAMAM dendrimers. *Colloids and Surfaces, B: Biointerfaces* **2014**, *118*, 164-71.
27. Roy, B.; Panda, A. K.; Parimi, S.; Ametov, I.; Barnes, T.; Prestidge, C. A., Physico-chemical Studies on the Interaction of Dendrimers with Lipid Bilayers. 1. Effect of Dendrimer Generation and Liposome Surface Charge. *J. Oleo Sci.* **2014**, *63* (11), 1185-1193.
28. Akesson, A.; Bendtsen, K. M.; Beherens, M. A.; Pedersen, J. S.; Alfredsson, V.; Cardenas Gomez, M., The effect of PAMAM G6 dendrimers on the structure of lipid vesicles. *Physical Chemistry Chemical Physics* **2010**, *12* (38), 12267-72.

29. Yanez Arteta, M.; Ainalem, M. L.; Porcar, L.; Martel, A.; Coker, H.; Lundberg, D.; Chang, D. P.; Soltwedel, O.; Barker, R.; Nylander, T., Interactions of PAMAM Dendrimers with Negatively Charged Model Biomembranes. *The journal of physical chemistry. B* **2014**, *118* (45), 12892-12906.
30. Kim, Y.; Kwak, Y.; Chang, R., Free energy of PAMAM dendrimer adsorption onto model biological membranes. *Journal of Physical Chemistry B* **2014**, *118* (24), 6792-6802.
31. Nyitrai, G.; Keszthelyi, T.; Bota, A.; Simon, A.; Toke, O.; Horvath, G.; Pal, I.; Kardos, J.; Heja, L., Sodium selective ion channel formation in living cell membranes by polyamidoamine dendrimer. *Biochim. Biophys. Acta* **2013**, *1828* (8), 1873-80.
32. Mansour, H.; Zograf, G., The relationship between water vapor absorption and desorption by phospholipids and bilayer phase transitions. *Journal of pharmaceutical sciences* **2007**, *96* (2), 377-396.
33. Neville, F.; Ivankin, A.; Konovalov, O.; Gidalevitz, D., A comparative study on the interactions of SMAP-29 with lipid monolayers. *Biochimica et Biophysica Acta, Biomembranes* **2010**, *1798* (5), 851-860.
34. Clifton, L. A.; Lad, M. D.; Green, R. J.; Frazier, R. A., Single amino acid substitutions in puroindoline-b mutants influence lipid binding properties. *Biochemistry* **2007**, *46* (8), 2260-2266.
35. Paiva, D.; Brezesinski, G.; Pereira Mdo, C.; Rocha, S., Langmuir monolayers of monocationic lipid mixed with cholesterol or fluorocholesterol: DNA adsorption studies. *Langmuir : the ACS journal of surfaces and colloids* **2013**, *29* (6), 1920-5.
36. Bohinc, K.; Brezesinski, G.; May, S., Modeling the influence of adsorbed DNA on the lateral pressure and tilt transition of a zwitterionic lipid monolayer. *Physical chemistry chemical physics : PCCP* **2012**, *14* (30), 10613-21.
37. Nowotarska, S. W.; Nowotarski, K. J.; Friedman, M.; Situ, C., Effect of structure on the interactions between five natural antimicrobial compounds and phospholipids of bacterial cell membrane on model monolayers. *Molecules* **2014**, *19* (6), 7497-7515.
38. Lad, M. D.; Birembaut, F.; Clifton, L. A.; Frazier, R. A.; Webster, J. R.; Green, R. J., Antimicrobial peptide-lipid binding interactions and binding selectivity. *Biophys. J.* **2007**, *92* (10), 3575-86.
39. Deleu, M.; Crowet, J. M.; Nasir, M. N.; Lins, L., Complementary biophysical tools to investigate lipid specificity in the interaction between bioactive molecules and the plasma membrane: A review. *Biochimica et biophysica acta* **2014**, *1838* (12), 3171-3190.
40. Brezesinski, G.; Mohwald, H., Langmuir monolayers to study interactions at model membrane surfaces. *Adv. Colloid Interface Sci.* **2003**, *100*, 563-584.

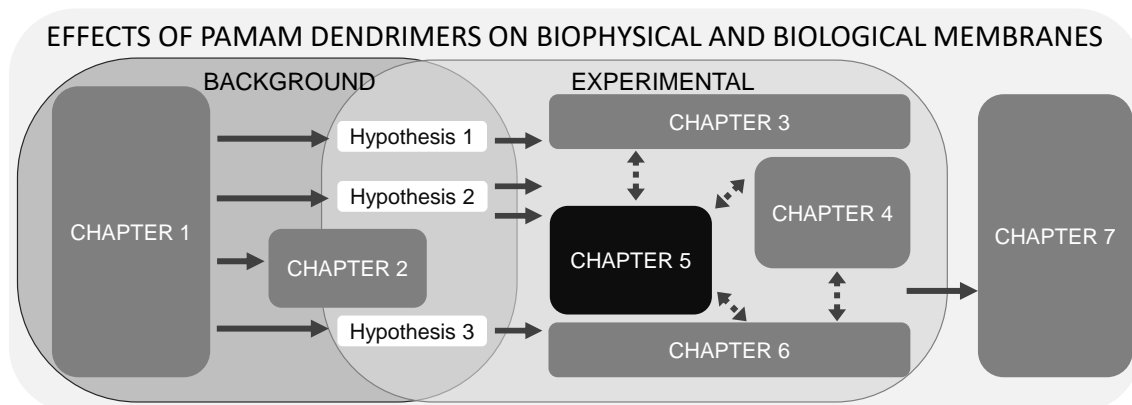
41. Epand, R. M.; Epand, R. F., Lipid domains in bacterial membranes and the action of antimicrobial agents. *Biochimica et Biophysica Acta, Biomembranes* **2009**, *1788* (1), 289-294.
42. Böhme, U.; Klenge, A.; Hänel, B.; Scheler, U., Counterion Condensation and Effective Charge of PAMAM Dendrimers. *Polymers* **2011**, *3* (4), 812-819.
43. Maiti, P. K.; Çağın, T.; Lin, S.-T.; Goddard, W. A., Effect of Solvent and pH on the Structure of PAMAM Dendrimers. *Macromolecules* **2005**, *38* (3), 979-991.
44. Bodewein, L.; Schmelter, F.; Di Fiore, S.; Hollert, H.; Fischer, R.; Fenske, M., Differences in toxicity of anionic and cationic PAMAM and PPI dendrimers in zebrafish embryos and cancer cell lines. *Toxicology and applied pharmacology* **2016**, *305*, 83-92.
45. Prieto, M. J.; Bacigalupe, D.; Pardini, O.; Amalvy, J. I.; Venturini, C.; Morilla, M. J.; Romero, E. L., Nanomolar cationic dendrimeric sulfadiazine as potential antitoxoplasmic agent. *International journal of pharmaceutics* **2006**, *326* (1-2), 160-8.
46. Kirkpatrick, G. J.; Plumb, J. A.; Sutcliffe, O. B.; Flint, D. J.; Wheate, N. J., Evaluation of anionic half generation 3.5-6.5 poly(amidoamine) dendrimers as delivery vehicles for the active component of the anticancer drug cisplatin. *Journal of inorganic biochemistry* **2011**, *105* (9), 1115-22.
47. Sweet, D. M.; Kolhatkar, R. B.; Ray, A.; Swaan, P.; Ghandehari, H., Transepithelial transport of PEGylated anionic poly(amidoamine) dendrimers: implications for oral drug delivery. *Journal of controlled release : official journal of the Controlled Release Society* **2009**, *138* (1), 78-85.
48. Oddone, N.; Lecot, N.; Fernandez, M.; Rodriguez-Haralambides, A.; Cabral, P.; Cerecetto, H.; Benech, J. C., In vitro and in vivo uptake studies of PAMAM G4.5 dendrimers in breast cancer. *J Nanobiotechnology* **2016**, *14* (1), 45.
49. Yavuz, B.; Bozdog Pehlivan, S.; Sumer Bolu, B.; Nomak Sanyal, R.; Vural, I.; Unlu, N., Dexamethasone - PAMAM dendrimer conjugates for retinal delivery: preparation, characterization and in vivo evaluation. *The Journal of pharmacy and pharmacology* **2016**, *68* (8), 1010-20.
50. Lombardo, D.; Calandra, P.; Bellocco, E.; Lagana, G.; Barreca, D.; Magazu, S.; Wanderlingh, U.; Kiselev, M. A., Effect of anionic and cationic polyamidoamine (PAMAM) dendrimers on a model lipid membrane. *Biochimica et biophysica acta* **2016**, *1858* (11), 2769-2777.
51. Keszthelyi, T.; Hollo, G.; Nyitrai, G.; Kardos, J.; Heja, L., Bilayer Charge Reversal and Modification of Lipid Organization by Dendrimers as Observed by Sum-Frequency Vibrational Spectroscopy. *Langmuir : the ACS journal of surfaces and colloids* **2015**, *31* (28), 7815-25.

52. Nowacka, O.; Shcharbin, D.; Klajnert-Maculewicz, B.; Bryszewska, M., Stabilizing effect of small concentrations of PAMAM dendrimers at the insulin aggregation. *Colloids and surfaces. B, Biointerfaces* **2014**, *116*, 757-60.
53. Shcharbin, D.; Klajnert, B.; Bryszewska, M., The effect of PAMAM dendrimers on human and bovine serum albumin at different pH and NaCl concentrations. *Journal of Biomaterials Science, Polymer Edition* **2005**, *16* (9), 1081-1093.
54. Sanders, M. R.; Clifton, L. A.; Neylon, C.; Frazier, R. A.; Green, R. J., Selected wheat seed defense proteins exhibit competitive binding to model microbial lipid interfaces. *Journal of agricultural and food chemistry* **2013**, *61* (28), 6890-900.
55. Arsenault, M.; Bedard, S.; Boulet-Audet, M.; Pezolet, M., Study of the Interaction of Lactoferricin B with Phospholipid Monolayers and Bilayers. *Langmuir : the ACS journal of surfaces and colloids* **2010**, *26* (5), 3468-3478.
56. Maget-Dana, R., The monolayer technique: a potent tool for studying the interfacial properties of antimicrobial and membrane-lytic peptides and their interactions with lipid membranes. *Biochimica Et Biophysica Acta-Biomembranes* **1999**, *1462* (1-2), 109-140.
57. Majoros, I.; Williams, C.; Becker, A.; Baker, J., Surface Interaction and Behavior of Poly(amidoamine) Dendrimers: Deformability and Lipid Bilayer Disruption. *Journal of Computational and Theoretical Nanoscience* **2009**, *6* (7), 1430-1436.
58. Mecke, A.; Majoros, I. J.; Patri, A. K.; Baker, J. R.; Holl, M. M.; Orr, B. G., Lipid bilayer disruption by polycationic polymers: the roles of size and chemical functional group. *Langmuir : the ACS journal of surfaces and colloids* **2005**, *21* (23), 10348-54.
59. Mecke, A.; Uppuluri, S.; Sassanella, T. M.; Lee, D. K.; Ramamoorthy, A.; Baker, J. R., Jr.; Orr, B. G.; Banaszak Holl, M. M., Direct observation of lipid bilayer disruption by poly(amidoamine) dendrimers. *Chemistry and physics of lipids* **2004**, *132* (1), 3-14.
60. Wang, Y. L.; Lu, Z. Y.; Laaksonen, A., Specific binding structures of dendrimers on lipid bilayer membranes. *Physical chemistry chemical physics : PCCP* **2012**, *14* (23), 8348-59.
61. Lee, H.; Larson, R. G., Coarse-grained molecular dynamics studies of the concentration and size dependence of fifth- and seventh-generation PAMAM dendrimers on pore formation in DMPC bilayer. *The journal of physical chemistry. B* **2008**, *112* (26), 7778-84.
62. Lee, H.; Larson, R. G., Molecular dynamics simulations of PAMAM dendrimer-induced pore formation in DPPC bilayers with a coarse-grained model. *The journal of physical chemistry. B* **2006**, *110* (37), 18204-11.
63. Evans, K.; Laszlo, J.; Compton, D., Carboxyl-terminated PAMAM dendrimer interaction with 1-palmitoyl-2-oleoyl phosphocholine bilayers. *Biochimica Et Biophysica Acta-Biomembranes* **2014**, *1838* (1), 445-455.

64. Li, Y.; Gu, N., Computer simulation of the inclusion of hydrophobic nanoparticles into a lipid bilayer. *J. Nanosci. Nanotechnol.* **2010**, *10* (11), 7616-9.
65. Wang, B.; Zhang, L.; Bae, S. C.; Granick, S., Nanoparticle-induced surface reconstruction of phospholipid membranes. *Proc. Natl. Acad. Sci. U. S. A.* **2008**, *105* (47), 18171-5.
66. Zheng, X.; Wang, T.; Jiang, H.; Li, Y.; Jiang, T.; Zhang, J.; Wang, S., Incorporation of Carvedilol into PAMAM-functionalized MWNTs as a sustained drug delivery system for enhanced dissolution and drug-loading capacity. *Asian Journal of Pharmaceutical Sciences* **2013**, *8* (5), 278-286.
67. Zolotarskaya, O. Y.; Xu, L.; Valerie, K.; Yang, H., Click synthesis of a polyamidoamine dendrimer-based camptothecin prodrug. *RSC Adv* **2015**, *5* (72), 58600-58608.
68. Pasut, G.; Veronese, F., State of the art in PEGylation: The great versatility achieved after forty years of research. *Journal of Controlled Release* **2012**, *161* (2), 461-472.
69. Fruijtier-Pöllöth, C., Safety assessment on polyethylene glycols (PEGs) and their derivatives as used in cosmetic products. *Toxicology* **2005**, *214* (1-2), 1-38.
70. Massenburg, D.; Lentz, B., Poly(ethylene glycol)-induced Fusion and Rupture of Dipalmitoylphosphatidylcholine Large, Unilamellar Extruded Vesicles. *Biochemistry* **1993**, *32* (35), 9172-9180.
71. Boni, L. T.; Stewart, T. P.; Hui, S. W., Alterations in phospholipid polymorphism by polyethylene glycol. *Journal of Membrane Biology* **1984**, *80* (1), 91-104.
72. Avaritt, B. R.; Swaan, P. W., Intracellular Ca²⁺ release mediates cationic but not anionic poly(amidoamine) (PAMAM) dendrimer-induced tight junction modulation. *Pharmaceutical research* **2014**, *31* (9), 2429-38.
73. Petrache, H. I.; Zemb, T.; Belloni, L.; Parsegian, V. A., Salt screening and specific ion adsorption determine neutral-lipid membrane interactions. *Proceedings of the National Academy of Sciences of the United States of America* **2006**, *103* (21), 7982-7.
74. Lodish, H., Intracellular Ion Environment and Membrane Electric Potential. In *Molecular Cell Biology*, 7th ed.; **Lodish, H.**; Berk, A.; Kaiser, C. A.; Krieger, M.; Bretscher, A.; Ploegh, H.; Amon, A.; Scott, M. P., Eds. W.H. Freeman & Co Ltd: New York, 2012; pp 483 - 494.
75. Aronson, P. S.; Boron, W. F.; Boulpaep, E. L., Transport of Solutes and Water. In *Medical physiology : a cellular and molecular approach*, 2 ed.; Boron, W. F.; Boulpaep, E. L., Eds. Saunders: Philadelphia, PA, 2012; pp 106-146.

76. Zhao, W.; Rog, T.; Gurtovenko, A. A.; Vattulainen, I.; Karttunen, M., Atomic-scale structure and electrostatics of anionic palmitoyloleoylphosphatidylglycerol lipid bilayers with Na⁺ counterions. *Biophysical journal* **2007**, 92 (4), 1114-24.

CHAPTER 5: BINDING OF PAMAM DENDRIMERS WITH DPPG LIPID MEMBRANE MODELS IS AFFECTED BY SOLVENT CONDITIONS



The manuscript is currently under finalization for submission to the Scientific Journal COLLOIDS SURFACE B BIOINTERFACE.

This chapter illustrates how changes in solvent (i.e. pH, residual methanol) can affect the binding behavior of PAMAM dendrimers to lipids in model membranes of increasing complexity. With the focus on pH and methanol effect, surface pressure measurements and neutron reflectometry were used to study activity of PAMAM G4.5 and G5 on DPPG lipid monolayers and bilayers respectively.

Neutron Reflectometry was carried out the ISIS Neutron and Muon Source (STFC) in Harwell. Following grants were used to obtain the data in this manuscript RB1710336, RB1520313 and RB1520310.

The estimated contribution of the candidate to the work of this chapter is 85 %.

- MW:** Conceptualization, Data curation, Funding acquisition, Investigation, Validation, Formal analysis, Project administration, Visualization, Writing – original draft
- OBF:** Investigation and Validation of Neutron Reflectometry Data
- LAC:** Methodology, Resource, Software, Supervision, Writing – review & editing
- FG:** Conceptualization, Funding acquisition, Supervision, Writing – review & editing
- RJG:** Conceptualization, Funding acquisition, Project administration, Supervision, Writing – review & editing
- MC** Investigation
- EK** Investigation

5 BINDING OF PAMAM DENDRIMERS WITH DPPG LIPID MEMBRANE MODELS AFFECTED BY SOLVENT CONDITIONS

Marleen Wilde^a, Olga B. Florek^a, Luke A. Clifton^b, Mario Campana^b, Elena Kabova^a, Francesca Greco^a, Rebecca R. Green^a

^aSchool of Pharmacy, University of Reading, PO Box 226, Whiteknights, Reading, Berkshire, RG6 6AP.

^bISIS Pulsed Neutron and Muon Source, Science and Technology Facilities Council, Rutherford Appleton Laboratory, Harwell Oxford Campus, Didcot, Oxfordshire, OX11 0QX

KEYWORDS

PAMAM, neutron reflectometry, surface pressure, monolayer, lipid bilayer, DPPG, penetration, adsorption

ACKNOWLEDGMENT

The neutron reflectometry work was supported by ISIS beam time awards for INTER (RB1520313, RB1520310) and SURF (RB1710336).

ABBREVIATIONS

DPPC 1,2-dipalmitoyl-*sn*-glycero-3-phosphocholine; DPPG 1,2-dipalmitoyl-*sn*-glycero-3-phospho-(1'-*rac*-glycerol), DMPG 1,2-dimyristoyl-*sn*-glycero-3-phospho-(1'-*rac*-glycerol), ER-FTIR external reflection Fourier transform infrared, UHQ ultrahigh quality

ABSTRACT

Poly(amidoamine) (PAMAM) dendrimers are a class of polymeric nanomolecules with diverse surface functionalities leading to a wide range of potential biomedical applications. Medium-sized generations, such as G5, are most promising candidates for drug- and gene-delivery and therefore, it is important to understand their interactions with biological membranes, their individual components and membrane environment. Here, we focus on the major membrane components – lipids – and aim to provide mechanistical insights into PAMAM-lipid interactions using simplified membrane models and biophysical methods. The interaction of full-generation G5 and half-generation G4.5 dendrimers with anionic DPPG lipid membrane models were evaluated as a function of pH and presence of methanol in the dendrimer solution. The effect of dendrimer charge and lipid surface pressure prior to dendrimer addition was monitored with surface pressure measurements on monolayers, whereas neutron reflectometry was used to study the pH and charge effect along with concentration-dependency on supported bilayers. We found that both pH and residual methanol in the solution environment significantly affected the intensity of PAMAM interactions with DPPG model membranes. At pH 4 and presence of 0.1 % methanol, both PAMAM G5 and G4.5 caused large changes in surface pressure of the monolayer (29.8 and 21.9 mN m⁻¹, respectively), which were reduced but still apparent under methanol-free conditions. In contrast, at pH 7, those changes were only a fraction of pH 4, and no changes were observed for G4.5 under methanol-free conditions. Neutron reflectometry revealed an adsorption layer onto the DPPG headgroups and change in the hydration levels.

5.1 INTRODUCTION

Commercially available poly(amidoamine) (PAMAM) dendrimers are pharmaceutical polymers defined by an initiator core with radially attached symmetrical branches and terminal surface functionalities^{1, 2}. Their unique architecture and tuneability of the individual structural components³ makes PAMAM dendrimers suitable candidates for drug and gene delivery⁴⁻⁶ and several other biomedical applications⁷. Nanotoxicity is a limiting factor for the clinical applicability of cationic PAMAMs⁸⁻¹⁰, but not for the more biocompatible PAMAMs with anionic (i.e. -COOH) or non-ionic (i.e. -OH) surface groups^{11, 12}. To overcome the cytotoxic effects, an understanding of the underlying mechanisms of PAMAM-cell interactions is crucial. Membrane lipids are likely a first point of contact, and therefore, simplified membrane models such as monolayers or supported bilayers are suitable systems to study the mechanistic effects of PAMAMs on cell membranes^{13, 14}.

Surface pressure changes can provide valuable information on membrane penetration and membrane rupture, and our previous work on PAMAM G4.5 and G5 demonstrated a concentration-dependent penetration behavior with a clear preference to anionic lipid monolayers compared to zwitterionic ones¹⁵. Another group used surface pressure measurements and coarse-grained molecular dynamics (MD) simulations to study PAMAM interaction with zwitterionic lipid monolayers and showed that penetration levels increased with higher dendrimer generation ($G3 < G5 < G7$) and charged surface groups (-OH < -NH₂)^{16, 17}. PAMAM properties were also shown to be driving factors in the interaction with lipid bilayers¹⁸⁻²⁰. Adsorption of cationic PAMAMs can cause strong perturbations of the lipid bilayer leading to dendrimer penetration and eventually hole formation as shown with biophysical techniques (i.e. X-ray scattering, atomic force microscopy (AFM), calorimetry)^{19, 21, 22} and in computational studies²³⁻²⁵. X-ray and neutron techniques, such as small-angle scattering or reflection, are increasingly used to study the effect of PAMAM on lipid membrane^{22, 26-28}, as they a) are compatible with monolayer and bilayers, b) are able to differentiate structures at an angstrom level, and c) are sensitive to changes in both, surface and interface structure.

However, to our knowledge, neutron reflectometry was yet not used to evaluate the effect of half-generation PAMAMs on anionic lipid bilayers. Additionally, most PAMAM – membrane studies employ an overall physiological, neutral pH range (pH 7 – 7.4), but do not consider the impact of localized acidic pH values (i.e. gastric pH, lysosome pH) or the composition of the solution environment. For example, in cell culture experiments, methanol is widely accepted as a well-tolerated solubility-enhancing co-solvent with low cytotoxic effects²⁹⁻³¹ but methanol concentrations as low as 0.08 % were reported to activate immune reaction in human T lymphocytes³². Furthermore, we showed previously that the solvent quality affects not only the conformation of PAMAM dendrimers in solution but also experimental readouts such as fluorescence or UV-Vis³³.

Therefore, this study uses surface pressure measurements and neutron reflectometry to probe the impact of the solution environment (i.e. pH, methanol as co-solvent) on the interaction behavior of full-generation (G5) and half-generation (G4.5) PAMAMs with anionic phosphatidylglycerol (PG) monolayers and bilayers. PG is a major bacterial lipid³⁴, but also reflects the anionic net charge of any biomembrane³⁵.

5.2 EXPERIMENTAL

5.2.1 Materials

Powdered phospholipids (1,2-dipalmitoyl-*sn*-glycero-3-phosphocholine (h-DPPC); 1,2-dipalmitoyl-d62-*sn*-glycero-3-phosphocholine (d-DPPC); 1,2-dipalmitoyl-*sn*-glycero-3-phospho-(1'-*rac*-glycerol) (sodium salt) (h-DPPG)) were purchased from Avanti Polar Lipids (USA) and used without further purification. Poly(amidoamine) dendrimers (PAMAM G4.5, G5) and deuterium oxide (D₂O) were obtained from Sigma-Aldrich (UK). Solvents and salts for buffers were purchased from Sigma-Aldrich (UK) and Fisher Scientific (UK). Ultrapure (UHQ grade) water was produced in-house by an ELGA water purifier. Phosphate buffers (I = 0.034 M) in either UHQ grade water or D₂O were used throughout.

For structural information on the phospholipids and dendrimers see Table 5-2 and Figure 5-4 in the Supplementary Material section 5.61.

5.2.2 Methodology

5.2.2.1 Surface pressure measurements

A Langmuir-Blodgett (LB) trough (Nima Technology Ltd, UK) equipped with barriers for monolayer compression was filled phosphate buffer and the DPPG lipid monolayers were created at the air/liquid interface. The surface pressure and its changes were monitored using the Wilhelmy plate method³⁶. Once the surface pressure was equilibrated at the targeted initial pressure of $22 \pm 1 \text{ mN m}^{-1}$ or $32 \pm 2 \text{ mN m}^{-1}$, PAMAM dendrimer solution was introduced phosphate buffer subphase. The resulting changes in surface pressure (ΔSP) were recorded a function of time. All experiments were repeated at least thrice. Basic data analysis was done in Microsoft[®] Excel followed by statistical analysis (One-way Analysis of Variance (ANOVA) and Bonferroni's multiple comparisons test) in GraphPad Prim version 8.4.1.

5.2.2.2 Solid-supported bilayer deposition for neutron reflectometry

The asymmetric lipid bilayers were assembled onto ozone cleaned, highly flat, polished silicon blocks (PI-KEM, UK) utilizing a purpose-built LB trough equipped with a deposition arm (KSV-Nima / Biolin Scientific, Finland)³⁷. The inner leaflet of the membrane was created by Langmuir-Blodgett deposition of either tail-hydrogenated h-DPPC or tail-deuterated d_{62} -DPPC onto the silicon surface submerged in UHQ water containing 5 mM of calcium chloride. Langmuir-Schaeffer deposition of h-DPPC or h-DDPG was used for the outer leaflet³⁸. For each experimental condition two bilayers were produced, one with fully hydrogenated tails (h-block) and one with deuterated tails at the inner leaflet (d-block). The silicon substrates with the deposited bilayers were then placed in a purpose-built solid-liquid flow cells and stored under cold condition before use in the reflectometry experiments.

5.2.2.3 Neutron reflectivity measurements on solid-supported bilayers

Reflectivity was measured on the specular, white beam INTER³⁹ and SURF⁴⁰ reflectometers at the ISIS Neutron and Muon Spallation Source, Rutherford Appleton Laboratory (Oxfordshire, UK) allowing for incident wavelengths of 1 – 16 Å and 0.5 – 7 Å respectively. The reflected intensity was recorded on INTER at angles of 0.7° and 2.3°; and on SURF at angles of 0.35°, 0.65° and 1.5°; with both reaching a momentum transfer (Q_z) range of $\sim 0.01 - 0.3 \text{ \AA}^{-1}$.

The bilayer-containing solid-liquid flow cells were placed on a variable angle sample stage and connected to a Hitachi-Merck HPLC pump to facilitate the exchange of isotopic contrast solutions. Prior to neutron beam alignment, the cells were rinsed with pure D₂O to remove residual CaCl₂ solution and potential precipitates from the inner cell volume.

Each lipid bilayer was characterized with three phosphate buffer solution contrasts (100 % D₂O; silicon-matched water (SMW): 38 % D₂O + 62 % H₂O; 100 % H₂O) and the same solution contrasts with added PAMAM dendrimer (0.06 mg mL⁻¹, 0.3 mg mL⁻¹), resulting in six isotopic contrasts per bilayer and 12 isotopic contrasts per experimental condition (h-block and d-block). For each contrast change, a total of 12 mL per contrast solution was flushed through the flow cell at a rate of 1.5 mL min⁻¹, then the solution was held static in the cell for 5 min before data collection started. Data frames for each contrast were collected until an equilibrium stage was achieved.

5.2.2.4 Reflectivity data analysis

The ISIS-own Matlab-based fitting package RasCal (version 2014 beta)⁴¹ was used for the analysis of the neutron reflectivity results. RasCal employs an optical matrix formalism^{42, 43} to fit layer models to the experimental reflectivity data and therefore provides structural insight into the surface assemblage. In this approach the interfacial structure is described as a series of layers between the silicon (Si) substrate (super phase) and the buffered water (subphase). Here, the layers consisted of a silicon oxide (SiO₂), inner headgroups (DPPC), inner tails (h-tails or d₆₂-tails), outer tails (h-tails), outer headgroups (DPPG) for

the lipid-only system, and an additional dendrimer layer (PAMAM G4.5 or G5) for the lipid-dendrimer systems. The buffered water subphase was defined according to the solution isotopic contrast (D_2O , SMW or H_2O), and the silicon super phase was assumed to be the same across all isotopic contrasts.

A RasCal custom model was used to define the interfacial structure describing the relationships between scattering length density (SLD), layer thickness, layer roughness and layer hydration. Parameters such as lipid mixing and mixing of headgroup-dendrimer were calculated. The SLDs for the individual components of the layers can be found in Table 5-3 in the Supplementary.

In RasCal, multiple data sets can be fitted simultaneously, and individual fitting parameters such as layer roughness or thickness can be fully or partially constrained across the data sets. Reflectivity data of all isotopic contrasts prior to and after PAMAM addition were fitted simultaneously, constraining substrate parameters (Si roughness and SiO_2 layer thickness, roughness, and hydration). Bilayer roughness was constrained to all layers of the lipid bilayer in each experimental condition. Lipid tails of the d-block were used to calculate lipid mixing and to monitor changes after interaction with the PAMAMs, and the outer layers (outer headgroup, dendrimer) were fitted unconstrained to determine potential dendrimer interactions.

Finally, model to data fit error estimation was achieved by applying RasCal's Bayesian Error estimation routine which employs a Bayesian Markov chain Monte Carlo algorithm⁴⁴. Parameters were estimated using 60,000 MCMC points, 6,000 Burn-in points and 3 repeat runs, and the best fit parameters were provided as distribution maxima and their 95 % confidence intervals. Total membrane thickness was calculated as sum of the distribution maxima of the layer thicknesses of inner headgroup, lipid tails and outer headgroup.

5.3 RESULTS AND DISCUSSION

5.3.1 Interactions with lipid monolayers

PAMAM G4.5 and G5 ($c = 0.06 \text{ mg mL}^{-1}$) were probed for their interactions with anionic DPPG monolayers under different pH conditions along with the effect of residual methanol (0.1 % vs. 0 %) in the phosphate buffer subphase. The initial surface pressure of the DPPG monolayer was $\sim 22 \pm 2 \text{ mN m}^{-1}$ and the resulting maximum changes in surface pressure (SP_{max}) after dendrimer addition are summarized in Figure 5-1a.

A clear pH-dependency was seen for both PAMAM G4.5 and G5, with highest values of SP_{max} observed at pH 4. Compared to pH 7, the surface pressure in the methanol-containing environment was nearly four times higher for PAMAM G4.5 and ~ 7 -fold increased for PAMAM G5 respectively (for both $p < 0.001$). Penetration of PAMAM G5 into the DPPG layer produced similar changes in surface pressure for pH 7 and pH 10, while for G4.5 the lowest SP_{max} was observed at pH 10.

The pH-dependency was also observed in methanol-free conditions and methanol was identified as contributing factor for PAMAM – membrane interactions. For both PAMAM G5 and G4.5 the SP_{max} values at pH 4 were 5 – 8 mN m^{-1} lower compared to the results with residual methanol, but still significantly higher than pH 7 ($p < 0.001$). PAMAM G4.5 was unable to penetrate the DPPG monolayer (no changes in surface pressure) at pH 7 ($p < 0.05$).

The lateral membrane pressure in more rigid lipid bilayers of biological systems was reported to be $\sim 31 - 35 \text{ mN m}^{-1}$ (e.g. erythrocyte membrane)⁴⁵, therefore we conducted a part of our study at a higher initial monolayer surface pressure (high IP) of $\sim 32.5 \pm 1.2 \text{ mN m}^{-1}$. We were particularly interested in the membrane activity of PAMAM G5 at physiologically relevant pH 4 and pH 7 as G5 already showed a considerable monolayer penetration at lower initial surface pressure (low IP, 0.1 % methanol), and its cationic charge is generally associated with cytotoxic effects.

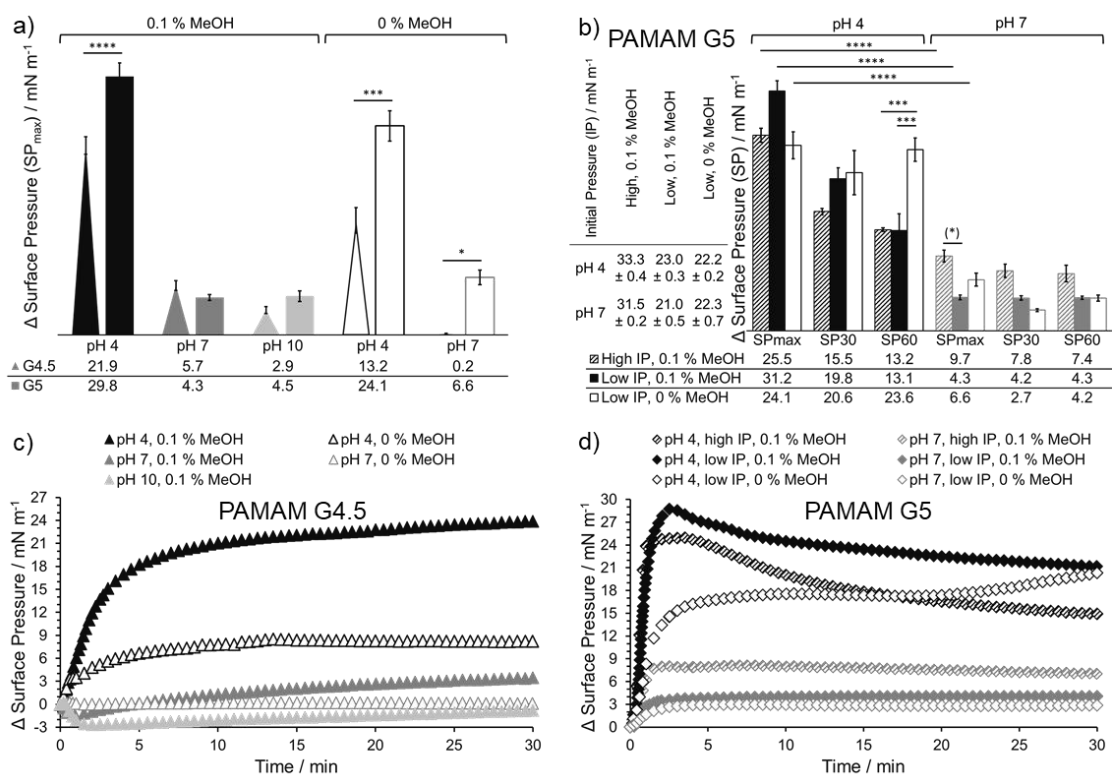


Figure 5-1 PAMAM G5 and G4.5 in phosphate buffer ($I = 0.034 \text{ M}$) interacting with DPPG monolayers. Panel a) Effect of methanol and pH on maximum changes in surface pressure (SP_{max}). Panel b) Impact of initial pressure (IP) before PAMAM G5 introduction on surface pressure changes at different pH. SP_{30} and SP_{60} are surface pressure changes measured at 30 min and 60 min after starting the PAMAM interaction. Panel c) Representative excerpts of initial 30 min of surface pressure changes over time for PAMAM G4.5 in different buffer conditions. Panel d) Exemplary excerpts of initial 30 min of surface pressure changes over time for PAMAM G5 in different buffer conditions and varying initial surface pressure. Data in panel a) and b) shown as $M \pm SEM$, $n \geq 3$. Statistical Analysis performed with Anova and Bonferroni; * $p \leq 0.05$; *** $p \leq 0.005$; **** $p < 0.001$. (*) $p = 0.0512$.

The differences in surface pressure changes after G5 addition at low IP and high IP are compared in Figure 5-1b. Most surface pressure changes were observed within the first half of the 60 min observation period, therefore values at half-time 30 min (SP_{30}) and endpoint 60 min (SP_{60}) are shown additionally to SP_{max} to give a flavor of the surface pressure behavior over time and representative kinetic profiles of the first 30 min are shown at Figure 5-1d (examples of the full 60 min profiles can be viewed in Figure 5-5 in the Supplementary section 5.6.2.1). A rapid increase to SP_{max} was seen within the first 5 min after PAMAM G5 addition. The interaction kinetics could be due to strong electrostatic attractions between the cationic PAMAM surface groups

and the anionic headgroups of DPPG as the number of primary amines was shown previously to linearly affect saturating stoichiometry and enthalpy of dendrimer–DMPG interactions⁴⁶. Furthermore, the resulting disturbances in the lipid membrane could be a contributing factor for the reported antibacterial activity of cationic PAMAMs^{47, 48}.

For pH 7 the surface pressure remained at the SP_{\max} plateau, but as illustrated in Figure 5-1b and 5-1d, the surface pressure at pH 4 decreased over time, known as relaxation, and the effect was less pronounced for high IP compared to low IP. The relaxation is a mechanism to deal with stress on the monolayers caused by the increased lateral pressure following the PAMAM penetration. Previous reports showed that monolayer relaxation and collapse mechanisms for rigid monolayers (i.e. high IP) include out-of-plane bending and folding, and for more fluid membranes (i.e. low IP) lipid stretching and shearing with material randomly leaving the surface⁴⁹. The 0.1 % methanol appeared to aid those processes, as under methanol-free conditions no decrease in surface pressure was observed after PAMAM G5 addition. In fact, after the rapid initial increase within the first 5 min and leveling at a plateau, a further slow increase of surface pressure was observed until reaching a second plateau at SP_{\max} values.

Interestingly, the SP_{\max} and SP_{30} values for the high IP were smaller than for the low IP at pH 4 compared to pH 7 where this trend was the opposite. At high IP, the lipid molecules had already a smaller area per molecule, which decreased more when the fully charged PAMAM molecules intercalated within the lipid layer and led to a lateral pressure increase. In fact, the total membrane pressure ($IP + SP_{\max}$) was $> 58 \text{ mN m}^{-1}$. Other researchers have shown that above a certain pressure which is lipid-specific, the monolayer will collapse and could form bilayer arrangements, which indicates a high IP might be able to only tolerate a small increase in pressure (less PAMAM penetration). For DPPG, Goto and coworkers⁵⁰ established a monolayer collapse pressure of 65 mN m^{-1} , which is not far above our total membrane pressure values of $\sim 58.8 \text{ mN m}^{-1}$ for high IP and 54.2 mN m^{-1} for low IP respectively.

At pH 7, the surface pressure changes at low and high IP were significantly smaller than pH 4, as PAMAM G5 carries a lower cationic net charge leading to reduced electrostatic attraction to the anionic DPPG headgroups. The surface pressure remained stable for both conditions after reaching the plateau within the first 5 min, but higher values overall were observed for high IP (near significant for SP_{\max} , $p = 0.0512$). The monolayer is more rigid at high IP, so even small amount of PAMAM penetration can cause higher increase in lateral pressure without restriction, as the total membrane pressure is far from the critical values seen for pH 4. However, it should be noted that surface pressure only indicates penetration but does not equate to surface excess of PAMAM at the interface where PAMAM may also be adsorbed below the lipid layer^{51, 52}.

Half-generation PAMAM G4.5 also interacted with DPPG monolayers in a pH-dependent manner with highest penetration levels at pH 4 (see Figure 5-1a), but the effect differed from those of full-generation PAMAM G5 in magnitude and interaction kinetics as illustrated in Figure 5-1 panels c and d. Overall, surface pressure changed at a much slower rate after addition of PAMAM G4.5 under all conditions, and SP_{\max} or a plateau was not achieved within the first 5 min. In the methanol-containing buffer environment at pH 7 and pH 10, an initial surface pressure dip before pressure stabilization and increase was observed, which was not seen for pH 4. Monolayer penetration and the related surface pressure increase was highest at pH 4 ($\sim 22 \text{ mN m}^{-1}$), where the tertiary amines in the dendrimer core were charged, and SP_{\max} values were significantly higher ($p < 0.001$) than those of the methanol-free buffer or higher pH conditions. At pH 7, no surface pressure changes were observed in the absence of methanol, indicating weak molecular interactions with PAMAM G4.5 and the need for the membrane-perturbing potency of methanol to facilitate penetration into DPPG monolayers. The assumed methanol effect on the DPPG monolayer is supported by previous studies showing that methanol interacted with membrane lipids, partitioned into the lipid headgroup areas, increased fluidity of lipid bilayers and decreased interfacial tension⁵³⁻⁵⁵. The impacts on the integrity of the lipid layer could have enabled adsorbed PAMAM G4.5 molecules to intercalate between the membrane lipids and this process was possibly aided

by hydrophobic interactions with the lipid tails. Previous studies reported the size and conformation of PAMAM G3.5 was smaller and more compact in methanol than in an aqueous solution^{56, 57} and this solvent quality driven effect could also contribute to the membrane penetration ability and penetration depth of half-generation PAMAMs. The observed inability to perturb the membrane under methanol-free conditions could be one of the reasons why anionic (half-generation) PAMAM were shown to be significantly less cytotoxic compared to their anionic counterparts^{11, 12}.

5.3.2 Interactions with lipid bilayers – neutron reflectometry

Whilst the monolayer experiments already provided valuable insights on the effect of solvent environment on the PAMAM – lipid interaction, the monolayer model has limited biological relevance as most natural membranes are made of lipid bilayers. Therefore, we decided to extend our PAMAM – lipid interactions studies to the more complex asymmetric bilayers and a different biophysical technique – neutron reflectometry (NR). The technique is interface- and surface-sensitive and informs on the location of different type of molecules relative to each other based on their distinct neutron scattering length density (SLD) (see Supplementary Table 5-3). We only studied the pH effect in this model system, as residual methanol was removed during to the PAMAM sample preparation to avoid undesired effects on the lipid bilayer coverage of the silicon substrate.

The first step was to characterize the lipid bilayers prior to any PAMAM addition. We used deuterated and hydrogenated lipids and to create the asymmetric DPPC-DPPG lipid bilayers and three solution contrasts (D_2O , silicon-matched water (SMW), H_2O) resulting in six contrasts for each experimental system. The large difference in H_2O and D_2O SLD enabled contrasting of otherwise chemically indistinguishable regions within the lipid bilayer. The D_2O contrast profile is particularly sensitive to lipid tail regions whereas the H_2O contrast can be used to detect interactions with the lipid heads⁵⁸. The lipid bilayers were then described with a five-layer model of the interface, which uses the minimum number of layers required to fit the

reflectivity data adequately⁵⁹. The lipid bilayer thicknesses ranged from ~ 54 - 61 Å, which agree with values for lipid bilayers at room temperature obtained by other researchers^{28, 60-62}. Some studies reported lower thickness values for DPPG bilayers (35 – 40 Å)^{63, 64}, however, those values were obtained at temperatures > 50°C – above their transition temperature, when the lipids were in the fluid phase (L_{α}). Our studies were conducted at room temperature, when both DPPC and DPPG were at the more ordered gel phase (L_{β}), where the lipid tails are more stretched and increase the overall bilayer thickness. Using the different SLDs of deuterated and hydrogenated tails, lipid tail mixing can be calculated. Increased tail mixing is a sign of lipid flip-flop between the leaflets and loss of asymmetry of the lipid bilayer. The asymmetry of the DPPC-DPPG bilayers was confirmed as less than 25 % lipid tail mixing was observed (see Supplementary Section 5.6.2.2., Table 5-4). For all systems, fitting of the individual bilayer regions returned similar hydration levels, smaller thickness values for the inner d-tail region compared to the outer h-tail regions, the smaller inner DPPC headgroups than outer DPPG headgroups.

Next, reflectivity of the lipid bilayers was measured again in all contrast conditions after addition of the PAMAM dendrimer solution and data was fitted with the same five-layer model as before but with an added PAMAM layer as illustrated in Figure 5-2.

At pH 7, PAMAM G4.5 showed a methanol-dependent penetration into the DPPG monolayer (see Figure 5-1), and therefore we were interested in the mode of bilayer interaction, if any, in a methanol-free environment. To our knowledge, we are the first to study half-generation PAMAM – lipid interactions with NR and therefore our results might shed light on the binding processes at the lipid interface. The fitted reflectivity profiles of all solution contrasts of the dDPPC:DPPG bilayer and the resulting layer SLD profiles before and after PAMAM G4.5 addition ($c = 0.06 \text{ mg mL}^{-1}$) are shown in Figure 5-2. Figure 5-2b illustrates the division of the bilayer into multiple layers, and that distinct changes in the SLDs can indicate interfacial areas potentially affected by PAMAM adsorption or penetration. Each layer of the model was fitted for hydration, layer thickness and roughness. Data for layer thickness and

hydration are summarized in Table 5-1, further fitted parameters can be found in Table 5-4 in the Supplementary.

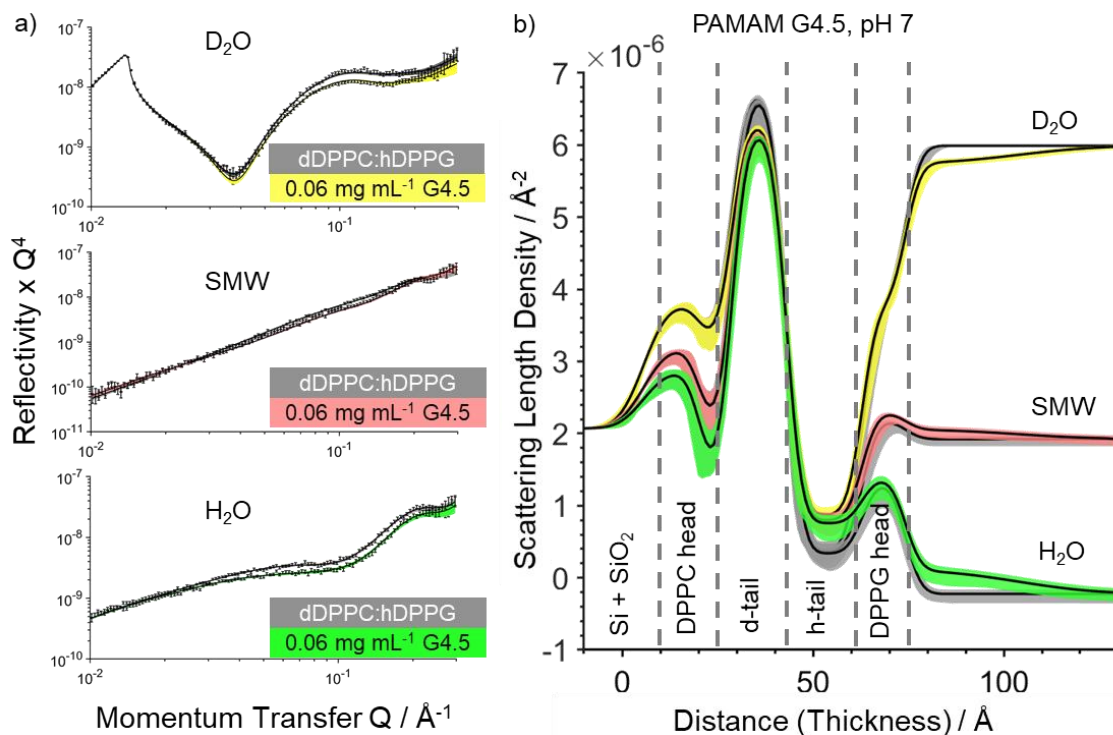


Figure 5-2 Interaction of PAMAM G4.5 with an asymmetric, deuterated bilayer (dDPPC-hDPPG) in phosphate buffer pH 7 ($I = 0.039 \text{ M}$). Panel a) Neutron reflectivity profiles and fits of the bilayer before (grey) and after PAMAM (coloured) interaction at 0.06 mg mL^{-1} . Averaged data points and error bars from multiple counts. Panel b) Scattering length density profiles derived from fits of the reflectivity profiles in different contrasts. In both panels, the shaded area accounts for the 95 % confidence interval of the data fits.

The results show that PAMAM G4.5 adsorbed as additional layer onto the DPPG headgroup, but only caused small changes to lipid bilayer itself, mainly shown by an increased lipid mixing (also known as flip-flop) and some intercalation ($\sim 5 \%$) only into the DPPG headgroup layer. These low-level changes to the lipid bilayer align with our lipid monolayer results, where in a methanol-free environment PAMAM G4.5 was not able to penetrate or disrupt the lipid layer at pH 7. At this pH, PAMAM G4.5 is a zwitterionic molecule with a negative net charge, with a small percentage of charged tertiary amines in the dendrimer core and most carboxylate surface groups charged³³. Therefore, with little electrostatic attraction to the anionic DPPG headgroups, intra- and inter-dendrimer interactions or attraction to the zwitterionic DPPC headgroups might

explain the observed changes to the bilayer. The PAMAM layer was fitted to ~90 % hydration indicating only ~10 % dendrimer coverage. The thickness was ~30 Å (about the diameter of one PAMAM molecule) and the roughness of ~ 16 Å suggested a patchy PAMAM adsorption.

Next, we probed PAMAM – lipid bilayer interactions at solution pH 4 since this condition led to the highest penetration levels for both PAMAM G4.5 and G5 during the monolayer studies. The dendrimer concentration was fixed to 0.06 mg mL⁻¹ to match the previous sets of experiments. Because of the proximity of the PAMAMs intrinsic SLD values to the SMW SLD, the effect on the lipid layer is best visible in the D₂O and H₂O contrasts, therefore, only those contrasts are shown in Figure 3.

Both dendrimer species show interactions in the reflectivity profiles (Figure 5-3, panel a and b), and the resulting fits revealed changes in the lipid tail hydration levels and the adsorption of a PAMAM layer onto the DPPG headgroups with similar hydration (~85 %) and roughness levels. The changes in the NR profiles appeared to be more pronounced for PAMAM G5, but it needs to be considered that those changes are related to the high number of exchangeable hydrogens within the dendrimer. The deuterium - hydrogen exchange might alter the SLDs of PAMAM G5 more than G4.5 and thus influence the results seen for different contrast solutions significantly. The level of dendrimer penetration into the DPPG headgroup layer was similar for both PAMAM (approx. 4 – 6 %) and comparable to pH 7. However, at pH 4, the asymmetry of the bilayer was retained, and no lipid flip-flopping occurred. Changes in the tail hydration levels were about 4 %, whereby G4.5 increased and G5 decreased the tail hydration. The differences in the apparent hydration of the layers may be linked to deeper penetration levels of the dendrimers into the hydrophobic lipid tail region, and our model might struggle to differentiate between species where multiple elements are present. The reflectometry technique is based on atomic SLDs and is therefore not sensitive to potential conformational changes of the dendrimers or lateral rearrangement of the lipid layer that possibly contribute to the observed tail hydrations at low pH. Overall, the results suggest a more effective penetration into tail layers of the bilayer at

pH 4 compared to pH 7, in line with our findings of DPPG monolayer experiments.

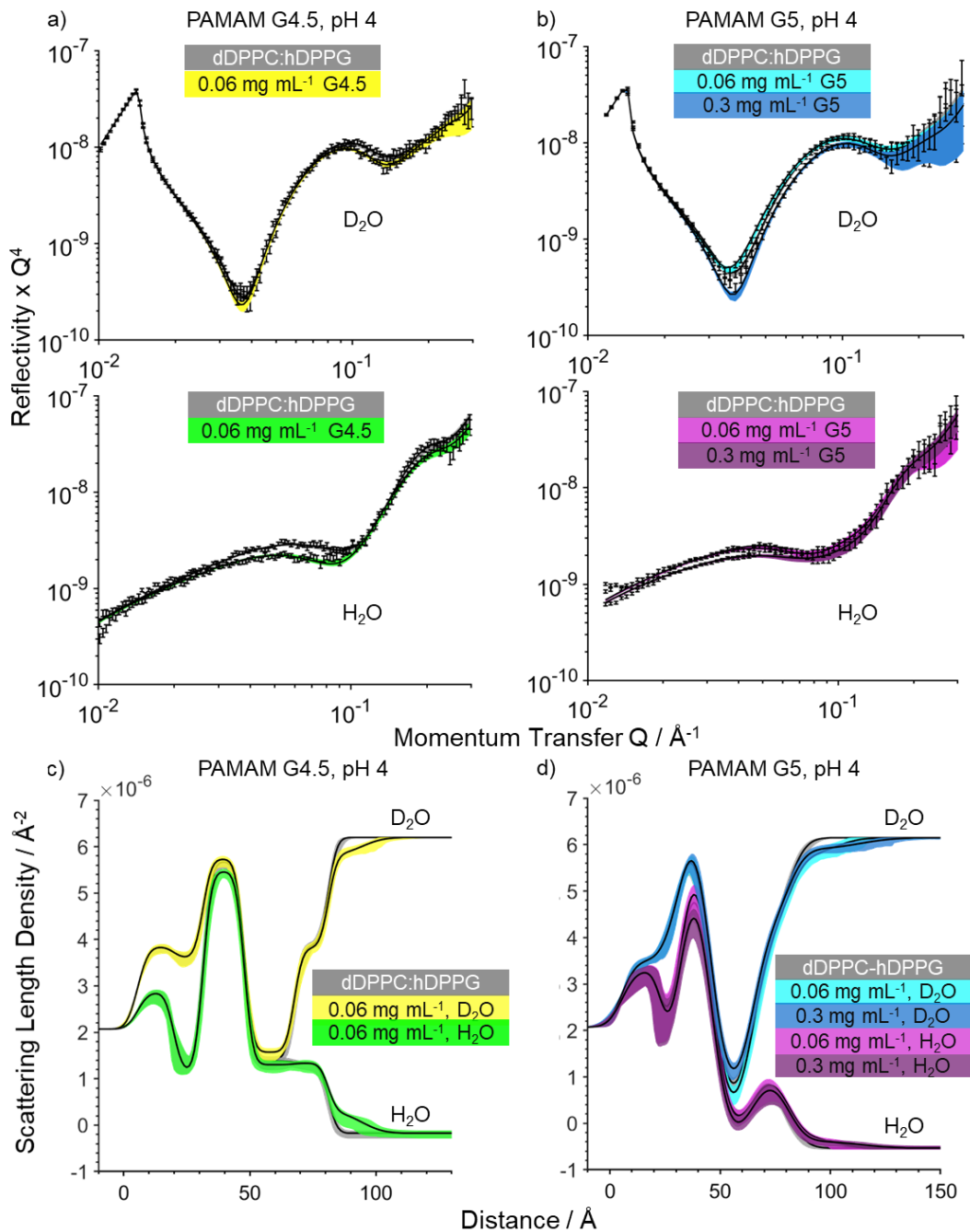


Figure 5-3 Interaction of PAMAM G4.5 and G5 with an asymmetric, deuterated bilayer (hDPPC-dDPPG) in deuterated and hydrogenated phosphate buffer pH 4 ($I = 0.039 M$). Neutron reflectivity profiles and fits of the bilayer before (light grey) and after PAMAM G4.5 (dark grey, panel a) and PAMAM G5 (panel c) interaction. Averaged data points and error bars from the scattering counts. Scattering length density profiles derived from fits of the reflectivity profiles in different contrasts for PAMAM G4.5 (panel b) and PAMAM G5 (panel d). In all panels, the shaded area accounts for the 95 % confidence interval of the data fits

In biological systems, acidic pH is a relevant parameter not only digestive organs, but also for cellular organelles such as lysosomes or endosomes, and our results suggest that low pH might enhance molecular interactions at the lipid interface. Biological studies reported higher cytotoxicity for NH₂-terminated PAMAM^{10, 11}, that was dependent on cell line and exposure time^{8, 9, 11}. Our previous study at pH 7 showed a concentration-dependent penetration behavior into DPPC and DPPG monolayers at concentrations up to 0.3 mg mL⁻¹¹⁵. The difference between surface pressure rise at 0.06 mg mL⁻¹ and 0.3 mg mL⁻¹ was ~3.5 mN m⁻¹, and the penetration levels were not proportional to the concentration increase and indicated a saturation of the monolayer towards the higher PAMAM concentrations. As we now observed significantly higher PAMAM – lipid interactions at biologically relevant pH 4, we decided to further study PAMAM G5 activity on DPPC:DPPG bilayers with an increased concentration of 0.3 mg mL⁻¹.

The reflectivity profiles and resulting fits for 0.3 mg mL⁻¹ PAMAM G5 can be found in Figure 5-3 panel b and d, overlaying the results for 0.06 mg mL⁻¹ for direct comparison. For both concentrations, lipid tail mixing was not affected by the addition of the dendrimer, however, the higher concentration led to 8-10 % higher tail hydration, indicating an effect of dendrimer onto the hydrophobic lipid tails region. The extent of dendrimer residing in the DPPG headgroup layer was minimal (< 0.02 %), but the adjacent PAMAM layer thickness and lipid hydration levels were the highest compared to any of the other systems studied. The overall higher hydration levels along with minimal PAMAM penetration into the headgroup region suggest that the dendrimers caused defects to the lipid layer, i.e. by pulling out individual lipid molecules from the bilayer without collapsing or stripping of the layer from the silicon support. A similar behavior was reported for full-generation PAMAMs interacting with phosphocholine bilayers and creating holes^{19, 21, 24}, and it was proposed the separated lipids form dendrimer-lipid aggregates, so called dendrisomes, with the free dendrimer molecules. The PAMAM layer at 0.3 mg mL⁻¹ concentration was ~ 32 Å (about 10 Å thicker than for 0.06 mg mL⁻¹) with high hydration levels > 90 %, which also supports a clustered, patchy adsorption of the dendrimers. In general, the higher G5

concentration introduced more pronounced disturbances to the lipid bilayer system but did not completely disrupt the bilayer's integrity. Considering the 5-fold concentration increase compared to 0.06 mg mL⁻¹, the changes overall were smaller than anticipated.

Table 5-1 Comparison of major fitting parameters in different PAMAM-lipid bilayer systems. Values in brackets reflect 95 % Confidence interval.

Layer	G4.5, pH 7, 0.06 mg mL ⁻¹	G4.5, pH 4, 0.06 mg mL ⁻¹	G5, pH 4, 0.06 mg mL ⁻¹	G5, pH 4, 0.3 mg mL ⁻¹
Layer Thickness / Å				
DPPC Headgroup	8.12 (7.05, 10.08)	11.50 (10.48, 12.48)		8.86 (7.42, 10.80)
Inner h-Tails	14.41 (13.93, 14.88)	16.41 (15.90, 16.86)		12.64 (12.08, 13.37)
Outer d-Tails	19.78 (19.26, 20.00)	19.75 (19.23, 19.99)		19.64 (18.84, 19.99)
DPPG Headgroup	11.45 (10.77, 12.15)	13.57 (12.92, 14.23)		16.09 (14.29, 17.95)
PAMAM Layer	29.52 (20.51, 37.05)	13.02 (3.10, 20.04)	21.53 (4.94, 32.64)	32.62 (14.34, 43.87)
Lipid Bilayer ^b	53.76	61.23		57.23
Lipid Bilayer + PAMAM ^b	83.28	74.25	78.76	89.85
Layer Hydration / %				
DPPC Headgroup	31.53 (27.92, 35.07)	38.27 (35.44, 40.96)		37.92 (30.16, 46.44)
Pre-PAMAM Tails	0.80 (0.04, 2.04)	0.33 (0.01, 0.98)		5.43 (2.12, 8.87)
DPPG Headgroup	35.88 (35.02, 38.18)	36.33 (35.05, 39.02)		44.20 (35.94, 52.01)
PAMAM Layer	89.81 (86.36, 92.61)	85.21 (70.36, 92.31)	87.33 (71.99, 93.72)	91.82 (85.58, 95.08)
Post-PAMAM Tails	1.83 (0.32, 3.49)	4.22 (2.95, 5.55)	2.64 (0.14, 6.19)	13.24 (9.77, 16.69)

^a CI = 95 % Confidence Interval, provided by Bayesian Error Analysis

^b Values represent the sum of the fitted parameters

5.4 CONCLUSIONS

We aimed to explore how experimental parameters such as solution pH and methanol content affect the interactions between lipid model membranes and amine-terminated PAMAM G5 as well as carboxylate-terminated G4.5 dendrimers using surface pressure measurements and neutron reflectometry. Understanding the implications of these parameters is important as they often form part in sample preparation and experimental set-up of biomedical PAMAM studies but also have a biological relevance in terms of variations in organ and cell organelles' pH.

Our findings show that the half-generation and full-generation PAMAM interacted differently with the model membranes. Generally, PAMAM G5 showed faster and higher penetration into the DPPG monolayers than PAMAM G4.5. Both PAMAMs induced changes to the DPPC-DPPG lipid bilayer system, but differences in the interaction were less pronounced than for the monolayer system. The PAMAM dendrimers caused charge- and concentration - dependent changes to lipid hydration levels, showed only minor headgroup layer penetration and adsorbed in clusters onto the DPPG headgroup.

Changing the solution pH from pH 7 to pH 4, led to a nearly 6-fold increase in surface pressure change for PAMAM G5 and ~ 3.5-fold increase for G4.5 implying increased penetration rates into the monolayers, potentially driven by electrostatic attraction of charged amines to the anionic DPPG headgroups. An increased interaction was also observed for the lipid bilayers, but not as distinctive as seen for the less rigid monolayers.

Presence of 0.1 % methanol in the system resulted in significantly higher PAMAM penetration levels into lipid monolayers, and this could be attributed to the membrane-perturbing effect of methanol aiding the dendrimer interaction. This was further supported by the inability of PAMAM G4.5 to induce surface pressure changes at pH 7 under methanol-free conditions. Additionally, the initial lateral pressure of the lipid monolayer prior to PAMAM G5 addition was also modulating the interaction intensity.

5.5 REFERENCES

1. Tomalia, D. A.; Baker, H.; Dewald, J.; Hall, M.; Kallos, G.; Martin, S.; Roeck, J.; Ryder, J.; Smith, P., A new class of polymers - Starburst-dendritic macromolecules. *Polym. J.* **1985**, *17* (1), 117-132.
2. Tomalia, D. A.; Naylor, A. M.; Goddard, W. A., Starburst Dendrimers: Molecular-Level Control of Size, Shape, Surface Chemistry, Topology, and Flexibility from Atoms to Macroscopic Matter. *Angew. Chem., Int. Ed. Engl.* **1990**, *29* (2), 138-175.
3. Fréchet, J. M., Functional polymers and dendrimers: reactivity, molecular architecture, and interfacial energy. *Science* **1994**, *263* (5154), 1710-5.

4. Abedi-Gaballu, F.; Dehghan, G.; Ghaffari, M.; Yekta, R.; Abbaspour-Ravasjani, S.; Baradaran, B.; Ezzati Nazhad Dolatabadi, J.; Hamblin, M. R., PAMAM dendrimers as efficient drug and gene delivery nanosystems for cancer therapy. *Applied Materials Today* **2018**, *12*, 177-190.
5. Li, J.; Liang, H.; Liu, J.; Wang, Z., Poly (amidoamine) (PAMAM) dendrimer mediated delivery of drug and pDNA/siRNA for cancer therapy. *International journal of pharmaceutics* **2018**, *546* (1-2), 215-225.
6. Daneshvar, N.; Abdullah, R.; Shamsabadi, F. T.; How, C. W.; Mh, M. A.; Mehrbod, P., PAMAM dendrimer roles in gene delivery methods and stem cell research. *Cell biology international* **2013**, *37* (5), 415-9.
7. Araújo, R. V. d.; Santos, S. d. S.; Igne Ferreira, E.; Giarolla, J., New Advances in General Biomedical Applications of PAMAM Dendrimers. *Molecules* **2018**, *23* (11), 2849.
8. Naha, P. C.; Mukherjee, S. P.; Byrne, H. J., Toxicology of Engineered Nanoparticles: Focus on Poly(amidoamine) Dendrimers. *Int J Environ Res Public Health* **2018**, *15* (2).
9. Sadekar, S.; Ghandehari, H., Transepithelial transport and toxicity of PAMAM dendrimers: implications for oral drug delivery. *Advanced drug delivery reviews* **2012**, *64* (6), 571-88.
10. Bodewein, L.; Schmelter, F.; Di Fiore, S.; Hollert, H.; Fischer, R.; Fenske, M., Differences in toxicity of anionic and cationic PAMAM and PPI dendrimers in zebrafish embryos and cancer cell lines. *Toxicology and applied pharmacology* **2016**, *305*, 83-92.
11. Thiagarajan, G.; Greish, K.; Ghandehari, H., Charge affects the oral toxicity of poly(amidoamine) dendrimers. *European journal of pharmaceutics and biopharmaceutics : official journal of Arbeitsgemeinschaft fuer Pharmazeutische Verfahrenstechnik e.V* **2013**, *84* (2), 330-4.
12. Janaszewska, A.; Mączyńska, K.; Matuszko, G.; Appelhans, D.; Voit, B.; Klajnert, B.; Bryszewska, M., Cytotoxicity of PAMAM, PPI and maltose modified PPI dendrimers in Chinese hamster ovary (CHO) and human ovarian carcinoma (SKOV3) cells. *New Journal of Chemistry* **2012**, *36* (2), 428-437.
13. Fox, L. J.; Richardson, R. M.; Briscoe, W. H., PAMAM dendrimer - cell membrane interactions. *Advances in colloid and interface science* **2018**, *257*, 1-18.
14. Jafari, M.; Mehrnejad, F.; Talandashti, R.; Doustdar, F.; Reza Vakili, M.; Lavasanifar, A., Effect of the lipid composition and cholesterol on the membrane selectivity of low generations PAMAM dendrimers: A molecular dynamics simulation study. *Applied Surface Science* **2021**, *540*, 148274.

15. Wilde, M.; Green, R. J.; Sanders, M. R.; Greco, F., Biophysical studies in polymer therapeutics: the interactions of anionic and cationic PAMAM dendrimers with lipid monolayers. *Journal of drug targeting* **2017**, *25* (9-10), 910-918.
16. Tian, F.; Lin, X.; Valle, R. P.; Zuo, Y. Y.; Gu, N., Poly(amidoamine) Dendrimer as a Respiratory Nanocarrier: Insights from Experiments and Molecular Dynamics Simulations. *Langmuir : the ACS journal of surfaces and colloids* **2019**, *35* (15), 5364-5371.
17. Lin, X.; Li, Y.; Gu, N., Molecular dynamics simulations of the interactions of charge-neutral PAMAM dendrimers with pulmonary surfactant. *Soft Matter* **2011**, *7* (8), 3882-3888.
18. Lombardo, D.; Calandra, P.; Bellocco, E.; Lagana, G.; Barreca, D.; Magazu, S.; Wanderlingh, U.; Kiselev, M. A., Effect of anionic and cationic polyamidoamine (PAMAM) dendrimers on a model lipid membrane. *Biochimica et biophysica acta* **2016**, *1858* (11), 2769-2777.
19. Mecke, A.; Majoros, I. J.; Patri, A. K.; Baker, J. R., Jr.; Holl, M. M.; Orr, B. G., Lipid bilayer disruption by polycationic polymers: the roles of size and chemical functional group. *Langmuir : the ACS journal of surfaces and colloids* **2005**, *21* (23), 10348-54.
20. Roy, B.; Panda, A. K.; Parimi, S.; Ametov, I.; Barnes, T.; Prestidge, C. A., Physico-chemical Studies on the Interaction of Dendrimers with Lipid Bilayers. 1. Effect of Dendrimer Generation and Liposome Surface Charge. *J. Oleo Sci.* **2014**, *63* (11), 1185-1193.
21. Berenyi, S.; Mihaly, J.; Wacha, A.; Toke, O.; Bota, A., A mechanistic view of lipid membrane disrupting effect of PAMAM dendrimers. *Colloids and Surfaces, B: Biointerfaces* **2014**, *118*, 164-71.
22. Fox, L. J.; Slastanova, A.; Taylor, N.; Wlodek, M.; Bikondoa, O.; Richardson, R. M.; Briscoe, W. H., Interactions between PAMAM dendrimers and DOPC lipid multilayers: Membrane thinning and structural disorder. *Biochimica et Biophysica Acta (BBA) - General Subjects* **2021**, *1865* (4), 129542.
23. Kelly, C. V.; Leroueil, P. R.; Orr, B. G.; Banaszak Holl, M. M.; Andricioaei, I., Poly(amidoamine) dendrimers on lipid bilayers II: Effects of bilayer phase and dendrimer termination. *Journal of Physical Chemistry B* **2008**, *112* (31), 9346-9353.
24. Lee, H.; Larson, R. G., Coarse-grained molecular dynamics studies of the concentration and size dependence of fifth- and seventh-generation PAMAM dendrimers on pore formation in DMPC bilayer. *The journal of physical chemistry. B* **2008**, *112* (26), 7778-84.
25. Majoros, I.; Williams, C.; Becker, A.; Baker, J., Surface Interaction and Behavior of Poly(amidoamine) Dendrimers: Deformability and Lipid Bilayer Disruption. *Journal of Computational and Theoretical Nanoscience* **2009**, *6* (7), 1430-1436.

26. Yanez Arteta, M.; Ainalem, M. L.; Porcar, L.; Martel, A.; Coker, H.; Lundberg, D.; Chang, D. P.; Soltwedel, O.; Barker, R.; Nylander, T., Interactions of PAMAM Dendrimers with Negatively Charged Model Biomembranes. *The journal of physical chemistry. B* **2014**, *118* (45), 12892-12906.
27. Ainalem, M.-L.; Campbell, R. A.; Khalid, S.; Gillams, R. J.; Rennie, A. R.; Nylander, T., On the Ability of PAMAM Dendrimers and Dendrimer/DNA Aggregates To Penetrate POPC Model Biomembranes. *The journal of physical chemistry. B* **2010**, *114*, 7229–7244.
28. Akesson, A.; Lind, T. K.; Barker, R.; Hughes, A.; Cardenas, M., Unraveling dendrimer translocation across cell membrane mimics. *Langmuir : the ACS journal of surfaces and colloids* **2012**, *28* (36), 13025-33.
29. Hamzeloo-Moghadam, M.; Taiebi, N.; Mosaddegh, M.; Eslami Tehrani, B.; Esmaeili, S., The effect of some cosolvents and surfactants on viability of cancerous cell lines. *Research Journal of Pharmacognosy* **2014**, *1* (3), 41-45.
30. Jover, R.; Ponsoda, X.; Castell, J. V.; Gómez-Lechón, M. J., Evaluation of the cytotoxicity of ten chemicals on human cultured hepatocytes: Predictability of human toxicity and comparison with rodent cell culture systems. *Toxicology in Vitro* **1992**, *6* (1), 47-52.
31. Oyama, Y.; Sakai, H.; Arata, T.; Okano, Y.; Akaike, N.; Sakai, K.; Noda, K., Cytotoxic effects of methanol, formaldehyde, and formate on dissociated rat thymocytes: a possibility of aspartame toxicity. *Cell Biol Toxicol* **2002**, *18* (1), 43-50.
32. Désy, O.; Carignan, D.; Caruso, M.; de Campos-Lima, P. O., Methanol Induces a Discrete Transcriptional Dysregulation that Leads to Cytokine Overproduction in Activated Lymphocytes. *Toxicological Sciences* **2010**, *117* (2), 303-313.
33. Wilde, M.; Wilde, C.; Edwards-Gayle, C. J. C.; Hamley, I. W.; Wang, Z.; Greco, F.; Green, R. J., pH and Methanol Responsive Conformational Changes of Poly(amidoamine) Dendrimers in Solution. *ACS Applied Polymer Materials* **2021**, *Manuscript submitted*.
34. Sohlenkamp, C.; Geiger, O., Bacterial membrane lipids: diversity in structures and pathways. *FEMS Microbiology Reviews* **2015**, *40* (1), 133-159.
35. van Meer, G.; Voelker, D.; Feigenson, G., Membrane lipids: where they are and how they behave. *Nature Reviews Molecular Cell Biology* **2008**, *9* (2), 112-124.
36. Rapp, B. E., Chapter 22 - Measuring Surface Tension and Free Surface Energy. In *Microfluidics: Modelling, Mechanics and Mathematics*, Rapp, B. E., Ed. Elsevier: Oxford, 2017; pp 453-465.
37. Hughes, A. V.; Howse, J. R.; Dabkowska, A.; Jones, R. A.; Lawrence, M. J.; Roser, S. J., Floating lipid bilayers deposited on chemically grafted

phosphatidylcholine surfaces. *Langmuir : the ACS journal of surfaces and colloids* **2008**, *24* (5), 1989-1999.

38. Tamm, L. K.; McConnell, H. M., Supported phospholipid bilayers. *Biophysical journal* **1985**, *47* (1), 105-113.

39. Webster, J.; Holt, S.; Dalgliesh, R., INTER the chemical interfaces reflectometer on target station 2 at ISIS. *Phys. B. (Amsterdam, Netherlands)* **2006**, *385-386*, 1164-1166.

40. Zarbakhsh, A.; Richardson, R. M.; Rennie, A.; Higgins, J. S.; Jones, R. A. L.; Fletcher, P.; Thomas, R. K.; Roser, S.; Dickinson, E., SURF - A second generation neutron reflectometer. 1995; pp 95-1002.

41. Hughes, A. V. *RasCal*, 2014 Beta; ISIS Spallation Neutron Source (Rutherford Appleton Laboratory): <http://sourceforge.net/projects/rscl/>, 2014.

42. Born, M.; Wolf, E., *Principles of Optics: Electromagnetic Theory of Propagation, Interference and Diffraction of Light*. 7 ed.; Cambridge University Press: Cambridge, 1999.

43. Doucet, M.; Archibald, R. K.; Heller, W. T., Machine learning for neutron reflectometry data analysis of two-layer thin films *. *Machine Learning: Science and Technology* **2021**, *2* (3), 035001.

44. Haario, H.; Laine, M.; Mira, A.; Saksman, E., DRAM: Efficient adaptive MCMC. *Statistics and Computing* **2006**, *16* (4), 339-354.

45. Demel, R. A.; Geurts van Kessel, W. S. M.; Zwaal, R. F. A.; Roelofsen, B.; van Deenen, L. L. M., Relation between various phospholipase actions on human red cell membranes and the interfacial phospholipid pressure in monolayers. *Biochimica et Biophysica Acta (BBA) - Biomembranes* **1975**, *406* (1), 97-107.

46. Kelly, C. V.; Liroff, M. G.; Triplett, L. D.; Leroueil, P. R.; Mullen, D. G.; Wallace, J. M.; Meshinchi, S.; Baker, J. R.; Orr, B. G.; Banaszak Holl, M. M., Stoichiometry and Structure of Poly(amidoamine) Dendrimer-Lipid Complexes. *ACS Nano* **2009**, *3* (7), 1886-1896.

47. Holmes, A. M.; Heylings, J. R.; Wan, K. W.; Moss, G. P., Antimicrobial efficacy and mechanism of action of poly(amidoamine) (PAMAM) dendrimers against opportunistic pathogens. *Int J Antimicrob Agents* **2019**, *53* (4), 500-507.

48. Xue, X.; Chen, X.; Mao, X.; Hou, Z.; Zhou, Y.; Bai, H.; Meng, J.; Da, F.; Sang, G.; Wang, Y.; Luo, X., Amino-terminated generation 2 poly(amidoamine) dendrimer as a potential broad-spectrum, nonresistance-inducing antibacterial agent. *AAPS J* **2013**, *15* (1), 132-42.

49. Pocivavsek, L.; Frey, S. L.; Krishan, K.; Gavrilov, K.; Ruchala, P.; Waring, A. J.; Walther, F. J.; Dennin, M.; Witten, T. A.; Lee, K. Y. C., Lateral stress relaxation and collapse in lipid monolayers. *Soft Matter* **2008**, *4* (10), 2019-2029.

50. Goto, T. E.; Caseli, L., Understanding the Collapse Mechanism in Langmuir Monolayers through Polarization Modulation-Infrared Reflection Absorption Spectroscopy. *Langmuir : the ACS journal of surfaces and colloids* **2013**, *29* (29), 9063-9071.
51. Tripp, B. C.; Magda, J. J.; Andrade, J. D., Adsorption of Globular Proteins at the Air/Water Interface as Measured via Dynamic Surface Tension: Concentration Dependence, Mass-Transfer Considerations, and Adsorption Kinetics. *J. Colloid Interface Sci.* **1995**, *173* (1), 16-27.
52. Lad, M. D.; Birembaut, F.; Frazier, R. A.; Green, R. J., Protein-lipid interactions at the air/water interface. *Physical chemistry chemical physics : PCCP* **2005**, *7* (19), 3478-3485.
53. Ingólfsson, H. I.; Andersen, O. S., Alcohol's effects on lipid bilayer properties. *Biophysical journal* **2011**, *101* (4), 847-855.
54. Joo, H.-J.; Ahn, S.-H.; Lee, H.-R.; Jung, S.-W.; Choi, C.-W.; Kim, M.-S.; Bae, M.-K.; Chung, I.-K.; Bae, S.-K.; Jang, H.-O.; Yun, I., The effect of methanol on the structural parameters of neuronal membrane lipid bilayers. *Korean J Physiol Pharmacol* **2012**, *16* (4), 255-264.
55. Ly, H. V.; Longo, M. L., The influence of short-chain alcohols on interfacial tension, mechanical properties, area/molecule, and permeability of fluid lipid bilayers. *Biophysical journal* **2004**, *87* (2), 1013-1033.
56. Lombardo, D., Liquid-like Ordering of Negatively Charged Poly(amidoamine) (PAMAM) Dendrimers in Solution. *Langmuir : the ACS journal of surfaces and colloids* **2009**, *25* (5), 3271-3275.
57. Micali, N.; Scolaro, L. M.; Romeo, A.; Lombardo, D.; Lesieur, P.; Mallamace, F., Structural properties of methanol-polyamidoamine dendrimer solutions. *Physical Review E* **1998**, *58* (5), 6229-6235.
58. Le Brun, A. P.; Clifton, L. A.; Holt, S. A.; Holden, P. J.; Lakey, J. H., Deuterium Labeling Strategies for Creating Contrast in Structure-Function Studies of Model Bacterial Outer Membranes Using Neutron Reflectometry. *Methods Enzymol.* **2016**, *566*, 231-52.
59. Clifton, L. A.; Neylon, C.; Lakey, J. H., Examining protein-lipid complexes using neutron scattering. *Methods Mol Biol* **2013**, *974*, 119-50.
60. Ashkar, R.; Nagao, M.; Butler, Paul D.; Woodka, Andrea C.; Sen, Mani K.; Koga, T., Tuning Membrane Thickness Fluctuations in Model Lipid Bilayers. *Biophysical Journal* **2015**, *109* (1), 106-112.
61. Florek, O. B.; Clifton, L. A.; Wilde, M.; Arnold, T.; Green, R. J.; Frazier, R. A., Lipid composition in fungal membrane models: effect of lipid fluidity. *Acta Crystallographica Section D* **2018**, *74* (12), 1233-1244.

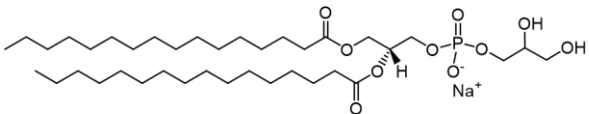
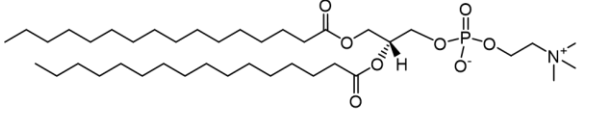
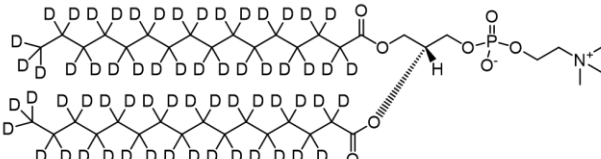
62. de Ghellinck, A.; Shen, C.; Fragneto, G.; Klosgen, B., Probing the position of resveratrol in lipid bilayers: A neutron reflectivity study. *Colloids and Surfaces B: Biointerfaces* **2015**, *134*, 65-72.
63. Zhuang, X.; Dávila-Contreras, E. M.; Beaven, A. H.; Im, W.; Klauda, J. B., An extensive simulation study of lipid bilayer properties with different head groups, acyl chain lengths, and chain saturations. *Biochimica et Biophysica Acta (BBA) - Biomembranes* **2016**, *1858* (12), 3093-3104.
64. Pan, J.; Heberle, F. A.; Tristram-Nagle, S.; Szymanski, M.; Koepfinger, M.; Katsaras, J.; Kučerka, N., Molecular structures of fluid phase phosphatidylglycerol bilayers as determined by small angle neutron and X-ray scattering. *Biochimica et Biophysica Acta (BBA) - Biomembranes* **2012**, *1818* (9), 2135-2148.

5.6 SUPPLEMENTARY

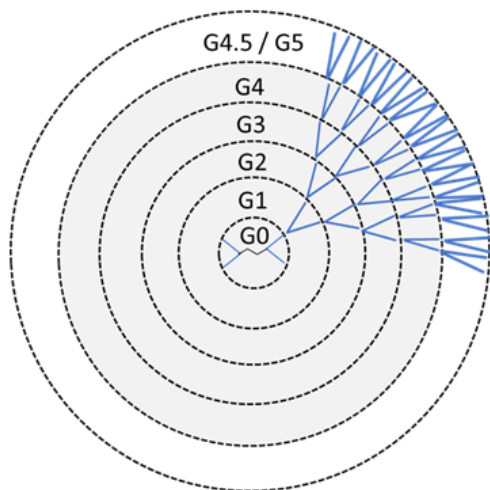
5.6.1 Supplementary materials

Structural information on the lipids and PAMAM dendrimers used in this study can be found in Table 5-2 and Figure 5-4 below.

Table 5-2 Summary of Avanti Phospholipids used in this study and their properties as provided by the manufacturer.

Name	Formula Weight	Chemical Structure
1,2-dipalmitoyl-sn-glycero-3-phospho-(1'-rac-glycerol) (sodium salt) (DPPG)	744.952	 The chemical structure shows two palmitoyl chains (16 carbons each) attached to the sn-glycerol backbone at the 1 and 2 positions. The 3-position is linked to a phosphate group, which is further connected to a 1'-rac-glycerol moiety. A sodium ion (Na+) is shown as a counterion.
1,2-dipalmitoyl-sn-glycero-3-phosphocholine (hDPPC)	734.039	 The chemical structure is similar to DPPG, but the phosphate group is linked to a choline group (N(CH3)3+) instead of a 1'-rac-glycerol moiety.
1,2-dipalmitoyl-d62-sn-glycero-3-phosphocholine (dDPPC)	796.421	 The chemical structure is similar to hDPPC, but the two palmitoyl chains are fully deuterated, with every carbon atom in the hydrocarbon chains labeled with a 'D'.

a) Branching Scheme



b) Parameters

	PAMAM G5	PAMAM G4.5
Chemical Formula	$[\text{NH}_2(\text{CH}_2)_2\text{NH}_2]:(\text{G}=5); \text{dendri}$ $\text{PAMAM}(\text{NH}_2)_{128}$	$[\text{NH}_2(\text{CH}_2)_2\text{NH}_2]:(\text{G}=4.5); \text{dendri}$ $\text{PAMAM}(\text{NHCH}_2\text{CH}_2\text{COONa})_{128}$
Molecular weight	28824.81	26251.86
Outermost generation	Full-generation	Half-generation
Surface branch structure		
Repetitive branch structure		
Core structure		

Figure 5-4 PAMAM dendrimer characteristics. a) Schematic representation of regular branching of PAMAM dendrimers. Number of surface groups/branches (Z) in each generation (G) can be calculated as follows: $Z = 4 \times 2^G$. b) Summary of key parameters of PAMAM dendrimers used in this study, chemical formula and molecular weight as provided by manufacturer.

5.6.2 Supplementary results

5.6.2.1 Monolayer experiments – surface pressure measurements.

Examples of the interaction kinetics of PAMAM dendrimers with DPPG monolayers are shown for the full length of the 60 min observation period in Figure 5-5.

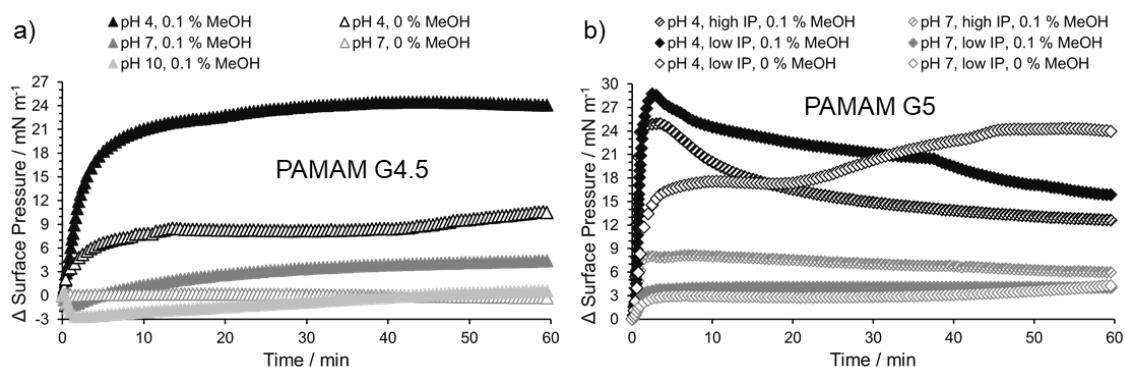


Figure 5-5 Representative profiles of 60 min of surface pressure changes over time under different experimental conditions for interactions of a) PAMAM G4.5 and b) PAMAM G5 with DPPG monolayers. IP stands for initial pressure and reflects the lipid monolayer surface pressure prior to PAMAM addition.

5.6.2.2 Bilayer experiments – neutron reflectometry

Neutron scattering length densities ρ (SLD) were calculated for the individual components of the layers based on atomic neutron scattering lengths and cross sections published by Sears in 1992¹. The SLDs were used to fit neutron reflectometry data to obtain layer hydration levels, thickness and roughness and are shown in Table 5-3. SMW stands for the silicon-matched water contrast.

Whilst the most important fitting results are already summarized in Table 5-1 of the main manuscript, detailed fitted parameters are compiled in Table 5-4 below.

Table 5-3 Neutron scattering length densities (ρ) of the components used to construct the layers for fitting the reflectivity data.

Component	(ρ) / x 10⁻⁶ Å⁻²
Silicon Oxide	3.41
DPPC headgroup	1.98
d-DPPC tail	7.45
h-DPPC tail	-0.37
h-DPPG tail	-0.37
DPPG headgroup in H ₂ O	2.20
DPPG headgroup in D ₂ O	2.54
DPPG headgroup in SMW	2.33
PAMAM G5 in H ₂ O	1.29
PAMAM G5 in D ₂ O	3.13
PAMAM G5 in SMW	1.99
PAMAM G4.5 in H ₂ O	3.12
PAMAM G4.5 in D ₂ O	3.51
PAMAM G4.5 in SMW	3.26
H ₂ O	-0.56
D ₂ O	6.35
SMW	2.07

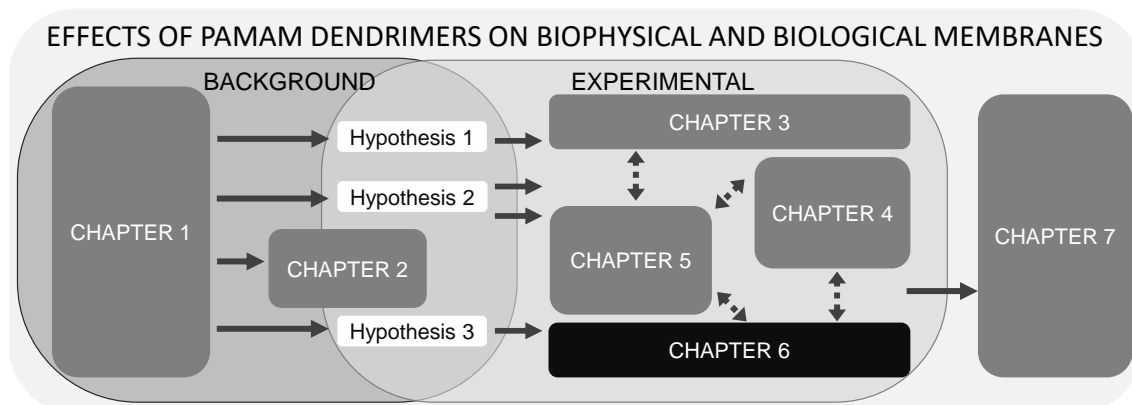
Table 5-4 Parameters derived from fitting incl. Bayesian error analysis. Values in brackets represent the 95 % confidence intervals.

Parameter	G4.5, pH 7, 0.06 mg mL ⁻¹	G4.5, pH 4, 0.06 mg mL ⁻¹	G5, pH 4, 0.06 mg mL ⁻¹	G5, pH 4, 0.3 mg mL ⁻¹
Substrate Roughness (Å)	5.0487 (3.6579, 6.2461)	3.3976 (3.0132, 4.2146)		5.1168 (3.2961, 7.2116)
Silicon Oxide Thickness (Å)	15.049 (13.199, 16.505)	14.338 (13.218, 15.598)		18.136 (15.422, 19.897)
Silicon Oxide Roughness (Å)	3.0911 (1.0966, 5.7346)	2.5634 (1.0576, 5.3799)		3.5829 (1.1368, 5.879)
Silicon Oxide Hydration (%)	14.904 (11.2, 17.963)	15.803 (12.818, 18.51)		3.3053 (0.25811, 6.7506)
DPPC Headgroup Thickness (Å)	8.1217 (7.0481, 10.079)	11.499 (10.48, 12.484)		8.8637 (7.4222, 10.798)
DPPC Headgroup Hydration (%)	31.533 (27.924, 35.069)	38.273 (35.437, 40.962)		37.917 (30.158, 46.439)
Bilayer Roughness (Å)	3.1289 (2.3892, 3.867)	2.6474 (2.0423, 3.4309)		6.3493 (5.6527, 7.0377)
Inner h-Tails Thickness (Å)	14.412 (13.925, 14.883)	16.412 (15.895, 16.861)		12.638 (12.083, 13.368)
Outer d-Tails Thickness (Å)	19.778 (19.256, 19.995)	19.751 (19.226, 19.991)		19.643 (18.839, 19.989)
Pre-PAMAM Tails Hydration (%)	0.79636 (0.042279, 2.0444)	0.32526 (0.010831, 0.98005)		5.4264 (2.1238, 8.8708)
Pre-PAMAM Tails Mix (%)	90.941 (89.131, 92.908)	77.596 (76.463, 78.914)		96.618 (93.972, 98.981)
DPPG Headgroup Thickness (Å)	11.451 (10.769, 12.145)	13.571 (12.919, 14.225)		16.086 (14.286, 17.949)
DPPG Headgroup Hydration (%)	35.877 (35.024, 38.175)	36.33 (35.05, 39.016)		44.197 (35.943, 52.006)
PAMAM in Headgroup (%)	4.817 (2.2449, 7.557)	4.0302 (1.0053, 8.2602)	6.1223 (1.7033, 11.244)	0.018984 (2.3333e ⁻⁰⁴ , 0.13557)
PAMAM Layer Thickness (Å)	29.519 (20.512, 37.054)	13.017 (3.1006, 20.044)	21.527 (4.9422, 32.64)	32.616 (14.335, 43.874)
PAMAM Layer Hydration (%)	89.805 (86.361, 92.612)	85.213 (70.364, 92.309)	87.33 (71.985, 93.721)	91.821 (85.579, 95.084)
PAMAM Layer Roughness (Å)	16.433 (10.45, 19.833)	6.7708 (0.56098, 13.436)	8.7421 (0.57931, 18.604)	12.359 (1.3171, 19.676)
Post-PAMAM Tails Hydration (%)	1.8294 (0.32362, 3.4912)	4.2235 (2.9496, 5.5467)	2.6385 (0.14351, 6.191)	13.237 (9.7726, 16.692)
Post-PAMAM Tails Mix (%)	85.387 (83.771, 87.202)	77.785 (76.593, 79.164)	97.246 (94.658, 99.476)	98.656 (96.101, 99.95)

5.6.3 References supplementary

1. Sears, V. F., Neutron scattering lengths and cross sections. *Neutron News* **1992**, 3 (3), 26-37.

CHAPTER 6: PAMAM DENDRIMERS AFFECT GRAM-POSITIVE BACTERIAL GROWTH



This last experimental chapter translates the findings from the previous biophysical studies into a biological membrane model. Bacteria are known for the high content of anionic lipids, especially PG, and are therefore an ideal model to probe PAMAM dendrimer effect on membrane lipids in a more physiological environment. Whilst the initial screening was performed with PAMAM dendrimers of different sizes, the more in-depth study concentrates on the medium-generation PAMAM G4.5 and G5 which allows direct comparisons to the previous biophysical studies.

The chapter is written in manuscript style for journal submission to match previous chapters.

The estimated contribution of the candidate to the work of this chapter is 95 %.

MW (50 %): Conceptualization, Data curation, Funding acquisition, Investigation, Validation, Formal analysis, Project administration, Visualization, Writing – original draft

GB: Conceptualization, Resources, Supervision, Writing – review & editing

FG: Funding acquisition, Supervision, Writing – review & editing

RJG: Funding acquisition, Supervision, Writing – review & editing

6 PAMAM DENDRIMERS AFFECT GRAM-POSITIVE BACTERIAL GROWTH

Marleen Wilde^a, Glyn Barrett^b, Rebecca J. Green^a, Francesca Greco^a

^aUniversity of Reading, SCFP, Pharmacy

^bUniversity of Reading, School of Biological Sciences

KEYWORDS

Dendrimer, PAMAM, screening, membrane, lipid, bacteria, gram-positive, gram-negative

ACKNOWLEDGEMENTS

The authors thank Marta Favaron (Erasmus student) for pre-liminary work on PAMAMS with bacterial work. We thank Dr Sarah Needs for gifting the ATCC bacterial strains. We also thank Simon Andrews (University of Reading, School of Biology) and Robert Jackson (previously University of Reading, School of Biology) for providing bacterial strains from isolates

ABSTRACT

PAMAM dendrimers were developed as carrier molecules for a wide range of therapeutic applications and were also trialed as adjuvants for antimicrobial agents. Following reports of activity and toxicity of the dendrimers on their own, this study aims to explore effects of full-generation and half-generation PAMAM on variety of bacterial strains, including clinically relevant ones to better understand the mechanism of action for the membrane toxicity.

We screened four different PAMAM (G5, G4.5, G3, G2.5) on 10 gram-negative and 8 gram-positive bacterial strains and found an increased activity against all gram-positive strains whereas only 50 % of the gram-negative strains responded to PAMA treatment. Following this broad screening, we selected PAMAM G5 and G4.5 to investigate active concentrations against selected, clinically relevant strains.

S. saprophyticus was most susceptible to PAMAM G5 with a MIC of 1 $\mu\text{g mL}^{-1}$ and for PAMAM G4.5 with an MIC of 10 $\mu\text{g mL}^{-1}$. MICs for PAMAM G5 were also determined for *S. aureus*, *E. coli* and *P. aeruginosa*. Furthermore, *P. aeruginosa* was most affected during the exponential growth phase, and a concentration-dependent decrease in bacterial generation times was observed.

In general, full-generation PAMAM showed a stronger antibacterial effect than half-generation PAMAM which can likely be attributed to the high cationic surface charge at pH 7 and therefore strong electrostatic interactions with anionic lipids in the bacterial membrane(s). Gram-positive strains were more susceptible to PAMAM treatment than gram-negative ones which could be explained by the higher proportion of anionic lipids (PG, CL) in gram-positive membranes.

6.1 INTRODUCTION

Dendrimers, a class of hyperbranched polymeric molecules, were developed for biomedical applications to improve solubility as well as targeted delivery of a wide range of pharmaceutical products. Poly (amidoamine) (PAMAM) dendrimers are a type of dendrimers which were first described by Tomalia and co-workers in the 1980s¹. The number of terminal surface groups increases exponentially with the generation number and can be functionalised to adjust solubility, miscibility and reactivity². Since then, PAMAM-type dendrimers have been widely researched and modified, and potential applications and functionalities reviewed a number of times (see for instance Shadrack *et al* 2018³, Kharwade *et al* 2020⁴, Dias *et al* 2020⁵).

More recently, PAMAM dendrimers were trialled for antimicrobial applications, either as carriers or conjugates for antibacterial^{6, 7} or antifungal drugs⁸, or modified as scaffolds for new PAMAM-derived active molecules^{9, 10}. However, very few studies focused on the membrane-active effects of native PAMAM dendrimers themselves¹¹. A comprehensive overview on antibacterial studies involving PAMAM and PAMAM-derivatives is provided in Table 6-1.

Whilst many of the studies show the antibacterial activity, the underlying mechanism is researched to a lesser extent. We propose that the antibacterial effect is somewhat related to the composition of bacterial membrane lipids and the ability of PAMAM dendrimers to interact with those. We demonstrated in our previous biophysical studies on membrane models¹², that medium-generation PAMAM G5 and G4.5 preferentially bind to anionic phosphatidylglycerols (PG) lipids, in which bacterial membranes¹³ especially those of gram positive bacteria¹⁴ are particularly enriched. Full-generation dendrimers with high numbers of cationic surface groups (high positive charge density) are known to interact strongly with anionic PG affecting membrane permeability and stability¹⁵ and even can cause hole formation and disruption of neutral zwitterionic membranes^{16, 17}.

Therefore, the overarching aim of this study is twofold: (a) establish to the potential antibacterial activity of native PAMAM dendrimers; and (b) investigate if our previous observations in model membranes explain any differences in antimicrobial behavior observed. Here, we chose to explore the activity of two half-generation

(G2.5, G4.5) and two full-generation (G3, G5) PAMAM of different size on a range of gram-positive and gram-negative bacteria. We also studied the effect of dendrimer concentration on selected bacteria stains using bacterial growth curves (turbidity measurements) and bacterial survival after PAMAM exposure.

Table 6-1 PAMAM-based systems in antibacterial research, mostly with amine-terminated PAMAM (exceptions are outlined in the footnotes). Bacteria used in this work are highlighted in grey.

Bacteria	Strain	PAMAM								undefined
		G1	G2	G3	G4	G5	G6	G7	G8	
<i>Gram-negative</i>										
<i>Acinetobacter baumannii</i>	Clinical						20	21		
	ATCC BAA-1605	18								
	ATCC 17957						20	21		
	LMG 1025		8	8						
	MDR	11	11	11,19	11					
<i>Acinetobacter johnsonii</i>	Undefined									22-24
<i>Aggregatibacter actinomycetemcomitans</i>	ATCC 43717	25								
	Undefined			26						26
<i>Escherichia coli</i>	Clinical						20	21		
	3215					12				
	7835					12				
	ABU 83972					12-14				
	ATCC 8739			30						
	ATCC 11230									31
	ATCC 11775					32				33
	ATCC 25922	11,18,34	8,11	8,11,19,35	11,36,37		20	21		
	ATCC 35218 (ESBL)	11	11	11,19	11					
	K-12 MG1655	11	11	11,19	11					38
	K-12 mutant LPS+									38
XJ74283 + MDR	11	11	11,19	11						

	XL-1					39		
	EHEC0157:H17	11	11	11,19	11			
	Undefined	10	10,40,41	6,42,43	7,9,41,44,45	44		22,23,46-49
<i>Enterobacter (klebsiella) aerogenes</i>	ATCC 13048							31
<i>Enterobacter cloacae</i>	ATCC 700323		8	8				
<i>Klebsiella oxytoca</i>	undefined		41	43	41			
<i>Klebsiella pneumoniae</i>	Clinical						20	21
	ATCC BAA-1706	18						
	ATCC BAA-1705b						20	21
	ATCC 13883	11,18	11	11,19	11			
	ATCC 700603		8	8				
	ESBL-KP XJ752970	11	11	11,19	11			
	UC57							31
<i>Porphyromonas gingivalis</i>	A7436	10						
	Undefined			11				26
<i>Proteus mirabilis</i>	Clinical						20	21
	ATCC 29906						20	21
<i>Proteus vulgaris</i>	ATCC 8427							31
<i>Pseudomonas aeruginosa</i>	Clinical					50	20	21
	ATCC BAA-1744	18						
	ATCC 9027			30				
	ATCC 19143	51	51	51	51			
	ATCC 19660			52		50,52		

	ATCC 27853	11,18,34	8,11	8,11,19	11,36		20	21	31
	PA01				37,53	54			
	PA (2219) Clinic					52			
	Undefined	55,56		55,56	9,44	44			22,24
<i>Salmonella enterica (paratyphi)</i>	ATCC 9150	11	11	11,19	11				
<i>Salmonella enterica (typhimurium)</i>	Clinical						20		
	ATCC 19430						20		
	ATCC 14028			19,57		57			
	MDR	11	11	11,19	11				
<i>Salmonella enterica (typhi)</i>	ATCC 19430						20		
<i>Shigella dysenteriae</i>	Clinical						20	21	
	ATCC 13313						20	21	
	Undefined			43					
<i>Shigella flexneri</i>	MDR	11	11	11,19	11				
<i>Gram-positive</i>									
<i>Actinomyces viscosus</i>	Undefined			26					26
<i>Bacillus cereus</i>	ATCC 7064								31
	ATCC 11778				37				
	Undefined								22-24
<i>Bacillus subtilis</i>	Clinical						20	21	
	ATCC 6633	34		30					
	ATCC 23857						20	21	
	Undefined		41	43	41				22-24

<i>Enterococcus (streptococcus) faecalis</i>	Clinical	8	8			27,29	
	210						
	ATCC 29212	8	8	36			
	Undefined		43				
<i>Lactococcus lactis</i>	MG1363						38
	Mutant VES5748						38
<i>Listeria monocytogenes</i>	ATCC 15313						31
<i>Mycobacterium smegmatis</i>	CCM 2067						31
<i>Sarcina lutea</i>	Undefined						22
<i>Staphylococcus aureus</i>	Clinical	8	8			20	21
	ATCC 4012					58	
	ATCC 6538P			59,60			31
	ATCC 25923	61	61	36,61		20	21
	ATCC 29213	11,51	8,11,51	8,11,35,51,52	11,51,36,37		
	ATCC 33807	34					
	ATCC 700699 (Mu50)	11	11	11	11	50,54	
	DSMZ 3463			30			
	MRSA ATCC 33591	51	51	51	51		
	MRSA ATCC 43300			30			
	MRSA ATCC BAA-1683		61	61	61		
	MRSA WHO-2	11	11	11	11		
	MRSA XJ75302	11	11	11	11		
	Undefined	18,56	40,41	42,43	9,41,44,45,56	44	47
<i>Staphylococcus epidermis</i>	ATCC 12228				36		
	ATCC 14990	11	11	11	11		

<i>Streptococcus gordonii</i>	DL1		62		63
<i>Streptococcus oralis</i>	ATCC 35037			37	
<i>Streptococcus mutans</i>	ATCC 25175	25,64			
	UA159		62		
	Undefined		26		26
<i>Streptococcus sanguinis</i>	ATCC 49297	25			
	SK1		62		

Surface groups other than -NH₂ only: [8] -NH₂, -OH; [30] dendritic hyperbranched PAMAM -ester, -amine; [31] -NH₂, -COOH; [32] -NH₂, -OH, -COOH (G3.5); [36] -NH₂ + -COOH (G4.5) reactant mixture; [38] -COOH; [44] -COOH (G4.5), -TRIS (G4); [47] -COOH (G-0.5, G0.5); [58] -COOH (G3.5); [62] -NH₂, -COOH;

6.2 EXPERIMENTAL

6.2.1 Materials

PAMAM dendrimers G2.5, G3, G4.5 and G5 in methanol solution, DMSO and methanol were sourced from Sigma Aldrich. Brain Heart Infusion (BHI) broth and agar plates were obtained from VWR International Ltd. Luria Bertani (LB) agar and broth and phosphate-buffered saline (PBS) pH 7.4 were provided in-house.

Bacterial strains used in this study are listed in Table 6-2 and were cultured in Luria Bertani⁶⁵ broth, except for *S. pyogenes* that required culture in heart-brain infusion broth.

6.2.2 Methods

PAMAM films were created by removing the methanol solvent under vacuum and rehydrated in growth broth for sample stock solutions (10 mg mL⁻¹). Final sample solutions were adjusted to contain 1 % methanol.

Stock cultures of the bacterial strains were kept at -80 °C in 7 % (v/v) DMSO. Prior to experiments the cultures were streaked onto Luria-Bertani Agar (LA) plates and incubated for a minimum of 18 h at 37 °C, except for the *Bacillus* species and *Arthrobacter* which were cultured at 27 °C. From these LA plates, cells from a single colony were then transferred into 5 mL Luria Bertani (LB) broth and grown overnight in a shaking incubator (150 rpm) at the respective culture temperature.

PAMAMs (1 mg mL⁻¹) with 1 % methanol as co-solvent were screened for their antimicrobial activity against all bacterial strains listed in Table 6-2. PAMAM G5 and G4.5 were assessed via a ten-fold dilution series (0.1, 0.01, 0.001 mg mL⁻¹) for their minimum inhibitory concentration (MIC) on selected bacterial strains (highlighted in Table 6-2).

Table 6-2 Overview of bacterial strains screened in this work. Highlighted strains were further studied for the effect of PAMAM concentration on bacterial survival.

Bacterial strain	Abbreviation	Incubation T / °C	Gram-Stain	Occurrence / General environment
<i>Arthrobacter sp.</i> JS443 NCBI:txid416011	JS443	27	Positive	Soil,
<i>Bacillus Cereus</i> isolate	<i>B. cereus</i>	27	Positive	Soil, food
<i>Bacillus Simplex</i> isolate	<i>B. simplex</i>	27	Positive	Soil, fungi
<i>Bacillus Subtilis</i> isolate QST713	<i>B. subtilis</i>	27	Positive	Soil, GIT of ruminants and humans
<i>Escherichia coli</i> ATCC® 25922™	<i>E. coli</i> 25922	37	Negative	GIT, food pathogen
<i>Escherichia coli</i> EDL933 (O157:H7) / ATCC® 43895™	<i>E. coli</i> EDL933	37	Negative	Food pathogen
<i>Escherichia coli</i> K12	<i>E. coli</i> K12	37	Negative	GIT
<i>Escherichia coli</i> OP50	<i>E. coli</i> OP50	37	Negative	GIT
<i>Klebsiella aerogenes</i> isolate	<i>K. aerogenes</i>	37	Negative	Nosocomial, opportunistic pathogen
<i>Klebsiella pneumoniae</i> <i>subsp. Pneumoniae</i> ATCC® 13883™	<i>K. pneumonia</i>	37	Negative	Nosocomial pathogen
<i>Pseudomonas aeruginosa</i> ATCC® 10145™	<i>P. aeruginosa</i> 10145	37	Negative	Nosocomial, opportunistic pathogen
<i>Pseudomonas aeruginosa</i> GH12	<i>P. aeruginosa</i> GH12	37	Negative	Nosocomial, opportunistic pathogen
<i>Salmonella enterica</i> <i>serovar Gallinarum</i> isolate	<i>S. gallinarum</i>	37	Negative	Poultry pathogen (host-specific)
<i>Salmonella enterica</i> <i>serovar Typhimurium</i> ST1	<i>S. typhimurium</i>	37	Negative	Food pathogen
<i>Staphylococcus aureus</i> <i>subsp. Aureus</i> ATCC® 12600™	<i>S. aureus</i> 12600	37	Positive	Respiratory pathogen
<i>Staphylococcus aureus</i> <i>subsp. Aureus</i> SH1000	<i>S. aureus</i> SH1000	37	Positive	Respiratory pathogen
<i>Staphylococcus saprophyticus</i> <i>subsp. Saprophyticus</i> ATCC® 15305™	<i>S. Saprophyticus</i> 15305	37	positive	Uropathogen
<i>Streptococcus pyogenes</i>	<i>S. pyogenes</i>	37	Positive	Unspecific, human pathogen

GIT: Gastrointestinal tract

For the screening of PAMAMs' effect on bacterial growth, a clear 96-well plate was prepared with 1 mg mL⁻¹ PAMAM (G2.5, G3, G4.5, G5) LB solution (198 µl per well) before 2 µl of the overnight bacterial culture was added to each well with LB alone as a negative control. In a temperature-controlled microplate reader (Tecan Spark), the 96-well plate was agitated for 10 s before the absorbance reading (optical density; OD) at 595 nm. Absorbance was measured every 15 min over 20 h.

For the bacterial survival assay, a 96-well plate was prepared with 198 µl PAMAM-LB solution per well (0.1, 0.01 and 0.001 mg mL⁻¹) and 2 µl of the bacterial culture was transferred into each well. Negative controls were the bacterial strains in pure LB medium and in LB with 1 % methanol co-solvent. Absorbance readings (after 10 s plate agitation) were taken at 595 nm every 15 min over a period of 20 h using a temperature-controlled Tecan plate reader. At 20 h post-incubation, 20 µl from each well was taken and serially diluted in PBS. Aliquots of 10 µl were pipetted onto LA plates and incubated for 18 – 24 h before enumeration of bacterial colony forming units (CFUs).

Data analysis was done using Microsoft Excel (Office 365). Experiments with full-generation PAMAM were repeated at least three times, half-generation PAMAM results derive from a minimum of two valid repeats. Statistical analysis was omitted due to incomplete datasets.

Bacterial colony forming units in the original cultures were calculated using the following equation:

$$CFU = (\text{number of colonies} \times \text{dilution factor}) \div \text{volume of aliquot (ml)}$$

The exponent (growth rate k) of the equation derived from an exponential fit to the bacterial growth curve was used to calculate bacterial generation time g

$$g = \frac{\ln 2}{k}$$

6.3 RESULTS AND DISCUSSION

6.3.1 Screening of bacterial strains

Two full-generation (G3, G5) and two half-generation (G2.5, G4.5) PAMAM were screened for their antibacterial activity on 18 bacterial strains. Absorbance readings (OD) at 20 h of incubation with 1 mg mL⁻¹ dendrimer solutions were normalized against the controls in Luria-Bertani broth and are summarized in a heatmap (Table 6-3). Generally, the antibacterial activity was stronger for the full-generation PAMAM than for the half-generation PAMAM, and growth of gram-positive bacterial strains was more affected than gram-negative strains. For instance, the absorbance of all gram-positive strains was reduced to 70 % or less after the exposure to full-generation PAMAMs, and for five of the 8 strains exposed to G5 the absorbance was < 25 % of that of the control. In comparison, only half of the gram-negative strains were affected by the PAMAM G5 treatment, and the absorbance was reduced to < 70 % for only two strains (*E. coli* 25922, *P. aeruginosa* 10145). Exposure to half-generation PAMAMs resulted in only minor reduction (up to 20 %) of the absorbance, except for *S. aureus* 12600 the absorbance was reduced to 50 – 60 % of the control.

Interestingly, for *Klebsiella aerogenes* and *Salmonella gallinarum*, all PAMAM dendrimers appeared to have a growth-promoting effect over the incubation period monitored. Thus far, there are no literature reports for antibacterial PAMAM activity against those strains available for direct comparison. However, studies on the related *Klebsiella pneumoniae* found significant growth inhibition for low generation PAMAMs (up to G4) at concentrations ranging from 6.25 – 125 µg mL⁻¹ ^{11,19} and 20 mg mL⁻¹ for PAMAM G5⁵⁷. They also screened *Salmonella paratyphi*, for which PAMAM concentrations ≤ 50 µg mL⁻¹ were sufficient to induce an inhibitory effect ^{11,19}. However, the results reported for *Salmonella typhimurium* are inconclusive, with one group reporting MICs from 12.5 – 125 µg mL⁻¹ for PAMAMs up to G4^{11,19,66}, but another group obtaining inhibitory results for G3 and G5 only for high concentrations (20 mg mL⁻¹)⁵⁸.

As there was no distinct difference in the observed results between the low-generation (G2.5, G3) and medium-generation (G4.5, G5) PAMAM, the medium-generation PAMAMs were chosen for further studies on selected strains.

Table 6-3 Antibacterial activity after 20 h incubation with 1 mg mL⁻¹ PAMAM dendrimer solution based on turbidity (OD₅₉₅).

		Half-generation		Full-generation		% of LB control
		G2.5	G4.5	G3	G5	
Gram - positive	<i>S. aureus</i> SH1000	53.4	75.23	9.99	67.85	
	<i>S. aureus</i> ATCC® 12600™	84.85	59.37	16.99	62.51	
	<i>S. saprophyticus</i> ATCC® 15305™	94.31	89.45	0.11	0.24	
	<i>Bacillus subtilis</i> (isolate)	86.85	93.15	7.01	4.44	
	<i>Bacillus cereus</i> (isolate)	95.23	103.93	3.73	21.41	
	<i>Bacillus simplex</i> (isolate)	104.36	101.11	31.33	24.91	
	<i>Arthrobacter</i> JS443	99.63	91.24	16.16	6.24	
	<i>Streptococcus pyrogenes</i>	78.51	84.86	28.12	33.63	
Gram - negative	<i>E. coli</i> EDL933 wt (O157:H7)	92.69	86.76	85.59	103.02	
	<i>E. coli</i> OP50	96.90	89.48	83.12	110.82	
	<i>E. coli</i> K12	92.99	96.69	98.77	88.86	
	<i>E. coli</i> ATCC® 25922™	89.92	88.09	55.00	64.42	
	<i>P. aeruginosa</i> GH12	95.23	93.82	83.71	81.85	
	<i>P. aeruginosa</i> ATCC® 10145™	91.76	88.97	119.22	36.44	
	<i>K. pneumonia</i> ATCC® 13883™	92.76	92.88	114.39	112.00	
	<i>K. aerogenes</i> (isolate)	106.52	106.60	127.91	133.16	
	<i>S. galinarum</i> (isolate)	135.09	133.24	136.49	122.47	
	<i>S. typhimurium</i> (isolate)	99.86	86.59	90.56	93.88	

6.3.2 Effect of PAMAM G5 on bacterial generation time

Generation time, also known as doubling time, is the time required for the binary fission of the bacterium and is usually determined during the log phase, where the bacterial culture grows at a constant and exponential rate. Overall, the antibacterial effects observed in this study were most pronounced for PAMAM G5, therefore only strains treated with the full-generation dendrimer were analyzed for their generation time.

The growth curves of all bacterial strains, except *P. aeruginosa* ATCC 10145, showed a lag phase, one constant log phase and a stationary phase. Bacterial generation times derived from an exponential fit of log phase are summarized in Table 6-4. *S. saprophyticus* growth was significantly slowed down by PAMAM G5 treatment, and a clear concentration-dependence was shown with doubling up of the generation time values at the highest PAMAM concentration compared to the control (168.2 min for 0.1 mg mL⁻¹, 83.7 min for control). In

general, the generation times observed in this study were in line with the range of values reported in literature for untreated bacteria⁶⁷, and for most strains there was no or only a mild PAMAM effect.

Table 6-4 Bacterial generation time for selected gram-positive and gram-negative bacterial strains affected by incubation with various concentrations of PAMAM G5.

Strain	Bacterial Generation Time (min)				
	PAMAM G5	0.1 mg mL ⁻¹	0.01 mg mL ⁻¹	0.001 mg mL ⁻¹	0 mg mL ⁻¹ (1 % MeOH)
<i>S. aureus</i> SH1000		50.7	43.8	50.4	48.1
<i>S. aureus</i> ATCC 12600		48.8	43.7	44.3	43.1
<i>S. saprophyticus</i> ATCC 15305		168.2	140.3	71.5	83.7
<i>E. coli</i> ATCC 25922		26.4	29.4	32.4	31.2
<i>K. pneumonia</i> ATCC 13883		25.4	23.6	26.5	26.1

Analysis of the growth curves of *P. aeruginosa* revealed a multi-step log phase (shown in Figure 6-1a), which is similar to reports on other untreated *Pseudomonas spp.*^{68,69}. Therefore, the log phase was divided in multiple sections, for which the individual generation time was determined. Increasing concentrations of PAMAM G5 resulted in faster generation times and at the highest concentration of 0.1 mg mL⁻¹ four different log growth sections could be identified and analyzed. The multiple steps suggest an adaptation mechanism to the surrounding conditions, i.e. availability of nutrients. The slower growth rates (sections II and IV) could indicate increased cell death, followed by autolysis and release of fresh nutrients which then triggered the following faster growth rate.

P. aeruginosa was also the only strain, for which a decline phase (starting after the peak in turbidity) was observed. The decline phase suggests cell death, which could be due to exhaustion of nutrients but also accumulation of toxic products potentially caused through the initially enhanced growth rate.

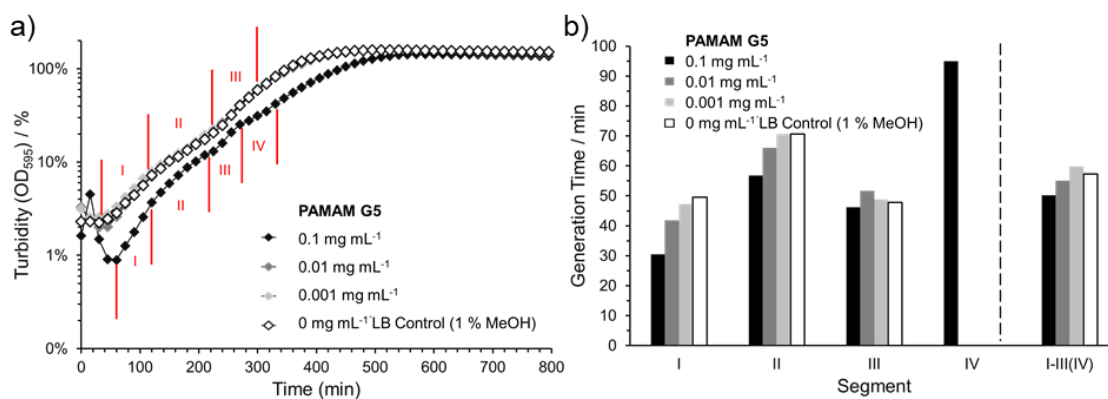


Figure 6-1 Effect of PAMAM G5 on the growth profile and generation time of *P. aeruginosa* ATCC 10145. Bacterial solutions were incubated for 20 h with PAMAM G5 and turbidity (optical density, OD) was measured every 15 min. The resulting growth profiles (panel a) were analyzed with an exponential fit which was used to calculate the generation times in panel b. As shown in panel a, the multiple phases for each growth curve were analyzed individually in segments and over the whole period of 255 min (I-III(IV)).

6.3.3 PAMAM effect on turbidity and bacterial survival

As shown in Table 6-3, the antibacterial effect was most pronounced for gram-positive strains. From the strains screened, the *Staphylococci* were the most clinically relevant ones and were therefore selected for PAMAM G5 and G4.5 MIC determination. Bacterial growth kinetics (absorbance) under PAMAM incubation was monitored in 15 min intervals over a period of 20 h. The OD₅₉₅ values at 20 h were normalized against the LB control which contained 1 % methanol as a co-solvent to account for the residual methanol in the diluted PAMAM samples. Where inhibition was observed in the complete growth kinetic profiles, the bacterial solution was diluted and plated onto solid media for enumeration of colony forming units. The CFUs were used to evaluate how many bacteria remained viable following PAMAM incubation, as the OD measurement cannot quantify dead (intact) and alive bacteria.

6.3.3.1 Gram-positive strains

The concentration effect of PAMAM G4.5 and G5 on the absorbance of gram-positive *Staphylococcus* strains is summarized in Figure 6-2. For the full-generation PAMAM, the most susceptible strain was *S. saprophyticus*. The inhibitory effect of G5 was shown for a concentration as low as 10 $\mu\text{g mL}^{-1}$,

which is comparable to the MIC₅₀ of Norfloxacin (4 µg mL⁻¹), a fluoroquinolone antibiotic tested on *S. saprophyticus* biofilms⁷⁰. The least effect was observed for *S. aureus* ATCC 12600. Overall, G4.5 had less pronounced effects on bacterial absorbance compared to PAMAM G5, but still showed some inhibitory effects on *S. aureus* SH1000.

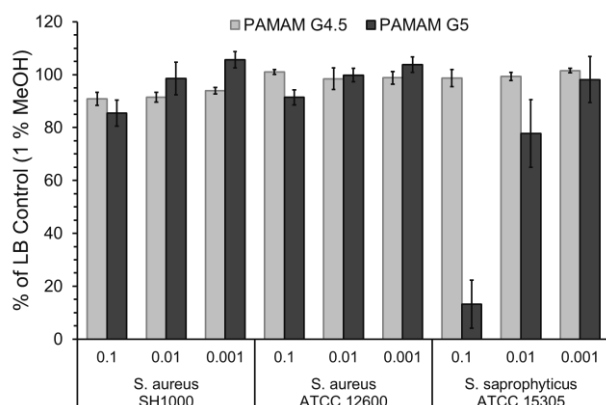


Figure 6-2 Concentration effect of full-generation PAMAM G5 and half-generation PAMAM G4.5 on gram-positive *Staphylococcus* strains after 20 h of incubation. Data derive from the OD values at timepoint 20 h and are normalized to the LB control with 1 % methanol as co-solvent. Values shown reflect mean \pm standard error of the mean (SEM).

For *S. saprophyticus* the results are summarized in Fig. 6-3 with panel a) showing the absolute numbers of colony forming units (CFU) per mL and panel b) the normalized % CFU to the PAMAM-free control. At the highest concentration tested (0.1 mg mL⁻¹), exposure to PAMAM G5 resulted in a reduction of 3 log₁₀ (10¹⁰ to 10⁷) in CFU. A decrease in this range can be considered a significant bactericidal effect⁷¹. However, even the lowest concentrations led to a decrease of the CFU mL⁻¹ which matches the trend observed for the turbidity. The MIC₅₀ for PAMAM G5 was determined to be < 0.01 mg mL⁻¹ and the minimum bactericidal concentration (MBC) 0.1 mg mL⁻¹.

Whilst the impact on the growth kinetics (turbidity) was less pronounced for PAMAM G4.5, CFU counts revealed a significant effect of PAMAM G4.5 at a concentration of 0.01 mg mL⁻¹, which related to a decrease of ~30 % in relation to the LB control (1 % MeOH). Interestingly, the higher concentration of 0.1 mg mL⁻¹ appeared to have no inhibitory effect.

S. aureus SH1000 was little affected by PAMAM treatment besides showing a concentration-dependent decrease in turbidity. CFU counts revealed no antibacterial effect on the survival / recovery of SH1000 after 20 h of exposure to PAMAM for neither G5 nor G4.5 and CFU counts were comparable to the control.

S. aureus 12600 was not affected by PAMAM G4.5 incubation but a MIC of 0.1 mg mL⁻¹ was determined for PAMAM G5 which resulted in 36.7 ± 0.6 % less CFUs compared to the LB control.

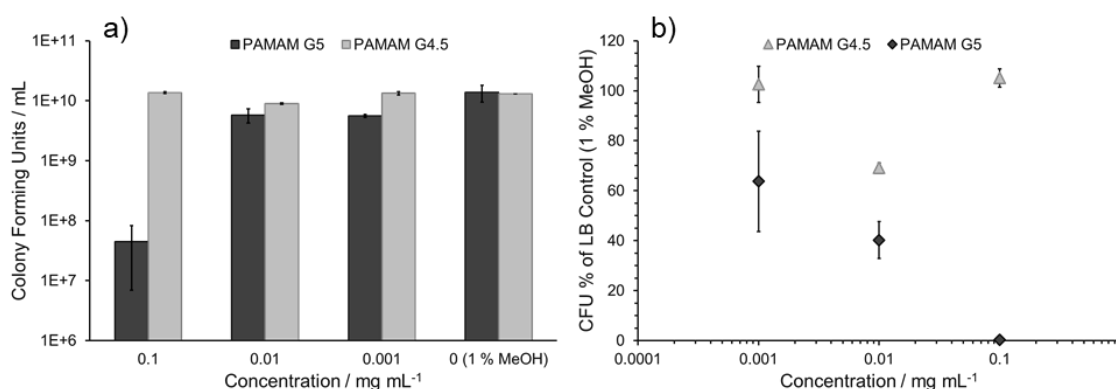


Figure 6-3 Effect of PAMAM dendrimers on the survival of *S. saprophyticus* after 20 h of incubation. Aliquots were incubated on LA plates for a minimum of 24 h before enumeration. Panel a) reflects the number of colony forming units (CFU) per 1 mL, the PAMAM-free control contained 1 % methanol. In panel, the absolute numbers of CFU / mL were normalized against the LB control (1 % methanol). For both panels, data reflect $M \pm SEM$, $n \geq 2$.

6.3.3.2 Gram-negative strains

Whilst the screening revealed less activity against gram-negative strains overall, a number of those strains are pathogens typically found in hospital settings and therefore interesting models for understanding the antibacterial effect of PAMAM. Overall, neither of the PAMAM species showed a clear trend in terms of growth inhibition or promotion across the strains screened. For further concentration-dependent investigation, *E. Coli* ATCC 26922, *P. aeruginosa* ATCC 10145 and *K. pneumonia* ATCC 13883 were chosen.

Considering the endpoint of turbidity growth kinetics after 20 h of incubation (shown in Figure 6-4), the most susceptible strain towards both PAMAM

dendrimers was *P. aeruginosa*. PAMAM G5 at 0.1 mg mL⁻¹ also inhibited *E. coli* growth, which was not affected by PAMAM G4.5. Interestingly, the half-generation PAMAM appeared to be more effective than G5 against *K. pneumonia*, albeit distinctive reduction in turbidity was only observed for 0.1 mg mL⁻¹.

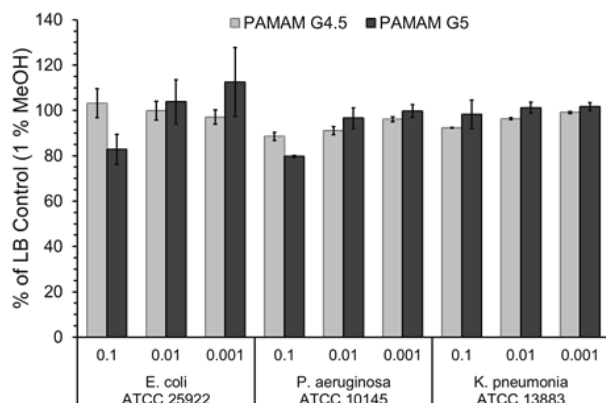


Figure 6-4 Concentration effect of full-generation PAMAM G5 and half-generation PAMAM G4.5 on common hospital pathogen strains after 20 h of incubation. Data derived from the OD values at timepoint 20 h and are normalized to the LB control with 1 % methanol as co-solvent. Values shown reflect mean \pm standard error of the mean (SEM).

A clearer picture emerged when CFUs after the 20 h PAMAM incubation were determined. PAMAM G4.5 showed no antibacterial effect on any of the gram-negative strains. Treatment with PAMAM G5 resulted in a concentration-dependent reduction of bacterial survival of *E. coli* and *P. aeruginosa*, which is illustrated in Figure 6-5. The strongest inhibition of 54 ± 8.5 % was observed for *P. aeruginosa* (MIC 0.01 mg mL⁻¹), but also *E. coli* survival was lowered by 33.3 ± 6.8 % (MIC 0.1 mg mL⁻¹).

Interestingly, both PAMAM species were observed to promote the growth of *K. pneumonia* (data not shown). The effect was more pronounced for G5 as well as with decreasing dendrimer concentration, with up to 85 % more CFUs compared to the LB control. It is possible that the medium – generation PAMAMs serve as nitrogen (N) substrate for the bacteria when degraded, which could lead to the increased growth activity seen in this study. The ability to utilize particular N sources as growth substrate depends on biochemical capacities; and the *Enterobacteriaceae* (the family *Klebsiella spp.* belong to)

were one of the families most commonly isolated from complex N-enrichments⁷². However, our results are not in line with observations reported in the literature, where smaller cationic PAMAM (up to G4) are reported to have a bactericidal effect on *K. pneumonia*¹¹.

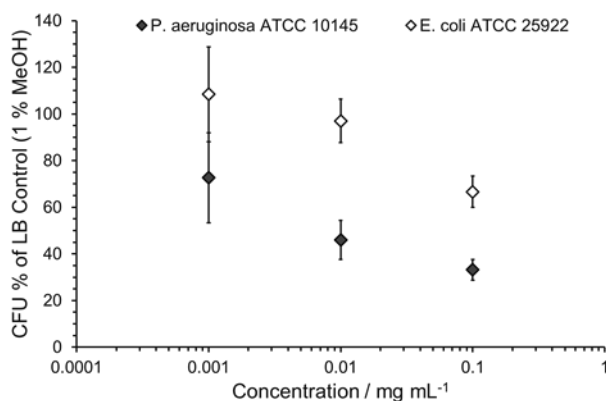


Figure 6-5 Effect of 20 h incubation with PAMAM G5 on the survival of *P. aeruginosa* ATCC 10145 and *E. coli* ATCC 25922. Colony-forming units (CFU) derived from the PAMAM-treated test solutions were normalized against the bacterial CFU of the PAMAM-free LB control (containing 1 % methanol). Data are shown as mean \pm SEM, $n \geq 4$.

6.3.4 Linking PAMAM effect to membrane lipid composition

The difference between gram-negative and gram-positive bacteria largely depends on the morphology and constituents of their cell envelopes^{73,74}. Specifically, gram-positive bacteria are surrounded by a cytoplasmic cell membrane and a thick peptidoglycan cell wall (20 – 80 nm). In comparison, gram-negative bacteria have a much thinner peptidoglycan layer (2-3 nm)⁷⁵ and an additional outer membrane containing lipopolysaccharide (LPS) as gram-negative specific lipid in the outer monolayer⁷⁶. Major bacterial lipids are the anionic phosphatidylglycerols (PG) and cardiolipin (CL), and the zwitterionic phosphatidylethanolamine (PE)¹³, however the proportion of those lipids is substantially different in gram-negative and gram-positive species as illustrated in Table 6-5 on selected species. In some strains, i.e. *S. aureus*, anionic phospholipids contribute up to 100 % of the net charge of the bacterial membrane. Substantial amounts of glycosyl diglycerides in addition to numerous other minor lipids were also found in some bacteria⁷⁷.

Phosphatidylcholines (PC) are zwitterionic major eukaryotic membrane lipids that occur rarely in bacterial membranes⁷⁸.

Table 6-5 Membrane lipid composition (%) of selected bacteria relevant to this study.

Bacterial Strain	PE	PG	CL	PS	PA	PC	Glycolipids	other
<i>E. coli</i> K-12 W3101 ⁷⁹	69	19	6.5					6
<i>E. coli</i> K12wt ⁸⁰	72-81	15-21	2-7					
<i>P. aeruginosa</i> POA ⁸¹	59.9	21.3	10.6					
<i>P. aeruginosa</i> ⁷⁸	73.2	11.8			0.8	11.8		
<i>P. aeruginosa</i> ⁸²	x	x	x					
<i>S. typhimurium</i> LT-2 wt ⁷⁹	75-78	18	3.2 - 4.5	0.2	0.2			0.7- 2.9
<i>S. typhimurium</i> ATCC 7136 ⁸³	72	8		6				14
<i>S. typhimurium</i> dam and/or seqA mutants ⁸⁴	75.2	19.4	5.3					
<i>S. aureus</i> ATCC 6538P ⁸⁵		66.6	30				3.4	
<i>S. aureus</i> Newman ⁸⁶		73.2	22.5		0.5			3.8
<i>S. aureus</i> Tazaki ⁸⁶		78.2	17.6		1.2			3.0
<i>S. aureus</i> U71 ⁸⁷		54- 95.4	15.3- 34.5					
<i>S. pyogenes</i> ⁸⁸ HSC5 ⁸⁹		x	x				x	

PE- phosphatidylethanolamine, PG- phosphatidylglycerol, CL – cardiolipin, PS phosphatidylserine, PA-phosphatidic acid, PC-phosphatidylcholine, x – no exact proportions provided

To date, the number of studies investigating antimicrobial efficacy of PAMAM dendrimers and underlying mechanism(s) is still limited albeit the binding preference of PAMAMs to anionic, bacterial phospholipids such phosphatidylglycerol has been established in biophysical⁹⁰ or simulation studies^{12,21}. Bacterial lipid composition was also shown as a modulator of antibacterial efficacy for a range of other molecules, i.e. antimicrobial peptides^{92,93}, ceragenin steroids⁹⁴, polymers⁹⁵.

Table 6-6 provides an overview of the few studies in which native PAMAM dendrimers (without modification or combinations with other molecules) were assessed for antimicrobial activity (MIC, MBC). The results of this study are included for comparison and highlighted in color. To date, most groups have used the more flexible small-generation PAMAMs^{1,19,52,58,96}, and only two groups trialed the efficacy of the more rigid, high-generation PAMAM^{20,21}. Interestingly, only Holmes *et al*⁹⁶ included a half-generation PAMAM G3.5 in

their study, which was shown to have a $MIC_{50} > 1000 \mu\text{g mL}^{-1}$ for *E. coli* ATCC 8739. The inhibitory effect was only observed at a comparably high MIC_{50} , which could explain why most groups focus on the more active full-generation PAMAMs that exhibit high cationic surface charges. In fact, our screening studies with PAMAM G2.5 and G4.5 (1 mg mL^{-1}) showed that the antibacterial effect, when observed, was much less than that of their full-generation counterparts. Significant inhibition at lower concentrations was only seen on gram-positive *S. Saprophyticus* after exposure to G4.5 ($MIC_{50} 10 \mu\text{g mL}^{-1}$).

Numerous antimicrobial molecules (i.e. antimicrobial peptides^{93,97}, (co)polymers^{98,99}, surfactants^{100,101}) are polycationic and membrane domains rich in anionic cardiolipin^{102,108} might provide a target for charge interactions affecting the membrane integrity. Possible membrane impacts include hydrophobic mismatch effects, chain stretching of the lipids close to the site of interaction, induced spontaneous membrane curvature and changes in lipid packaging¹⁰⁴. Furthermore, the polycationic molecules likely promote phase separation between anionic and zwitterionic lipids^{13,105}, which could be driven by simultaneous interaction with multiple anionic lipid headgroups and could result in membrane defects. Additional cation-structure related factors, such as ability for conformational adaption or hydrophobicity levels sufficient for membrane partitioning are supporting the antimicrobial efficacy of those molecules¹⁰². Full-generation PAMAM dendrimers of medium size, such as the G5 used in this study, have aforementioned properties and are therefore suitable molecules to study antibacterial activity and underlying modes of action.

We propose that antibacterial activity of PAMAM dendrimers is related to membrane lipid binding, but there are other potential ways the dendrimers could interact with bacterial cells and exhibit toxicity, i.e. binding to non-lipid membrane constituents^{38,63} or intracellular targets⁵³. However, as bacterial membrane lipids are the first point of contact for the dendrimers before being able to access internal targets, interaction with the lipids and resulting effects on membrane integrity and lipid arrangements can be assumed the first mode of action. The high content of anionic lipids provides electrostatic attraction to the

cationic surface groups of the full-generation PAMAM and further hydrophobic interactions with the core and lipid tails might aid the intercalation into the lipid bilayer, where the dendrimers can cause further damage. Considering the gram-negative and gram-positive lipid compositions in Table 6-5 and the higher anionic lipid proportion, this could explain the more pronounced antibacterial PAMAM G5 effects observed for the gram-positive *Staphylococcus* strains compared to the gram-negative strains. Unfortunately, no lipidomics analysis was available in the literature for *S. saprophyticus* and therefore we are unable to explain the stronger PAMAM susceptibility for this strain compared to the other gram-positive *S. aureus* strains, but it is noteworthy that also the half-generation PAMAM G4.5 with deprotonated carboxyl surface groups was able to cause an inhibitory effect.

Table 6-6 Literature-reported PAMAM effect on survival of gram-positive and gram-negative bacteria. Data with grey background derive from this study and are included for comparison. Concentrations are provided in $\mu\text{g mL}^{-1}$.

Bacteria	Strain	G1	G2	G3	G3.5	G4	G4.5	G5	G6	G7
Gram-negative										
<i>Acinetobacter baumannii</i>	Clinical								MIC 25.0; MBC 200.0 ²⁰	MIC 4.0; MBC 128.0 ²¹
	ATCC 17957								MIC 2.5; MBC 200.0 ²⁰	MIC 4.0; MBC 128.0 ²¹
	MDR	MIC >100 ¹¹	MIC 25 ¹¹	MIC 25 ^{11,19}		MIC 50 ¹¹				
<i>Escherichia coli</i>	Clinical								MIC 25.0; MBC 200.0 ²⁰	MIC 4.0; MBC 128.0 ²¹
	ATCC 25922	MIC 50 ¹¹	MIC 6.25 ¹¹	MIC 12.5 ^{11,19}		MIC 12.5 ¹¹	No MIC	MIC 100	MIC 2.5; MBC 100 ²⁰	MIC 4.0; MBC 128.0 ²¹
	ATCC 35218 (ESBL)	MIC 50 ¹¹	MIC 6.25 ¹¹	MIC 12.5 ¹¹ ; MIC 15.6 ¹⁹		MIC 12.5 ¹¹				
	K-12 MG 1655	MIC >100 ¹¹	MIC 6.25 ¹¹	MIC 12.5 ^{11,19}		MIC 12.5 ¹¹				
	MDR XJ74283 (clinical isolate)	MIC >100 ¹¹	MIC 12.5 ¹¹	MIC 50 ¹¹ ; MIC 15.6 ¹⁹		MIC >100 ¹¹				
	EHEC O157:H7	MIC 50 ¹¹	MIC 6.25 ¹¹	MIC 12.5 ^{11,19} ; MIC 5000; MBC > 20000 ⁵⁷		MIC 12.5 ¹¹		MIC 20000; MBC >20000 ⁵⁷		
	ATCC 8739									
ATCC 8277				MIC ₅₀ 4.9 ⁹⁶	MIC ₅₀ >1000 ⁹⁶					
ATCC 11775					MIC ₅₀ 22000 ³²	MIC ₅₀ 3.8 ³²				

<i>Klebsiella pneumoniae</i>	Clinical							MIC 0.25 MBC 100.0 ²⁰	MIC 4.0; MBC 128.0 ²¹
	ATCC 49131							MIC 0.25 MBC 100.0 ²⁰	MIC 2.0; MBC 128.0 ²¹
	ATCC 13883 ESBL-KP XJ752970 (clinical isolate) ATCC 10031	MIC 50 ¹¹ MIC >100 ¹¹	MIC 6.25 ¹¹ MIC 100 ¹¹	MIC 12.5 ^{11,19} MIC >100 ¹¹ ; MIC 125 ¹⁹		MIC 12.5 ¹¹ MIC >100 ¹¹	No MIC	No MIC	
			MIC 20000; MBC > 20000 ⁵⁷				MIC 20000; MBC > 20000 ⁵⁷		
<i>Proteus mirabilis</i>	Clinical							MIC 2.5; MBC 100.0 ²⁰	MIC 1.0; MBC 64.0 ²¹
	ATCC 29906							MIC 2.5; MBC 100.0 ²⁰	MIC 2.0; MBC 64.0 ²¹
<i>Pseudomonas aeruginosa</i>	Clinical							MIC 2.5; MBC 100.0 ²⁰	MIC 4.0; MBC 128.0 ²¹
	ATCC 27853	MIC 50 ¹¹	MIC 6.25 ¹¹	MIC 12.5 ^{11,19}		MIC 12.5 ¹¹		MIC 2.5; MBC 100.0 ²⁰	MIC 4.0; MBC 128.0 ²¹
	ATCC 19660			MIC 6.3 ⁵²				MIC 12.5 ⁵² MIC ₅₀ 1.550	
	ATCC 9027			MIC 20000; MBC > 20000 ⁵⁷				MIC 20000; MBC > 20000 ⁵⁷	
	ATCC 10145						No MIC	MIC 10.0	
<i>Salmonella enterica (paratyphi)</i>	ATCC 9150	MIC 50 ¹¹	MIC 3.12 ¹¹	MIC 12.5 ^{11,19}		MIC 12.5 ¹¹			

<i>Salmonella enterica</i> (<i>typhimurium</i>)	Clinical						MIC 0.25; MBC 25.0 ²⁰		
	ATCC 19430						MIC 0.025; MBC 2.5 ²⁰		
	MDR	MIC >100 ¹¹	MIC 100 ¹¹	MIC 100 ¹¹ ; MIC 125 ¹⁹		MIC 100 ¹¹			
	ATCC 14028			MIC 20000; MBC > 20000 ⁵⁷ MIC 12.5 ¹⁹			MIC 20000; MBC >20000 ⁵⁷		
<i>Shigella dysenteriae</i>	Clinical						MIC 0.25; MBC 50.0 ²⁰	MIC 1.0; MBC 64.0 ²¹	
	ATCC 13313						MIC 0.25; MBC 50.0 ²⁰	MIC 2.0; MBC 64.0 ²¹	
<i>Shigella flexneri</i>	MDR	MIC 50 ¹¹	MIC 6.25 ¹¹	6.25 ^{11,19}		MIC 12.5 ¹¹			
Gram- positive									
<i>Bacillus subtilis</i>	Clinical						MIC 0.25; MBC 50.0 ²⁰	MIC 2.0; MBC 64.0 ²¹	
	ATCC 23857						MIC 0.25; MBC 50.0 ²⁰	MIC 2.0; MBC 64.0 ²¹	

<i>Staphylococcus aureus</i>	Clinical							MIC 0.25; MBC 100.0 ²⁰	MIC 4.0; MBC 128.0 ²¹
	ATCC 25923							MIC 0.25; MBC 100.0 ²⁰	MIC 4.0; MBC 128.0 ²¹
	ATCC 29213	MIC 50 ¹¹	MIC 6.25 ¹¹	MIC 6.25 ¹¹ ; MIC 6.3 ⁵²		MIC 6.25 ¹¹		MIC 12.5 ⁵² ; MIC ₅₀ 20.8 ⁵⁰	
	VIR SA Mu50	MIC 50 ¹¹	MIC 6.25 ¹¹	MIC 6.25 ¹¹		MIC 12.5 ¹¹			
	MRSA WHO-2	MIC 50 ¹¹	MIC 3.12 ¹¹	MIC 6.25 ¹¹		MIC 6.25 ¹¹			
	MRSA XJ75302 (clinical isolate)	MIC 50 ¹¹	MIC 6.25 ¹¹	MIC 6.25 ¹¹		MIC 6.25 ¹¹			
	ATCC 6538			MIC 1250; MBC > 20000 ⁵⁷				MIC 2500; MBC > 20000 ⁵⁷	
	MRSA ATCC 33591			MIC 2500; MBC > 20000 ⁵⁷				MIC 2500; MBC > 20000 ⁵⁷	
ATCC 11832 ATCC 12600		MIC ₅₀ 26.7 ⁹⁶	MIC ₅₀ 9.4 ⁹⁶	MIC > 250 ⁹⁶	MIC ₅₀ 6.0 ⁹⁶	No MIC	MIC ₅₀ 2.9 ⁹⁶ MIC 100.0		
<i>Staphylococcus epidermis</i>	ATCC 14990	MIC 25 ¹¹	MIC 0.78 ¹¹	MIC 1.56 ¹¹				MIC 3.12 ¹¹	
<i>Staphylococcus saprophyticus</i>	ATCC 15305						MIC 10.0	MIC 1.0 MBC 100.0	

6.3.5 Conclusion

Microbiology methods are an important tool in biomedical research, especially when investigating infectious diseases or the activity of new antimicrobial drugs. Bacteria, fungi, and yeasts are common target organisms that are generally more robust and easier to culture than eukaryotic cell lines, and are, in combination with lipidomics, useful models for studying molecule - membrane interactions.

Here, a range of PAMAM dendrimer species were studied for their antibacterial efficacy on several gram-negative and gram-positive bacterial strains. For all susceptible strains, the full-generation PAMAMs (G3, G5) with cationic surface groups were more active than the half-generation counterparts (G2.5, G4.5) with anionic surface moieties.

Both, PAMAM G4.5 and G5 had an inhibitory effect *S. saprophyticus* and MICs could be determined for both dendrimer species. MICs were also obtained for *S. aureus* ATCC12600, *E. coli* ATCC 25922 and *P. aeruginosa* ATCC 10145, but only for PAMAM G5.

In general, all three gram-negative strains were less impacted in their growth kinetics than the three gram-positive strains, which could be attributed to the higher anionic lipid content of the gram-positive cell envelop and resulting stronger electrostatic interactions between cationic PAMAM surface groups and anionic lipid heads.

6.4 REFERENCES

1. Tomalia, D. A.; Baker, H.; Dewald, J.; Hall, M.; Kallos, G.; Martin, S.; Roeck, J.; Ryder, J.; Smith, P., A new class of polymers - Starburst-dendritic macromolecules. *Polym. J.* **1985**, *17* (1), 117-132.
2. Fréchet, J. M., Functional polymers and dendrimers: reactivity, molecular architecture, and interfacial energy. *Science* **1994**, *263* (5154), 1710-5.
3. Shadrack, D. M.; Swai, H. S.; Munissi, J. J. E.; Mubofu, E. B.; Nyandoro, S. S., Polyamidoamine Dendrimers for Enhanced Solubility of Small Molecules and Other

Desirable Properties for Site Specific Delivery: Insights from Experimental and Computational Studies. *Molecules* **2018**, *23* (6), 1419.

4. Kharwade, R.; More, S.; Warokar, A.; Agrawal, P.; Mahajan, N., Starburst pamam dendrimers: Synthetic approaches, surface modifications, and biomedical applications. *Arabian Journal of Chemistry* **2020**, *13* (7), 6009-6039.
5. Dias, A. P.; da Silva Santos, S.; da Silva, J. V.; Parise-Filho, R.; Igne Ferreira, E.; Seoud, O. E.; Giarolla, J., Dendrimers in the context of nanomedicine. *International journal of pharmaceutics* **2020**, *573*, 118814.
6. Ma, M.; Cheng, Y.; Xu, Z.; Xu, P.; Qu, H.; Fang, Y.; Xu, T.; Wen, L., Evaluation of polyamidoamine (PAMAM) dendrimers as drug carriers of anti-bacterial drugs using sulfamethoxazole (SMZ) as a model drug. *European journal of medicinal chemistry* **2007**, *42* (1), 93-8.
7. Cheng, Y.; Qu, H.; Ma, M.; Xu, Z.; Xu, P.; Fang, Y.; Xu, T., Polyamidoamine (PAMAM) dendrimers as biocompatible carriers of quinolone antimicrobials: an in vitro study. *European journal of medicinal chemistry* **2007**, *42* (7), 1032-8.
8. Winnicka, K.; Wroblewska, M.; Wieczorek, P.; Sacha, P. T.; Trynieszewska, E. A., The effect of PAMAM dendrimers on the antibacterial activity of antibiotics with different water solubility. *Molecules* **2013**, *18* (7), 8607-17.
9. Neelgund, G. M.; Oki, A.; Luo, Z., Antimicrobial activity of CdS and Ag₂S quantum dots immobilized on poly(amidoamine) grafted carbon nanotubes. *Colloids and surfaces. B, Biointerfaces* **2012**, *100*, 215-21.
10. Wen, Y.; Yao, F.; Sun, F.; Tan, Z.; Tian, L.; Xie, L.; Song, Q., Antibacterial action mode of quaternized carboxymethyl chitosan/poly(amidoamine) dendrimer core-shell nanoparticles against Escherichia coli correlated with molecular chain conformation. *Mater Sci Eng C Mater Biol Appl* **2015**, *48*, 220-7.
11. Xue, X.; Chen, X.; Mao, X.; Hou, Z.; Zhou, Y.; Bai, H.; Meng, J.; Da, F.; Sang, G.; Wang, Y.; Luo, X., Amino-terminated generation 2 poly(amidoamine) dendrimer as a potential broad-spectrum, nonresistance-inducing antibacterial agent. *AAPS J* **2013**, *15* (1), 132-42.
12. Wilde, M.; Green, R. J.; Sanders, M. R.; Greco, F., Biophysical studies in polymer therapeutics: the interactions of anionic and cationic PAMAM dendrimers with lipid monolayers. *Journal of drug targeting* **2017**, *25* (9-10), 910-918.
13. Epand, R. M.; Epand, R. F., Bacterial membrane lipids in the action of antimicrobial agents. *Journal of Peptide Science* **2011**, *17* (5), 298-305.
14. Cronan, J. E., Bacterial membrane lipids: where do we stand? *Annual review of microbiology* **2003**, *57*, 203-24.
15. Chen, C. Z.; Cooper, S. L., Interactions between dendrimer biocides and bacterial membranes. *Biomaterials* **2002**, *23* (16), 3359-3368.

16. Mecke, A.; Majoros, I. J.; Patri, A. K.; Baker, J. R.; Holl, M. M.; Orr, B. G., Lipid bilayer disruption by polycationic polymers: the roles of size and chemical functional group. *Langmuir : the ACS journal of surfaces and colloids* **2005**, *21* (23), 10348-54.
17. Mecke, A.; Uppuluri, S.; Sassanella, T. M.; Lee, D. K.; Ramamoorthy, A.; Baker, J. R., Jr.; Orr, B. G.; Banaszak Holl, M. M., Direct observation of lipid bilayer disruption by poly(amidoamine) dendrimers. *Chemistry and physics of lipids* **2004**, *132* (1), 3-14.
18. Ngu-Schwemlein, M.; Chin, S. F.; Hileman, R.; Drozdowski, C.; Upchurch, C.; Hargrove, A., Carbon nanodots as molecular scaffolds for development of antimicrobial agents. *Bioorg Med Chem Lett* **2016**, *26* (7), 1745-9.
19. Xue, X. Y.; Mao, X. G.; Li, Z.; Chen, Z.; Zhou, Y.; Hou, Z.; Li, M. K.; Meng, J. R.; Luo, X. X., A potent and selective antimicrobial poly(amidoamine) dendrimer conjugate with LED209 targeting QseC receptor to inhibit the virulence genes of gram negative bacteria. *Nanomedicine : nanotechnology, biology, and medicine* **2015**, *11* (2), 329-39.
20. Rastegar, A.; Nazari, S.; Allahabadi, A.; Falanji, F.; Akbari Dourbash, F. A. D.; Rezai, Z.; Alizadeh Matboo, S.; Hekmat-Shoar, R.; Mohseni, S. M.; Majidi, G., Antibacterial activity of amino- and amido- terminated poly (amidoamine)-G6 dendrimer on isolated bacteria from clinical specimens and standard strains. *Med J Islam Repub Iran* **2017**, *31*, 64.
21. Gholami, M.; Mohammadi, R.; Arzanlou, M.; Akbari Dourbash, F.; Kouhsari, E.; Majidi, G.; Mohseni, S. M.; Nazari, S., In vitro antibacterial activity of poly (amidoamine)-G7 dendrimer. *BMC Infect Dis* **2017**, *17* (1), 395.
22. Grabchev, I.; Vasileva-Tonkova, E.; Staneva, D.; Bosch, P.; Kukeva, R.; Stoyanova, R., Impact of Cu(II) and Zn(II) ions on the functional properties of new PAMAM metallodendrimers. *New Journal of Chemistry* **2018**, *42* (10), 7853-7862.
23. Staneva, D.; Vasileva-Tonkova, E.; Bosch, P.; Grozdanov, P.; Grabchev, I., Synthesis and Characterization of a New PAMAM Metallodendrimer for Antimicrobial Modification of Cotton Fabric. *Macromolecular Research* **2018**, *26* (4), 332-340.
24. Grabchev, I.; Vasileva-Tonkova, E.; Staneva, D.; Bosch, P.; Kukeva, R.; Stoyanova, R., Synthesis, spectral characterization, and in vitro antimicrobial activity in liquid medium and applied on cotton fabric of a new PAMAM metallodendrimer. *International Journal of Polymer Analysis and Characterization* **2018**, *23* (1), 45-57.
25. Backlund, C. J.; Sergesketter, A. R.; Offenbacher, S.; Schoenfisch, M. H., Antibacterial efficacy of exogenous nitric oxide on periodontal pathogens. *J Dent Res* **2014**, *93* (11), 1089-94.

26. Yang, L.; Wang, X.; Suchyta, D. J.; Schoenfisch, M. H., Antibacterial Activity of Nitric Oxide-Releasing Hyperbranched Polyamidoamines. *Bioconjugate chemistry* **2018**, *29* (1), 35-43.
27. Zhu, Z.; Yu, F.; Chen, H.; Wang, J.; Lopez, A. I.; Chen, Q.; Li, S.; Long, Y.; Darouiche, R. O.; Hull, R. A.; Zhang, L.; Cai, C., Coating of silicone with mannoside-PAMAM dendrimers to enhance formation of non-pathogenic Escherichia coli biofilms against colonization of uropathogens. *Acta Biomater* **2017**, *64*, 200-210.
28. Lopez, A. I.; Kumar, A.; Planas, M. R.; Li, Y.; Nguyen, T. V.; Cai, C., Biofunctionalization of silicone polymers using poly(amidoamine) dendrimers and a mannose derivative for prolonged interference against pathogen colonization. *Biomaterials* **2011**, *32* (19), 4336-46.
29. Zhu, Z.; Wang, J.; Lopez, A. I.; Yu, F.; Huang, Y.; Kumar, A.; Li, S.; Zhang, L.; Cai, C., Surfaces Presenting alpha-Phenyl Mannoside Derivatives Enable Formation of Stable, High Coverage, Non-pathogenic Escherichia coli Biofilms against Pathogen Colonization. *Biomater Sci* **2015**, *3* (6), 781-880.
30. Labena, A.; Kabel, K. I.; Farag, R. K., One-pot synthesise of dendritic hyperbranched PAMAM and assessment as a broad spectrum antimicrobial agent and anti-biofilm. *Mater Sci Eng C Mater Biol Appl* **2016**, *58*, 1150-9.
31. Tulu, M.; Aghatabay, N. M.; Senel, M.; Dizman, C.; Parali, T.; Dulger, B., Synthesis, characterization and antimicrobial activity of water soluble dendritic macromolecules. *European journal of medicinal chemistry* **2009**, *44* (3), 1093-9.
32. Wang, B.; Navath, R. S.; Menjoge, A. R.; Balakrishnan, B.; Bellair, R.; Dai, H.; Romero, R.; Kannan, S.; Kannan, R. M., Inhibition of bacterial growth and intramniotic infection in a guinea pig model of chorioamnionitis using PAMAM dendrimers. *International Journal of Pharmaceutics (Amsterdam, Netherlands)* **2010**, *395* (1-2), 298-308.
33. Arakaki, A.; Takahashi, M.; Hosokawa, M.; Matsunaga, T.; Tanaka, T., Bacterial Inactivation by Applying an Alternating Electromagnetic Field Using PAMAM Dendron-modified Magnetic Nanoparticles. *Electrochemistry* **2016**, *84* (5), 324-327.
34. Zainul Abid, C. K. V.; Jackeray, R.; Jain, S.; Chattopadhyay, S.; Asif, S.; Singh, H., Antimicrobial Efficacy of Synthesized Quaternary Ammonium Polyamidoamine Dendrimers and Dendritic Polymer Network. *Journal of Nanoscience and Nanotechnology* **2016**, *16* (1), 998-1007.
35. Yu, S.; Li, G.; Liu, R.; Ma, D.; Xue, W., Dendritic Fe₃O₄@Poly(dopamine)@PAMAM Nanocomposite as Controllable NO-Releasing Material: A Synergistic Photothermal and NO Antibacterial Study. *Advanced Functional Materials* **2018**, *28* (20), 1707440.
36. Strydom, S. J.; Rose, W. E.; Otto, D. P.; Liebenberg, W.; de Villiers, M. M., Poly(amidoamine) dendrimer-mediated synthesis and stabilization of silver

sulfonamide nanoparticles with increased antibacterial activity. *Nanomedicine : nanotechnology, biology, and medicine* **2013**, *9* (1), 85-93.

37. VanKoten, H. W.; Dlakic, W. M.; Engel, R.; Cloninger, M. J., Synthesis and Biological Activity of Highly Cationic Dendrimer Antibiotics. *Molecular pharmaceuticals* **2016**, *13* (11), 3827-3834.
38. Beaussart, A.; Beloin, C.; Ghigo, J. M.; Chapot-Chartier, M. P.; Kulakauskas, S.; Duval, J. F. L., Probing the influence of cell surface polysaccharides on nanodendrimer binding to Gram-negative and Gram-positive bacteria using single-nanoparticle force spectroscopy. *Nanoscale* **2018**, *10* (26), 12743-12753.
39. Wong, P. T.; Tang, S. Z.; Tang, K.; Coulter, A.; Mukherjee, J.; Gam, K.; Baker, J. R.; Choi, S. K., A lipopolysaccharide binding heteromultivalent dendrimer nanoplatform for Gram negative cell targeting. *J Mater Chem B* **2015**, *3* (6), 1149-1156.
40. He, G.; Zhu, C.; Ye, S.; Cai, W.; Yin, Y.; Zheng, H.; Yi, Y., Preparation and properties of novel hydrogel based on chitosan modified by poly(amidoamine) dendrimer. *International journal of biological macromolecules* **2016**, *91*, 828-37.
41. Maleki, A.; Shahmoradi, B.; Hayati, B.; Jebelli, M. A.; Daraei, H.; Joo, S. W., Synthesis of halogenated nanodendrimer as novel antimicrobial agents in water treatment. *Desalin Water Treat* **2017**, *64*, 101-108.
42. Charles, S.; Vasanthan, N.; Kwon, D.; Sekosan, G.; Ghosh, S., Surface Modification of Poly(amidoamine) (PAMAM) Dendrimer as Antimicrobial Agents. *Tetrahedron letters* **2012**, *53* (49), 6670-6675.
43. Mofrad, A. S.; Mohammadi, M. J.; Mansoorian, H. J.; Khaniabadid, Y. O.; Jebeli, M. A.; Khanjani, N.; Khoshgoftar, M.; Yari, A. R., The antibacterial effect of G3-poly-amidoamine dendrimer on gram negative and gram positive bacteria in aqueous solutions. *Desalin Water Treat* **2018**, *124*, 223-231.
44. Balogh, L.; Swanson, D. R.; Tomalia, D. A.; Hagnauer, G. L.; McManus, A. T., Dendrimer–Silver Complexes and Nanocomposites as Antimicrobial Agents. *Nano Letters* **2001**, *1* (1), 18-21.
45. Shang, K.; Qiao, Z.; Sun, B.; Fan, X.; Ai, S., An efficient electrochemical disinfection of E. coli and S. aureus in drinking water using ferrocene–PAMAM–multiwalled carbon nanotubes–chitosan nanocomposite modified pyrolytic graphite electrode. *Journal of Solid State Electrochemistry* **2013**, *17* (6), 1685-1691.
46. Ghosh, S.; Banthia, A. K., Biocompatibility and antibacterial activity studies of polyamidoamine (PAMAM) dendron, side chain dendritic oligourethane (SCDOU). *Journal of biomedical materials research. Part A* **2004**, *71* (1), 1-5.
47. Sadeghi-Kiakhani, M.; Safapour, S., Functionalization of poly(amidoamine) dendrimer-based nano-architectures using a naphthalimide derivative and their

fluorescent, dyeing and antimicrobial properties on wool fibers. *Luminescence* **2016**, *31* (4), 1005-12.

48. Ghosh, S., Antibacterial Effects of Silver Doped Polyethyleneglycol Based Polyamidoamine Side Chain Dendritic Polyurethane. *Journal of Macromolecular Science, Part A* **2005**, *42* (6), 765-770.

49. Aryabadie, S.; Sadeghi-Kiakhani, M.; Arami, M., Antimicrobial and Dyeing studies of treated cotton fabrics by prepared Chitosan-PAMAM Dendrimer/Ag Nano-emulsion. *Fibers and Polymers* **2015**, *16* (12), 2529-2537.

50. Calabretta, M.; Kumar, A.; McDermott, A.; Cai, C., Antibacterial activities of poly(amidoamine) dendrimers terminated with amino and poly(ethylene glycol) groups. *Biomacromolecules* **2007**, *8* (6), 1807-1811.

51. Worley, B. V.; Schilly, K. M.; Schoenfisch, M. H., Anti-Biofilm Efficacy of Dual-Action Nitric Oxide-Releasing Alkyl Chain Modified Poly(amidoamine) Dendrimers. *Molecular pharmaceutics* **2015**, *12* (5), 1573-83.

52. Lopez, A. I.; Reins, R. Y.; McDermott, A. M.; Trautner, B. W.; Cai, C., Antibacterial activity and cytotoxicity of PEGylated poly(amidoamine) dendrimers. *Molecular bioSystems* **2009**, *5* (10), 1148-56.

53. Brockman, S. M.; Bodas, M.; Silverberg, D.; Sharma, A.; Vij, N., Dendrimer-based selective autophagy-induction rescues DeltaF508-CFTR and inhibits *Pseudomonas aeruginosa* infection in cystic fibrosis. *PLoS One* **2017**, *12* (9), e0184793.

54. Wang, L.; Erasquin, U. J.; Zhao, M.; Ren, L.; Zhang, M. Y.; Cheng, G. J.; Wang, Y.; Cai, C., Stability, antimicrobial activity, and cytotoxicity of poly(amidoamine) dendrimers on titanium substrates. *ACS Appl. Mater. Interfaces* **2011**, *3* (8), 2885-94.

55. Lu, Y.; Slomberg, D. L.; Shah, A.; Schoenfisch, M. H., Nitric oxide-releasing amphiphilic poly(amidoamine) (PAMAM) dendrimers as antibacterial agents. *Biomacromolecules* **2013**, *14* (10), 3589-98.

56. Worley, B. V.; Slomberg, D. L.; Schoenfisch, M. H., Nitric oxide-releasing quaternary ammonium-modified poly(amidoamine) dendrimers as dual action antibacterial agents. *Bioconjugate chemistry* **2014**, *25* (5), 918-27.

57. Serri, A.; Mahboubi, A.; Zarghi, A.; Moghimi, H. R., PAMAM-dendrimer Enhanced Antibacterial Effect of Vancomycin Hydrochloride Against Gram-Negative Bacteria. *J Pharm Pharm Sci* **2018**, *22* (1), 10-21.

58. Choi, S. K.; Myc, A.; Silpe, J. E.; Sumit, M.; Wong, P. T.; McCarthy, K.; Desai, A. M.; Thomas, T. P.; Kotlyar, A.; Holl, M. M.; Orr, B. G.; Baker, J. R., Jr., Dendrimer-based multivalent vancomycin nanoplatfor for targeting the drug-resistant bacterial surface. *ACS Nano* **2013**, *7* (1), 214-28.

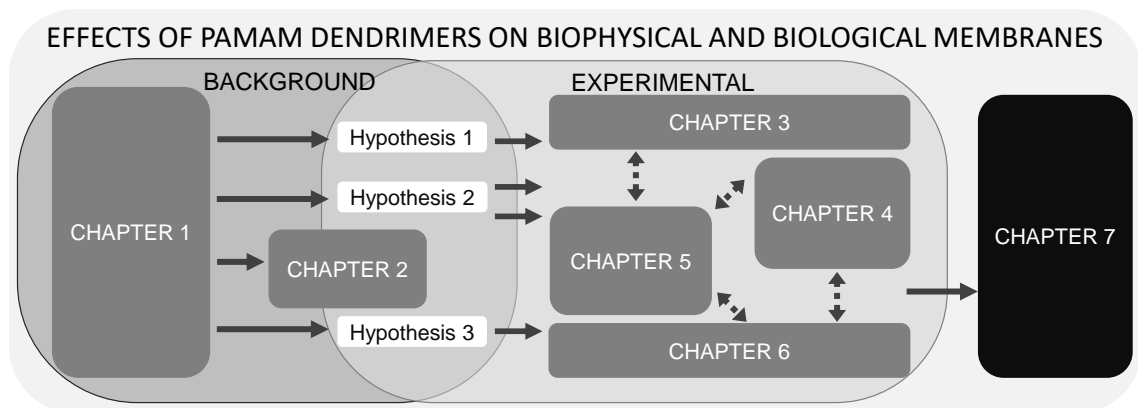
59. Yang, H.; Lopina, S. T., Penicillin V-conjugated PEG-PAMAM star polymers. *J Biomater Sci Polym Ed* **2003**, *14* (10), 1043-56.
60. Ghosh, S.; Yadav, S.; Vasanthan, N.; Sekosan, G., A study of antimicrobial property of textile fabric treated with modified dendrimers. *J Appl Polym Sci* **2010**, *115* (2), 716-722.
61. Sonawane, S. J.; Kalhapure, R. S.; Rambharose, S.; Mocktar, C.; Vepuri, S. B.; Soliman, M.; Govender, T., Ultra-small lipid-dendrimer hybrid nanoparticles as a promising strategy for antibiotic delivery: In vitro and in silico studies. *International journal of pharmaceutics* **2016**, *504* (1-2), 1-10.
62. Ge, Y.; Ren, B.; Zhou, X.; Xu, H. H. K.; Wang, S.; Li, M.; Weir, M. D.; Feng, M.; Cheng, L., Novel Dental Adhesive with Biofilm-Regulating and Remineralization Capabilities. *Materials (Basel)* **2017**, *10* (1).
63. Eichler, M.; Katur, V.; Scheideler, L.; Haupt, M.; Geis-Gerstorfer, J.; Schmalz, G.; Ruhl, S.; Muller, R.; Rupp, F., The impact of dendrimer-grafted modifications to model silicon surfaces on protein adsorption and bacterial adhesion. *Biomaterials* **2011**, *32* (35), 9168-79.
64. Backlund, C. J.; Worley, B. V.; Schoenfish, M. H., Anti-biofilm action of nitric oxide-releasing alkyl-modified poly(amidoamine) dendrimers against *Streptococcus mutans*. *Acta Biomater* **2016**, *29*, 198-205.
65. Malke, H., J. SAMBROCK, E. F. FRITSCH and T. MANIATIS, Molecular Cloning, A Laboratory Manual (Second Edition), Volumes 1, 2 and 3. 1625 S., zahlreiche Abb. und Tab. Cold Spring Harbor 1989. Cold Spring Harbor Laboratory Press. \$ 115.00. ISBN: 0-87969-309-6. *Journal of Basic Microbiology* **1990**, *30* (8), 623-623.
66. Yang, T.; Wu, B.; Yue, X.; Jin, L.; Li, T.; Liang, X.; Ding, S.; Feng, K.; Huang, G.; Zhang, J., Rapid detection of *Salmonella* in milk with a nuclear magnetic resonance biosensor based on a streptavidin-biotin system and a polyamidoamine-dendrimer-targeted gadolinium probe. *Journal of Dairy Science* **2021**, *104* (2), 1494-1503.
67. Gibson, B.; Wilson, D. J.; Feil, E.; Eyre-Walker, A., The distribution of bacterial doubling times in the wild. *Proceedings of the Royal Society B: Biological Sciences* **2018**, *285* (1880), 20180789.
68. Wang, M.-Z.; Lai, B.-M.; Dandekar, A. A.; Yang, Y.-S.; Li, N.; Yin, J.; Shen, D.-S., Nitrogen Source Stabilization of Quorum Sensing in the *Pseudomonas aeruginosa* Bioaugmentation Strain SD-1. *Appl Environ Microb* **2017**, *83* (16), e00870-17.
69. Farisa Banu, S.; Rubini, D.; Rakshitaa, S.; Chandrasekar, K.; Murugan, R.; Wilson, A.; Gowrishankar, S.; Pandian, S. K.; Nithyanand, P., Antivirulent Properties of Underexplored *Cinnamomum tamala* Essential Oil and Its Synergistic Effects with DNase against *Pseudomonas aeruginosa* Biofilms – An In Vitro Study. *Frontiers in Microbiology* **2017**, *8* (1144).

70. Martins, K. B.; Ferreira, A. M.; Pereira, V. C.; Pinheiro, L.; Oliveira, A. d.; Cunha, M. d. L. R. d. S. d., In vitro Effects of Antimicrobial Agents on Planktonic and Biofilm Forms of *Staphylococcus saprophyticus* Isolated From Patients With Urinary Tract Infections. *Frontiers in Microbiology* **2019**, *10* (40).
71. Pankey, G. A.; Sabath, L. D., Clinical Relevance of Bacteriostatic versus Bactericidal Mechanisms of Action in the Treatment of Gram-Positive Bacterial Infections. *Clinical Infectious Diseases* **2004**, *38* (6), 864-870.
72. Ghosh, S.; Ayayee, P. A.; Valverde-Barrantes, O. J.; Blackwood, C. B.; Royer, T. V.; Leff, L. G., Initial nitrogen enrichment conditions determines variations in nitrogen substrate utilization by heterotrophic bacterial isolates. *BMC Microbiology* **2017**, *17* (1), 87.
73. Pasquina-Lemonche, L.; Burns, J.; Turner, R. D.; Kumar, S.; Tank, R.; Mullin, N.; Wilson, J. S.; Chakrabarti, B.; Bullough, P. A.; Foster, S. J.; Hobbs, J. K., The architecture of the Gram-positive bacterial cell wall. *Nature* **2020**, *582* (7811), 294-297.
74. Beveridge, T. J., Structures of Gram-Negative Cell Walls and Their Derived Membrane Vesicles. *Journal of Bacteriology* **1999**, *181* (16), 4725-4733.
75. Wada, A.; Kono, M.; Kawauchi, S.; Takagi, Y.; Morikawa, T.; Funakoshi, K., Rapid Discrimination of Gram-Positive and Gram-Negative Bacteria in Liquid Samples by Using NaOH-Sodium Dodecyl Sulfate Solution and Flow Cytometry. *PLOS ONE* **2012**, *7* (10), e47093.
76. Beutler, B., LPS in microbial pathogenesis: promise and fulfilment. *Journal of endotoxin research* **2002**, *8* 5, 329-35.
77. Hänel, F., C. Radledge and S. G. Wilkinson (Editors), *Microbial Lipids Volume I. XVIII + 393 S., 32 Abb., 156 Tab.* London–San Diego–New York–Berkeley–Boston–Sydney–Tokyo—Toronto 1988. Academic Press (Harcourt Brace Javanovich Publishers). £ 110.00. ISBN: 0–12–582304–5. *Journal of Basic Microbiology* **1990**, *30* (1), 63-63.
78. Albelo, S. T.; Domenech, C. E., Carbons from choline present in the phospholipids of *Pseudomonas aeruginosa*. *FEMS Microbiology Letters* **1997**, *156* (2), 271-274.
79. Ames, G. F., Lipids of *Salmonella typhimurium* and *Escherichia coli*: structure and metabolism. *J Bacteriol* **1968**, *95* (3), 833-43.
80. Morein, S.; Andersson, A. S.; Rilfors, L.; Lindblom, G., Wild-type *Escherichia coli* cells regulate the membrane lipid composition in a "window" between gel and non-lamellar structures. *J Biol Chem* **1996**, *271* (12), 6801-6809.
81. Conrad, R. S.; Gilleland, H. E., Jr., Lipid alterations in cell envelopes of polymyxin-resistant *Pseudomonas aeruginosa* isolates. *J Bacteriol* **1981**, *148* (2), 487-97.

82. Pinkart, H. C.; White, D. C., Lipids of *Pseudomonas*. In *Pseudomonas*, 1998; pp 111-138.
83. Tomlins, R. I.; Watkins, T. R.; Gray, R. J., Membrane lipid alterations and thermal stress in *Salmonella typhimurium* 7136. *Appl Environ Microb* **1982**, *44* (5), 1110-1117.
84. Aloui, A.; Mihoub, M.; Sethom, M. M.; Chatti, A.; Feki, M.; Kaabachi, N.; Landoulsi, A., Effects of dam and/or seqA Mutations on the Fatty Acid and Phospholipid Membrane Composition of *Salmonella enterica* Serovar Typhimurium. *Foodborne Pathogens and Disease* **2010**, *7* (5), 573-583.
85. Beining, P. R.; Huff, E.; Prescott, B.; Theodore, T. S., Characterization of the lipids of mesosomal vesicles and plasma membranes from *Staphylococcus aureus*. *J Bacteriol* **1975**, *121* (1), 137-43.
86. Hayami, M.; Okabe, A.; Kariyama, R.; Abe, M.; Kanemasa, Y., Lipid Composition of *Staphylococcus aureus* and Its Derived L-forms. *Microbiology and Immunology* **1979**, *23* (6), 435-442.
87. White, D. C.; Frerman, F. E., Extraction, characterization, and cellular localization of the lipids of *Staphylococcus aureus*. *J Bacteriol* **1967**, *94* (6), 1854-67.
88. Cohen, M.; Panos, C., Membrane Lipid Composition of *Streptococcus pyogenes* and Derived L Form*. *Biochemistry* **1966**, *5* (7), 2385-2392.
89. Rosch, J. W.; Hsu, F. F.; Caparon, M. G., Anionic Lipids Enriched at the ExPortal of *Streptococcus pyogenes*. *Journal of Bacteriology* **2007**, *189* (3), 801-806.
90. Yanez Arteta, M.; Ainalem, M.-L.; Porcar, L.; Martel, A.; Coker, H.; Lundberg, D.; Chang, D. P.; Soltwedel, O.; Barker, R.; Nylander, T., Interactions of PAMAM Dendrimers with Negatively Charged Model Biomembranes. *The Journal of Physical Chemistry B* **2014**, *118* (45), 12892-12906.
91. Jafari, M.; Mehrnejad, F.; Talandashti, R.; Doustdar, F.; Reza Vakili, M.; Lavasanifar, A., Effect of the lipid composition and cholesterol on the membrane selectivity of low generations PAMAM dendrimers: A molecular dynamics simulation study. *Applied Surface Science* **2021**, *540*, 148274.
92. Edwards-Gayle, C. J. C.; Barrett, G.; Roy, S.; Castelletto, V.; Seitsonen, J.; Ruokolainen, J.; Hamley, I. W., Selective Antibacterial Activity and Lipid Membrane Interactions of Arginine-Rich Amphiphilic Peptides. *ACS Applied Bio Materials* **2020**, *3* (2), 1165-1175.
93. Furci, L.; Secchi, M., Chapter 6 - AMPs and Mechanisms of Antimicrobial Action. In *Antimicrobial Peptides in Gastrointestinal Diseases*, Cho, C. H., Ed. Academic Press: 2018; pp 97-131.

94. Epand, R. F.; Savage, P. B.; Epand, R. M., Bacterial lipid composition and the antimicrobial efficacy of cationic steroid compounds (Ceragenins). *Biochimica et Biophysica Acta (BBA) - Biomembranes* **2007**, *1768* (10), 2500-2509.
95. Prevette, L. E.; Benish, N. C.; Schoenecker, A. R.; Braden, K. J., Cell-penetrating compounds preferentially bind glycosaminoglycans over plasma membrane lipids in a charge density- and stereochemistry-dependent manner. *Biophysical Chemistry* **2015**, *207*, 40-50.
96. Holmes, A. M.; Heylings, J. R.; Wan, K. W.; Moss, G. P., Antimicrobial efficacy and mechanism of action of poly(amidoamine) (PAMAM) dendrimers against opportunistic pathogens. *Int J Antimicrob Agents* **2019**, *53* (4), 500-507.
97. Hale, J. D. F.; Hancock, R. E. W., Alternative mechanisms of action of cationic antimicrobial peptides on bacteria. *Expert Review of Anti-infective Therapy* **2007**, *5* (6), 951-959.
98. Guo, J.; Qin, J.; Ren, Y.; Wang, B.; Cui, H.; Ding, Y.; Mao, H.; Yan, F., Antibacterial activity of cationic polymers: side-chain or main-chain type? *Polymer Chemistry* **2018**, *9* (37), 4611-4616.
99. Epand, R. F.; Mowery, B. P.; Lee, S. E.; Stahl, S. S.; Lehrer, R. I.; Gellman, S. H.; Epand, R. M., Dual Mechanism of Bacterial Lethality for a Cationic Sequence-Random Copolymer that Mimics Host-Defense Antimicrobial Peptides. *Journal of Molecular Biology* **2008**, *379* (1), 38-50.
100. Colomer, A.; Pinazo, A.; Manresa, M. A.; Vinardell, M. P.; Mitjans, M.; Infante, M. R.; Pérez, L., Cationic Surfactants Derived from Lysine: Effects of Their Structure and Charge Type on Antimicrobial and Hemolytic Activities. *Journal of medicinal chemistry* **2011**, *54* (4), 989-1002.
101. Zhou, C.; Wang, Y., Structure–activity relationship of cationic surfactants as antimicrobial agents. *Current Opinion in Colloid & Interface Science* **2020**, *45*, 28-43.
102. Epand, R. M.; Epand, R. F., Lipid domains in bacterial membranes and the action of antimicrobial agents. *Biochimica et Biophysica Acta, Biomembranes* **2009**, *1788* (1), 289-294.
103. Mukhopadhyay, R.; Huang, K. C.; Wingreen, N. S., Lipid Localization in Bacterial Cells through Curvature-Mediated Microphase Separation. *Biophysical journal* **2008**, *95* (3), 1034-1049.
104. Tribet, C.; Vial, F., Flexible macromolecules attached to lipid bilayers: impact on fluidity, curvature, permeability and stability of the membranes. *Soft Matter* **2008**, *4* (1), 68-81.
105. Epand, R. M.; Walker, C.; Epand, R. F.; Magarvey, N. A., Molecular mechanisms of membrane targeting antibiotics. *Biochimica et Biophysica Acta (BBA) - Biomembranes* **2016**, *1858* (5), 980-987.

CHAPTER 7: DISCUSSION AND CONCLUSION



This final chapter is a discussion of all the previous chapters in the wider context and draws a number of conclusion for the potential future direction of the project.

7 DISCUSSION AND CONCLUSION

Over the last 5-6 years (duration of this project), there has been a trend to explore new areas for potential PAMAM dendrimers applications – such as biological sensing (i.e. for tracking of cancer cells¹ or detection of bacteria²) or PAMAMs as bioactive agents themselves. Of particular relevance to this thesis is the increased focus on the antimicrobial activity of PAMAM dendrimers³⁻⁶ and their delivery of antibacterial⁷⁻⁹ or antifungal¹⁰⁻¹² agents as well as incorporation in antimicrobial textiles¹³⁻¹⁵.

Rising incidences of viruses diseases such as Dengue fever or the most recent coronavirus pandemic triggered research into novel applications of PAMAM and its derivatives, such as an optical sensor with the integrated PAMAM for the detection of dengue E protein¹⁶ or a silver redox probe modified with chitosan and PAMAM dendrimer-coated silicon quantum dots as a genosensor for the early detection of COVID19¹⁷. Transactivator of transcription (TAT)-conjugated PAMAM dendrimers were successfully employed in a mouse model as transdermal DNA vaccine delivery system for the virulent H5N1 influenza virus¹⁸. Sialyllactose-conjugated PAMAM were shown to be efficient as inhibitors of avian and human influenza virus strains¹⁹, and antiviral properties of native PAMAM dendrimers were reported against Middle East respiratory syndrome coronavirus²⁰.

The most exciting recent development is that OP-101, a PAMAM-based drug delivery system licensed for use in neuroinflammatory diseases (Alzheimer's, Adrenoleukodystrophy, Amyotrophic Lateral Sclerosis), has successfully entered and passed a Phase I clinical trial. It is currently in Phase II to address the excessive inflammation and cytokine production in severe COVID-19 cases²¹. OP-101, marketed by Opheris/ Ashvattha Therapeutics, is a PAMAM G4 dendrimer functionalized with N-Acetylcysteine on the surface²².

Parallel to the developing biomedical applications of PAMAM dendrimers, research on improved membrane models has evolved. More complex lipid

membrane models have been developed for biophysical applications, such a lipid bilayer based nanodiscs or bicelles^{23, 24} or lipid droplets^{25, 26} that include membrane curvature which is missing in conventional bilayer models. Bilayer models such as supported bilayers or tethered bilayers were developed further to create freer lipid movement and mimic membrane asymmetry²⁷⁻²⁹ and introduce membrane curvature³⁰. Some research groups were able to implement membrane channels^{31, 32} and membrane proteins^{33, 34} into their models. More complex biophysical models of the gram-negative bacterial outer membrane³⁵ or fungal membrane³⁶ were also reported.

Advances in computational research led to more realistic bacterial membrane composition with multi-lipid systems^{37, 38} and native membrane proteins³⁹, but also to more physiological models for eukaryotic plasma membrane types⁴⁰⁻⁴². For both, bacterial and eukaryotic models, lipid rafts and domains⁴³⁻⁴⁶, lipid-protein binding sites⁴⁷⁻⁴⁹, lipid-mediated protein clustering⁵⁰⁻⁵², and membrane curvature⁵³⁻⁵⁵ were increasingly addressed by membrane researchers providing clearer insights into natural membrane dynamics and potential points of molecular interaction.

This chapter aims to: (a) provide a summary of the key results of the thesis body (7.1); (b) critically evaluate selected, most significant findings and their relevance to the wider research community (7.2); and (c) assess opportunities for future research, taking in consideration most recent advances in PAMAM and membrane research (7.3).

7.1 KEY FINDINGS

In chapter 3, we showed the importance of careful evaluation of solvent conditions as this can have impact on multiple molecule properties (i.e. structural arrangement, intrinsic fluorescence). We showed that pH and resulting charge state of functional groups for the surface and dendrimer core considerably affect the molecular conformation (shape and size) of PAMAM G4.5 and G5, which is in line with literature on full-generation PAMAM G1-8⁵⁶⁻⁶⁰. There are only few reports exploring the structural behavior of half-generation

PAMAMs⁶¹⁻⁶³, and our study is the first to address the impact of solution pH as modulator of half-generation PAMAMs molecular structure.

Furthermore, even small quantities of methanol, which is often used to improve solubility, can affect the experimental endpoints such as fluorescence or absorbance. PAMAM fluorescence was reported to be dependent on solvent⁶⁴⁻⁶⁶, but so far, very few studies addressed solvent-mixtures⁶⁷ and to our knowledge, none of them included residual methanol.

Chapter 4 utilizes the most simplistic membrane model of lipid monolayers to study binding behavior of PAMAM G4.5 (COOH) and G5 (NH₃). At pH 7, the surface groups of both dendrimers are fully charged, which was identified as a driver for the binding preference to and penetration into anionic DPPG monolayers. Our results are in line with strong adsorption to and embedding in sodium dodecyl sulfate monolayers (anionic surfactant) seen for PAMAM G4 and G8⁶⁸. Electrostatic interactions of PAMAM G4.5 and G5 with solid-supported DPPC-DPPG bilayers were causing changes to the interfacial water structure and charge density, and G5 additionally affected the alkyl chain conformation of the lipid tails⁶⁹.

We observed that higher PAMAM concentrations were required for penetration into zwitterionic DPPC monolayers and changes to the lipid order, and the dependency of membrane interactions on PAMAM /lipid molar ratio was also reported for phosphatidylcholine bilayer models⁷⁰⁻⁷².

The effect of the solvent environment (pH, residual methanol) on PAMAM interactions with membrane models was explored in Chapter 5. Methanol is a common (co-)solvent to increase the solubility of biologically active molecules, but residual methanol in the experimental system is rarely considered as contributor to cell membrane effects⁷³⁻⁷⁵ However, our studies showed that it can affect membrane fluidity and lipid order such that the degree of PAMAM penetration is higher with residual methanol present. Interestingly, the strong membrane binding effect from monolayer models (especially for pH 4) was not the same degree for the more complex asymmetric DPPC-DPPG bilayers at neither low nor neutral pH. Whilst pH – responsiveness of PAMAM dendrimers

was shown in structural studies^{57, 59, 76} and utilized in developing pH-controlled drug carrier systems⁷⁷⁻⁷⁹, so far very few studies focused on the environment pH as relevant modulator of PAMAM binding to biological cell components such as lipids⁸⁰ or proteins⁸¹. Most membrane interaction studies assume a neutral pH, which does not reflect the pH range of the different organs or cell organelles, and the work of this thesis aims to address this deficit in the literature.

Considering the PAMAM binding preference to PG, which is a major headgroup of bacterial lipids, in Chapter 6 we used bacteria as models to better understand the antibiotic effect of PAMAM dendrimers reported in literature^{3, 8, 82}. The majority of antibacterial studies were focused on smaller full-generation PAMAM, up to G4^{3, 8, 83, 84} and very few included less active half-generation G3.5^{4, 82} for which no inhibitory effect was seen. The half-generation PAMAM G2.5 and G4.5 in our study showed antibacterial activity but less compared to their full-generation counterparts G3 and G5. However, a MIC was determined for G4.5 on gram-positive *S. Saprophyticus*. In general, the full-generation PAMAM effect was more pronounced for gram-positive bacteria than for gram-negative strains, and the MICs for G5 are in line with the values reported for G4-G6 on literature on strains of the same bacteria family^{6, 83-85}. The stronger effect on gram-positive strains was correlated to the higher anionic lipid content in the cell envelop, i.e. PG or CL, and the resulting electrostatic attraction of the full-generations' cationic surface groups to the lipid heads, which upon close contact can then enable disruptive interactions with the hydrophobic membranes and other membrane components.

7.2 SIGNIFICANCE TO THE WIDER RESEARCH FIELD

The findings from this interdisciplinary work shall be of interest not only for PAMAM research but also for the broader field polymer therapeutics research. Solvent composition and pH is relevant to anyone exploring the therapeutic molecules aimed at *in vivo* use and should be taken in consideration for potential membrane interactions, molecule charge effect as well as for the design and development of pH-responsive delivery systems. (Co-)Solvent

properties were also shown to impact on experimental endpoints, such as commonly used fluorescence or UV/Vis absorbance, and their contribution to the overall experimental findings so far is often underestimated. There are two main areas in the wider research field which this thesis' contribution warrant a more detailed discussion: the use of membrane models and their biological translation, and the role of half generation PAMAMs.

7.2.1 Membrane models and their translatability, a critical assessment

Throughout the work of thesis, a variety of model membranes with increasing complexity was used – lipid monolayers, supported bilayers and bacterial membranes. Lipid monolayers are a suitable model system to study the contributions of individual properties in the systems, i.e. lipid head charge, dendrimer surface charge, pH or composition of the surrounding solvent. However, their simplistic nature does not reflect the more complex interactions in a biological system, where most membranes are made of bilayers. Even when using mixed-lipid systems based on reported phospholipid membrane compositions⁸⁶⁻⁸⁸, they are still only modelling one leaflet under unphysiological conditions of the air-water interface.

Bilayer lipid models in a contained liquid environment, as used for our neutron reflectometry experiments, are a more physiological approach to investigate PAMAM-lipid interactions as the lateral pressure and the resulting limited lipid mobility are more realistic. Supported bilayers are widely used as membrane models^{69, 89}, and fabricating them via the Langmuir-Blodgett technique enables finetuning of the lipid composition of each layer^{36, 90}. Other groups have been using the simpler method of vesicle-deposition⁹¹⁻⁹³, but this has the disadvantage that the lipid asymmetry cannot be controlled. Recently, new supported bilayer fabrication techniques such as the bicelle method and solvent-assisted lipid bilayer (SALB) have been reported^{94, 95}, but they have yet to be established. However, both, monolayers and supported bilayers are flat membrane models and are lacking the natural membrane curvature.

To include membrane curvature, several membrane interaction studies utilized liposomes, such as MLVs or small, large or giant unilamellar vesicles as

membrane model. PAMAM-liposome interactions were studied with a range of techniques, such as solution NMR^{96, 97}, SANS/SAXS^{70, 71}, different types of microscopy^{98, 99}, calorimetry^{100, 101}, UV-Vis and Fluorescence^{102, 103}, but they have the major disadvantage that they can have poor stability and over time, vesicles might aggregate, fuse or break. The molecular shape of lipids determines their ability to form curves and careful consideration is required when selecting the lipids to form the liposomes and their suitability for usage in flat membrane models for comparison. Additionally, the lipid distribution across the leaflets is random and cannot be controlled as easily as with flat bilayer models which makes it more difficult to determine PAMAM lipid binding preferences when using mixed-lipid systems.

So, is it even possible to relate findings across those membrane models and are those different membrane models required?

The strong PAMAM penetration effect observed in our lipid monolayers studies was not seen to the same degree during the lipid bilayer experiments, but this does not mean that those seemingly different observations cannot be explained. For one, surface pressure is very sensitive to changes in the lipid packing but not to where and how many molecules have penetrated the layer or adsorbed onto the headgroups without penetrating. Therefore, even one aggregate of molecules can have the same strong effect on surface pressure than multiple individual molecules. On the other hand, with neutron reflectivity adsorption layers, penetration levels, coverage, and distribution of PAMAM molecules affect the scattering profiles and can be quantified, but changes in lateral lipid packing do not reflect very well with this technique. The results of those two experimental techniques cannot be compared directly, but they provide complementary information on the interactions happening on the lipid interface and therefore justify the need for a variety of membrane models depending on the research question to be answered.

However, there is still a big difference between existing biophysical lipid membrane models and biological membranes. First, the biophysical experimental are often not using near-biological conditions, and even

experimental temperature can majorly affect PAMAM-membrane interactions¹⁰⁴. Second, the complexity of biological membrane composition is very difficult to model artificially and not all biological membrane components are known and/or available for custom membrane fabrication. Some researchers increased the complexity of their biophysical models by using multi-lipid mixtures, i.e. Roy *et al*⁹⁹ trialed PAMAM G3, G4 and G5 on for their effect on various binary lipid vesicles, but this still does not account for potential interactions with other natural membrane components such as proteins or receptors.

In this work, we used bacteria as biological membrane models to correlate the observed toxic effects to bacterial lipid compositions reported in literature. Previously, the antibacterial PAMAM effect was mainly investigated for their therapeutic use as antimicrobial agent^{3, 5, 105} or suitability of carrier of antibiotics^{8, 106, 107} but the exploration of the mechanisms underlying the bacterial toxicity was neglected in those studies.

There is still a gap between biophysical reports of PAMAMs' activity towards anionic membranes¹⁰⁸⁻¹¹⁰ and the correlation to their biological effects across the used models, that could be addressed through using more complex biophysical systems^{35, 111} or multi-component models for molecular simulations^{38, 42} or a combination of both.

7.2.2 Half-generation PAMAMs – an overlooked drug-delivery system?

Main biomedical research focus thus far was on the seemingly more attractive full-generation, polycationic PAMAMs (NH₃ terminus) for drug and nucleic acid delivery, which also are more cytotoxic than the OH- or COOH-terminated dendrimers¹¹²⁻¹¹⁵, therefore there are generally fewer reports on half-generation PAMAMs available.

No hemotoxicity was observed for PAMAM G6.5 on platelet morphology, activation states, and hemostatic functions¹¹⁶, but a recent study on the blood coagulation and fibrinolysis system with PAMAM G1.5, G2.5 and G3.5 revealed a strong effect on the plasminogen activation and conformation¹¹⁷. The anionic surface groups of the same half-generation PAMAMs were also shown to

increase the porosity and membrane permeability of Caco-2 cell monolayers^{118, 119} without affecting the cell morphology¹²⁰, which enabled the dendrimers to translocate through the membrane – an important property of a potential drug-delivery system. Another study demonstrated a good biocompatibility of PAMAM G1.5, G3.5 and G5.5 with lung tissue with rapid uptake into the respiratory epithelia via endocytic, size-dependent transport¹²¹. Thiagarajan et al¹¹⁴ showed that PAMAM G3.5 and G6.5 showed no signs of oral toxicity in mice up to doses of 500 mg kg⁻¹ and a bioavailability of 9.4 % after 4 h for 1 mg mL⁻¹ G6.5 at ¹²², which further evidences the biocompatibility of half-generation PAMAMs. As shown by Sweet *et al*¹²³ PEGylation might improve the biocompatibility even further, by increasing cellular uptake of the dendrimers at the same time. A study addressing the immunocompatibility of PAMAM dendrimers, did not observe immunoreactivity for PAMAM G3.5¹²⁴.

However, biophysical studies on PAMAM G1.5 and G4.5 interacting with POPC bilayers, revealed dendrimer-size dependent interaction mechanism¹⁰², where smaller dendrimers were more membrane destructive than the larger ones. The smaller G1.5 produced defects on supported bilayers with some mass loss and increased leakage of fluorescence dye from liposomes, whereas G4.5 adsorbed and caused local (supported) bilayer swelling and decrease in liposome leakage, probably by increase of lipid packing when intercalating into the membrane. An earlier study by Shcharbin *et al*¹²⁵ reported a membrane disrupting effect of G5 on planar lipid bilayers made of egg yolk PC whereas G4.5 did not affect the membrane integrity which was attributed to the zwitterionic nature of both the membrane and PAMAM G4.5. In contrast, our study (chapter 4) with the same PAMAMs showed that both penetrated DPPC monolayers but did not cause membrane disruption. However, PAMAM G5.5 and G7.5 were reported to cause hole formation on supported DMPC bilayers, which was partially temporary, and the causation was not clear as the extended study of the process was focused on full-generation PAMAM⁹⁷. An atomistic molecular dynamics study investigated interactions of PAMAMs carrying different surfaces charges (NH₃⁺, COO⁻, Ac (neutral)) with DMPC bilayers¹²⁶ showed a greater binding of the lipid bilayer of the two charged dendrimers, but

more deformation of the Ac-terminated PAMAM during the process. Furthermore, the hydrophobic core was significantly involved in the stronger dendrimer binding to the fluid compared to the gel phase lipids, and this effect was most pronounced for carboxyl terminated PAMAM containing most hydrophobic components. Another experimental study on membrane activity of PAMAM G5 and G4.5 used supported bilayers of DPPC and DPPG⁶⁹ and observed more significant membrane interactions with the DPPG leaflets. Stronger binding affinity and lipid tail packing and ordering changes were shown for PAMAM G5 compared to G4.5, in line with our observations (Chapter 4 & 5).

The PG lipid family is a major component of bacterial membranes, but antimicrobial assessment of half-generation PAMAMs and PAMAM-derivatives with anionic functionalities revealed much lesser or no antibacterial activities compared to cationic PAMAM. However, G3.5 was reported to antibacterial activity against *E. coli*^{81, 82} and *S. aureus*⁴ and, in our studies (see chapter 6), we found a significant inhibitory effect of G4.5 on *S. saprophyticus*, which could be considered for future development of antimicrobial medicines or drug-delivery systems.

Recently, more research groups are considering the beneficial properties of half-generation PAMAM, maybe due to the biocompatibility limitations of the cationic full-generation PAMAMs, and new biomedical applications have been developed. Carboxyl terminated PAMAMs have been investigated as delivery system for cancer drugs or imaging agents targeted at the sentinel lymph node^{127, 128}. PAMAM G4.5 coated with mixed lanthanide oxide nanoparticles as dual imaging system¹²⁹ and PAMAM G4.5 conjugated to anti-body interleukin-6 (IL-6)¹³⁰ were successfully trialed for bioimaging in HeLa cells, and a dendritic nanoplatform based on a G5-succinamic acid was applied as triple modality theranostic to HepG2 cells¹³¹. A PEGylated PAMAM G4.5 – camptothecin conjugate was evaluated on human glioma cell line U1242 as a sustained-release prodrug¹³² and a PEGylated G3.5 – carboplatin conjugate showed a high drug load and a sustained-release pattern¹³³.

Efficacy of a PAMAM G4.5 – doxorubicin conjugate was shown *in vitro* and *in vivo* for the treatment of metastatic lung tumor using a pH-stimulated sustained drug release mechanism¹³⁴. PAMAM G4.5 and G3.5 were shown to increase the solubility of candesartan cilexetil, a hypertension drug, to a higher degree than amine-terminated PAMAMs¹³⁵. The solubility of sulfamethoxazole, an antibiotic, was increased by PAMAM G1.5, G2.5 and G3.5 and followed a sustained release pattern¹³⁶. Ocular drug delivery seems to be another potential application for PAMAMs with anionic surface groups, shown for dexamethasone as model drug in *in vitro* and *in vivo* studies^{137, 138}. Dental applications appear to be an emerging field for half-generation PAMAM, which are reported to promote biomineralization of demineralized dentin¹³⁹ and dentinal tubule occlusion¹⁴⁰ and inhibit dental degradation by host-derived matrix metalloproteinases¹⁴¹. Advances were also made for ex-vivo diagnostic application of carboxyl terminated PAMAMs, i.e. with the development of an immunosensor for detection of cardiac troponin I in serum samples¹⁴².

Nonetheless, in comparison to the wealth of applications suggested for the full-generation PAMAMs, the pool of available reports on the more biocompatible half-generation PAMAM is still rather small and highlights an area that is seemingly underdeveloped and requires more attention from biomedical researchers.

7.3 CONCLUSIONS AND FUTURE DEVELOPMENT OPPORTUNITIES

Being commercialized as Starbust® dendrimers with Starpharma, PAMAM dendrimers have already found their way on the market in *in vitro* applications. Stratus CS®, available from Siemens Healthcare Diagnostics (originally marketed by Dade Behring, a Baxter Healthcare subsidiary), utilizes PAMAM G5 for diagnosing cardiac biomarkers^{143, 144}. Qiagen has marketed SuperFect® and Polyfect®, transfection agents which use PAMAM G6 delivery vectors for plasmic DNA and siRNA nucleic acids¹⁴⁵⁻¹⁴⁷. Furthermore, an anthrax sensor called ALERT ticket™ based on PAMAM technology is manufactured by the U.S. army lab.

The work presented in this thesis has highlighted that a better understanding of PAMAMs' physicochemical properties under more realistic conditions is crucial to assess their biological interactions more accurately and eventually enable improved efficacy and specificity of dendrimer-based drug design which is essential for the entry of PAMAM-based medicines into clinical trials.

In fact, we found that the behavior of functional groups of the dendrimer core related to the environmental pH are not fully considered in existing studies exploring the PAMAM effect on membranes. Furthermore, whilst model membranes with easily adjustable individual components are very versatile and suitable for a wide range of techniques, they are often too simplistic to reflect realistic conditions (as discussed in section 7.2.1). Therefore, the observations cannot be readily translated into more complex biological systems and the actual PAMAM-membrane behavior might be significantly different to what was seen in the simplistic models.

In my opinion, there is still a scope to increase the biological relevance of future biophysical experiments with model membranes, for example by refining the experimental conditions to mimic more closely the *in vivo* environment. A lot of research so far, including our own, was conducted under room temperature, therefore a first step could be to adapt the models to use temperature-controlled systems and techniques. In fact, Tian *et al* 2019¹⁰⁴ studied PAMAM interaction with DPPC monolayers and reported significant differences between results obtained room-temperature and at body temperature.

To date, phosphate buffer at neutral pH is a standard on most biophysical experiments. However, body fluids are more complex in nature, i.e., variety of electrolyte composition / concentration and solution pH or presence of mobile soluble proteins and enzymes. Calcium specifically is an important modulator of membrane processes where the ions are involved in signal transduction and ion channel gating. Our own studies (see Chapter 4) showed that the presence of physiological levels of sodium chloride in the solution environment can affect the extent of the PAMAM penetration. The pH of body fluids ranges from highly acidic in the stomach to slightly alkaline in the intestine, and although

absorption of oral therapeutics is happening under those varying conditions, not many reports on active molecule-membrane interaction address those acidic or alkaline conditions. Hence, biophysical studies with model membranes could become more biologically relevant, by adapting solution conditions to body temperature, organ-specific pH and adjusting the electrolyte content to reflect intra-/extracellular ion composition.

In my view, another point that is particularly important to consider in future investigations is the use of knowledge from lipidomic data for the design of membrane models (i.e., target cell-type specific lipid mixes) and interpretation of data from studies involving biological membranes. Over the last years, the methods in lipidomics and proteomics advanced significantly and an increasing number of reports on cell membrane compositions and components is available. A recent study using a 'shotgun lipidomics' approach, studied an extensive range of tissues, primary, membrane isolations, cultured cell types and different extraction procedures and found 400-800 different lipid species per sample¹⁴⁸. Future membrane models should make more use of reports like the aforementioned to select suitable lipids for a near-biological lipid composition of the target cell type to model. Equally, researchers using biological model such bacteria or cell lines could also benefit from including lipidomic analysis to their repertoire to study, for example, the lipid up- or down-regulation effect caused by interaction with the active molecule. Those changes in membrane lipid composition might be related to antimicrobial resistance¹⁴⁹ or adaptation mechanisms of cancer cells¹⁵⁰, and thus also interesting for future studies involving PAMAM dendrimers with proven antimicrobial or cancer-selective activity.

Another potential direction of the current project could be a wider exploration of the antimicrobial activity of selected PAMAM dendrimers, either just on bacteria or also involving medically relevant yeasts and fungi. The existing reports do not delve deep into the causation of the observed growth inhibition and there is plenty of scope to explore this avenue in relation to membrane lipids, directly on bacteria, on more complex bacterial membrane models such as the one for gram-negative membranes reported by Clifton *et al*⁵ and/or near-

real simulation models³⁸. Once the mechanism of action and membrane effect is better understood, it will hopefully enable PAMAM-based drugs or drug-delivery systems to be developed for combating the increasing problem of antimicrobial resistance.

7.4 REFERENCES

1. Xu, J.; Wang, X.; Yan, C.; Chen, W., A Polyamidoamine Dendrimer-Based Electrochemical Immunosensor for Label-Free Determination of Epithelial Cell Adhesion Molecule- Expressing Cancer Cells. *Sensors* **2019**, *19* (8), 1879.
2. Yang, T.; Wu, B.; Yue, X.; Jin, L.; Li, T.; Liang, X.; Ding, S.; Feng, K.; Huang, G.; Zhang, J., Rapid detection of *Salmonella* in milk with a nuclear magnetic resonance biosensor based on a streptavidin–biotin system and a polyamidoamine-dendrimer-targeted gadolinium probe. *Journal of Dairy Science* **2021**, *104* (2), 1494-1503.
3. Xue, X.; Chen, X.; Mao, X.; Hou, Z.; Zhou, Y.; Bai, H.; Meng, J.; Da, F.; Sang, G.; Wang, Y.; Luo, X., Amino-terminated generation 2 poly(amidoamine) dendrimer as a potential broad-spectrum, nonresistance-inducing antibacterial agent. *AAPS J* **2013**, *15* (1), 132-42.
4. Holmes, A. M.; Heylings, J. R.; Wan, K. W.; Moss, G. P., Antimicrobial efficacy and mechanism of action of poly(amidoamine) (PAMAM) dendrimers against opportunistic pathogens. *Int J Antimicrob Agents* **2019**, *53* (4), 500-507.
5. Gholami, M.; Mohammadi, R.; Arzanlou, M.; Akbari Dourbash, F.; Kouhsari, E.; Majidi, G.; Mohseni, S. M.; Nazari, S., In vitro antibacterial activity of poly (amidoamine)-G7 dendrimer. *BMC Infect Dis* **2017**, *17* (1), 395.
6. Rastegar, A.; Nazari, S.; Allahabadi, A.; Falanji, F.; Akbari Dourbash, F. A. D.; Rezai, Z.; Alizadeh Matboo, S.; Hekmat-Shoar, R.; Mohseni, S. M.; Majidi, G., Antibacterial activity of amino- and amido- terminated poly (amidoamine)-G6 dendrimer on isolated bacteria from clinical specimens and standard strains. *Med J Islam Repub Iran* **2017**, *31*, 64.
7. Winnicka, K.; Wroblewska, M.; Wiczorek, P.; Sacha, P. T.; Trynieszewska, E. A., The effect of PAMAM dendrimers on the antibacterial activity of antibiotics with different water solubility. *Molecules* **2013**, *18* (7), 8607-17.
8. Xue, X. Y.; Mao, X. G.; Li, Z.; Chen, Z.; Zhou, Y.; Hou, Z.; Li, M. K.; Meng, J. R.; Luo, X. X., A potent and selective antimicrobial poly(amidoamine) dendrimer conjugate with LED209 targeting QseC receptor to inhibit the virulence genes of gram negative bacteria. *Nanomedicine : nanotechnology, biology, and medicine* **2015**, *11* (2), 329-39.

9. Jiang, G.; Liu, S.; Yu, T.; Wu, R.; Ren, Y.; van der Mei, H. C.; Liu, J.; Busscher, H. J., PAMAM dendrimers with dual-conjugated vancomycin and Ag-nanoparticles do not induce bacterial resistance and kill vancomycin-resistant Staphylococci. *Acta Biomater* **2021**, *123*, 230-243.
10. Jose, J.; Charyulu, R. N., Prolonged drug delivery system of an antifungal drug by association with polyamidoamine dendrimers. *Int J Pharm Investig* **2018**, *6* (2), 123-7.
11. Winnicka, K.; Wroblewska, M.; Wieczorek, P.; Sacha, P. T.; Trynieszewska, E., Hydrogel of ketoconazole and PAMAM dendrimers: formulation and antifungal activity. *Molecules* **2012**, *17* (4), 4612-24.
12. Winnicka, K.; Sosnowska, K.; Wieczorek, P.; Sacha, P. T.; Trynieszewska, E., Poly(amidoamine) dendrimers increase antifungal activity of clotrimazole. *Biol Pharm Bull* **2011**, *34* (7), 1129-33.
13. Grabchev, I.; Vasileva-Tonkova, E.; Staneva, D.; Bosch, P.; Kukeva, R.; Stoyanova, R., Impact of Cu(II) and Zn(II) ions on the functional properties of new PAMAM metallodendrimers. *New Journal of Chemistry* **2018**, *42* (10), 7853-7862.
14. Grabchev, I.; Vasileva-Tonkova, E.; Staneva, D.; Bosch, P.; Kukeva, R.; Stoyanova, R., Synthesis, spectral characterization, and in vitro antimicrobial activity in liquid medium and applied on cotton fabric of a new PAMAM metallodendrimer. *International Journal of Polymer Analysis and Characterization* **2018**, *23* (1), 45-57.
15. Staneva, D.; Vasileva-Tonkova, E.; Bosch, P.; Grozdanov, P.; Grabchev, I., Synthesis and Characterization of a New PAMAM Metallodendrimer for Antimicrobial Modification of Cotton Fabric. *Macromolecular Research* **2018**, *26* (4), 332-340.
16. Mustapha Kamil, Y.; Al-Rekabi, S. H.; Yaacob, M. H.; Syahir, A.; Chee, H. Y.; Mahdi, M. A.; Abu Bakar, M. H., Detection of dengue using PAMAM dendrimer integrated tapered optical fiber sensor. *Scientific Reports* **2019**, *9* (1), 13483.
17. Farzin, L.; Sadjadi, S.; Sheini, A.; Mohaghehpour, E., A nanoscale genosensor for early detection of COVID-19 by voltammetric determination of RNA-dependent RNA polymerase (RdRP) sequence of SARS-CoV-2 virus. *Microchimica Acta* **2021**, *188* (4), 121.
18. Bahadoran, A.; Ebrahimi, M.; Yeap, S. K.; Safi, N.; Moeini, H.; Hair-Bejo, M.; Hussein, M. Z.; Omar, A. R., Induction of a robust immune response against avian influenza virus following transdermal inoculation with H5-DNA vaccine formulated in modified dendrimer-based delivery system in mouse model. *International journal of nanomedicine* **2017**, *12*, 8573-8585.
19. Günther, S. C.; Maier, J. D.; Vetter, J.; Podvalnyy, N.; Khanzhin, N.; Hennet, T.; Stertz, S., Antiviral potential of 3'-sialyllactose- and 6'-sialyllactose-conjugated

dendritic polymers against human and avian influenza viruses. *Scientific Reports* **2020**, *10* (1), 768.

20. Kandeel, M.; Al-Taher, A.; Park, B. K.; Kwon, H.-J.; Al-Nazawi, M., A pilot study of the antiviral activity of anionic and cationic polyamidoamine dendrimers against the Middle East respiratory syndrome coronavirus. *Journal of Medical Virology* **2020**, *92* (9), 1665-1670.

21. Therapeutics, A. Inflammation. <http://avttx.com/pipeline/inflammation/> (accessed 07/05/2021).

22. Kannan, S.; Dai, H.; Navath, R. S.; Balakrishnan, B.; Jyoti, A.; Janisse, J.; Romero, R.; Kannan, R. M., Dendrimer-Based Postnatal Therapy for Neuroinflammation and Cerebral Palsy in a Rabbit Model. *Science Translational Medicine* **2012**, *4* (130), 130ra46-130ra46.

23. Dos Santos Morais, R.; Delalande, O.; Pérez, J.; Mouret, L.; Bondon, A.; Martel, A.; Appavou, M.-S.; Le Rumeur, E.; Hubert, J.-F.; Combet, S., Contrast-Matched Isotropic Bicelles: A Versatile Tool to Specifically Probe the Solution Structure of Peripheral Membrane Proteins Using SANS. *Langmuir : the ACS journal of surfaces and colloids* **2017**, *33* (26), 6572-6580.

24. Rouck, J. E.; Krapf, J. E.; Roy, J.; Huff, H. C.; Das, A., Recent advances in nanodisc technology for membrane protein studies (2012–2017). *FEBS Letters* **2017**, *591* (14), 2057-2088.

25. Chen, Y.; Okur, H. I.; Lütgebaucks, C.; Roke, S., Zwitterionic and Charged Lipids Form Remarkably Different Structures on Nanoscale Oil Droplets in Aqueous Solution. *Langmuir : the ACS journal of surfaces and colloids* **2018**, *34* (3), 1042-1050.

26. Chen, Y.; Jena, K. C.; Lütgebaucks, C.; Okur, H. I.; Roke, S., Three Dimensional Nano “Langmuir Trough” for Lipid Studies. *Nano Letters* **2015**, *15* (8), 5558-5563.

27. Luchini, A.; Nzulumike, A. N. O.; Lind, T. K.; Nylander, T.; Barker, R.; Arleth, L.; Mortensen, K.; Cárdenas, M., Towards biomimics of cell membranes: Structural effect of phosphatidylinositol triphosphate (PIP3) on a lipid bilayer. *Colloids and Surfaces B: Biointerfaces* **2019**, *173*, 202-209.

28. Rondelli, V.; Brocca, P.; Tranquilli, N.; Fragneto, G.; Del Favero, E.; Cantù, L., Building a biomimetic membrane for neutron reflectivity investigation: Complexity, asymmetry and contrast. *Biophysical Chemistry* **2017**, *229*, 135-141.

29. Andersson, J.; Köper, I.; Knoll, W., Tethered Membrane Architectures—Design and Applications. *Frontiers in Materials* **2018**, *5* (55).

30. Cheney, P. P.; Weisgerber, A. W.; Feuerbach, A. M.; Knowles, M. K., Single Lipid Molecule Dynamics on Supported Lipid Bilayers with Membrane Curvature. *Membranes* **2017**, *7* (1), 15.

31. Shen, Y.-x.; Song, W.; Barden, D. R.; Ren, T.; Lang, C.; Feroz, H.; Henderson, C. B.; Saboe, P. O.; Tsai, D.; Yan, H.; Butler, P. J.; Bazan, G. C.; Phillip, W. A.; Hickey, R. J.; Cremer, P. S.; Vashisth, H.; Kumar, M., Achieving high permeability and enhanced selectivity for Angstrom-scale separations using artificial water channel membranes. *Nature Communications* **2018**, *9* (1), 2294.
32. Kocsis, I.; Sorci, M.; Vanselous, H.; Murail, S.; Sanders, S. E.; Licsandru, E.; Legrand, Y.-M.; van der Lee, A.; Baaden, M.; Petersen, P. B.; Belfort, G.; Barboiu, M., Oriented chiral water wires in artificial transmembrane channels. *Science Advances* **2018**, *4* (3), eaao5603.
33. Meredith, S. A.; Yoneda, T.; Hancock, A. M.; Connell, S. D.; Evans, S. D.; Morigaki, K.; Adams, P. G., Model Lipid Membranes Assembled from Natural Plant Thylakoids into 2D Microarray Patterns as a Platform to Assess the Organization and Photophysics of Light-Harvesting Proteins. *Small* **2021**, *17* (14), 2006608.
34. Miehl, J.; Goricanec, D.; Hagn, F., A Split-Intein-Based Method for the Efficient Production of Circularized Nanodiscs for Structural Studies of Membrane Proteins. *ChemBioChem* **2018**, *19* (18), 1927-1933.
35. Clifton, L. A.; Skoda, M. W.; Daulton, E. L.; Hughes, A. V.; Le Brun, A. P.; Lakey, J. H.; Holt, S. A., Asymmetric phospholipid: lipopolysaccharide bilayers; a Gram-negative bacterial outer membrane mimic. *J. R. Soc., Interface* **2013**, *10* (89), 20130810.
36. Florek, O. B.; Clifton, L. A.; Wilde, M.; Arnold, T.; Green, R. J.; Frazier, R. A., Lipid composition in fungal membrane models: effect of lipid fluidity. *Acta Crystallogr D Struct Biol* **2018**, *74* (Pt 12), 1233-1244.
37. Piggot, T. J.; Holdbrook, D. A.; Khalid, S., Electroporation of the E. coli and S. Aureus Membranes: Molecular Dynamics Simulations of Complex Bacterial Membranes. *The Journal of Physical Chemistry B* **2011**, *115* (45), 13381-13388.
38. Pluhackova, K.; Horner, A., Native-like membrane models of E. coli polar lipid extract shed light on the importance of lipid composition complexity. *BMC Biology* **2021**, *19* (1), 4.
39. Hsu, P.-C.; Samsudin, F.; Shearer, J.; Khalid, S., It Is Complicated: Curvature, Diffusion, and Lipid Sorting within the Two Membranes of Escherichia coli. *The Journal of Physical Chemistry Letters* **2017**, *8* (22), 5513-5518.
40. Ingólfsson, H. I.; Melo, M. N.; van Eerden, F. J.; Arnarez, C.; Lopez, C. A.; Wassenaar, T. A.; Periole, X.; de Vries, A. H.; Tieleman, D. P.; Marrink, S. J., Lipid Organization of the Plasma Membrane. *Journal of the American Chemical Society* **2014**, *136* (41), 14554-14559.
41. Ingólfsson, H. I.; Carpenter, T. S.; Bhatia, H.; Bremer, P.-T.; Marrink, S. J.; Lightstone, F. C., Computational Lipidomics of the Neuronal Plasma Membrane. *Biophysical Journal* **2017**, *113* (10), 2271-2280.

42. Domicевичa, L.; Koldsø, H.; Biggin, P. C., Multiscale molecular dynamics simulations of lipid interactions with P-glycoprotein in a complex membrane. *Journal of Molecular Graphics and Modelling* **2018**, *80*, 147-156.
43. Lin, X.; Lorent, J. H.; Skinkle, A. D.; Levental, K. R.; Waxham, M. N.; Gorfe, A. A.; Levental, I., Domain Stability in Biomimetic Membranes Driven by Lipid Polyunsaturation. *The Journal of Physical Chemistry B* **2016**, *120* (46), 11930-11941.
44. Sodt, Alexander J.; Pastor, Richard W.; Lyman, E., Hexagonal Substructure and Hydrogen Bonding in Liquid-Ordered Phases Containing Palmitoyl Sphingomyelin. *Biophysical journal* **2015**, *109* (5), 948-955.
45. Bennett, W. F. D.; Shea, J.-E.; Tieleman, D. P., Phospholipid Chain Interactions with Cholesterol Drive Domain Formation in Lipid Membranes. *Biophysical journal* **2018**, *114* (11), 2595-2605.
46. López, C. A.; Unkefer, C. J.; Swanson, B. I.; Swanson, J. M. J.; Gnanakaran, S., Membrane perturbing properties of toxin mycolactone from *Mycobacterium ulcerans*. *PLOS Computational Biology* **2018**, *14* (2), e1005972.
47. Briones, R.; Aponte-Santamaría, C.; de Groot, B. L., Localization and Ordering of Lipids Around Aquaporin-0: Protein and Lipid Mobility Effects. *Frontiers in Physiology* **2017**, *8* (124).
48. Hedger, G.; Koldsø, H.; Chavent, M.; Siebold, C.; Rohatgi, R.; Sansom, M. S. P., Cholesterol Interaction Sites on the Transmembrane Domain of the Hedgehog Signal Transducer and Class F G Protein-Coupled Receptor Smoothed. *Structure* **2019**, *27* (3), 549-559.e2.
49. Hedger, G.; Rouse, S. L.; Domański, J.; Chavent, M.; Koldsø, H.; Sansom, M. S. P., Lipid-Loving ANTs: Molecular Simulations of Cardiolipin Interactions and the Organization of the Adenine Nucleotide Translocase in Model Mitochondrial Membranes. *Biochemistry* **2016**, *55* (45), 6238-6249.
50. Travers, T.; López, C. A.; Van, Q. N.; Neale, C.; Tonelli, M.; Stephen, A. G.; Gnanakaran, S., Molecular recognition of RAS/RAF complex at the membrane: Role of RAF cysteine-rich domain. *Scientific Reports* **2018**, *8* (1), 8461.
51. Mondal, S.; Khelashvili, G.; Weinstein, H., Not Just an Oil Slick: How the Energetics of Protein-Membrane Interactions Impacts the Function and Organization of Transmembrane Proteins. *Biophysical journal* **2014**, *106* (11), 2305-2316.
52. Gahbauer, S.; Pluhackova, K.; Böckmann, R. A., Closely related, yet unique: Distinct homo- and heterodimerization patterns of G protein coupled chemokine receptors and their fine-tuning by cholesterol. *PLOS Computational Biology* **2018**, *14* (3), e1006062.

53. Baoukina, S.; Ingólfsson, H. I.; Marrink, S. J.; Tieleman, D. P., Curvature-Induced Sorting of Lipids in Plasma Membrane Tethers. *Advanced Theory and Simulations* **2018**, *1* (8), 1800034.
54. Sodt, Alexander J.; Pastor, Richard W., Molecular Modeling of Lipid Membrane Curvature Induction by a Peptide: More than Simply Shape. *Biophysical journal* **2014**, *106* (9), 1958-1969.
55. Patel, Dhilon S.; Park, S.; Wu, Emilia L.; Yeom, Min S.; Widmalm, G.; Klauda, Jeffery B.; Im, W., Influence of Ganglioside GM1 Concentration on Lipid Clustering and Membrane Properties and Curvature. *Biophysical journal* **2016**, *111* (9), 1987-1999.
56. Liu, Y.; Bryantsev, V. S.; Diallo, M. S.; Goddard Iii, W. A., PAMAM Dendrimers Undergo pH Responsive Conformational Changes without Swelling. *Journal of the American Chemical Society* **2009**, *131* (8), 2798-2799.
57. Maiti, P. K.; Bagchi, B., Diffusion of flexible, charged, nanoscopic molecules in solution: Size and pH dependence for PAMAM dendrimer. *The Journal of chemical physics* **2009**, *131* (21), 214901.
58. Maiti, P. K.; Goddard, W. A., Solvent Quality Changes the Structure of G8 PAMAM Dendrimer, a Disagreement with Some Experimental Interpretations. *The Journal of Physical Chemistry B* **2006**, *110* (51), 25628-25632.
59. Maiti, P. K.; Çağın, T.; Lin, S.-T.; Goddard, W. A., Effect of Solvent and pH on the Structure of PAMAM Dendrimers. *Macromolecules* **2005**, *38* (3), 979-991.
60. Garcia-Fernandez, E.; Paulo, P. M. R., Deswelling and Electrolyte Dissipation in Free Diffusion of Charged PAMAM Dendrimers. *The Journal of Physical Chemistry Letters* **2014**, *5* (8), 1472-1478.
61. Lombardo, D., Liquid-like Ordering of Negatively Charged Poly(amidoamine) (PAMAM) Dendrimers in Solution. *Langmuir* **2009**, *25* (5), 3271-3275.
62. Paulo, P. M. R.; Lopes, J. N. C.; Costa, S. M. B., Molecular Dynamics Simulations of Charged Dendrimers: Low-to-Intermediate Half-Generation PAMAMs. *The Journal of Physical Chemistry B* **2007**, *111* (36), 10651-10664.
63. Pilkington, G. A.; Pedersen, J. S.; Briscoe, W. H., Dendrimer Nanofluids in the Concentrated Regime: From Polymer Melts to Soft Spheres. *Langmuir* **2015**, *31* (11), 3333-3342.
64. Konopka, M.; Janaszewska, A.; Klajnert-Maculewicz, B., Intrinsic Fluorescence of PAMAM Dendrimers—Quenching Studies. *Polymers* **2018**, *10* (5), 540.
65. Staneva, D.; Bosch, P.; Asiri, A. M.; Taib, L. A.; Grabchev, I., Studying pH dependence of the photophysical properties of a blue emitting fluorescent PAMAM

dendrimer and evaluation of its sensor potential. *Dyes and Pigments* **2014**, *105*, 114-120.

66. Chu, C. C.; Imae, T., Fluorescence Investigations of Oxygen-Doped Simple Amine Compared with Fluorescent PAMAM Dendrimer. *Macromolecular rapid communications* **2009**, *30* (2), 89-93.

67. Jasmine, M. J.; Kavitha, M.; Prasad, E., Effect of solvent-controlled aggregation on the intrinsic emission properties of PAMAM dendrimers. *Journal of Luminescence* **2009**, *129* (5), 506-513.

68. Yanez Arteta, M.; Campbell, R. A.; Nylander, T., Adsorption of Mixtures of Poly(amidoamine) Dendrimers and Sodium Dodecyl Sulfate at the Air–Water Interface. *Langmuir : the ACS journal of surfaces and colloids* **2014**, *30* (20), 5817-5828.

69. Keszthelyi, T.; Hollo, G.; Nyitrai, G.; Kardos, J.; Heja, L., Bilayer Charge Reversal and Modification of Lipid Organization by Dendrimers as Observed by Sum-Frequency Vibrational Spectroscopy. *Langmuir : the ACS journal of surfaces and colloids* **2015**, *31* (28), 7815-25.

70. Lombardo, D.; Calandra, P.; Bellocco, E.; Lagana, G.; Barreca, D.; Magazu, S.; Wanderlingh, U.; Kiselev, M. A., Effect of anionic and cationic polyamidoamine (PAMAM) dendrimers on a model lipid membrane. *Biochimica et biophysica acta* **2016**, *1858* (11), 2769-2777.

71. Lombardo, D.; Calandra, P.; Magazu, S.; Wanderlingh, U.; Barreca, D.; Pasqua, L.; Kiselev, M. A., Soft nanoparticles charge expression within lipid membranes: The case of amino terminated dendrimers in bilayers vesicles. *Colloids and Surfaces B-Biointerfaces* **2018**, *170*, 609-616.

72. Smith, P. E. S.; Brender, J. R.; Dürr, U. H. N.; Xu, J.; Mullen, D. G.; Banaszak Holl, M. M.; Ramamoorthy, A., Solid-State NMR Reveals the Hydrophobic-Core Location of Poly(amidoamine) Dendrimers in Biomembranes. *Journal of the American Chemical Society* **2010**, *132* (23), 8087-8097.

73. López, R. R.; G. Font de Rubinat, P.; Sánchez, L.-M.; Tsering, T.; Alazzam, A.; Bergeron, K.-F.; Mounier, C.; Burnier, J. V.; Stiharu, I.; Nerguizian, V., The effect of different organic solvents in liposome properties produced in a periodic disturbance mixer: Transcutol®, a potential organic solvent replacement. *Colloids and Surfaces B: Biointerfaces* **2021**, *198*, 111447.

74. Paxman, J.; Hunt, B.; Hallan, D.; Zarbock, S. R.; Woodbury, D. J., Drunken Membranes: Short-Chain Alcohols Alter Fusion of Liposomes to Planar Lipid Bilayers. *Biophysical journal* **2017**, *112* (1), 121-132.

75. Hu, L.-X.; Tian, F.; Martin, F. L.; Ying, G.-G., Biochemical alterations in duckweed and algae induced by carrier solvents: Selection of an appropriate solvent in toxicity testing. *Environmental Toxicology and Chemistry* **2017**, *36* (10), 2631-2639.

76. Reis, P. B. P. S.; Vila-Viçosa, D.; Campos, S. R. R.; Baptista, A. M.; Machuqueiro, M., Role of Counterions in Constant-pH Molecular Dynamics Simulations of PAMAM Dendrimers. *ACS Omega* **2018**, 3 (2), 2001-2009.
77. Maingi, V.; Kumar, M. V. S.; Maiti, P. K., PAMAM Dendrimer–Drug Interactions: Effect of pH on the Binding and Release Pattern. *The Journal of Physical Chemistry B* **2012**, 116 (14), 4370-4376.
78. Devarakonda, B.; Otto, D. P.; Judefeind, A.; Hill, R. A.; de Villiers, M. M., Effect of pH on the solubility and release of furosemide from polyamidoamine (PAMAM) dendrimer complexes. *International journal of pharmaceuticals* **2007**, 345 (1), 142-153.
79. Nguyen, T. L.; Nguyen, T. H.; Nguyen, C. K.; Nguyen, D. H., Redox and pH Responsive Poly (Amidoamine) Dendrimer-Heparin Conjugates via Disulfide Linkages for Letrozole Delivery. *BioMed Research International* **2017**, 2017, 8589212.
80. Tian, W.-d.; Ma, Y.-q., pH-responsive dendrimers interacting with lipid membranes. *Soft Matter* **2012**, 8 (9), 2627-2632.
81. Shcharbin, D.; Klajnert, B.; Bryszewska, M., The effect of PAMAM dendrimers on human and bovine serum albumin at different pH and NaCl concentrations. *Journal of Biomaterials Science, Polymer Edition* **2005**, 16 (9), 1081-1093.
82. Wang, B.; Navath, R. S.; Menjoge, A. R.; Balakrishnan, B.; Bellair, R.; Dai, H.; Romero, R.; Kannan, S.; Kannan, R. M., Inhibition of bacterial growth and intramniotic infection in a guinea pig model of chorioamnionitis using PAMAM dendrimers. *International Journal of Pharmaceutics (Amsterdam, Netherlands)* **2010**, 395 (1-2), 298-308.
83. Serri, A.; Mahboubi, A.; Zarghi, A.; Moghimi, H. R., PAMAM-dendrimer Enhanced Antibacterial Effect of Vancomycin Hydrochloride Against Gram-Negative Bacteria. *J Pharm Pharm Sci* **2018**, 22 (1), 10-21.
84. Calabretta, M.; Kumar, A.; McDermott, A.; Cai, C., Antibacterial activities of poly(amidoamine) dendrimers terminated with amino and poly(ethylene glycol) groups. *Biomacromolecules* **2007**, 8 (6), 1807-1811.
85. Lopez, A. I.; Reins, R. Y.; McDermott, A. M.; Trautner, B. W.; Cai, C., Antibacterial activity and cytotoxicity of PEGylated poly(amidoamine) dendrimers. *Molecular BioSystems* **2009**, 5 (10), 1148-56.
86. Hoyo, J.; Torrent-Burgues, J.; Tzanov, T., Lipid-lipid interactions of Escherichia coli mimetic inner membrane at human physiological temperature. *Gen Physiol Biophys* **2020**, 39 (2), 195-202.
87. Sanders, M. R.; Clifton, L. A.; Frazier, R. A.; Green, R. J., Role of Lipid Composition on the Interaction between a Tryptophan-Rich Protein and Model

Bacterial Membranes. *Langmuir : the ACS journal of surfaces and colloids* **2016**, *32* (8), 2050-2057.

88. Ciumac, D.; Gong, H.; Campbell, R. A.; Campana, M.; Xu, H.; Lu, J. R., Structural elucidation upon binding of antimicrobial peptides into binary mixed lipid monolayers mimicking bacterial membranes. *J. Colloid Interface Sci.* **2021**, *598*, 193-205.

89. Nyitrai, G.; Keszthelyi, T.; Bota, A.; Simon, A.; Toke, O.; Horvath, G.; Pal, I.; Kardos, J.; Heja, L., Sodium selective ion channel formation in living cell membranes by polyamidoamine dendrimer. *Biochim. Biophys. Acta* **2013**, *1828* (8), 1873-80.

90. Kurniawan, J.; Ventrice de Souza, J. F.; Dang, A. T.; Liu, G.-y.; Kuhl, T. L., Preparation and Characterization of Solid-Supported Lipid Bilayers Formed by Langmuir–Blodgett Deposition: A Tutorial. *Langmuir : the ACS journal of surfaces and colloids* **2018**, *34* (51), 15622-15639.

91. Parimi, S.; Barnes, T.; Prestidge, C., PAMAM Dendrimer Interactions with Supported Lipid Bilayers: A Kinetic and Mechanistic Investigation. *Langmuir : the ACS journal of surfaces and colloids* **2008**, *24* (23), 13532-13539.

92. Fox, L. J.; Slastanova, A.; Taylor, N.; Wlodek, M.; Bikondoa, O.; Richardson, R. M.; Briscoe, W. H., Interactions between PAMAM dendrimers and DOPC lipid multilayers: Membrane thinning and structural disorder. *Biochimica et Biophysica Acta (BBA) - General Subjects* **2021**, *1865* (4), 129542.

93. Ainalem, M.-L.; Campbell, R. A.; Khalid, S.; Gillams, R. J.; Rennie, A. R.; Nylander, T., On the Ability of PAMAM Dendrimers and Dendrimer/DNA Aggregates To Penetrate POPC Model Biomembranes. *The journal of physical chemistry. B* **2010**, *114*, 7229–7244.

94. Jackman, J. A.; Cho, N.-J., Supported Lipid Bilayer Formation: Beyond Vesicle Fusion. *Langmuir : the ACS journal of surfaces and colloids* **2020**, *36* (6), 1387-1400.

95. Cho, N.-J., Emerging Approaches to Fabricate Supported Lipid Bilayers: Moving Beyond Vesicles. *Biophysical journal* **2018**, *114* (3), 15a.

96. Berenyi, S.; Mihaly, J.; Wacha, A.; Toke, O.; Bota, A., A mechanistic view of lipid membrane disrupting effect of PAMAM dendrimers. *Colloids and Surfaces, B: Biointerfaces* **2014**, *118*, 164-71.

97. Mecke, A.; Uppuluri, S.; Sassanella, T. M.; Lee, D. K.; Ramamoorthy, A.; Baker, J. R., Jr.; Orr, B. G.; Banaszak Holl, M. M., Direct observation of lipid bilayer disruption by poly(amidoamine) dendrimers. *Chemistry and physics of lipids* **2004**, *132* (1), 3-14.

98. Akesson, A.; Bendtsen, K. M.; Beherens, M. A.; Pedersen, J. S.; Alfredsson, V.; Cardenas Gomez, M., The effect of PAMAM G6 dendrimers on the structure of lipid vesicles. *Physical Chemistry Chemical Physics* **2010**, *12* (38), 12267-72.

99. Roy, B.; Guha, P.; Nahak, P.; Karmakar, G.; Maiti, S.; Mandal, A. K.; Bykov, A. G.; Akentiev, A. V.; Noskov, B. A.; Tsuchiya, K.; Torigoe, K.; Panda, A. K., Biophysical Correlates on the Composition, Functionality, and Structure of Dendrimer–Liposome Aggregates. *ACS Omega* **2018**, *3* (9), 12235-12245.
100. Gardikis, K.; Hatziantoniou, S.; Viras, K.; Wagner, M.; Demetzos, C., A DSC and Raman spectroscopy study on the effect of PAMAM dendrimer on DPPC model lipid membranes. *International journal of pharmaceutics* **2006**, *318* (1-2), 118-123.
101. Klajnert, B.; Epan, R. M., PAMAM dendrimers and model membranes: differential scanning calorimetry studies. *International journal of pharmaceutics* **2005**, *305* (1-2), 154-66.
102. Evans, K.; Laszlo, J.; Compton, D., Carboxyl-terminated PAMAM dendrimer interaction with 1-palmitoyl-2-oleoyl phosphocholine bilayers. *Biochimica Et Biophysica Acta-Biomembranes* **2014**, *1838* (1), 445-455.
103. Åkesson, A.; Lundgaard, C. V.; Ehrlich, N.; Pomorski, T. G.; Stamou, D.; Cárdenas, M., Induced dye leakage by PAMAM G6 does not imply dendrimer entry into vesicle lumen. *Soft Matter* **2012**, *8* (34), 8972-8980.
104. Tian, F. J.; Lin, X.; Valle, R. P.; Zuo, Y. Y.; Gu, N., Poly(amidoamine) Dendrimer as a Respiratory Nanocarrier: Insights from Experiments and Molecular Dynamics Simulations. *Langmuir : the ACS journal of surfaces and colloids* **2019**, *35* (15), 5364-5371.
105. Lu, Y.; Slomberg, D. L.; Shah, A.; Schoenfisch, M. H., Nitric oxide-releasing amphiphilic poly(amidoamine) (PAMAM) dendrimers as antibacterial agents. *Biomacromolecules* **2013**, *14* (10), 3589-98.
106. Ma, M.; Cheng, Y.; Xu, Z.; Xu, P.; Qu, H.; Fang, Y.; Xu, T.; Wen, L., Evaluation of polyamidoamine (PAMAM) dendrimers as drug carriers of anti-bacterial drugs using sulfamethoxazole (SMZ) as a model drug. *European journal of medicinal chemistry* **2007**, *42* (1), 93-8.
107. Cheng, Y.; Qu, H.; Ma, M.; Xu, Z.; Xu, P.; Fang, Y.; Xu, T., Polyamidoamine (PAMAM) dendrimers as biocompatible carriers of quinolone antimicrobials: an in vitro study. *European journal of medicinal chemistry* **2007**, *42* (7), 1032-8.
108. Wilde, M.; Green, R. J.; Sanders, M. R.; Greco, F., Biophysical studies in polymer therapeutics: the interactions of anionic and cationic PAMAM dendrimers with lipid monolayers. *Journal of drug targeting* **2017**, *25* (9-10), 910-918.
109. Yanez Arteta, M.; Ainalem, M. L.; Porcar, L.; Martel, A.; Coker, H.; Lundberg, D.; Chang, D. P.; Soltwedel, O.; Barker, R.; Nylander, T., Interactions of PAMAM Dendrimers with Negatively Charged Model Biomembranes. *The journal of physical chemistry. B* **2014**, *118* (45), 12892-12906.
110. Roy, B.; Panda, A. K.; Parimi, S.; Ametov, I.; Barnes, T.; Prestidge, C. A., Physico-chemical Studies on the Interaction of Dendrimers with Lipid Bilayers. 1.

Effect of Dendrimer Generation and Liposome Surface Charge. *J. Oleo Sci.* **2014**, *63* (11), 1185-1193.

111. Semeraro, E. F.; Marx, L.; Frewein, M. P. K.; Pabst, G., Increasing complexity in small-angle X-ray and neutron scattering experiments: from biological membrane mimics to live cells. *Soft Matter* **2021**, *17* (2), 222-232.

112. Jevprasesphant, R.; Penny, J.; Jalal, R.; Attwood, D.; McKeown, N.; D'Emanuele, A., The influence of surface modification on the cytotoxicity of PAMAM dendrimers. *International Journal of Pharmaceutics (Amsterdam, Netherlands)* **2003**, *252* (1-2), 263-266.

113. Pryor, J. B.; Harper, B. J.; Harper, S. L., Comparative toxicological assessment of PAMAM and thiophosphoryl dendrimers using embryonic zebrafish. *Int. J. Nanomed.* **2014**, *9*, 1947-56.

114. Thiagarajan, G.; Greish, K.; Ghandehari, H., Charge affects the oral toxicity of poly(amidoamine) dendrimers. *European journal of pharmaceutics and biopharmaceutics : official journal of Arbeitsgemeinschaft fuer Pharmazeutische Verfahrenstechnik e.V* **2013**, *84* (2), 330-4.

115. Patel, M.; De Paoli, S. H.; Elhelu, O. K.; Farooq, S.; Simak, J., Cell membrane disintegration and extracellular vesicle release in a model of different size and charge PAMAM dendrimers effects on cultured endothelial cells. *Nanotoxicology* **2019**, *13* (5), 664-681.

116. Jones, C. F.; Campbell, R. A.; Franks, Z.; Gibson, C. C.; Thiagarajan, G.; Vieira-de-Abreu, A.; Sukavaneshvar, S.; Mohammad, S. F.; Li, D. Y.; Ghandehari, H.; Weyrich, A. S.; Brooks, B. D.; Grainger, D. W., Cationic PAMAM Dendrimers Disrupt Key Platelet Functions. *Molecular pharmaceutics* **2012**, *9* (6), 1599-1611.

117. Aisina, R.; Mukhametova, L.; Ivanova, E., Influence cationic and anionic PAMAM dendrimers of low generation on selected hemostatic parameters in vitro. *Materials Science and Engineering: C* **2020**, *109*, 110605.

118. Lin, Y.-L.; Khanafer, K.; El-Sayed, M. E. H., Quantitative evaluation of the effect of poly(amidoamine) dendrimers on the porosity of epithelial monolayers. *Nanoscale* **2010**, *2* (5), 755-762.

119. Kitchens, K. M.; Kolhatkar, R. B.; Swaan, P. W.; Eddington, N. D.; Ghandehari, H., Transport of poly(amidoamine) dendrimers across Caco-2 cell monolayers: Influence of size, charge and fluorescent labeling. *Pharm. Res.* **2006**, *23* (12), 2818-26.

120. Kitchens, K.; Foraker, A.; Kolhatkar, R.; Swaan, P.; Ghandehari, H., Endocytosis and interaction of poly (amidoamine) dendrimers with Caco-2 cells. *Pharmaceutical research* **2007**, *24* (11), 2138-2145.

121. Morris, C. J.; Aljayyousi, G.; Mansour, O.; Griffiths, P.; Gumbleton, M., Endocytic Uptake, Transport and Macromolecular Interactions of Anionic PAMAM

- Dendrimers within Lung Tissue. *Pharmaceutical research* **2017**, *34* (12), 2517-2531.
122. Thiagarajan, G.; Sadekar, S.; Greish, K.; Ray, A.; Ghandehari, H., Evidence of oral translocation of anionic G6.5 dendrimers in mice. *Molecular pharmaceuticals* **2013**, *10* (3), 988-98.
123. Sweet, D. M.; Kolhatkar, R. B.; Ray, A.; Swaan, P.; Ghandehari, H., Transepithelial transport of PEGylated anionic poly(amidoamine) dendrimers: implications for oral drug delivery. *Journal of controlled release : official journal of the Controlled Release Society* **2009**, *138* (1), 78-85.
124. Serchenya, T.; Shcharbin, D.; Shyrochyna, I.; Sviridov, O.; Terekhova, M.; Dzmitruk, V.; Abashkin, V.; Apartsin, E.; Mignani, S.; Majoral, J.-P.; Ionov, M.; Bryszewska, M., Immunoreactivity changes of human serum albumin and alpha-1-microglobulin induced by their interaction with dendrimers. *Colloids and Surfaces B: Biointerfaces* **2019**, *179*, 226-232.
125. Shcharbin, D.; Drapeza, A.; Loban, V.; Lisichenok, A.; Bryszewska, M., The breakdown of bilayer lipid membranes by dendrimers. *Cellular & molecular biology letters* **2006**, *11* (2), 242-8.
126. Kelly, C. V.; Leroueil, P. R.; Orr, B. G.; Banaszak Holl, M. M.; Andricioaei, I., Poly(amidoamine) dendrimers on lipid bilayers II: Effects of bilayer phase and dendrimer termination. *Journal of Physical Chemistry B* **2008**, *112* (31), 9346-9353.
127. Niki, Y.; Ogawa, M.; Makiura, R.; Magata, Y.; Kojima, C., Optimization of dendrimer structure for sentinel lymph node imaging: Effects of generation and terminal group. *Nanomedicine: Nanotechnology, Biology and Medicine* **2015**, *11* (8), 2119-2127.
128. Nagai, K.; Sato, T.; Kojima, C., Design of a dendrimer with a matrix metalloproteinase-responsive fluorescence probe and a tumor-homing peptide for metastatic tumor cell imaging in the lymph node. *Bioorganic & Medicinal Chemistry Letters* **2021**, *33*, 127726.
129. Mekuria, S. L.; Addisu, K. D.; Chou, H.-Y.; Hailemeskel, B. Z.; Tsai, H.-C., Potential fluorescence and magnetic resonance imaging modality using mixed lanthanide oxide nanoparticles. *Colloids and Surfaces B: Biointerfaces* **2018**, *167*, 54-62.
130. Mekuria, S. L.; Tsai, H.-C., Preparation of self-assembled core-shell nano structure of conjugated generation 4.5 poly (amidoamine) dendrimer and monoclonal Anti-IL-6 antibody as bioimaging probe. *Colloids and Surfaces B: Biointerfaces* **2015**, *135*, 253-260.
131. Cao, J.; Ge, R.; Zhang, M.; Xia, J.; Han, S.; Lu, W.; Liang, Y.; Zhang, T.; Sun, Y., A triple modality BSA-coated dendritic nanoplatfor for NIR imaging, enhanced tumor penetration and anticancer therapy. *Nanoscale* **2018**, *10* (19), 9021-9037.

132. Zolotarskaya, O. Y.; Xu, L.; Valerie, K.; Yang, H., Click synthesis of a polyamidoamine dendrimer-based camptothecin prodrug. *RSC Advances* **2015**, *5* (72), 58600-58608.
133. Vu, M. T.; Bach, L. G.; Nguyen, D. C.; Ho, M. N.; Nguyen, N. H.; Tran, N. Q.; Nguyen, D. H.; Nguyen, C. K.; Hoang Thi, T. T., Modified Carboxyl-Terminated PAMAM Dendrimers as Great Cytocompatible Nano-Based Drug Delivery System. *International journal of molecular sciences* **2019**, *20* (8), 2016.
134. Zhong, Q.; Bielski, E. R.; Rodrigues, L. S.; Brown, M. R.; Reineke, J. J.; da Rocha, S. R. P., Conjugation to Poly(amidoamine) Dendrimers and Pulmonary Delivery Reduce Cardiac Accumulation and Enhance Antitumor Activity of Doxorubicin in Lung Metastasis. *Molecular pharmaceutics* **2016**, *13* (7), 2363-2375.
135. Ertürk, A. S.; Gürbüz, M. U.; Tülü, M., The effect of PAMAM dendrimer concentration, generation size and surface functional group on the aqueous solubility of candesartan cilexetil. *Pharmaceutical Development and Technology* **2017**, *22* (1), 111-121.
136. Gürbüz, M. U.; Ertürk, A. S.; Tülü, M., Synthesis of surface-modified TREN-cored PAMAM dendrimers and their effects on the solubility of sulfamethoxazole (SMZ) as an analog antibiotic drug. *Pharmaceutical Development and Technology* **2017**, *22* (5), 678-689.
137. Souza, J. G.; Dias, K.; Silva, S. A.; de Rezende, L. C.; Rocha, E. M.; Emery, F. S.; Lopez, R. F., Transcorneal iontophoresis of dendrimers: PAMAM corneal penetration and dexamethasone delivery. *Journal of controlled release : official journal of the Controlled Release Society* **2015**, *200*, 115-24.
138. Yavuz, B.; Bozdogan Pehlivan, S.; Sumer Bolu, B.; Nomak Sanyal, R.; Vural, I.; Unlu, N., Dexamethasone - PAMAM dendrimer conjugates for retinal delivery: preparation, characterization and in vivo evaluation. *The Journal of pharmacy and pharmacology* **2016**, *68* (8), 1010-20.
139. Xie, F.; Wei, X.; Li, Q.; Zhou, T., *In vivo* analyses of the effects of polyamidoamine dendrimer on dentin biomineralization and dentinal tubules occlusion. *Dental Materials Journal* **2016**, *35* (1), 104-111.
140. Qin, H.; Long, J.; Zhou, J.; Wu, L.; Xie, F., Use of phosphorylated PAMAM and carboxylated PAMAM to induce dentin biomimetic remineralization and dentinal tubule occlusion. *Dental Materials Journal* **2021**, *advpub*.
141. Wu, Q.; Shan, T.; Zhao, M.; Mai, S.; Gu, L., The inhibitory effect of carboxyl-terminated polyamidoamine dendrimers on dentine host-derived matrix metalloproteinases *in vitro* in an etch-and-rinse adhesive system. *Royal Society Open Science* **2019**, *6* (10), 182104.
142. Akter, R.; Jeong, B.; Lee, Y.-M.; Choi, J.-S.; Rahman, M. A., Femtomolar detection of cardiac troponin I using a novel label-free and reagent-free dendrimer

- enhanced impedimetric immunosensor. *Biosensors and Bioelectronics* **2017**, *91*, 637-643.
143. Singh, P., Dendrimers and their applications in immunoassays and clinical diagnostics. *Biotechnology and Applied Biochemistry* **2007**, *48*, 1-9.
144. Singh, P.; Moll, F.; Lin, S. H.; Ferzli, C.; Yu, K. S.; Koski, R. K.; Saul, R. G.; Cronin, P., Starburst dendrimers: enhanced performance and flexibility for immunoassays. *Clinical Chemistry* **1994**, *40* (9), 1845-1849.
145. Akhtar, S.; Chandrasekhar, B.; Attur, S.; Yousif, M. H.; Benter, I. F., On the nanotoxicity of PAMAM dendrimers: Superfect® stimulates the EGFR-ERK1/2 signal transduction pathway via an oxidative stress-dependent mechanism in HEK 293 cells. *International Journal of Pharmaceutics (Amsterdam, Netherlands)* **2013**, *448* (1), 239-46.
146. Tang, M. X.; Redemann, C. T.; Szoka, F. C., In vitro gene delivery by degraded polyamidoamine dendrimers. *Bioconjugate chemistry* **1996**, *7* (6), 703-14.
147. Akhtar, S.; Al-Zaid, B.; El-Hashim, A. Z.; Chandrasekhar, B.; Attur, S.; Yousif, M. H. M.; Benter, I. F., Cationic Polyamidoamine Dendrimers as Modulators of EGFR Signaling In Vitro and In Vivo. *PLOS ONE* **2015**, *10* (7), e0132215.
148. Symons, J. L.; Cho, K.-J.; Chang, J. T.; Du, G.; Waxham, M. N.; Hancock, J. F.; Levental, I.; Levental, K. R., Lipidomic atlas of mammalian cell membranes reveals hierarchical variation induced by culture conditions, subcellular membranes, and cell lineages. *Soft Matter* **2021**, *17* (2), 288-297.
149. Gutschmann, T.; Hagge, S. O.; David, A.; Roes, S.; Böhling, A.; Hammer, M. U.; Seydel, U., Lipid-mediated resistance of Gram-negative bacteria against various pore-forming antimicrobial peptides. *Journal of Endotoxin Research* **2005**, *11* (3), 167-173.
150. Ma, Y.; Zhang, S.; Jin, Z.; Shi, M., Lipid-mediated regulation of the cancer-immune crosstalk. *Pharmacological Research* **2020**, *161*, 105131.